

UNIVERSITÄTSKLINIKUM HAMBURG-EPPENDORF

Zentrum für Experimentelle Medizin
Institut für Computational Neuroscience
Direktor: Prof. Dr. Claus C. Hilgetag

Architecture and Connectivity of the Cerebral Cortex

Dissertation

zur Erlangung des Doktorgrades PhD
an der Medizinischen Fakultät der Universität Hamburg

vorgelegt von

Sarah F. Beul

aus Perleberg

Hamburg 2019

**Angenommen von der
Medizinischen Fakultät der Universität Hamburg am: 02.12.2019**

**Veröffentlicht mit Genehmigung der
Medizinischen Fakultät der Universität Hamburg.**

Prüfungsausschuss, der/die Vorsitzende: Prof. Dr. Claus Hilgetag

Prüfungsausschuss, zweite/r Gutachter/in: Prof. Dr. Udo Schumacher

dritter Gutachter: Dr. Marc Tittgemeyer

Contents

1	Introduction	1
1.1	Architecture varies throughout the cortex	2
1.2	Intrinsic circuitry	3
1.2.1	Intrinsic circuitry in granular cortex	5
1.2.2	Interlaminar inhibition in mouse cortex	5
1.3	Extrinsic circuitry	7
1.3.1	Laminar projection patterns regulate information processing .	8
1.4	Possible measures to explain the organisation of cortical connectivity	9
1.4.1	Architectonic differentiation	9
1.4.2	Cellular morphological measures	11
1.4.3	Cortical thickness	12
1.4.4	Spatial proximity	13
1.4.5	Cortical hierarchy	13
1.5	Connectivity data	14
1.6	Possible developmental mechanism underlying the organisation of cortical connectivity	14
1.6.1	Aspects of neural development that prescribe spatio-temporal trajectories of cortical growth	17
1.6.2	An <i>in silico</i> model for assessing spatio-temporal growth trajec- tories	20
1.6.3	Expansion of the <i>in silico</i> model to probe the emergence of laminar patterns of projection origins	20
1.7	Overview of performed studies	23

1.7.1	Tentative intrinsic circuitry in agranular cortex	23
1.7.2	Testing the architectonic type principle and other frameworks in cat and macaque	24
1.7.3	Testing the relative merit of multiple measures of cortical struc- ture	24
1.7.4	Testing the applicability of the architectonic type principle to the developing cortex	26
1.7.5	Testing the hypothesised mechanistic underpinnings of the architectonic type principle	27
2	Methods	30
2.1	Connectivity data sets	30
2.1.1	Cat cortex	30
2.1.2	Macaque cortex	34
2.2	Potential explanatory measures	38
2.2.1	Cortical architecture	38
2.2.2	Cortical thickness	43
2.2.3	Spatial proximity	44
2.2.4	Hierarchical level	46
2.3	Analysis procedures and statistical tests	46
2.3.1	Tests for group differences	46
2.3.2	Correlations	47
2.3.3	Relative projection frequency	47
2.3.4	Classification of connection existence	47
2.4	Simulating the development of cortico-cortical connections: Existence of connections	52
2.4.1	Variants of the <i>in silico</i> model	52
2.4.2	Connection formation	57
2.4.3	Properties of the simulated cortical sheet	58
2.4.4	Analyses	59
2.5	Simulating the development of cortico-cortical connections: Laminar patterns of connection origins	65

2.5.1	Model expansion	66
2.5.2	Analyses of laminar patterns	71
2.5.3	Analyses of connection existence	72
3	Results	73
3.1	Intrinsic circuitry varies with architectonic differentiation	73
3.2	Comparison of the architectonic type principle, distance model and hierarchical model in the cat cortex	75
3.2.1	Relationship of projection existence to structural measures	76
3.2.2	Combining architectonic type difference and border distance allows the classification of connection existence	78
3.2.3	Relation of architecture with connection topology	80
3.2.4	Connection range	83
3.2.5	Laminar projection profiles	84
3.3	Comparison of the architectonic type principle, the distance model and the thickness model in the macaque cortex	85
3.3.1	Relations among structural measures	85
3.3.2	Relationship of projection existence to structural measures	86
3.3.3	Combining neuron density ratio and Euclidean distance allows the classification of connection existence	86
3.3.4	Relation of architecture with connection topology	89
3.3.5	Laminar patterns of projection origins	90
3.4	Neuron density is a better predictor of cortico-cortical connectivity than cellular morphological measures	91
3.4.1	Macroscopic and microscopic morphological measures are interrelated	92
3.4.2	Neuron density is most consistently related to the existence of projections	93
3.4.3	Distance and dendritic tree size are related to projection strength	97
3.4.4	Neuron density is consistently related to laminar patterns of projection origins	100
3.4.5	Neuron density is correlated with area degree	100

3.4.6	Discarding very weak projections does not affect observed relationships	104
3.5	The architectonic type principle captures laminar projection patterns early in development	104
3.5.1	Immature projection patterns correlate with adult differentiation measures	105
3.5.2	Loss of visual input does not substantially alter the gradient of projection patterns	107
3.6	Mechanistic underpinnings of the architectonic type principle explored by simulation experiments: Existence of connections	108
3.6.1	Connection statistics	111
3.6.2	Contributions of distance and density difference to connectivity patterns	111
3.6.3	Number of connections per area	116
3.6.4	Prediction of empirical connection existence from simulated networks	117
3.7	Mechanistic underpinnings of the architectonic type principle explored by simulation experiments: Laminar patterns of connection origins	124
3.7.1	At baseline settings, supragranular contribution was not correlated with relative differentiation	124
3.7.2	Delay in infragranular compartment growth did not affect laminar projection patterns	125
3.7.3	Delay in supragranular compartment growth resulted in negative correlation of supragranular contribution with relative differentiation	127
3.7.4	Scaling of supragranular density did not result in representative laminar patterns of projection origins	129
3.7.5	Divergence in axon elongation resulted in laminar patterns of projection origins that exhibited the empirically observed relation to relative differentiation	132
3.7.6	Combinations of features	134
4	Discussion	135

4.1	The architectonic type principle captures cortico-cortical connectivity across mammalian cortices	137
4.1.1	Relationship among structural measures	138
4.1.2	Connection existence can be classified based on architectonic differentiation and spatial proximity	140
4.1.3	Topological features are related to architectonic differentiation	142
4.1.4	Methodological considerations	143
4.1.5	Connectivity is not optimised solely for minimal wiring	147
4.1.6	Cortical thickness is not a suitable predictor of connectivity .	147
4.1.7	A cortical hierarchy is not a suitable predictor of connectivity	148
4.1.8	The architectonic type principle is further corroborated	149
4.2	Compared to measures of neuron morphology, neuron density is a superior indicator of connectivity features	150
4.2.1	Limitations of the explanatory power of the cellular measures	154
4.2.2	Developmental mechanisms may regulate the covariation of architectonic measures	154
4.2.3	Local cortical architecture, features of cortico-cortical connections and areas' functional roles are tightly interrelated	156
4.2.4	Neuron density is a powerful predictor of connectivity features	159
4.3	The architectonic type principle is already applicable in the developing cortex	160
4.4	Possible mechanistic underpinnings of the architectonic type principle	163
4.4.1	Spatio-temporal growth trajectories determine essential properties of the final connectome	164
4.4.2	Realistic network properties emerge from empirically grounded growth trajectories	166
4.4.3	Simulation results validate the mechanistic explanations hypothesised to underlie the architectonic type principle	168
4.4.4	Simulating the development of laminar projection patterns . .	170
4.4.5	Limitations and future extensions	177

4.4.6	Realistic networks of inter-areal connections can be generated from an <i>in silico</i> model realising spatio-temporal interactions in the forming tissue	182
4.5	Conclusions	183
4.5.1	Architecture and intrinsic connectivity vary across the cortex .	184
4.5.2	The architectonic type principle comprehensively accounts for features of connectivity in the mammalian cortex	184
4.5.3	The architectonic type principle may emerge from spatio-temporal interactions during brain development	186
5	Summary	189
5.1	English Summary	189
5.2	Deutsche Zusammenfassung	190
	Bibliography	192
	Acknowledgements	233
A	Prior publications	235
B	Curriculum Vitae	237
C	Supplementary figures	239
D	Supplementary tables	257
E	Eidesstattliche Erklärung	278

List of Figures

1.1	Architectonic differentiation and laminar patterns of projections . . .	3
1.2	Interlaminar inhibition varies across mouse cortex	6
1.3	Neurodevelopmental assumptions and overview of the <i>in silico</i> model	16
2.1	Architectonic type in the cat cortex	39
2.2	Variation of cytoarchitectonic features across the macaque cortex . .	41
2.3	Developmental trajectories of growth layouts	55
2.4	Validation procedure for measures of simulation-to-empirical classification performance	64
2.5	Features of the expanded <i>in silico</i> model	68
3.1	Intrinsic circuitry in the mammalian cortex	74
3.2	Cumulative percentages of present projections in the cat cortex . . .	77
3.3	Interrelations of structural measures in the cat cortex	77
3.4	Correlation of structural measures with relative frequencies of present projections in the cat cortex	78
3.5	Results of linear discriminant analysis	79
3.6	Distribution of architectonic types across modules of cortical areas in the cat cortex	81
3.7	Degree distribution of cortical areas in the cat cortex	82
3.8	Mean number of projections across architectonic types in the cat cortex	83
3.9	Correlation of structural measures with assigned directionalities of projections	84

3.10 Comparison of neuron density similarity and distance for projection frequency	87
3.11 Classification of projection existence in the macaque cortex from neuron density similarity and Euclidean distance	88
3.12 Variation of topological properties with neuron density in the macaque cortex	90
3.13 Variation of laminar patterns of projection origins with structural measures in the macaque cortex	91
3.14 Relative structural measures differ between connected and unconnected pairs of areas in the macaque cortex	93
3.15 Classification of connection existence by logistic regression in the macaque cortex	94
3.16 Projection strength varies with relative structural measures in the macaque cortex	99
3.17 Laminar projection patterns vary with relative structural measures in the macaque cortex	101
3.18 Area degree varies with structural measures in the macaque cortex	102
3.19 Laminar projection patterns in immature macaque cortex	106
3.20 Laminar projection patterns in the macaque cortex after enucleation	108
3.21 Connection statistics of simulation experiments	112
3.22 Correlation of distance and absolute density difference with relative connection frequency <i>in silico</i>	113
3.23 Logistic regression performance for classification of simulation data from simulation data	114
3.24 Correlation of area degree with neuron density <i>in silico</i>	116
3.25 Classification accuracy for prediction of empirical connection existence from simulation data	119
3.26 Youden index for prediction of empirical connection existence from simulation data	120
3.27 Percentage of empirical connectivity data that were classified from simulation data	121
3.28 Correlation of supragranular contribution with neuron density difference <i>in silico</i>	126

3.29 Neuron density scaling did not result in realistic laminar patterns of projection origins	131
3.30 Abolishing the ordered neuron density gradient decreased the positive correlation observed for axon elongation scaling	133
4.1 The architectonic basis of the mammalian connectome	139
4.2 Projection patterns in the context of cortical structural variation . . .	152
4.3 Structure and function of brain areas and connections are interlinked	157
4.4 Summary of changes in laminar projection patterns	162
4.5 Number and relation of neurogenetic and architectonic gradients . .	167
4.6 Realistic laminar patterns can arise from an interaction of spatio-temporal gradients in neurogenesis with gradients in cell-intrinsic properties	174
C.1 True positive rate and false positive rate for classification of projection existence in the macaque cortex	240
C.2 Youden index J for classification of projection existence in the macaque cortex	241
C.3 Developmental trajectories of all 21 growth layouts	243
C.4 Correlation of relative connection frequency with distance and absolute density difference for all growth layouts	244
C.5 Correlation of area degree with neuron density for all growth layouts	246
C.6 Supragranular contribution across source area densities	250
C.7 Correlation of area degree with neuron density	251
C.8 Simulation-to-empirical classification performance	253
C.9 Axon elongation without ordered succession of neuron density values	253
C.10 Pairwise combination of features	254
C.11 Combination of all features	255
C.12 Classification of connection existence using logistic regression in simulated cortical sheets of different sizes	256

List of Tables

2.1	Summary of growth layouts	54
3.1	Correlation between structural measures in the macaque cortex . . .	92
3.2	Structural measures in connected and unconnected pairs of areas in the macaque cortex	94
3.3	Classification of connection existence by logistic regression in the macaque cortex	95
3.4	Correlation between projection strength and structural measures in the macaque cortex	98
3.5	Correlation between laminar projection patterns and structural measures in the macaque cortex	101
3.6	Correlation between area degree and structural measures in the macaque cortex	103
3.7	Summary of correspondence between simulation results and empirical observations	110
3.8	Analysis of variance on classification performance of <i>realistically oriented density gradient</i> growth layouts	123
3.9	<i>Post-hoc</i> comparisons for classification performance of <i>realistically oriented density gradient</i> growth layouts	123
D.1	Anatomical abbreviations in the cat cortex	258
D.2	Projection data and structural measures in the cat cortex	259
D.3	Classification of unsampled projections in the macaque cortex	266
D.4	Correspondence of areas in the macaque cortex across parcellations .	268

D.5	Structural measures in connected and unconnected pairs of macaque cortex areas in reduced data set	269
D.6	Classification of connection existence by logistic regression in reduced data set	270
D.7	Correlation between projection strength and structural measures in reduced data set	271
D.8	Correlation between area degree and structural measures in reduced data set	272
D.9	Projection data in the immature macaque cortex	273
D.10	Correlations of laminar projection patterns and architectonic differentiation in the immature macaque cortex	274
D.11	Correlations with laminar projection patterns after enucleation	274
D.12	Summary of connectivity statistics, correlation with relative projection frequency, classification performance logistic regression, and correlation with area degree <i>in silico</i>	275
D.13	Summary classification of empirical connectivity from simulated connectivity	276

Introduction

The cerebral cortex is arguably one of the most complex physical systems that exist. Untangling the intricate relations of the myriad elements of the grey matter is one of the formidable challenges of science, as already pronounced by Santiago Ramón y Cajal:

“Devotion to the cerebral hemispheres, enigma of enigmas, was old in me...the supreme cunning of the structure of the grey matter is so intricate that it defies and will continue to defy for many centuries the obstinate curiosity of investigators. That apparent disorder of the cerebral jungle, so different from the regularity and symmetry of the spinal cord and of the cerebellum, conceals a profound organisation of the utmost subtlety which is at present inaccessible.”

— (Cajal, 1937)

Decades later, the picture has become more refined, but a comprehensive understanding of cortical organisation still remains a fundamental scientific challenge.

In the following chapters, I will describe insights we gained into the organisation of cortico-cortical connectivity in the mammalian brain by exploring the explanatory power of the architectonic type principle, which was proposed in its current form by Helen Barbas (1986). By framing the axonal connections between brain areas in terms of the respective compositions of areas, this principle affords a suitable vantage point for understanding how multiple dimensions of brain organisation relate to each other. I will detail evidence from the immature and adult states in the macaque as well as the adult cat cortex, indicating that the structure and the function of brain areas are tightly interlinked. I will argue that this interdependence arises from

a combination of the structure of individual areas with the structural features of the connections linking areas. Importantly, and crucial to its status as a principle, the architectonic type principle can be grounded in mechanistic explanations of its emergence, which we probed in simulation experiments.

Most of the work presented in this dissertation has been published in peer-reviewed journals, and a complete list of the publications I (co-)authored in the context of this dissertation can be found in Appendix A. The publications from which text has been excerpted are referenced at the end of each section. Since I accomplished none of the presented work alone, I will make use of plural verb forms throughout.

1.1 Architecture varies throughout the cortex

A crucial step in understanding the organisation of the cerebral cortex was the recognition that it is locally structured into horizontal compartments ('layers') as well as vertical units ('columns') which both may be of functional relevance. Traditionally, the isocortex has been characterised in the context of a six-layered scheme (Brodmann, 1909; Vogt, 1910; von Economo, 2009), as opposed to three-layered allocortex. This scheme is, however, subject to substantial variation in the relative prominence of layers and does not hold in a considerable number of cortical areas. Nonetheless, and in spite of his acknowledgment that "the distinction of six layers can be both arbitrary and conventional" (von Economo, 2009), already von Economo himself asserted that "on practical grounds, we retain the six-layer division" (von Economo, 2009). Indeed, the simplified concept of a uniformly six-layered isocortex has prevailed (Zilles and Amunts, 2012a) and become generally accepted.

But instead of all parts of the cortex being uniformly differentiated, architectonic differentiation changes gradually across the cortex (Brodmann, 1909; Sanides, 1970; von Economo, 1927, 2009; Zilles and Amunts, 2012b), as illustrated in Figure 1.1A for the human brain. Cortical architecture can be defined by a number of structural features, including the neuron density of cortical areas, as well as the number of identifiable cortical layers, myelin density and a number of receptor markers and specialised inhibitory neurons (Barbas and Pandya, 1989; Dombrowski et al., 2001; von Economo, 1927, 2009; Zilles and Amunts, 2012b). The spectrum of differentiation ranges from clearly eulaminate areas, such as striate (primary visual) cortex in primates, to agranular areas that lack the inner granular layer (layer 4, L4), and have few identifiable sublayers as well as very low neuron density.

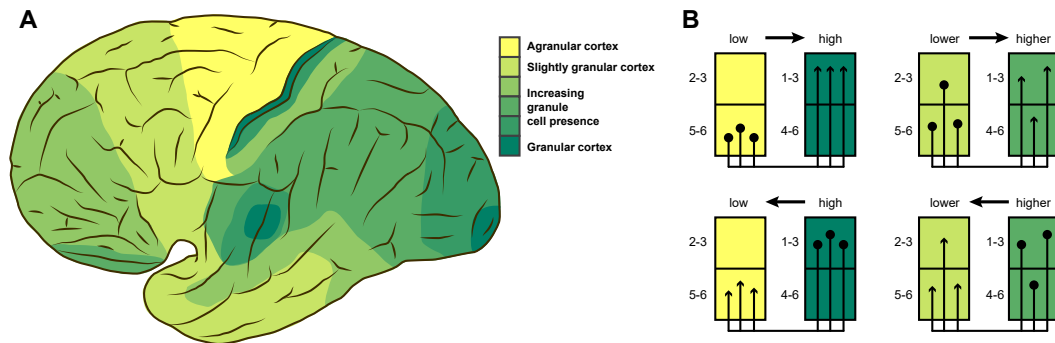


Figure 1.1: Architectonic differentiation and laminar patterns of projections. **(A)** Architectonic differentiation varies across the cortex. This lateral view of the human brain shows broad variations in granule cell presence as described by von Economo (2009). **(B)** Laminar origin and termination patterns of extrinsic cortico-cortical connections vary according to the relative architectonic differentiation of the connected areas. Projection origins (terminations) shift from infragranular to supragranular layers, as the source (target) area becomes more strongly differentiated. This rule results in unilaminar profiles for projections between areas that are unequal in their differentiation, and multilaminar profiles for areas with more similar differentiation. **(A)** adapted from von Economo (2009), **(B)** adapted from Barbas and Rempel-Clower (1997).

In between these two extremes, one can find areas that are still eulaminar, but without the remarkable clarity of differentiation or dense packing of neurons found in striate cortex, such as prestriate cortex, as well as dysgranular areas with a lower density of neurons, a dissolving inner granular layer and fewer identifiable sublayers. Quantitative differences in many aspects of the structural organisation of cortical tissue have been extensively demonstrated (e.g. Beaulieu and Colonnier, 1989; DeFelipe et al., 1999; Dombrowski et al., 2001; Yáñez et al., 2005; Collins et al., 2010).

Parts of this section have been published in Beul and Hilgetag (2015) and Beul et al. (2017).

1.2 Intrinsic circuitry

Within cortical areas, the multitude of present neurons are connected across layers by short-range, intrinsic connections, forming the local microcircuit. The radial organisation of the cortex became a subject of interest when vertical columns spanning all cortical layers were proposed to exist (Lorente de Nó, 1949; Mountcastle, 1957), with

uniform columns repeating across the cortex to form an intermediate-level neural substrate for information processing. Within these columns, connectivity across cortical layers appeared stereotypical (Szentagothai, 1978; Gilbert and Wiesel, 1983). While there is still considerable debate about the existence, the precise definition and the extent of heterogeneity in the cellular composition of cortical columns (Rakic, 2008; da Costa and Martin, 2010; Rockland, 2010; Smith, 2010a,b,c,d; Carlo and Stevens, 2013; Herculano-Houzel et al., 2013), the concept of radial cortical organisation was later extended to the notion of a ‘canonical’ microcircuit (Douglas et al., 1989; Douglas and Martin, 1991, 2004), as a generic template of intrinsic cortical circuitry. The computations performed by such a fundamental neuronal circuit are thought to be prescribed by the intrinsic circuitry within a cortical column, with functional specificity added by patterns of axonal inputs and outputs to and from the column. Substantial work has been devoted to the computational performance and theoretical properties of the ‘canonical’ microcircuit (e.g. Douglas et al., 1989, 1995; Haeusler and Maass, 2007; George and Hawkins, 2009; Haeusler et al., 2009; Wagatsuma et al., 2011; Bastos et al., 2012; Habenschuss et al., 2013). In the primate prefrontal cortex, the ‘canonical’ microcircuit was shown to be subject to modifications from the striate circuit (Heinzle et al., 2007; Godlove et al., 2014). More generally, abundant data is available on variants of intrinsic connectivity in cortical regions such as prefrontal cortex (Melchitzky et al., 2001), somatosensory cortex (Lübke and Feldmeyer, 2007; Petersen, 2007; Lefort et al., 2009; Feldmeyer et al., 2013) or auditory cortex (Barbour and Callaway, 2008; Oviedo et al., 2010; Watkins et al., 2014). Nonetheless, the notion of a ‘canonical’ microcircuit, which has gained popularity especially in the computational neuroscience community and has also inspired neuroengineering solutions (e.g. Merolla et al., 2014), is still largely based on work in one particular cortical area, the striate cortex. Moreover, much of this work has concentrated on the cat and non-human primate brain (Douglas and Martin, 2007c). Striate cortex is not only special in the amount of probing it has undergone, but is also exceptional in its architectonic differentiation. Striate cortex is the cortical region with the highest neuron density, sporting numbers substantially higher than the remainder of the cortex (Schüz and Palm, 1989; Collins et al., 2010; Cahalane et al., 2012; Herculano-Houzel et al., 2013). The number of (sub)layers that can be identified is also higher in striate cortex than in other regions of the cortex.

The variation in local cortical structure needs to be taken into account when describing a ‘canonical’ microcircuit, because it is unlikely for the patterns of inter- and intra-laminar connections to be uniform in spite of strong variations of their structural substrate. Indeed, experimental results, for example from rodent barrel

cortex, demonstrate that intrinsic connectivity is not uniform across the cortex (Sato et al., 2008; Meyer et al., 2013; Reyes-Puerta et al., 2014).

1.2.1 Intrinsic circuitry in granular cortex

Over the last decades, general features of intrinsic circuitry in striate cortex have emerged from studies in the cat and non-human primate. Connections are proposed to form a processing loop across cortical layers, where recurrent excitation and inhibition are interlinked, which leads to amplification of inputs into the cortical column and appropriate modulation of the ensuing activity (Markram et al., 2004; Douglas and Martin, 2004, 2007c; Bannister, 2005; Lübke and Feldmeyer, 2007). To probe the local microcircuitry, diverse experimental methods with different degrees of sensitivity and reliability have been used. Two investigations that supplied the most comprehensive data on cat striate cortex employed electrophysiological and morphological approaches, respectively. Thomson and colleagues (2002) used dual intracellular recordings to characterise synaptic connections across cortical layers. Binzegger and colleagues (2004) reconstructed the morphology of neurons in striate cortex in three dimensions and estimated the number of synaptic contacts between different cell types. Both data sets have been adapted and used in various studies, for example, in the construction of computational models (e.g. Haeusler and Maass, 2007; Haeusler et al., 2009; Bastos et al., 2012; Du et al., 2012; Potjans and Diesmann, 2014). But even though the same model system, cat striate cortex, was considered across these studies, there currently exists no definite scheme of this area's intrinsic circuitry. There are, for example, diverging data on whether recurrent excitation occurs between layer 3 (L3) and layer 5 (L5) or between L4 and L3 (cf. Thomson et al. (2002); Thomson and Bannister (2003) versus Binzegger et al. (2004); Douglas and Martin (2004)).

1.2.2 Interlaminar inhibition in mouse cortex

Such discrepancies may be reconciled by future experimental findings. In contrast, reports of differences in interlaminar activation patterns across cortical regions point towards the existence of genuine variations in intrinsic circuitry across the brain. Kätzel and colleagues (2011) used genetically targeted photostimulation to comprehensively map inhibitory-to-excitatory connectivity in three distinct regions of mouse

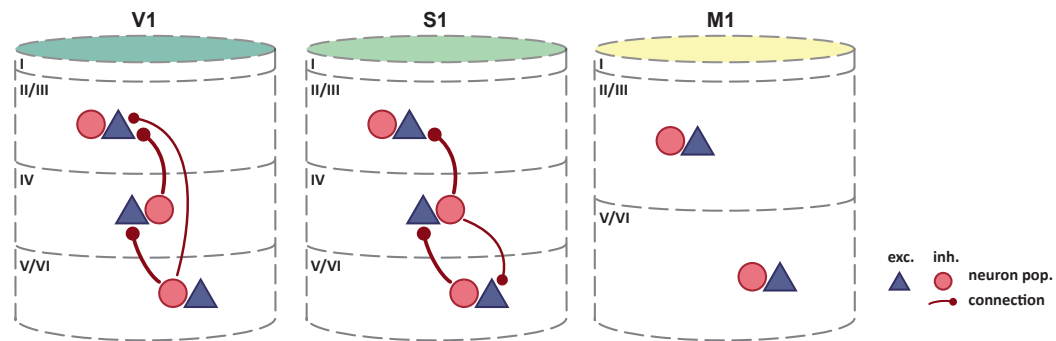


Figure 1.2: Interlaminar inhibition varies across mouse cortex. As architectonic differentiation becomes weaker, the abundance of interlaminar inhibitory-to-excitatory connectivity decreases. By contrast, intralaminar connectivity, including intralaminar inhibition, appears relatively unchanged (Intra-laminar connections, which are all-to-all, are not shown). Column colors follow the color coding of architectonic differentiation in Figure 1.1: yellow-weakly differentiated cortex to dark green-strongly differentiated cortex. Adapted by permission from Macmillan Publishers Ltd: Kätzel and colleagues (2011).

cortex. They assessed intra- and interlaminar connectivity in striate cortex, primary somatosensory and primary motor cortex. As mentioned before, striate cortex is by far the most differentiated cortical region, even in the rodent brain (Herculano-Houzel et al., 2013), where it is less well differentiated than for example in the primate. Primary somatosensory cortex, although still clearly eulaminar, is already much less dense and comprises fewer distinguishable sublayers, while primary motor cortex is even less architectonically differentiated (Collins et al., 2010; Herculano-Houzel et al., 2013). Primary motor cortex thus ranges in the lower end of the differentiation spectrum with dysgranular cortical regions, although it is sometimes classified as agranular (lacking an inner granular layer, L4): see Shipp (2005) and García-Cabezas and Barbas (2014) for an extensive discussion of this issue. Other than probing connectivity in three cortical regions processing different modalities, this study can, therefore, be used to demonstrate potential differences regarding intrinsic circuitry in three areas occupying different positions in the differentiation spectrum. While Kätzel and colleagues (2011) report relatively uniform patterns of intralaminar inhibition across these three cortical regions, interlaminar inhibitory-to-excitatory connectivity differed substantially (Figure 1.2). In striate cortex, considerable interlaminar inhibition was observed between all layers (L2/3, L4, L5/6). In primary somatosensory cortex, a similar pattern of interlaminar inhibition was reported, but without inhibition between L2/3 and L5/6. In primary motor cortex, in contrast, no substantial inhibition between L2/3, L4, and L5/6 was evident. Thus, across the three sampled regions, interlaminar inhibitory-to-excitatory connectivity was progressively weaker in less architectonically differentiated areas. By interpreting the results this way, we

assume that they reflect genuine variation in the presence of interlaminar inhibition, and not the impact of other aspects of structural variation across the studied areas. For example, systematic differences in cellular morphology across the sampled areas could lead to skewed results from applying the same measurement approach to all areas. Nonetheless, these observations support the notion that intrinsic circuitry cannot be uniform in the face of considerable variation of the structural substrate, as is the case in regions of the cerebral cortex with profoundly differing architectonic differentiation.

This section has been published in Beul and Hilgetag (2015).

1.3 Extrinsic circuitry

Brain regions of differing local architecture and intrinsic connectivity are linked by extrinsic cortico-cortical connections and thus joined into the anatomical substrate for the elaborate information processing performed in the brain. Structural connections impose strong constraints on functional interactions among brain areas (Park and Friston, 2013), and it is thus essential to understand the principles that underlie the organisation of connections which give rise to the topological properties of the cortex. Cortico-cortical connections form networks that are neither regular nor random, but characteristically link specific brain regions.

Evidence accumulated from detailed quantitative studies of the connectome of cat, monkey and human cerebral cortex (Young, 1992; Scannell et al., 1995, 1999; Hilgetag et al., 2000a; Kaiser and Hilgetag, 2006; Zamora-López et al., 2010; Bassett et al., 2010; Modha and Singh, 2010; Harriger et al., 2012; Goulas et al., 2014a) has revealed a common large-scale topology that has been related to both behavioral measures and disease conditions in humans (Li et al., 2009; Fang et al., 2012) and been the subject of further wide-ranging investigations (Modha and Singh, 2010; Xu et al., 2010; Zamora-López et al., 2010, 2011; Power et al., 2013; Towlson et al., 2013; Ball et al., 2014; Collin et al., 2014; Crossley et al., 2014; Senden et al., 2014; Tomasi et al., 2014; Wang et al., 2014; van den Heuvel et al., 2016; Rubinov, 2016).

This topology, observed across several species, is characterised by dense connectivity among neighbouring areas of the same major processing modules (visual, auditory, somato-motor, fronto-limbic), with relatively few direct long-range connections between them (Kaiser and Hilgetag, 2006). Inter-modal integration is largely served

by a collection of spatially distributed hub-module areas, which possess widespread connections and are strongly interconnected among themselves, and hence have been designated a 'rich-club' (Colizza et al., 2006; Zamora-López et al., 2011; Bullmore and Sporns, 2012; Harriger et al., 2012). While the 'rich-club' is a costly feature in several aspects of cortical organisation (Collin et al., 2014), including the disproportionate occupancy of white matter volume and associated high energy expenditure, this organisation can also be considered functionally efficient for providing locally specialised (intra-modal) as well as longer-range (cross-modal) integration, and has been likened to the complex global infrastructure underlying human social and transport networks (Bassett and Bullmore, 2006).

While these topological properties concern the existence, that is, the absence or presence of a connection, another feature of cortico-cortical connections that needs to be explained is the laminar pattern of their origin and termination, which exhibits striking regularities (Rockland and Pandya, 1979; Pandya and Yeterian, 1985; Felleman and Van Essen, 1991; Hilgetag et al., 1996).

1.3.1 Laminar projection patterns regulate information processing

The specific laminar composition of connections is crucial to their function, given that neurons in the different layers, differing in morphology, are endowed with distinct processing capabilities. In fact, lamination itself may only be relevant to the extent that it reflects the arrangement of particular types of brain cells (Larkum et al., 2018). It has been shown that oscillations of particular frequencies dominate in different cortical layers (Buffalo et al., 2011; Xing et al., 2012; Roberts et al., 2013; Bastos et al., 2015). Since these oscillations are associated with communication in specific directions ('feedforward' /'feedback') (van Kerkoerle et al., 2014; Bastos et al., 2015; Mejias et al., 2016; Michalareas et al., 2016), they are likely related to the laminar patterns of cortico-cortical connections (Bastos et al., 2015). Moreover, oscillations across different frequency bands are a crucial feature in theories of brain function such as predictive coding (Bastos et al., 2012), they underlie executive processes such as working memory regulation (reviewed in Miller et al., 2018) and they have been identified to be causal for self-reflective awareness in humans (Voss et al., 2014). The laminar specifics of cortico-cortical connections therefore have implications for a wide spectrum of functions, as certain types of connections are crucial for processes up to cognition and conscious perception in humans (reviewed in Larkum, 2013).

Hence, integrating the characteristics of cortico-cortical connectivity with intrinsic

circuitry in source and target areas is important for understanding experimental results. This integration is, however, also profoundly useful in deriving powerful models of cortical function. For example, validated regularities can be harnessed to infer missing data points in empirical data sets and build better performing models than possible with the incomplete data alone. This approach has, for example, been gainfully employed in the construction of computational models of cortical network function (Schmidt et al., 2018a,b).

The presence of nonrandom features in brain networks points to the existence of organising factors, but the principles that govern the characteristic organisation of cortico-cortical connectivity remain elusive. We hypothesise that inherent structural properties of the cortex account for prominent characteristics of the cortical connectome, as captured by the architectonic type principle (Barbas, 1986).

Parts of this section have been published in Beul et al. (2015), Beul et al. (2017) and Beul et al. (2018) and submitted for peer-review in Beul and Hilgetag (2019b).

1.4 Possible measures to explain the organisation of cortical connectivity

1.4.1 Architectonic differentiation

One comprehensive framework that captures many aspects of the organisation of structural connectivity in the mammalian brain is the architectonic type principle (Barbas, 1986; Barbas and Rempel-Clower, 1997) (reviewed in Barbas, 2015; García-Cabezas et al., 2019; Hilgetag et al., 2019). It represents connections in terms of the relative architectonic differentiation between brain areas and has been shown to account well for multiple features of cortico-cortical projections across the entire cortex of different mammalian species. To quantify architectonic differentiation, the property that the architectonic type principle is based on, comprehensive measures of area composition, such as architectonic type and overall neuron density, have been employed.

Originally developed qualitatively in the classic studies of Pandya and Sanides (1973), Barbas and coworkers systematically extended the architectonic type principle in quantitative studies across a variety of cortical systems and connection targets in

several mammalian species, including prefrontal, parietal, temporal and occipital projection systems, and contralateral as well as subcortical projections (e.g. Barbas, 1986; Barbas and Rempel-Clover, 1997; Rempel-Clover and Barbas, 2000; Dombrowski et al., 2001; Barbas et al., 2005; Medalla and Barbas, 2006; Ghashghaei et al., 2007; Medalla et al., 2007; Hilgetag and Grant, 2010; Goulas et al., 2014c; Hilgetag et al., 2016; Goulas et al., 2017).

The most intricate property of structural connections that is well captured by the architectonic type principle are the distributions of projection neurons' somata and synaptic connections across cortical layers. These laminar projection patterns have been shown to vary gradually as the difference in architectonic differentiation between the two connected areas changes (Barbas, 1986, 2015; García-Cabezas et al., 2019; Hilgetag et al., 2019), such that graded differences in cortical architecture can account for the graded patterns observed in the distribution of projection origins and targets across cortical layers (Barbas, 1986; Barbas and Rempel-Clover, 1997; Barbas et al., 2005; Medalla and Barbas, 2006; Hilgetag and Grant, 2010; Hilgetag et al., 2016). Specifically, a positive correlation has been observed, such that the contribution to a projection from the supragranular layers becomes stronger, the more differentiated the source area is than the target area. This means that projections from areas of weaker differentiation are formed increasingly from infragranular layers as they target areas of increasingly stronger differentiation, while projections from areas of stronger differentiation are formed increasingly from the supragranular layers as they target areas of weaker differentiation. These stereotypic laminar patterns found in non-human primate cortex are illustrated in Figure 1.1B, showing distinctly infra- and supragranular origins and terminations for projections between areas of weak differentiation and areas of strong differentiation, while these patterns change gradually towards multilaminar origin and termination profiles as the difference in differentiation between the connected areas becomes less pronounced.

In addition to the laminar patterns of projections, other features of cortico-cortical connectivity have been found to relate to relative architectonic differentiation. For example, greater similarity in architectonic differentiation of cortical areas has been found to be associated with higher connection frequency between them, above and beyond the explanatory power of spatial proximity (Goulas et al., 2017) (for reviews see Barbas, 2015; Pandya et al., 2015).

The architectonic type principle was originally described for ipsilateral connections of the macaque prefrontal cortex (Barbas, 1986), but it has since been confirmed for a considerable number of brain systems and species, as well as contralateral connections, suggesting a mammalian-general organisational principle. The general applicability of this principle was further supported in a recent study which performed

prediction analyses that transferred information across mammalian species (Goulas and Hilgetag, 2016). Specifically, by training a classifier on the relationship between cortical structure and connections in a first species, area-to-area connectivity in a second species could be reliably predicted from structural variations of cortical areas in the second species without making changes to the classifier.

While architectonic differentiation varies to a certain extent in any mammalian species, there are notable differences across species both in the highest level of differentiation that occurs in the cortex (in some species, only low levels of differentiation are present), as well as in the range of variation in differentiation (in some species, most areas are of similar differentiation, while in others very different levels of differentiation are present across the cortex). This leads to predictions about the extent to which the architectonic type principle is apparent in different species, since shallow gradients in architectonic differentiation appear to go hand in hand with smaller differences in laminar projection patterns (Goulas et al., 2019b).

1.4.2 Cellular morphological measures

By now it is evident that cortical architecture is intricate and varies considerably throughout the cortex. The measures of overall area composition used to capture architectonic differentiation collapse the complex cortical structure into a single parameter, but of course, diverse aspects of cortical architecture have been measured at different spatial scales. Such measures comprise macroscopic features, such as the laminar appearance of cortical areas, including the thickness of cortical layers and the density and distribution of different types of neurons or glia across layers (Dombrowski et al., 2001; Barbas, 2015). Further macroscopic features are the density of receptors of different neurotransmitter systems (Zilles and Amunts, 2009; Palomero-Gallagher and Zilles, 2017; Zilles and Palomero-Gallagher, 2017) and myeloarchitecture (Nieuwenhuys et al., 2015; Nieuwenhuys and Broere, 2017). In addition, cells within cortical areas have been characterised by a large number of microscopic morphological and physiological measures, such as the density of synaptic spines (Elston et al., 2005; Ballesteros-Yáñez et al., 2006) or firing patterns (Cauli et al., 1997; Dégenétais et al., 2002; Otsuka and Kawaguchi, 2008; Oswald et al., 2013).

Given the abundance of possible features, it remains unclear whether there are aspects of cortical architecture that carry more weight in determining cortico-cortical connectivity than others, particularly than overall architectonic differentiation. Especially

well documented are cellular morphological measures obtained for pyramidal cells in cortical layer 3 (L3), based on extensive immunohistochemical analyses (e.g. Elston and Rosa, 1997). These measures comprise the cross section of the soma, the total spine count of an average pyramidal neuron, the peak dendritic spine density, and the size of the dendritic tree. These measures have been used to quantify ‘pyramidal complexity’ in a previous report that found a relation to topological measures of the macaque connectome (Scholtens et al., 2014). Microscopic, cellular morphological measures appear to be closely correlated with each other, as we also describe below (Section 3.4.1). In primates, neurons show a tendency to become larger, have more complex dendritic arbors and be more spiny towards the frontal cortex (reviewed in Charvet and Finlay, 2014). Characteristics of cellular morphology are crucial for how an area can process incoming information. Spine morphology and the spatial arrangement of dendrites directly affect the electrical and biochemical properties of synapses on pyramidal neurons (reviewed in Spruston, 2008; Yuste, 2010), and spine number and density affect the opportunity for neuronal interactions (reviewed in DeFelipe, 2011). These cellular properties, therefore, directly relate to information processing capabilities of cortical populations, especially with regard to the integration of information from numerous sources (Charvet and Finlay, 2014). In line with the areas’ position in the inter-areal circuitry, morphology in prefrontal association areas allows for a broader integration of inputs (Bianchi et al., 2013; Buckner and Krienen, 2013). Moreover, variation in cellular morphological characteristics across species presumably also reflects differences in the complexity of cortical circuits and specifics of information processing, which plausibly have wide-ranging implications for cognition, memory and learning (DeFelipe, 2011).

1.4.3 Cortical thickness

One other factor that has received much attention in the study of possible relations between brain morphology and connectivity is cortical thickness, an attractive possibility, because thickness can be assessed non-invasively by magnetic resonance imaging (MRI). Cortical thickness has been related to neuron density (Cullen et al., 2006; la Fougère et al., 2011) and suggested as an indicator of overall cortical composition (Narr et al., 2005; Lerch et al., 2006; He et al., 2007). Cortical thickness covariations have been treated as a surrogate of anatomical connectivity (but see Gong et al., 2012). The structural networks inferred from cortical thickness have been explored with respect to their topological properties, association with functional connectivity, and relationship to behavioral traits (e.g. Chen et al., 2008, 2011;

Bernhardt et al., 2014; Tewarie et al., 2014b) (for a review see Evans, 2013). Given this strong interest in the possible significance of cortical thickness, we assessed this parameter as an anatomical covariate of structural connectivity, phrasing it as the ‘thickness model’.

1.4.4 Spatial proximity

Since brains are physical objects that exist in space, an inevitable property of the cortex is spatial proximity between areas. The ‘distance model’ proposes that the relative spatial position of areas across the cortex systematically influences the existence (Young, 1992; Klyachko and Stevens, 2003) and strength (Douglas and Martin, 2007b) of connections between them. Specifically, the model assumes that connections are more frequent, and more dense, among neighbouring regions and sparser or absent between remote regions, an arrangement consistent with minimisation of axonal wiring costs (Young, 1992; Ercsey-Ravasz et al., 2013). Salin and Bullier (1995) further proposed that the laminar locations of projection origins and terminations also change gradually according to the physical distance between connected cortical regions.

1.4.5 Cortical hierarchy

The ‘hierarchical model’ assigns relevance to rankings of cortical areas which have been constructed from the laminar origin and termination patterns of cortico-cortical projections (Felleman and Van Essen, 1991; Scannell et al., 1995). These patterns were interpreted as directional information on projections, for example, ‘forward’, ‘backward’ and ‘lateral’ (Rockland and Pandya, 1979; Felleman and Van Essen, 1991), and hierarchical rankings were constructed so as to fit projection directions with a minimal number of constraint violations (Hilgetag et al., 1996, 2000b; Reid et al., 2009). The level differences separating source and target areas in such hierarchies were then related to the areas’ connectivity, in particular quantitative measures of the relative distribution of projection origins in the upper and deep cortical layers (Barone et al., 2000; Vezoli et al., 2004).

Parts of this section have been published in Beul and Hilgetag (2015), Beul et al. (2015), Beul et al. (2017), Beul et al. (2018) and Beul and Hilgetag (2019a) and

submitted for peer-review in Beul and Hilgetag (2019b).

1.5 Connectivity data

As outlined above, the intricate organisation of cortico-cortical connectivity still poses many questions, both with respect to the fully developed adult state as well as the developmental processes shaping it. To probe the explanatory power of the different presented measures regarding this organisation, we employed tract-tracing data detailing axonal connections in two mammalian species, cat and macaque monkey. For the cat, connection existence data was available for the adult state (Scannell et al., 1995), including a categorisation of laminar projection patterns. For the macaque monkey, we were able to make use of a wealth of data describing the existence of connections in the adult state (Markov et al., 2014a), as well as the laminar patterns of projection origins in both the adult (Markov et al., 2014b; Chaudhuri et al., 2015) and the immature state (Kennedy et al., 1989; Batardière et al., 2002; Magrou et al., 2018). Moreover, derived from these data, measures of topology were available for both species. These included the number of maintained connections, also termed area degree, as well as a division of the network of cortical areas into core and peripheral areas (Zamora-López et al., 2010; Ercsey-Ravasz et al., 2013) and a clustering of cortical areas into functional modules (Zamora-López et al., 2010; Goulas et al., 2014b).

1.6 Possible developmental mechanism underlying the organisation of cortical connectivity

It has been extensively demonstrated empirically that the architectonic type principle captures much of the regularity in cortico-cortical connectivity by capitalising on regularities in cortical architecture. Further substantiation of the architectonic type principle calls for a mechanistic explanation of how the described relationships between architecture and connectivity may emerge. From early on, the origin of this relationship has been hypothesised to be linked to developmental events (Barbas, 1986). Specifically, the observed close relationship between variations in cortical

1.6. Possible developmental mechanism underlying the organisation of cortical connectivity

structure and axonal connections may arise from an interplay between the ontogenetic time course of neurogenesis and concurrent connection formation (Barbas, 2015; Hilgetag et al., 2016; Barbas and García-Cabezas, 2016). Areas which develop during different time windows were suggested to be afforded distinct opportunities to connect, with self-organisation rather than precisely targeted connection formation leading to the strikingly regular final connectivity patterns (cf. Kaiser, 2017). Put differently, it has been hypothesised that spatio-temporal interactions in the forming tissue, and specifically the relative timing of neurogenesis across the cortex, determine the connectivity patterns between cortical areas. Empirically, such a relationship has, for example, been observed in the olfactory system of the rat (Bayer and Altman, 1987).

We explored whether this suggested mechanism may be capable of generating cortico-cortical connectivity consistent with empirical observations and the architectonic type principle using systematic computational simulation experiments (Figure 1.3). To this end, we implemented an *in silico* model of the growing two-dimensional cortical sheet of a single cerebral hemisphere that was progressively populated by neurons and divided into cortical areas. Model neurons randomly grew their axons across the cortical sheet and stochastically formed connections with potential postsynaptic targets (similar, for example, to simulation experiments in Kaiser and Hilgetag (2004) and Kaiser et al. (2009)). We assessed the resulting network of simulated structural connections between cortical areas in the same way as in experimental studies (e.g. Section 3.2 and Section 3.3) and compared the results to the empirical observations. Since we constrained the model to a single hemisphere, the simulated connections represent ipsilateral connectivity. Following this general approach, we characterised a number of variants of the *in silico* model of the growing cortical sheet, which differed in their adherence to empirical observations about developmental processes, specifically the spatio-temporal sequence of neurogenesis across the cortex. By comparing the networks generated from these variants, we could infer which aspects of the proposed mechanistic underpinnings of the architectonic type principle, particularly, which neurodevelopmental assumptions, were necessary to approximate empirical ipsilateral cortical connectivity.

We conducted two sets of simulation experiments. In the first set, we probed which assumptions allowed us to generate networks that were consistent with the architectonic type principle with respect to the existence of connections. After establishing those, we expanded our *in silico* model to explore how laminar patterns of projections origins could emerge that conformed to expectations which were based on the architectonic type principle.

1.6. Possible developmental mechanism underlying the organisation of cortical connectivity

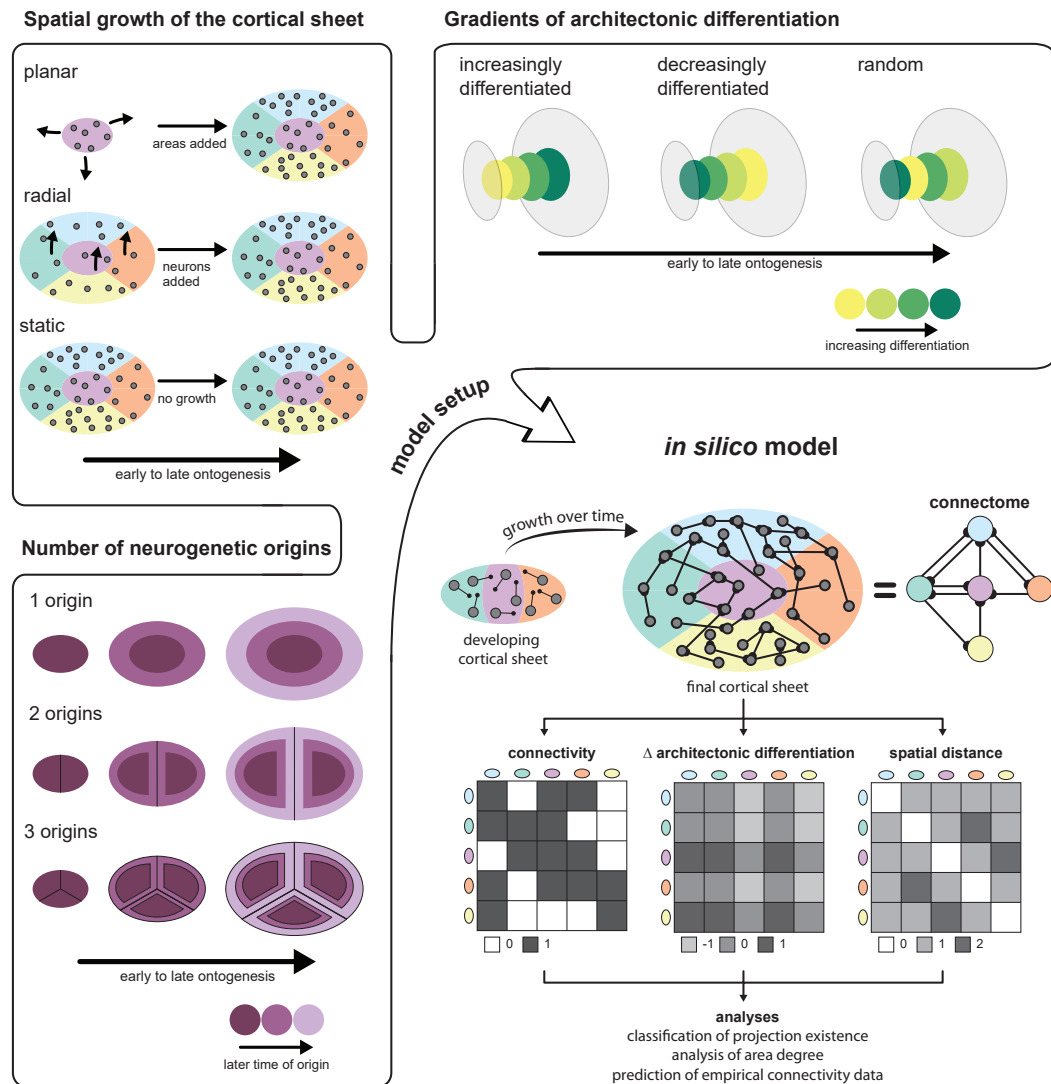


Figure 1.3: Neurodevelopmental assumptions and overview of the *in silico* model. The figure illustrates the assumptions regarding neurogenesis that were varied in the *in silico* model. The spatial growth of the cortical sheet of a single hemisphere was modelled in three possible ways: First, planar growth, in which the neurons comprising a cortical area develop at the same time and the cortical sheet expands as more areas materialise. Second, radial growth, in which neurons across the entire extent of the final cortical sheet develop at the same time, and the final complement of neurons is reached by gradual growth of neurons at a constant rate. Third, no growth, that is, a static cortical sheet on which the final complement of neurons is already present from the onset. Regarding the gradients of architectonic differentiation, we considered three possible relationships between the time at which an area was formed (time of neurogenesis) and its architectonic differentiation, approximated by neuron density. First, areas could be more differentiated the later in ontogenesis they were formed (increasingly differentiated). This scenario corresponds to the realistically oriented density gradient we incorporated in the *in silico* model. Second, areas could be less differentiated the later their time of origin was (decreasingly differentiated). This scenario corresponds to the inversely oriented density gradient in the *in silico* model. Third, there could be no gradient of differentiation aligned with

Figure 1.3: (cont.) neurogenetic timing, that is, the neuron density of newly formed areas varied randomly throughout ontogenesis. As a third factor that determined the spatio-temporal growth trajectory of the cortical sheet, we considered the number of neurogenetic origins. There could either be a single origin, such that more recently formed areas occupied the fringes of the cortical sheet, or there could be two or three origins. In this case, recently formed areas would be interleaved with areas that were formed earlier, as the neurogenetic origins were moved apart by addition of areas around them. From these assumptions on neurogenetic processes shaping the cortical sheet, we set up different variants of an *in silico* model in which axons grew randomly across the developing cortical sheet and stochastically formed connections. We translated the resulting neuron-level connectivity to area-level connectivity and extracted structural measurements from the simulated cortical sheet. As in previous studies of mammalian connectomes, we considered the difference in architectonic differentiation between areas and their spatial distance. Thus, we simulated sets of measures which we could then analyse in the same way as the empirical data, and compared the results to empirical findings. Specifically, we used simulated architectonic differentiation and spatial distance to classify whether a connection existed in the final simulated network; we probed whether there was an association between simulated architectonic differentiation and the number of connections maintained by an area; and we used a classifier trained on the simulated data to predict connection existence in two sets of empirical connectivity data, from the cat and the macaque cortex.

1.6.1 Aspects of neural development that prescribe spatio-temporal trajectories of cortical growth

We explicitly incorporated three aspects of corticogenesis in our simulations, which are briefly described here.

Neurogenetic origins

First, the cortical sheet is established through neurogenesis spreading out from spatial origins, or primordial points (where the earliest neuronal populations are observed on the developing cortex), so that the surface of the cortex expands over time. This expansion is accompanied by a gradient in the time of onset of neurogenesis across the cortical sheet, which we refer to as the planar gradient of time of neurogenesis (Sidman et al., 1959; Angevine and Sidman, 1961; Hicks and D'Amato, 1968; Caviness, 1982; Smart and Smart, 1982; McSherry, 1984; McSherry and Smart, 1986; Bayer and Altman, 1991; Takahashi et al., 1995; Miyama et al., 1997; Shaw et al., 2008). Developmental studies indicate that neurogenesis proceeds from at least two points of origin (Bayer and Altman, 1991; Shaw et al., 2008; Gogtay et al., 2006), with new neurons successively increasing the extent of cortical tissue between these

neurogenetic origins. This progression entails that areas formed earlier become further separated on the cortical sheet as new areas are generated. Moreover, there is a superimposed radial gradient in the progression of neurogenesis (Sidman et al., 1959; Angevine and Sidman, 1961; Caviness, 1982; Kölliker, 1896; Rakic, 1974) (which was not included in this first set of simulation experiments), resulting in the characteristic inside-out generation sequence of neurons across layers (meaning that, with the exception of neurons in layer 1, neurons in lower cortical layers are generated before neurons in upper cortical layers). In contradistinction to the findings outlining a planar gradient in the onset of neurogenesis, as described above, it has also been suggested that the onset of neurogenesis is simultaneous across the cortex (Rakic et al., 1986; Rakic, 2002). To contrast these two interpretations, we included both alternatives in our simulation experiments, as described in more detail below.

Temporal gradient in architectonic differentiation

Second, cortical areas that are generated later are generally more architectonically differentiated (Barbas and García-Cabezas, 2016; Shaw et al., 2008; Charvet and Finlay, 2014; Charvet et al., 2015) (also briefly reviewed in Hilgetag et al. (2016)). Gradual changes in cortical architecture along two trends were described already several decades ago (Dart, 1934; Abbie, 1940, 1942; Sanides, 1962, 1972) (reviewed in Barbas, 2015; Pandya et al., 2015). In brief, the two foci of least differentiated cortex are the allocortical three-layered archicortex (hippocampus) and paleocortex (olfactory cortex). These cortices are surrounded by periallocortex, where additional layers can be discerned, but without the clear laminar organisation found in the isocortex. Proisocortex, the next stage of differentiation, has a definite laminar organisation, but is missing a well-developed layer 4. Finally, there are different levels of isocortex with increasing demarcation of laminar boundaries and prominence of layer 4. More recently, changes in cell cycle kinetics across the forming cortical sheet and genetic correlates of the neurogenetic gradients have been described (Takahashi et al., 1995; Miyama et al., 1997; Suter et al., 2007; Caviness et al., 2008, 2009), which elucidate how gradual changes in cortical architecture are effected and provide an association between time of origin and architectonic differentiation. Particularly, a lengthening in the cell cycle along the planar neurogenetic gradient is accompanied by a successive increase in the proportion of progenitor cells differentiating into neurons with each cell cycle. In combination with the mentioned relation between time of origin and final laminar position of neurons, this mechanism results in a relatively increased number of supragranular layer neurons in later generated sections

of the cortical sheet. Thus, a positive correlation can be observed between time of origin and neuron density across the cortex (Charvet et al., 2015). This link has been corroborated by findings in the human cortex, which directly traced systematic architectonic variation of the cortex to the timing of development (Barbas and García-Cabezas, 2016). A lengthening of the overall developmental time period, and with it the neurogenetic interval, appears to be responsible for increased neuron numbers both within the cortex of a given species, as well as across species which differ in their overall level of architectonic differentiation (Charvet and Finlay, 2014; Charvet et al., 2015; Finlay and Darlington, 1995). In fact, it has been suggested that cortical architecture correlates not only with neurogenetic time windows during ontogenesis, but also with the succession of architectural differentiation observed during brain evolution (Sanides, 1962; Shaw et al., 2008). This finding suggests that phylogenetic age has a bearing on architectural gradients. It has repeatedly been reported that areas at similar points in the architectonic differentiation spectrum, as well as within the two described trends of architectonic progression, are preferentially linked, even if they are dispersed throughout the brain (reviewed in Pandya et al., 2015). The link to phylogeny, added to this correlation between architectonic progression and associated connectivity, thus, further points towards a developmental origin of the interrelations captured by the architectonic type principle.

Immediate, unspecific, stochastic formation of connections

The third aspect of neurogenesis which we incorporated into our simulations is that axon outgrowth starts concurrently with, or immediately after, neuronal migration (Caviness et al., 2008; Schwartz et al., 1991; Easter et al., 1993; Barnes and Polleux, 2009; Donahoo and Richards, 2009), and appears to be largely unspecific spatially (Cahalane et al., 2011). We, therefore, assumed that connection formation starts as soon as neurons were placed in the cortical sheet. Further assumptions derived from these observations were that axons grow randomly across the cortical sheet (i.e., with no particular spatial orientation) and that they indiscriminately form connections once they are close enough to a potential target neuron, a mechanism that has been named Peters's Rule (Braitenberg and Schüz, 1998; Binzegger et al., 2004). Thus, the process of connection formation can be described as stochastic, and has been simulated in this way in previous computational models of connection development, for example by Kaiser and colleagues (2009). This mechanism entails that the probability of a neuron forming a connection is only dependent on the probability of its axon finding a target neuron. Since neurons that are far apart are separated

by a larger number of neurons that could accommodate the axon, the probability of connecting to a specific target neuron is lower, the larger the distance between two particular neurons is. In effect, there is a positive correlation between the spatial proximity and connection probability of different neurons.

1.6.2 An *in silico* model for assessing spatio-temporal growth trajectories

The spatio-temporal dynamics of corticogenesis that emerge from the combination of these empirically grounded assumptions were hypothesised to result in the establishment of realistic cortico-cortical connectivity. In particular, we expected interactions between the spatial and temporal aspects of neurogenesis to lead to the formation of connections which are consistent with the predictions of the architectonic type principle concerning the relationship between areas' relative architectonic differentiation and the existence of connections (connection frequencies). Our simulation experiments, thus, contribute the first systematic exploration of the neurodevelopmental mechanisms that have been hypothesised to underlie the architectonic type principle (Barbas, 1986, 2015; Hilgetag et al., 2016; Dombrowski et al., 2001).

In summary, we implemented several aspects of neurogenesis in an *in silico* model of the growing mammalian cerebral cortex. These aspects were then modified in some variants of the model, so that they either corresponded to, or violated, empirically observed phenomena. This strategy allowed us to compare the cortico-cortical connectivity resulting from hypothetical variants that differed in their assumptions, where some of these assumptions were empirically grounded and others were not. The approach enabled us to assess the merits of mechanisms which have been proposed to link cortical structure and connectivity through the architectonic type principle.

1.6.3 Expansion of the *in silico* model to probe the emergence of laminar patterns of projection origins

Observing the developmental events that shape cortico-cortical connectivity during the course of ontogenesis in sufficient detail to answer the question of how laminar projection patterns emerge remains challenging at best. Therefore, we extended our *in silico* model of cortical development to explore some features that could possibly be relevant for the formation of laminar projection patterns.

In the second set of simulation experiments, we tested the effect of adding four features to the *in silico* model: a delay in the growth of the infragranular compartment relative to layer 1, a delay in the growth of the supragranular compartment relative to the infragranular compartment, a scaling of the neuron density in the supragranular compartment, and a scaling in the elongation of neurons' axons. The first three of these modified spatio-temporal patterns of neurogenesis, while the fourth feature affected properties of individual neurons.

The two delays in the growth of the laminar compartment straightforwardly mirror the radial gradient in neurogenesis that can be observed for cortical neurons (Sidman et al., 1959; Angevine and Sidman, 1961; Rakic, 1974; Caviness, 1982) by assigning neurons to birth cohorts according to laminar compartments. With the exception of layer 1 neurons (which are formed first), neurons that are born later come to populate successively more superficial positions in the cortical sheet. Thus, the cortical sheet forms in an inside-out manner with infragranular layer neurons at a particular position of the cortical sheet born before neurons in the supragranular layers.

As architectonic differentiation becomes stronger and neuron density becomes higher, density increases especially in the supragranular layers of the mammalian cortex (Charvet et al., 2015; Finlay and Uchiyama, 2015; Pandya et al., 2015). The cell cycle kinetics underlying the transition from progenitor cells to differentiated neurons have been described in detail (Takahashi et al., 1995; Miyama et al., 1997; Suter et al., 2007; Caviness et al., 2008, 2009; Dehay et al., 2015) and explain this selective increase. As neurogenesis progresses across the cortical sheet, cell cycles lengthen and the proportion of progenitor cells that differentiate into neurons successively increases with each cell cycle. On the level of cortical areas, this results in a positive correlation between time of origin and neuron density (Cahalane et al., 2014; Charvet et al., 2015). In addition, since later cycles lengthen the most and yield neurons destined for the upper layers, as cycles become longer and overall neuron density increases, the effect is particularly pronounced in the supragranular layers (Finlay and Darlington, 1995; Charvet and Finlay, 2014). We implemented this notable increase in relative supragranular neuron density by scaling the neuron density of the supragranular compartment to be relatively higher than infragranular compartment neuron density, and this difference to be larger the more differentiated an area was.

As architectonic differentiation becomes stronger, there are many changes beyond an increase in neuron density. For example, myelination, cellular markers of synaptic stability and plasticity, as well as neurotransmitter receptor complement change across the spectrum of architectonic differentiation (Dombrowski et al., 2001; Nieuwenhuys et al., 2015; García-Cabezas et al., 2017; Zilles and Palomero-Gallagher, 2017;

Burt et al., 2018; Holley et al., 2018), and properties of cell morphology such as soma cross section, dendritic tree size and dendritic spine density are correlated with neuron density (cf. Section 3.4). As a final modification, we therefore probed which effects on laminar projection patterns could arise from changes to cell-intrinsic properties across the differentiation spectrum. We chose to manipulate axon elongation, because two observations, detailed below, create a tentative link between gradual changes in architectonic differentiation and the laminar position of cells best equipped for maintaining longer projections. First, there is a striking shift in the laminar distribution of larger neurons across the cortex, which has been termed externopyramidization (Sanides, 1962, 1970). Depending on whether larger neurons are predominantly found in the infragranular or in the supragranular layers, areas can be classified as internopyramidal or externopyramidal, respectively. Thus, in internopyramidal areas the ratio of supragranular neuron size to infragranular neuron size is smaller than it is in externopyramidal areas. This ratio of neuron sizes changes gradually across the cortex and coincides with the degree of architectonic differentiation, such that supragranular neuron size tends to be relatively larger compared to infragranular neuron size in more differentiated areas (reviewed in Goulas et al., 2018). Second, multiple lines of evidence suggest that neuron size is related to axon length (reviewed in Goulas et al., 2018) (although this does not speak to the direction of the causality, that is, whether larger neurons maintain longer connections or whether the formation of longer connections induces neuron somata to become larger). For example, considerations of metabolic cost (Laughlin et al., 1998; Laughlin and Sejnowski, 2003), attainable conduction velocities (Lawson and Waddell, 1991; Tomasi et al., 2012) and synaptic efficacy (Germuska et al., 2006; Medalla and Barbas, 2010; Innocenti et al., 2014; Innocenti and Caminiti, 2017) suggest that larger neurons are particularly capable of maintaining projections across larger distances. Taken together, these observations suggest that in areas of different architectonic differentiation the neurons that are best suited for forming longer projections are situated in different layers, and thus, as hypothesised before (Goulas and Hilgetag, 2016; Goulas et al., 2018), that externopyramidization might be associated with shifts in laminar patterns of projection origins. We therefore constructed our *in silico* manipulation of axon elongation to mirror the changes in relative neuron size observed across the spectrum of architectonic differentiation.

In summary, we expanded our *in silico* model of cortical sheet development by implementing four features that reflect further neurodevelopmental processes. Through a series of systematic simulation experiments we then probed which features affected the simulated laminar patterns of projection origins, drawing inferences about the likely mechanism underlying the emergence of the architectonic type principle in the

mammalian cortex.

Parts of this section have been published in Beul et al. (2018) and submitted for peer-review in Beul and Hilgetag (2019b).

1.7 Overview of performed studies

In the remaining chapters, I will describe in detail the studies we performed to contribute to the formulation of fundamental organisational principles of the mammalian cortex, working towards taming the complexity of cortical organisation. We related essential features of cortico-cortical connectivity, such as connection existence, laminar patterns of projection origins, and topological properties, to characteristics of cortical areas, such as the similarity in architectonic differentiation and spatial proximity of area pairs, in both adult and immature states. Our analyses further corroborated the presence of the architectonic type principle and advanced to probing its mechanistic underpinnings.

1.7.1 Tentative intrinsic circuitry in agranular cortex

Since the variation of architectonic differentiation is an aspect of cortical organisation that is often insufficiently considered in discussions of intrinsic circuitry, we wanted to raise awareness of the importance of architectonic differences, by providing a first approximation of general features of intrinsic circuitry in agranular regions of the cerebral cortex. We did this by assimilating information from the available literature on inter- and intralaminar connectivity in the agranular frontal cortex of the rodent brain, in order to present a tentative model of intrinsic circuitry in cortical regions on the opposite end of the differentiation spectrum than has previously been predominantly considered for such models. This variation is crucial for applying insights gained from such model circuits in a realistic way, for example in the biological grounding of *in silico* experiments (e.g. Merolla et al., 2014).

To compile the tentative circuitry, we made use of data that can shed light on the intrinsic microcircuitry in agranular cortex. We chose to concentrate on the rodent brain, capitalising on the relative abundance of experimental data available for this popular animal model. In comparison, fewer studies report on intrinsic circuitry in

non-human primates, and only a small proportion of those considered agranular cortical regions, which are relatively infrequent in the primate brain. By focusing on the rodent brain, we can therefore provide a more detailed sketch of the intrinsic circuitry in agranular cortex without having to incorporate data across a wide range of species, which would have been a more uncertain approach.

1.7.2 Testing the architectonic type principle and other frameworks in cat and macaque

To assess the extent to which the mentioned explanatory frameworks could account for features of structural cortico-cortical connectivity, we compared how measures of overall architectonic differentiation and spatial proximity related to the existence, strength, and laminar patterns of projections as well as to topological properties in the adult cat and macaque cortex. In the cat cortex, we could additionally probe the association with cortical hierarchy, while in the macaque cortex, we could additionally consider cortical thickness.

Importantly, the conceptual frameworks which we examine here have been developed and tested extensively for connections of the visual (Young, 1992; Barone et al., 2000; Vezoli et al., 2004; Douglas and Martin, 2007b) and prefrontal cortex of the macaque monkey (Barbas, 1986; Barbas and Pandya, 1989; Barbas and Rempel-Clower, 1997; Klyachko and Stevens, 2003; Barbas et al., 2005; Medalla and Barbas, 2006). Thus, their application to connections spanning the whole cortex in the macaque as well as one further species, the cat, provides an excellent test of the frameworks' generality.

1.7.3 Testing the relative merit of multiple measures of cortical structure

The results we report in the cat and macaque cortex corroborate the usefulness of the architectonic type principle in making sense of cortico-cortical connectivity. However, as detailed above, cortical architecture is associated with a plethora of features, which can be condensed to measures of overall architectonic differentiation. Since it is not inherently obvious whether any of the features are especially relevant to the organisation of cortico-cortical connectivity, we analysed the relation of multiple architectonic features to cortical connectivity in the adult macaque cortex, to assess the features' inter-dependence and to identify which of them were most frequently and strongly related to structural cortical connectivity. To be able to evaluate the

relative merit of the architectonic features, we devised our analyses such that all features were included conjointly and interrelations between them were taken into consideration, instead of analysing each measure separately and applying a false discovery rate correction to the significance threshold.

We considered four essential aspects of connectivity, namely the existence and strength of projections, the laminar patterns of projection origins, and the number of connections maintained by an area, the so-called area degree. We probed two groups of measures of architectonic features for their relation to these aspects of structural connectivity. The first group comprised the two macroscopic (area-based) structural features of neuron density and spatial proximity. The second group included the four microscopic (cellular) morphological measures of soma cross section, dendritic spine count, dendritic peak spine density and dendritic tree size. Both groups of measures have been individually linked to some features of the macaque connectome in previous reports (e.g. Scholtens et al., 2014; Hilgetag et al., 2016; Section 3.3), but have not yet been combined in a comprehensive analysis that can disclose their comparative relevance.

We considered neuron density because it has been shown to consistently relate to essential aspects of cortico-cortical connectivity, such as the distribution of projection origins and terminations across cortical layers (i.e., laminar projection patterns), the existence of projections, or topological properties of cortical connectivity (Barbas, 1986; Barbas and Rempel-Clower, 1997; Barbas et al., 2005; Barbas, 2015; Hilgetag et al., 2016). Neuron density is an objective, quantifiable measure of overall architectonic differentiation that is characteristic of different cortices (e.g. Dombrowski et al., 2001).

We also included spatial proximity, not as a measure of cortical architecture, but as an additional macroscopic feature of physically embedded cortical areas that has been shown to be related to connection existence (Young, 1992; Markov et al., 2013a) and strength (Douglas and Martin, 2007b; Ercsey-Ravasz et al., 2013), but not laminar projection patterns (e.g. Barbas et al., 2005; Hilgetag et al., 2016).

Cortical thickness is appealing as a further macroscopic measure because it is relatively easy to measure, also non-invasively. Its relevance to connectivity in healthy and diseased brains has been explored widely (e.g. Lerch et al., 2006; He et al., 2007; Chen et al., 2008, 2011; Tewarie et al., 2014b) (reviewed in Evans, 2013), and it is known to be inversely related to neuron density in the primate brain (von Economo, 1927). However, notwithstanding its appeal as a convenient measure, the usefulness of cortical thickness measures on their own remains open to discussion (Gong et al., 2012) and, rather than considering them individually, thickness

measures have recently been used as just one of many measures obtained through MRI to characterise cortical structure (Seidlitz et al., 2018). Moreover, in a direct multivariate comparison with neuron density performed as part of the analyses in adult macaque cortex (Section 3.3), we already found cortical thickness to be less informative regarding structural connectivity. Therefore, we did not include cortical thickness in these comparative analyses.

In summary, we contrast the relative contribution of each of six measures (neuron density, spatial proximity, L3 pyramidal cell soma cross section, dendritic spine count, dendritic peak spine density and dendritic tree size) for characterising inter-areal connections in the macaque cerebral cortex. Specifically, we considered four essential features of connectivity: projection existence, projection strength, laminar patterns of projection origins, and the number of connections maintained by an area. By employing analyses designed to account for interrelations between the structural measures, we show that not all measures were equally relevant in predicting connectivity, and that neuron density in particular emerged as the most essential and informative feature for explaining multiple properties of structural cortico-cortical connections. These findings suggest that neuron density constitutes a fundamental architectonic marker of cortical areas that is closely related to diverse macroscopic and microscopic structural cortical features, with implications for cortical function and development.

1.7.4 Testing the applicability of the architectonic type principle to the developing cortex

As described in the preceding, it has been suggested that a principle as widely applicable as the architectonic type principle should emerge from spatio-temporal interactions during ontogeny, without the need for sensory input or other major external influences (Barbas, 1986, 2015; Barbas and García-Cabezas, 2016; Hilgetag et al., 2016). However, observing the formation of structural connections, which happens concurrently with the formation of the brain itself, is an onerous endeavour and only little experimental data is available.

One essential feature of these connections are their laminar patterns of projection origins, which, as mentioned before, are strikingly regular and well-captured by the architectonic type principle (Rockland and Pandya, 1979; Barbas, 1986; Barbas and Rempel-Clower, 1997; Rempel-Clower and Barbas, 2000). They represent a connectional feature that is important for structure-function brain theories (Friston,

2010; Feldman Barrett and Simmons, 2015), but how these laminar patterns are shaped during ontogeny is not entirely clear. Since the architectonic type principle is the most central predictor of laminar projection patterns in multiple species as documented so far (cf. Barbas, 2015; Hilgetag et al., 2019), there are two prominent questions about the origin of this relationship between architectonic differentiation and laminar patterns. First, it is not clear if the relation of architectonic differentiation and laminar origin of connections pertains only to the adult state of the cerebral cortex. It has been shown that the laminar origin of connections is not uniform, but already biased, across areas early in development (Barone et al., 1995). Hence, does the architectonic type principle reflect graded differences in the laminar origin of connections already in prenatal and neonatal states of the connectivity or do the laminar origin patterns of areas undergo drastic reconfigurations which alter the initial bias and thereby eventually give rise to the architectonic type principle in the adult animal? In addition to the extent to which a biased distribution of laminar origins constitutes a preconfiguration of the adult state, a second question concerns the mechanisms that effect the refinement of laminar projection patterns. These could be intrinsic factors, such as apoptosis or plasticity mechanisms, or extrinsic factors, such as synaptic activity resulting from sensory input. Enucleation experiments allow inferring the influence of the visual input on the formation of cortical areas and connections (e.g. Karlen and Krubitzer, 2009), and are thus helpful in deciphering the influence of external stimuli on the formation of connectional features.

Making use of tract-tracing data detailing laminar patterns of projection origins obtained in the immature macaque cortex (Kennedy et al., 1989; Batardière et al., 2002; Magrou et al., 2018), we demonstrate the extent to which the architectonic type principle applies to connectional data from early development and enucleated animals, presenting data which indicate that processes very early during ontogenesis are sufficient to establish laminar projection patterns which are consistent with the architectonic type principle.

1.7.5 Testing the hypothesised mechanistic underpinnings of the architectonic type principle

These results, demonstrating the applicability of the architectonic type principle already in the immature mammalian cortex, encouraged us to search for the mechanisms leading to the emergence of the architectonic type principle in early ontogenesis. Given the dearth of pertinent empirical data, we chose to perform simulation experiments, using an *in silico* model of the developing cortical sheet to probe the

hypothesised mechanistic underpinnings of the architectonic type principle. To reiterate, it has been suggested that the architectonic type principle could emerge from spatio-temporal interactions in the developing brain (Barbas, 1986; Dombrowski et al., 2001; Barbas, 2015; Hilgetag et al., 2016), where correlations of time of origin with both distance between cortical areas (and thus their probability to connect to each other) and with the architectonic differentiation of cortical areas (where areas that are formed later are of stronger differentiation) would interact to result in the empirically observed correlations of connectivity with architectonic differentiation.

In a first set of simulation experiments, we explored the effects of different spatio-temporal patterns of neurogenesis on the resulting connectivity, with a focus on the existence of connections. By varying the spatio-temporal trajectory of the simulated neurogenesis while keeping the rules governing axon outgrowth and connection formation constant, we were able to create variants of the *in silico* model which differed exclusively by the specifics of when and where neurons were generated. Thus, all differences in the resulting connectivity were due to the variations in spatio-temporal growth trajectories. Our results demonstrate that a prescribed targeting of inter-areal connection sites was not necessary for obtaining a realistic replication of the experimentally observed relation between connection patterns and architectonic differentiation. Instead, we found that spatio-temporal interactions within the forming cortical sheet were sufficient if a small number of empirically well-grounded assumptions were met, namely (i) planar, expansive growth of the cortical sheet around two points of origin as neurogenesis progressed, (ii) stronger architectonic differentiation of cortical areas for later neurogenetic time windows, and (iii) stochastic connection formation. Thus, our results highlight a potential mechanism of how relative architectonic differentiation and cortical connectivity become linked during development. Moreover, we successfully predicted connectivity in two species, cat and macaque, from simulated cortico-cortical connection networks, which further underscored the general applicability of mechanisms through which the architectonic type principle can explain cortical connectivity in terms of the relative architectonic differentiation of cortical regions.

Hence, these simulation experiments provide the first support of the suggested mechanistic explanation for the emergence of the architectonic type principle by showing that simple interactions between the time and place of neurogenesis can result in structural networks that capture many of the relationships concerning connection existence observed in empirical mammalian cortico-cortical connections. Obviously, more features of connectivity, beyond their existence, are of interest, and this first set of simulation experiments did not address how the characteristic laminar patterns of projection origins arise that originally prompted the formulation of the

architectonic type principle (Barbas, 1986). Therefore, in a second set of simulation experiments, we modified the *in silico* model of the developing cortical sheet, probing how the distribution of projection origins across laminar compartments was affected either by changes in the spatio-temporal patterns of neurogenesis or by gradual changes in cell-intrinsic properties. Our simulation experiments only replicated the changes in laminar origin patterns, which are observed empirically across the spectrum of architectonic differentiation, when we introduced cellular heterogeneity, modifying a cell-intrinsic property. These results suggest that factors beyond spatio-temporal interactions in the forming cortical sheet mediate the specification of laminar projection patterns.

Parts of this section have been published in Beul and Hilgetag (2015), Beul et al. (2015), Beul et al. (2018) and Beul and Hilgetag (2019a) and submitted for peer-review in Beul and Hilgetag (2019b).

Methods

2.1 Connectivity data sets

2.1.1 Cat cortex

For the cat cerebral cortex, qualitative measures of cortico-cortical connections were extracted from an extensive collation of published reports of anatomical tract-tracing experiments, the traditional standard for measuring cortical connectivity, compiled by Scannell and colleagues (1995). The data set that was provided for download in conjunction with the article includes 1,400 projections, which are mapped onto a parcellation consisting of 65 brain regions. The data set comprises the most complete summary of cortico-cortical connections in the cat to date. Even close to 25 years after its publication, this collation from 96 articles still represents the majority of anatomical tracing data available for this species, since few new tract-tracing results on the cat cortex have been published in the meantime. The data set has been widely interrogated (and cited more than 350 times as of September 2019, according to Web of Science, <http://apps.webofknowledge.com>), for example to investigate structural and dynamic properties of the cat cortical connectome (Müller-Linow et al., 2008; Zamora-López et al., 2009, 2010; Gómez-Gardeñes et al., 2010; Zamora-López et al., 2011; Tang et al., 2012; Bailey et al., 2013; de Reus and van den Heuvel, 2013). One reason for this popularity is that the data set collates data from direct anatomical methods for tracing cortical connections in both anterograde and

retrograde directions. The spatial resolution (which is at the level of individual cells and synapses) and reliability of this approach exceed that of indirect diffusion-based tractography methods (Alger, 2012; Griffa et al., 2013).

Existence of projections

Existence of projections was given qualitatively as either absent ('0') or present, where the presence was described by ordinal weights as sparse ('1'), intermediate ('2'), or dense ('3'). Importantly, projections weighted as '0' were explicitly reported to be absent in the original literature, whereas no assumption was made about unknown projections (67% of all potential projections among the areas). This distinction between absent and unknown projections was made in the companion data set provided for download by Scannell and colleagues (1995), but not in the results published in the article itself. We conducted the majority of analyses on a version of the data set converted to binary projection status, which rated projections as either absent or present and discarded information on projection density. This binarisation enabled us to normalise projection frequencies across the tested variables, for example controlling for the fact that the data set contained information about a larger number of connections across shorter distances. An alternative approach for treating connection weights would have been to normalise projection frequencies separately for each ordinal density category. This approach would have yielded separate results for each density class, but not provided a comprehensive picture of the impact of the structural variables on connectivity overall.

For 954 of the 1,400 projections in the database (218 absent, 736 present) we were able to assess both spatial proximity and relative architectonic differentiation, expressed as border distance, Δ_{dist} , and architectonic type difference, Δ_{type} . For a subset of 308 projections (93 absent, 215 present), we could include additional information for hierarchical level difference, Δ_{level} , in the analyses (see Section 2.2 for details). An overview of all available cat cortex projection data together with the associated structural measures is given in Supplementary Table D.2.

Qualitative information on the presence or absence of connections is an undirected measure, as is the distance between two cortical areas, Δ_{dist} . To meaningfully correlate these undirected variables with the directed variables Δ_{type} and Δ_{level} , we reduced the latter two variables to their magnitude, that is, their absolute values, $|\Delta_{\text{type}}|$ and $|\Delta_{\text{level}}|$.

We characterised the spatial range of the projections of cortical areas by assessing

the distances of all afferent and efferent connections to and from each area, by computing the proportions of its projections formed by short (distance 1 and 2) as well as long (distance 4 and 5) connections, respectively. These proportions provided a simplified and robust measure of the projection distance profile of individual areas, from which we computed aggregate measures of connection ranges for groups of areas.

Laminar patterns of projections

Laminar projection patterns were available for a subset of 133 projections linking 22 cortical areas of the cat visual system. Scannell and colleagues (1995) classified the direction of projections as ‘ascending’, ‘lateral’, or ‘descending’ according to criteria laid out by Felleman and Van Essen (1991). Specifically, projections were classified as ‘ascending’, if they originated from the supragranular layers or in a bilaminar pattern from supra- and infragranular layers, and terminated predominantly in layer 4. ‘Lateral’ projections originated from both supra- and infragranular layers, and terminated in a columnar pattern throughout all cortical layers. ‘Descending’ projections originated either from infragranular layers or from both supra- and infragranular layers, and terminated in supra- and/or infragranular layers, avoiding layer 4 in their terminations (Felleman and Van Essen, 1991, their Figure 3).

Based on this classification of projection directions, Scannell and colleagues derived an anatomical hierarchy of the cat visual system by arranging cortical areas such that a maximum number of ‘ascending’ projections pointed to higher levels and a maximum of ‘descending’ projections pointed to lower levels of the hierarchy.

The projection directions (Scannell et al., 1995; Hilgetag et al., 2000b, their Figure 4) contain information on laminar projection origins and terminations in a pre-interpreted form. To assess the relationship between laminar projection patterns and structural factors, we used this set of 133 classified projections to calculate rank correlations of projection direction with Δ_{type} as well as Δ_{level} . For these calculations, projection direction was consolidated in three categories: ‘ascending’, ‘lateral’, and ‘descending’. We included all projections whose direction classification had been marked as unreliable, due to insufficient or contradictory data (Hilgetag et al., 2000b, their Figure 4), into the laminar categories that were indicated for them.

To relate the projection directions to other measures, we considered them as ordinal values, by arranging them in the order of (‘ascending’, ‘lateral’, ‘descending’). For one projection analysed by Scannell and colleagues (1995) and Hilgetag and colleagues

(2000b), no Δ_{type} was available, because it targeted a region which had not been assigned an architectonic type. The present analyses were thus conducted on 132 projections.

The relation of projection direction to spatial proximity between cortical areas could not be evaluated using this data set, because spatial proximity is an undirected measure. Projection direction classified into three categories as used here, however, has no magnitude which could be evaluated independent of its direction, so that no meaningful combination of spatial proximity with an undirected adaptation of laminar projection patterns could be obtained.

Topological measures

Hubs and modules Zamora-López and colleagues (2010) used the data set provided by Scannell and colleagues (1995) to analyse the connectivity of the entire cerebral cortex in the cat from a network-theoretical perspective and identified a ‘rich-club’ module of 11 hub areas, based on the internal density of links between high-degree nodes. The cortical areas constituting this hub meta-module were part of four other anatomical modules (visual, auditory, somatosensory-motor, and fronto-limbic) previously identified by different network-theoretical approaches (Scannell and Young, 1993; Young, 1993; Young et al., 1994; Hilgetag et al., 2000a; Sporns et al., 2004). These module classifications provide an opportunity to study the association between structural measures and connection features at a larger-scale level of cortical organisation. As Zamora-López and colleagues included only 53 of the 65 cortical areas of the original data set in their analyses, we restricted our analyses of the module features to the 48 areas which were both included in their analyses and possessed an architectonic type rating.

Area degree and weighted area degree The degree of a cortical area is the number of projections it takes part in, conceptualising individual areas as nodes in the graph-theoretical sense. Here we added the number of afferent projections (in-degree) to the number of efferent projections (out-degree) for each area to obtain its overall degree. Projections commonly comprise a strongly varying number of neurons, with projection strengths ranging over several orders of magnitude from only a few neurons to several thousand neurons (Scannell et al., 2000; Hilgetag and Grant, 2000; Markov et al., 2011, 2014a). Therefore, we also computed node strength (the weighted area degree) by weighting each projection with its strength prior to summing up the present projections. As projection strength was rated ordinally in

the data set provided by Scannell and colleagues (1995), we approximated the actual metric projection strength to vary over three orders of magnitude across sparse, intermediate and dense projections. We assigned weights of 10^0 , 10^1 , and 10^2 to these respective descriptive categories to take into account the typical exponential distribution of projection densities (Hilgetag and Grant, 2000; Markov et al., 2014a). Moreover, we separately rank-correlated the number of projections with architectonic type for the projections of each ordinal strength.

Note that area degree is a connectivity measure that is a property of cortical areas, rather than of cortico-cortical projections. Therefore, a smaller number of data points were available than in other analyses, which assessed properties of projections.

2.1.2 Macaque cortex

Existence of projections

We analysed an extensive, up-to-date set of anatomical tract-tracing data in the adult macaque cortex (*Macaca fascicularis* and *Macaca mulatta*) (Markov et al., 2014a). Based on injections of retrograde tracer in 29 cortical areas (represented in the accompanying parcellation, the M132 atlas (Markov et al., 2014a)), Markov and colleagues quantified labelled neurons found in all 91 areas of the M132 atlas that project to these injected sites. Within each area, labelled neurons ranged from a minimum of 1 neuron to a maximum of 262,279 neurons. The resulting data set provided information on 2610 cortico-cortical connections between 91 areas, within a 91×29 subgraph of the complete (91×91) connectivity matrix of the M132 atlas. That is, projections targeting about a third of the cortex are included in this data set. For projections found to be present, projection strength was given as the fraction of labelled neurons outside of the injected region (FLNe), thus normalising the number of projection neurons between two areas to the total number of labelled neurons for the respective injection, as done previously (e.g. Barbas and Rempel-Clower, 1997; Medalla and Barbas, 2006). In the data set, projections were included as present without a threshold on projection strength, that is, even a single labelled axon was considered to constitute a present projection. Most cortical areas were injected only once, but controls for consistency between repeated injections were performed in a few areas.

To assess the relation of the structural measures with projection existence, we transformed projection strength to a binary measure (absent vs. present). To assess

the relation of the structural measures with projection strength, we considered the natural logarithm, $\ln(\text{FLNe})$. The use of a logarithmic scale was indicated, since the most extreme FLNe value was more than three standard deviations above the mean FLNe value (Buzsáki and Mizuseki, 2014). Moreover, while conjointly assessing the relative predictive power of microscopic and macroscopic structural measures (Section 3.4), we also considered ranked projection strength, to account for the fact that areas that receive many afferent projections might have smaller FLNe values per projection than areas that receive only few afferents. To circumvent this potential bias whereby projections from areas with many afferents could artifactually be considered too weak through the normalisation by the number of neurons labelled per injection, we ranked afferent projections per target area. Specifically, the strongest projection that targeted each of the injected areas (since retrograde tracers were used, only injected areas receive projections in the used data set) was ranked highest (as rank 1), and successively weaker projections were ranked accordingly (by increasing rank number), up to the number of afferents, which differed between areas. This ranking made projection strength dependent only on the relative strength of a given projection to projections from the same injection. Thus, ranking projections by strength allowed us to assess how projection strength was related to the structural measures independent of the precise strength of a projection in terms of the number of neurons and the number of afferents an injected area received, alleviating any distortions that may be caused by these factors.

Laminar patterns of projections

Adult cortex In addition, we analysed the laminar patterns of projection origins for this data set (Markov et al., 2014b; Chaudhuri et al., 2015), which were published separately from the main part of the data set (Markov et al., 2014a). The distribution of projection origins across cortical layers was expressed as the supragranular contribution to a projection, specifically the fraction of labelled neurons originating in supragranular layers, $N_{\text{SG}}\%$. For each projection, $N_{\text{SG}}\%$ was computed as the number of neurons labelled in supragranular layers divided by the sum of neurons labelled in supragranular and infragranular layers. To relate $N_{\text{SG}}\%$ to the undirected measure of spatial proximity, we also transformed it to an undirected measure of inequality in laminar patterns, $|N_{\text{SG}}\%|$, where $|N_{\text{SG}}\%| = |N_{\text{SG}}\% - 50| * 2$ (cf. Hilgetag and Grant, 2010). Values of $N_{\text{SG}}\%$ around 0 and 1 (i.e., 0% and 100% supragranular contribution), thus, translated to larger values of $|N_{\text{SG}}\%|$, indicating a more pronounced inequality in the distribution of origins of projection neurons between infra-

and supragranular layers and hence deviation from a columnar (bilaminar) pattern of projection origins.

We based our analyses regarding $N_{SG}\%$ on the subset of projections comprising more than 20 neurons (neuron numbers for each projection are provided in Markov and colleagues (2014a)). Thus, we excluded very sparse projections for which assessment of the distribution of projection neurons in cortical layers was not considered reliable, as was done previously (cf. Barbas et al., 2005). Note that sparse projections were only excluded from analyses involving $N_{SG}\%$, but not from analyses considering binary projection existence.

A first subset of laminar projection data was published in Markov and colleagues (2014b), detailing 625 projections originating in 11 of the 29 injected areas and targeting all 91 areas. After thresholding, 429 projections with reliable information on laminar patterns remained. We used this data in our analyses of the relative merit of different explanatory frameworks in the macaque cortex (Section 3.3). Information on projection origins for all 29 injected areas was published in Chaudhuri and colleagues (2015), providing information on all 1602 present projections. After thresholding, 1132 projections remained. We used this data set in our assessment of the relative predictive power of microscopic and macroscopic structural measures (Section 3.4).

Immature cortex Measures of laminar projection patterns in the developing macaque cortex were taken from three published reports (Kennedy et al., 1989; Batardière et al., 2002; Magrou et al., 2018). Kennedy and colleagues (1989) injected retrograde tracers in the neonate and adult striate cortex (area V1) of cynomolgus monkeys (*Macaca irus*). They evaluated labelled projection neurons in the posterior bank of the lunate sulcus (area V2), on the prelunate gyrus (area V4), and in the posterior bank and fundus of the superior temporal sulcus (STS, which we interpreted to correspond to areas FST, PGa and STPi in the M132 parcellation (Markov et al., 2014a)). For each observed projection, they determined the fraction of labelled neurons that originated in supragranular layers ($N_{SG}\%$). Batardière and colleagues (2002) followed a similar approach, injecting retrograde tracer in area V4 of macaque monkeys (*Macaca fascicularis*) at different fetal stages (embryonic day 112 to embryonic day 140) and in adult monkeys. They evaluated labelled projections neurons across 10 brain areas and also determined the contribution from supragranular neurons ($N_{SG}\%$) for each projection (Batardière et al., 2002, their Figure 7A).

Magrou and colleagues (2018) performed bilateral enucleation (removal of the eyes) in macaque monkey (*Macaca fascicularis*) fetuses between embryonic days 58 and 73. Retrograde tracers were injected into areas V2 and V4 postnatally, at postnatal

day 16 and postnatal month 10, respectively. Labelled projection neurons were evaluated across 18 and 16 brain areas, respectively, and the fraction of labelled neurons originating in supragranular layers ($N_{SG}\%$) was determined. We compared the contribution from supragranular neurons in enucleated monkeys to $N_{SG}\%$ -values from intact adult macaque monkeys reported by Chaudhuri and colleagues (2015). All $N_{SG}\%$ -values that we considered in our analyses of the immature state are summarised in Supplementary Table D.9.

Topological measures

Network core The data set describing cortico-cortical connectivity in the adult macaque cortex (Markov et al., 2014a) contains a 29×29 subgraph of injected areas, which provides information about all possible connections among the injected areas. This edge-complete subgraph makes it possible to perform analyses without uncertainty related to possible connections that were not sampled. Due to the wide distribution of the injected areas across the cortex, the 29×29 subgraph is expected to have similar properties as the complete network which incorporates all 91 areas (Ercsey-Ravasz et al., 2013). Ercsey-Ravasz and colleagues (2013) used the edge-complete subgraph to identify areas belonging to a ‘network core’ with a high density of connections among areas. This network core is similar to the concept of a rich-club, as discussed in recent studies (van den Heuvel et al., 2012; Crossley et al., 2013; Tomasi et al., 2014; Towlson et al., 2013; van den Heuvel and Sporns, 2013b,a; Ball et al., 2014; Collin et al., 2014; Crossley et al., 2014). Ercsey-Ravasz and colleagues (2013) identified 17 core areas in the 29×29 subgraph, assigning the remaining 12 areas to the network periphery.

Area degree As mentioned above, the data set (Markov et al., 2014a) contained the 29×29 subgraph of injected areas for which all possible connections have been examined. To assess overall area degree, we considered only areas within this edge-complete subgraph, computing the overall degree of each area as the sum of the number of its efferent and afferent projections. While conjointly assessing the relative predictive power of microscopic and macroscopic structural measures (Section 3.4), we also separately considered the number of efferent projections, out-degree, and the number of afferent projections, in-degree. In-degree was computed both within the 29×29 edge-complete subgraph, and cortex-wide, using all reported projections between the 91 cortical areas (i.e., it was also computed on the 91×29 graph). Please note that since degree is an area-based measure of connectivity, fewer data points

were available for area degree than for the projection-based connectivity measures.

Parts of this section have been published in Beul et al. (2015), Beul et al. (2017) and Beul and Hilgetag (2019a).

2.2 Potential explanatory measures

Multiple frameworks have been investigated as candidates for making sense of the remarkable complexity that characterises the organisation of cortico-cortical connections in the mammalian cortex. Each of these frameworks is associated with one or more empirical measures, which are detailed below. Collectively, I will refer to these measures as structural measures, because they concern the cortex and not the connections linking areas, thus referring to the structural substrate of connectivity.

2.2.1 Cortical architecture

Architectonic differentiation

In the mammalian cortex, the spectrum of architectonic differentiation ranges from areas of low overall neuron density, with few layers and lacking an inner granular layer (agranular areas), to dense areas with six distinct layers (eulaminar areas). The striate cortex, for example, has a much higher overall neuron density not only within the cortical visual system, but also among all other parts of the cerebral cortex (Pandya et al., 1988; Hilgetag et al., 2016; Zilles, 2006; O’Kusky and Colonnier, 1982; Schüz and Palm, 1989; Collins et al., 2010; Cahalane et al., 2012; Herculano-Houzel et al., 2013). Intermediate to these two extremes are areas of lower neuron densities with a sparse inner granular layer (dysgranular areas), and areas with six layers but without the exceptional clarity of layers and sublayers or remarkable neuron density of striate cortex. The architectonic type principle is based on this comprehensive assessment of cortical architecture. To quantify overall architectonic differentiation, two measures have been used: architectonic type and neuron density.

Architectonic type Architectonic differentiation can be operationalised qualitatively by ranking cortical areas into architectonic types, an ordinal measure which projects

see Hilgetag and Grant (2010). Using these criteria, 49 areas across the whole cat cortex were ranked. Figure 2.1 depicts the assigned architectonic types in the cortical parcellation of Scannell and colleagues (1995). From this architectonic type ranking, we determined the difference between the architectonic types, Δ_{type} (cf. Barbas, 1986), of any two of the cortical areas with a defined architectonic type, where $\Delta_{\text{type}} = \text{type}_{\text{source area}} - \text{type}_{\text{target area}}$.

Neuron density A quantitative measure that reflects architectonic differentiation is overall neuron density (Dombrowski et al., 2001). We used an unbiased quantitative stereologic approach to estimate neuron density in the macaque cortex from coronal sections that were stained to mark neurons using either Nissl stain or immunohistochemical staining for neuronal nuclei-specific antibody (NeuN), which labels neurons but not glia, using a microscope-computer interface (StereoInvestigator, MicroBright-Field Inc., Williston, VT). We verified that there was a close correspondence between measures derived from both staining methods in a sample of areas for which both measures were available ($r = 0.99$, $p = 0.001$), and accordingly transformed density measures from different staining methods to a common reference frame. The neuron density measurements used here have partly been published previously (Dombrowski et al., 2001; Hilgetag et al., 2016). In total, neuron density measures were available for 48 of the 91 areas of the M132 parcellation (Figure 2.2). Within the 29×29 subgraph of areas injected with retrograde tracer, neuron densities were available for 14 of the 17 core areas and 10 of the 12 non-core areas.

We quantified how similar areas were in their neuron density by computing the log-ratio of neuron density values for each pair of areas (which is equivalent to the difference of the logarithms of the area densities). Specifically, $\log\text{-ratio}_{\text{density}} = \ln(\text{density}_{\text{source area}}/\text{density}_{\text{target area}})$. This procedure enabled us to directly relate each sampled projection to the density ratio of its source and target area. The use of a logarithmic scale was indicated, since the most extreme value of the neuron density measures was more than three standard deviations above the mean of the considered neuron densities (Buzsáki and Mizuseki, 2014). For analyses which required considering an undirected equivalent of the actual neuron density ratio, we used the absolute value of the log-ratio, $|\log\text{-ratio}_{\text{density}}|$. To relate the neuron density ratio to ranked projections strength, we also ranked the absolute value of the log-ratio of neuron density, $|\log\text{-ratio}_{\text{density}}|$, separately per target area. That is, the smallest absolute neuron density ratio was ranked highest (as rank 1) for each injected area, and successively larger absolute neuron density ratios were ranked accordingly (increasing rank number). Hence, areas of similar neuron density (small absolute ratio) were ranked higher than areas of strongly diverging neuron density

2.2. Potential explanatory measures

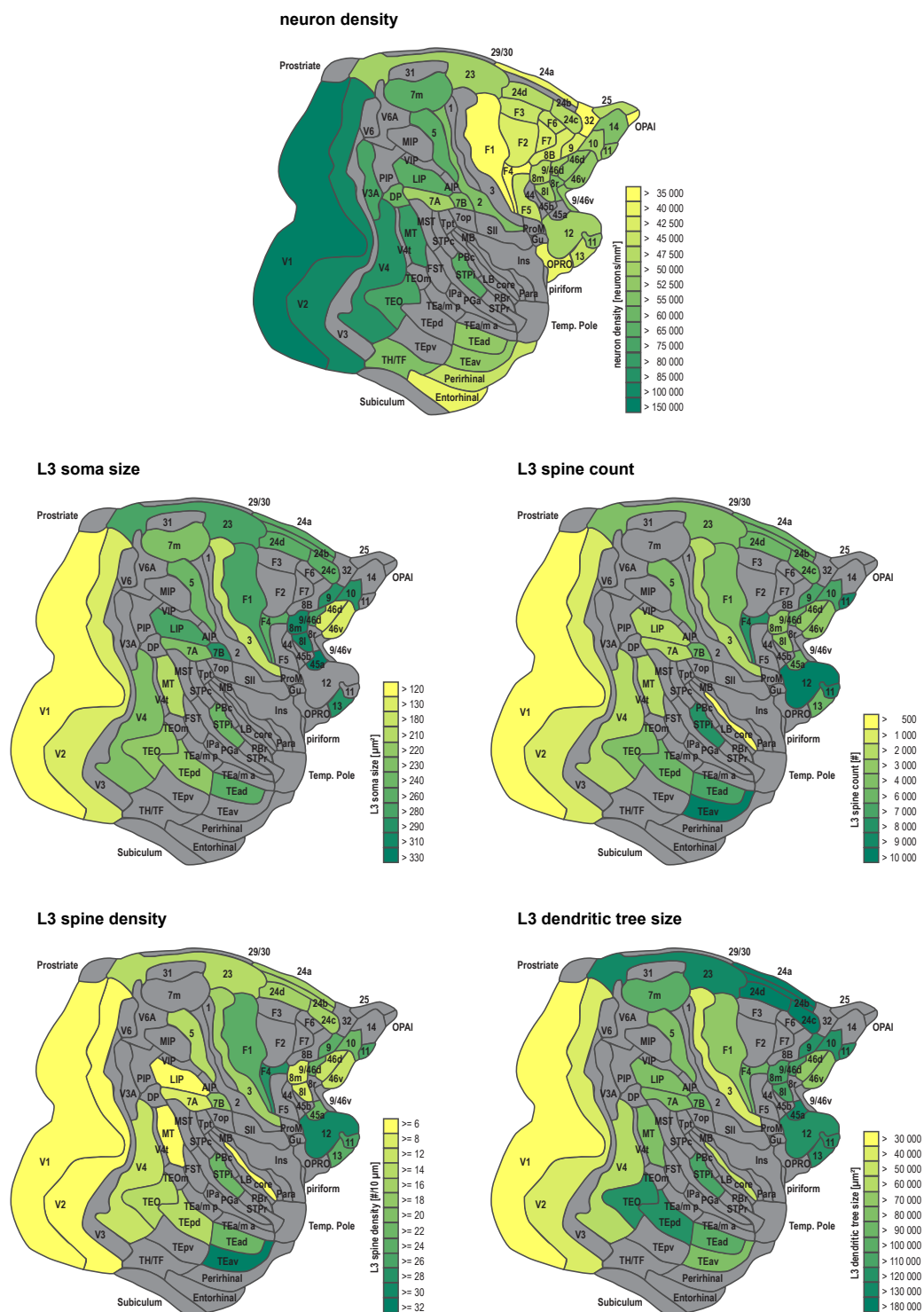


Figure 2.2: Variation of cytoarchitectonic features across the macaque cortex.

Figure 2.2: Variation of cytoarchitectonic features across the macaque cortex. Variation of neuron density, L3 neuron soma cross section, L3 dendritic spine count, L3 dendritic spine density and L3 dendritic tree size depicted on the M132 parcellation (Markov et al., 2014a). For grey areas, no values were available. See Supplementary Table D.4 for correspondences between areas in the M132 parcellation and alternative parcellations. Abbreviations as in Markov et al. (2014a).

(large absolute ratio) relative to each of the injected areas.

From the available neuron density measures we were able to determine the relative architectonic profile for 1128 of the sampled projections. After applying a threshold of constituent neurons to exclude potentially unreliable $N_{SG}\%$ values (discarding projections comprising less than 20 neurons), this included 172 projections with an associated $N_{SG}\%$ for the subset of projection published in Markov and colleagues (2014b) and 521 projections with an associated $N_{SG}\%$ for the complete set of injections published in Chaudhuri and colleagues (2015).

Cellular morphological measures

Measures of cellular morphology characterise individual cells, and thus provide an impression of an area's constituting elements, but not of its overall architectonic differentiation. The measures of cellular morphology we considered were mostly reported by Elston and colleagues (Elston and Rosa, 1997, 1998a,b; Elston et al., 1999a,b; Elston, 2000; Elston et al., 2001; Elston and Rockland, 2002; Elston et al., 2005, 2009, 2010a,b, 2011a,b; Coskren et al., 2015; Gilman et al., 2017). Specifically, four aspects of L3 pyramidal neuron morphology were measured across the macaque cortex: the cross section of the cell soma (soma cross section), the average total spine count on the basal dendritic tree (spine count), the peak density of dendritic spines (spine density), and the size of the basal dendritic tree (dendritic tree size). Spine density was measured as the number of spines per 10 μm dendrite segment, and peak spine density was then calculated as the average density along the five consecutive 10 μm segments that yielded the highest spine density (see e.g. Elston and Rosa, 1998b). Supplementary Table D.4 gives an overview of the correspondence between the parcellations used in the morphological data references and the M132 parcellation, as well as the relevant reports. Specifically, in the M132 parcellation, soma cross section was available for 30 areas, spine count and spine density for 33 areas, and dendritic tree size for 34 areas (Figure 2.2). The soma cross section may be related to the overall size of a neuron, which would be characterised by

further properties such as soma surface area and soma volume. However, given the varying shapes of somata, inferences from the cross-sectional area to overall soma size are not straightforward. Such inferences are further impaired by the difficulty of measuring the cross section at comparable locations across different neurons. For example, some measures of cross-sectional area that we included in our analyses were taken at the level of the basal dendritic tree (e.g. Elston et al., 2011b), while others were taken at the widest point of the cell body (e.g. Elston and Rosa, 1997; Gilman et al., 2017). To quantify how similar areas were in the four morphological measures across the cortex, we computed the difference of their values for each pair of areas, where $\Delta_{\text{morphological measure}} = \text{measure}_{\text{source area}} - \text{measure}_{\text{target area}}$. This resulted in $\Delta_{\text{soma cross section}}$, $\Delta_{\text{spine count}}$, $\Delta_{\text{spine density}}$, and $\Delta_{\text{tree size}}$. Each of these difference measures was converted to an undirected variable by computing its absolute value, $|\Delta_{\text{soma cross section}}|$, $|\Delta_{\text{spine count}}|$, $|\Delta_{\text{spine density}}|$, and $|\Delta_{\text{tree size}}|$, where appropriate. To relate the four morphological measures to ranked projections strength, we ranked their absolute difference measures separately per target area, analogous to the ranking described for the absolute neuron density ratio above. That is, smaller absolute difference measures were ranked highest (rank 1), and successively larger absolute difference measures were ranked accordingly (increasing rank number).

2.2.2 Cortical thickness

To evaluate the thickness model in the macaque cortex, we used cortical thickness data extracted from an anatomical T1-weighted magnetic resonance (MR) brain scan of one male adult macaque monkey (*Macaca mulatta*) supplied by Helen Barbas. Animals were obtained through the New England Primate Research Center (1 Pinehill Rd, Southborough, MA 01772, USA). Procedures were designed to minimise animal suffering and to reduce the number of animals used. Detailed protocols of the procedures were approved by the Institutional Animal Care and Use Committee at Harvard Medical School and Boston University School of Medicine in accordance with NIH guidelines (DHEW Publication no. [NIH] 80-22, revised 1996, Office of Science and Health Reports, DRR/NIH, Bethesda, MD, USA). During MR data acquisition, the animal was anaesthetised with propofol (loading dose, 2.5 - 5mg/kg, i.v.; continuous rate infusion, 0.25 - 0.4mg/(kg min)). MR data were acquired on a 3 Tesla Philips Achieva MRI scanner using a three-dimensional magnetisation prepared rapid acquisition gradient-echo (3DMPRAGE) sequence with 0.6mm isotropic voxels (130 slices, TR = 7.09ms, TE = 3.16ms, FOV = 155 × 155mm²). Cortical reconstruction and volumetric segmentation were performed using the Freesurfer image analysis

suite (<http://surfer.nmr.mgh.harvard.edu/>). The resulting surface reconstruction was registered to the M132 atlas (Markov et al., 2014a) using the Caret software (Van Essen et al., 2001) (<http://www.nitrc.org/projects/caret/>). Cortical thickness was then extracted for all 91 areas in both hemispheres using Freesurfer by Konrad Wagstyl. We report results for mean thickness values of the left and right hemisphere. Cortical thickness data (registered to a different atlas) extracted from these MR data have been used in a previous publication (Wagstyl et al., 2015).

The thickness measurements extracted from MR data were well correlated with microscopic measurements of histological sections (Dombrowski et al., 2001). Corresponding histological and MR measurements for 33 areas were available, resulting in $r = 0.62$, $p < 0.001$ for the left hemisphere, $r = 0.48$, $p < 0.01$ for the right hemisphere, and $r = 0.56$, $p < 0.001$ for mean thickness values of the left and right hemisphere.

To quantify relative thickness across the cortex in order to compare thickness in pairs of connected areas, we computed the log-ratio of thickness values for each pair of areas analogous to the log-ratio of neuron density, where $\log\text{-ratio}_{\text{thickness}} = \ln(\text{thickness}_{\text{source area}}/\text{thickness}_{\text{target area}})$. We transformed the log-ratio of cortical thickness to an undirected equivalent, $|\log\text{-ratio}_{\text{thickness}}|$, where appropriate. Relative thickness of areas was included for all 2610 projections sampled by Markov and colleagues (2014a), also encompassing all 429 projections analysed with respect to $N_{\text{SG}}\%$ after thresholding for a minimum of 20 constituent neurons (using the subset of data on laminar projection patterns published in Markov and colleagues (2014b)).

2.2.3 Spatial proximity

To evaluate the distance model, which is based on the spatial proximity of cortical areas, in the cat and macaque cortex, we relied on three different measures of the distance between areas.

Border distance

To characterise the spatial separation of areas across the cortical sheet in the cat cortex, we computed their border distance, which is a pragmatic and widely used measure (e.g. Young, 1992; Barbas et al., 2005) for estimating inter-areal distance in the absence of reliable three-dimensional area coordinates (also see Section

4.1.4.2). As part of their connectivity data collation, Scannell and colleagues (1995) published a spatial adjacency matrix for their parcellation that indicates common area borders (their Figure 6). In some cases, there was an apparent mismatch between the information in this adjacency matrix and the parcellation shown in the paper (Scannell et al., 1995, their Figure 1). In most of these cases, we gave priority to information from the matrix, except where the map was unambiguous. Specifically, the following changes were made to the spatial adjacency matrix: we removed adjacencies of area 17 with areas CGp and RS; and we added adjacencies of area 18 with areas 20a and 20b; of area CGa with areas 17, 4 and 6m; of area SVA with areas 18, 20b and RS; of area SIV with area Ig and of area 4g with area 6m (Supplementary Table D.1 provides a list of abbreviations used for area names, see Scannell and colleagues (1995) for further details). From the spatial adjacency relations, we calculated the shortest distances between all pairs of areas, Δ_{dist} ; that is, we determined the minimum number of borders separating any two areas within the cortical parcellation adopted by Scannell and colleagues.

Euclidean distance

In our analyses of the relative merit of different explanatory frameworks in the macaque cortex (Section 3.3), we operationalised the spatial proximity of all 91 cortical areas by the Euclidean distance between their mass centers, obtained from the Scalable Brain Atlas (<http://scalablebrainatlas.incf.org>). This widely used interval measure of projection length represents a pragmatic estimate of the spatial proximity of pre- and postsynaptic neurons located in different brain areas (e.g. Salvador et al., 2005; Achard et al., 2006; Bassett et al., 2008; Alexander-Bloch et al., 2013; Goñi et al., 2014; Vértes et al., 2012; Tewarie et al., 2014a).

Geodesic distance

In our assessment of the relative predictive power of microscopic and macroscopic structural measures (Section 3.4), we quantified the spatial proximity of cortical areas using the geodesic distance between the mass centers of all 91 areas, which are provided as supplementary material with the study of Markov and colleagues (2013a). To relate the spatial proximity to ranked projections strength, we ranked geodesic distance separately per target area, analogous to the ranking described

for the absolute neuron density ratio above. That is, the smallest distance was ranked highest (rank 1), and successively larger distances were ranked accordingly (increasing rank number).

2.2.4 Hierarchical level

To evaluate the hierarchical model in the cat cortex, we computed the hierarchical level difference between any two areas within the visual system. This analysis was confined to the visual module, because no equivalent hierarchical schemes exist for the other major modules of the cat cortical connectome. We used the hierarchy of the cat visual system as derived by Scannell and colleagues (1995, their Figure 2) to determine the difference in hierarchical level, Δ_{level} , where $\Delta_{\text{level}} = \text{level}_{\text{source area}} - \text{level}_{\text{target area}}$ (as in, e.g., Barone et al., 2000; Hilgetag and Grant, 2010). To exclude the possibility that our results hold only for this particular hierarchy, we alternatively computed Δ_{level} from the hierarchy of the cat visual system as proposed by Hilgetag and colleagues (2000b, their Figure 12). In the analyses, we rectified an oversight in this published hierarchy diagram by reducing the level of area 17 (area V1) to level 1, placing it on the same level as area 18 (area V2).

Parts of this section have been published in Beul et al. (2015), Beul et al. (2017) and Beul and Hilgetag (2019a).

2.3 Analysis procedures and statistical tests

If not indicated otherwise, all analyses were performed using Matlab (The MathWorks, Inc., Natick, MA, USA) and tests and correlations were pre-assigned a two-tailed significance level $\alpha = 0.05$.

2.3.1 Tests for group differences

To test two groups of ordinal measures for equality of their medians, for example the structural measures associated with two groups of projections, we computed

Wilcoxon rank sum test statistics (W).

To test two groups of interval measures for equality of their means, we computed two-tailed independent samples t-tests and reported the t-statistic t , degrees of freedom df and the associated measure of effect size r , where $r = (t^2 / (t^2 + df))^{1/2}$.

To test for equality of more than two groups of ordinal as well as interval measures, we computed Kruskal–Wallis test statistics (H). We calculated Jonckheere–Terpstra test statistics (JT) to assess trends across multiple groups of ordinal measures. JT was computed using IBM SPSS Statistics Version 19 (IBM Corporation, Armonk, NY, USA).

2.3.2 Correlations

To assess relations between interval variables, we computed Pearson’s correlation coefficient r and its associated p-value. For ordinal variables, we computed Spearman’s rank correlation coefficient ρ and its associated p-value.

2.3.3 Relative projection frequency

To characterise the distribution of present and absent projections across the range of each structural measure, while accounting for differences in sampling, we computed relative frequencies of projections that were present. Specifically, we partitioned each structural measure into bins and normalised the number of present projections in each bin by the total number of studied projections (i.e., absent and present projections that fell into the respective bin). This procedure allowed us to obtain a measure of the relative frequency of present projections which is robust against disparities in sampling across a structural measure’s range (e.g., when more projections were sampled across a short than a long spatial distance). We verified that results were robust against changes in bin size.

2.3.4 Classification of connection existence

To assess how well an explanatory framework accounted for patterns in the existence of cortico-cortical connections, we used a range of classification procedures. By

evaluating how well the structural measures enabled the classification of connection existence, individually or in conjunction, we were able to generate insights into the principles underlying the characteristics of connection existence.

Linear discriminant analysis

To assess the distribution of present and absent projections in the cat cortex across the variables $|\Delta_{\text{type}}|$ and Δ_{dist} more closely, we performed a linear discriminant analysis (Klecka, 1980; Burns and Burns, 2008). A linear discriminant analysis determines a linear combination of predictive variables that optimally separates distinct classes of a dependent variable. We used $|\Delta_{\text{type}}|$ and Δ_{dist} as predictive variables, and existence of projections as the dependent variable. Given the non-significant correlation of relative projection frequencies with $|\Delta_{\text{level}}|$ (see Section 3.2.1), we did not include $|\Delta_{\text{level}}|$ into the linear discriminant analysis. We assumed uniform prior probabilities for the two classes of the dependent variable ('absent' and 'present'). The linear discriminant analysis then provides a posterior probability for each combination of $|\Delta_{\text{type}}|$ and Δ_{dist} , which can be used to classify new data points (unknown connections) as either absent or present.

To account for the fact that not all combinations of the predictive variables can occur equally often (e.g., combinations of $|\Delta_{\text{type}}| = 1$ and $\Delta_{\text{dist}} = 1$ are frequent in this cortical parcellation, while combinations of $|\Delta_{\text{type}}| = 4$ and $\Delta_{\text{dist}} = 4$ are not), we normalised the numbers of absent and present projections of a specific combination of $|\Delta_{\text{type}}|$ and Δ_{dist} by the maximally possible number of co-occurrences of that combination. This resulted in proportions $\%_{\text{absent}}$ and $\%_{\text{present}}$ of projections at each point in the predictive variable space. Note that $\%_{\text{absent}} + \%_{\text{present}} \neq 100$, which reflects the fact that there is a remaining percentage of projections which have not been examined. To transform the resulting percentages into cases suitable as input for the linear discriminant analysis, we constructed, for each combination of $|\Delta_{\text{type}}|$ and Δ_{dist} , $N_{\text{a}} = \%_{\text{absent}}$ cases with the respective values of the predictive variables and a dependent variable rating of '0' (absent), and $N_{\text{p}} = \%_{\text{present}}$ cases with the same predictive variables but a dependent variable rating of '1' (present). Compared to using the raw data as input for the linear discriminant analysis, this procedure adjusts the relative importance of examined projections by taking into account how thoroughly the underlying predictive variable space was sampled.

Cross-validation was performed by randomly excluding 10% of the data from the training set and using this test set to validate the obtained model. We tested model

performance at seven different classification thresholds, starting at 0.60 and increasing in 0.05 increments to 0.90. Connections were assigned the status ‘present’, if the posterior probability for the presence of connections at their associated $|\Delta_{\text{type}}|$ and Δ_{dist} was equal to or larger than the classification threshold, and assigned the status ‘absent’, if their associated posterior probability was equal to or smaller than 1 minus the classification threshold (i.e., 0.40, decreasing in 0.05 increments to 0.10). We did not classify the status of connections with associated posterior probabilities that fell into the intermediate range. We computed prediction accuracy to assess classification performance, where accuracy equalled the number of correct predictions divided by the total number of predictions. We calculated this measure separately for predictions assigning either the status absent (correct absent), the status present (correct present) or all predictions (correct total). We performed 200 cross-validation cycles and report averaged results.

Support vector machine

In our analyses of the relative merit of different explanatory frameworks in the macaque cortex (Section 3.3), we combined the structural measures in a different probabilistic predictive model for classifying the existence of projections. We built this model using a binary support vector machine classifier (i.e., used for two-class learning), which received the structural measures associated with the projections as independent variables (features) and information about projection existence (i.e., projection status ‘absent’ or ‘present’) as the dependent variable (labels, comprising two classes). Euclidean distance, absolute log-ratio of neuron density and absolute log-ratio of cortical thickness were used as features in different combinations.

For training the support vector machine classifier, we used a linear kernel function and standardised the independent variables prior to classification. Moreover, we assumed uniform prior probabilities for the learned classes and assigned a symmetric cost function, that is, all types of errors were weighted equally. Classification scores obtained from the trained classifier were transformed to the posterior probability that an observation was classified as ‘present’, p_{present} . To assess performance of the classification procedure, we used five-fold cross-validation. To this end, we randomly partitioned all available observations into five folds of equal size. After training the support vector machine classifier on a training set comprising four folds, we used the resulting posterior probabilities to predict the status of the remaining fold (20% of available observations) that comprised the test set. Similarly to the procedure followed in the linear discriminant analysis, we used two classification

rules derived from a common threshold probability. (1) We assigned the status ‘present’ to all observations whose posterior probability exceeded the threshold probability, that is, observations with $p_{\text{present}} > p_{\text{threshold}}$. (2) We assigned the status ‘absent’ to all observations with $p_{\text{present}} < 1 - p_{\text{threshold}}$. The approach was applied to thresholds from $p_{\text{threshold}} = 0.50$ to $p_{\text{threshold}} = 1.00$, in increments of 0.025. By increasing the threshold probability, we therefore narrowed the windows in the feature space for which classification was possible. For thresholds of $p_{\text{threshold}} \leq 0.50$, the classification windows would overlap. In particular, there would be an overlap between parts of the feature space corresponding to classification as ‘present’ with parts corresponding to classification as ‘absent’, and observations would therefore be classified twice. For this reason, we did not consider thresholds below $p_{\text{threshold}} = 0.50$. For each threshold, we computed performance as described below and averaged results across the five cross-validation folds. To make performance assessment robust against variability in the partitioning of observations, we report performance measures averaged across 100 rounds of the five-fold cross-validation.

We assessed classification performance by computing prediction accuracy, the fraction of correct predictions relative to all predictions. Accuracy was also separately assessed for positive and negative predictions, yielding precision and negative predictive value as the fraction of correct positive or correct negative predictions relative to all positive or negative predictions, respectively. We also computed which fraction of observations in the test set was assigned a prediction at a given threshold. As further performance measures, we computed sensitivity (true positive rate) and specificity (true negative rate) at the evaluated thresholds. We also computed the false positive rate ($1 - \text{specificity}$). To quantify performance based on sensitivity and specificity, we computed the Youden index J as $J = \text{sensitivity} + \text{specificity} - 1$ (Youden, 1950; Fluss et al., 2005). J is a measure of how well a binary classifier operates above chance level, with $J = 0$ indicating chance performance and $J = 1$ indicating perfect classification. Since J is defined at each threshold, to obtain a single summary measure we computed the mean of J across the more conservative thresholds $p_{\text{present}} = 0.85$ to $p_{\text{present}} = 1.00$ for all 100 cross-validation runs. Results did not change if the maximum J across all thresholds was considered instead (Supplementary Figure C.2B).

To assess statistical null performance of the classification procedure, we performed a permutation analysis. The analysis was equal to the classification procedure described above, with the exception of an additional step prior to the partitioning of observations into cross-validation folds. Here, for each round of cross-validation, the labels were randomly permuted. Thereby, the correspondence between features and true labels of observations was removed. In the permutation analysis, we used

Euclidean distance and the absolute log-ratio of neuron density as features, based on the feature combination that led to the best results, and averaged performance measures across 1000 rounds of five-fold cross-validation.

Logistic regression

In our assessment of the relative predictive power of microscopic and macroscopic structural measures (Section 3.4), we performed multivariate logistic regression analyses using projection existence as the binary dependent variable and different combinations of the relative structural measures as covariates. Specifically, we considered $|\log\text{-ratio}_{\text{density}}|$, geodesic distance, $|\Delta_{\text{soma cross section}}|$, $|\Delta_{\text{spine count}}|$, $|\Delta_{\text{spine density}}|$, and $|\Delta_{\text{tree size}}|$. The relative structural measures were converted to z-scores, so that the resulting regression coefficients were standardised. We also included a constant intercept term in each model. All covariates were entered into the model simultaneously. We report the standardised regression coefficients, the t-statistic, and its associated p-value.

For the logistic regression, we assessed model classification performance in three different ways. First, we calculated the generalised coefficient of determination, R^2 , adjusted for the number of covariates, which indicates which proportion of the variance in the dependent variable is explained by the covariates. Second, we computed the Youden index J (Youden, 1950; Fluss et al., 2005), where $J = \text{sensitivity} + \text{specificity} - 1$. As mentioned above, by taking into account both sensitivity (true positive rate) and specificity (true negative rate), the Youden index is a comprehensive summary measure of classification performance. We considered values of J below 0.25 to indicate negligible classification performance, values of 0.25 and above to indicate weak performance, values of 0.40 and above to indicate moderate performance, and values of 0.50 and above to indicate good classification performance. Third, we calculated classification accuracy, that is, which proportion of all predictions was correct.

Parts of this section have been published in Beul et al. (2015), Beul et al. (2017) and Beul and Hilgetag (2019a).

2.4 Simulating the development of cortico-cortical connections: Existence of connections

To investigate possible mechanistic underpinnings of the architectonic type principle, we created an *in silico* model of the developing cortical sheet. In a first set of simulation experiments, we addressed how the existence of connections could be influenced by spatio-temporal patterns of neurogenesis. We first describe the variants of the *in silico* model we considered and how we simulated the formation of cortico-cortical connections on a forming cortical sheet, representing a single hemisphere. We then detail how we analysed the resulting simulated networks.

Connection formation was simulated to take place on a two-dimensional, rectangular cortical sheet, where neuron somata and axon terminals were assigned two-dimensional coordinates without spatial extent. Somata were arranged in rectangular cortical areas which differed in their surface density of neurons. Neuron density has been shown to be a good indicator of a cortical area's overall degree of architectonic differentiation (Dombrowski et al., 2001) and has been used previously to relate differentiation to connectivity in the macaque brain (e.g. Hilgetag et al., 2016). Hence, we used neuron density as a central marker for architectonic differentiation, with higher neuron density corresponding to a stronger degree of differentiation. We did not adjust the absolute magnitude of neuron density to empirical values, but did choose the range of neuron densities such that it was similar to empirically observed variation in neuron densities across the cortex, with about a five-fold increase between areas of lowest and highest neuron density (cf. Hilgetag et al., 2016). We implemented neuron density as number of somata per unit area of cortical sheet ($\#/arbitrary\ unit^2$). All cortical areas were defined to be of the same size. From these two constraints on neuron density and area size, it followed that areas of different densities contained different numbers of neurons. Within an area, somata were spaced equidistantly.

2.4.1 Variants of the *in silico* model

The generation of the cortical sheet across time was simulated in a number of different settings of the *in silico* model, which we call variants or growth layouts. These growth layouts systematically differed in where and when neurons were generated on the forming cortical sheet, that is, they had different spatio-temporal

growth trajectories. Below, we describe all growth layouts and their correspondence to neurodevelopmental findings in detail. An overview is provided in Table 2.1, and Figure 2.3 as well as Supplementary Figure C.3 give a visualisation of cortical sheet development over time for the different growth layouts.

All considered spatio-temporal growth trajectories were grouped into five sets of growth layouts. These sets differed with respect to whether cortical areas were generated by planar, expansive growth, whether there was radial growth, and in the final gradient of neuron density around neurogenetic origins.

In growth layouts with planar growth, the cortical sheet expanded, as, with each growth event, new cortical areas emerged around neurogenetic origins. Each new cortical area was grown within one time step, thus all constituent neurons appeared on the cortical sheet simultaneously. Neurogenesis occurred on the outer fringes of the portion of the cortical sheet already generated around each origin of neurogenesis. For more than one neurogenetic origin, this process entailed that newly generated areas moved previously generated areas apart on the cortical sheet, increasing the spatial distance in between them. Thus, planar growth mimicked the empirically observed planar gradient in onset of neurogenesis (see Section 1.6.1.1).

Radial growth, in contrast, did not expand the cortical sheet over time. Here, the cortical sheet had its final dimension already at the start of corticogenesis and cortical areas did not differ with respect to the time of onset of neurogenesis, but instead in the length of their neurogenetic interval. During each growth event, neurons were added at a constant rate across the entire cortical sheet. Areas with lower neuron density finished generating their complement of neurons earlier in time than areas with a higher neuron density, which needed to generate a larger number of neurons. Radial growth thus reproduced an alternative interpretation of studies of neurogenetic timing (see Section 1.6.1.1).

Growth events, during which the cortical sheet was generated, were distributed across the fixed simulated length of time. For both planar and radial growth, they were timed in such a manner that all neurons had grown after one third of the simulation length, and the remaining time steps could be used for connection formation by all neurons. These three main properties of spatio-temporal growth of the cortical sheet were combined in the five sets of growth layouts, with each set containing three (or in one case nine) growth layouts, as follows: The first set, the *realistically oriented density gradient* growth layouts, grew by planar growth. Here, newly generated areas were of higher neuron density than previously grown areas. That is, there was a positive correlation between time of origin and neuron density, which appeared as a distinct gradient in neuron density around the neurogenetic origins on the final

2.4. Simulating the development of cortico-cortical connections: Existence of connections

set	growth mode	# origins	final gradient of neuron density around origins	planar growth of cortical sheet	radial growth of cortical sheet	# areas	# growth events	total # neurons	abbreviation
realistically oriented gradient	1D 1 row	1				25	12	24897	1D-1row-1or
	1D 2 rows	1				50	12	49794	1D-2row-1or
	2D	1				81	5	40838	2D-1or
	1D 1 row	2	realistically oriented			26	6	26550	1D-1row-2or
	1D 2 rows	2		✓	✗	52	6	53100	1D-2row-2or
	2D	2				162	5	81676	2D-2or
	1D 1 row	3				27	4	28215	1D-1row-3or
	1D 2 rows	3			54	4	56430	1D-2row-3or	
2D	3			196	4	100248	2D-4or		
inverse gradient	1D 1 row	2	inverse			26	6	23910	inverse-1D-1row-2or
	1D 2 rows	2		✓	✗	52	6	47820	inverse-1D-2row-2or
	2D	2				162	5	38994	inverse-2D-2or
radial	1D 1 row	2	realistically oriented			26	6	26550	radial-1D-1row-2or
	1D 2 rows	2		✗	✓	52	6	53100	radial-1D-2row-2or
	2D	2				162	5	81676	radial-2D-2or
static	1D 1 row	2	realistically oriented			26	1	26550	static-1D-1row-2or
	1D 2 rows	2		✗	✗	52	1	53100	static-1D-2row-2or
	2D	2				162	1	81676	static-2D-2or
random	1D 1 row	2	no gradient / random			26	6	26550	random-1D-1row-2or
	1D 2 rows	2		✓	✗	52	6	53100	random-1D-2row-2or
	2D	2				162	5	81676	random-2D-2or

Table 2.1: Summary of growth layouts. This table indicates the set, growth mode and number of neurogenetic origins for each of the 21 growth layouts. For each set, the determining properties of the spatio-temporal growth trajectory are indicated. Moreover, for each growth layout the total numbers of areas, growth events and neurons are included. Abbreviations and background colours introduced here are used throughout the figures and tables.

2.4. Simulating the development of cortico-cortical connections: Existence of connections

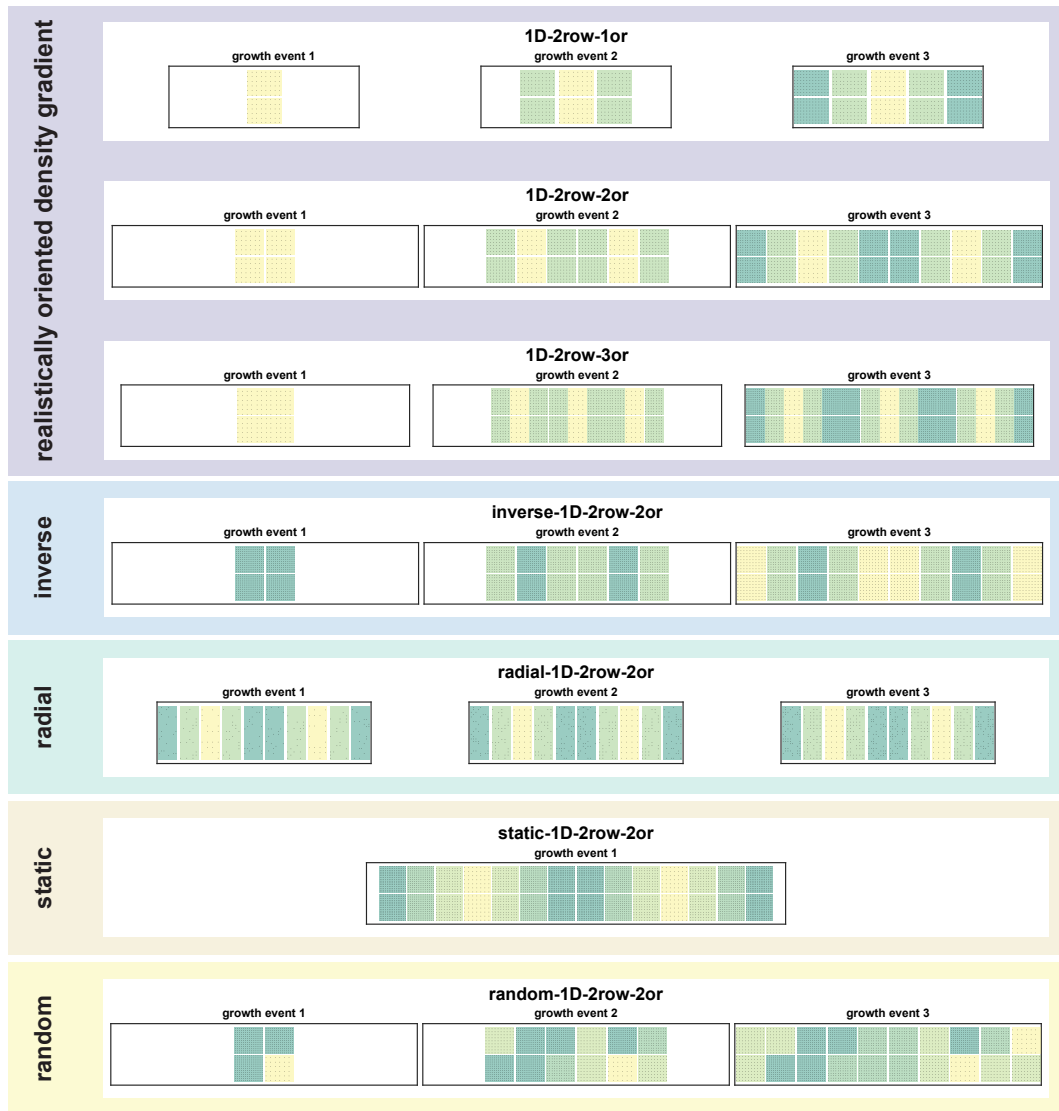


Figure 2.3: Developmental trajectories of growth layouts. The figure illustrates the spatio-temporal growth trajectory for different growth layouts. The successive population of the cortical sheet with neurons is shown for the first three growth events. For static growth, all neurons grow simultaneously, hence only one growth event is shown. Here, all growth layouts of growth mode 1D 2 rows are shown. See Supplementary Figure C.3 for an illustration of the developmental trajectories of all 21 growth layouts.

cortical sheet. The second set, the *inverse neuron density gradient* growth layouts, grew by planar growth like sets 1 and 5. However, in these *inverse gradient* growth layouts, newly generated areas were of lower neuron density than previously grown areas, that is, there was a negative correlation between time of origin and neuron density. The third set, the *radial* growth layouts, grew by radial growth. The final density gradient was identical to sets 1 and 4, but for the *radial* growth layouts, this pattern was caused by a positive correlation between length of the neurogenetic interval and neuron density, instead of a correlation between the time of onset of neurogenesis and neuron density. The fourth set, *static* growth layouts, did not in fact grow at all. All neurons were grown during the first growth event, thus the cortical sheet was fully formed from the beginning of the simulation. The final density gradient was identical to sets 1 and 3. Finally, in the fifth set, the *random* growth layouts, the cortical sheet grew by planar growth. The resulting final cortical sheet had no directed gradient of neuron density around the neurogenetic origins. Instead, each newly generated area was randomly assigned a neuron density. Possible density values were drawn from the neuron densities found on the final cortical sheet of the first set, *realistically oriented neuron density gradient*.

For each of these five sets, we implemented three different growth modes to mitigate influences of any specific choice of spatial implementation. Each growth mode was implemented around two neurogenetic origins. The three growth modes were as follows: First, one-dimensional growth with one row of areas (*1D 1row* growth layouts), where new areas grew to the left and right of neurogenetic origins (i.e., along the x-dimension of the cortical sheet) and there was only one row of cortical areas. Second, we implemented one-dimensional growth with two rows of areas (*1D 2rows* growth layouts), where, again, areas were added to the left and right of neurogenetic origins, but there were two rows of areas stacked in the y-dimension of the cortical sheet. Third, we implemented two-dimensional growth (*2D* growth layouts), where new areas were added on all sides of neurogenetic origins (i.e., in both the x- and y-direction of the cortical sheet). In this growth mode, each successive growth event led to an exponentially increasing number of added areas, and for set 1, *realistically oriented density gradient*, an unproportionally high number of areas of the highest neuron density, which did not accurately reflect the composition of the mammalian cerebral cortex. However, as stated above, we simulated the different growth modes to alleviate side-effects that might unintentionally arise from any particular spatial layout. Considering results across these specific implementations vastly reduced the risk of misinterpretation. We therefore included the two-dimensional growth mode as a further control, despite its unrealistic rendering of the cortical sheet.

As mentioned before, each of the 15 growth layouts that were described so far was

implemented around two origins of neurogenesis (5 sets x 3 growth modes x 1 number of origins). For set 1, *realistically oriented neuron density gradient*, we additionally considered two different numbers of origins for each growth mode. Specifically, we included growth around one neurogenetic origin and growth around three or four neurogenetic origins for *1D* and *2D* growth modes, respectively. These further six growth layouts allowed us to test whether the exact number of neurogenetic origins meaningfully influenced final connectivity.

Thus, we considered a total of 21 growth layouts (5 sets x 3 growth modes x 1 number of origins + 1 set x 3 growth modes x 2 numbers of origins). We simulated 100 instances of the spatio-temporal development of each of these 21 growth layouts.

Correspondence to empirical observations

The five sets were designed to correspond to some aspects of empirical neurodevelopmental findings and to violate others. Set 1, which features planar growth and a *realistically oriented density gradient*, represents a fiducial reproduction of the empirically grounded assumptions we described in Chapter 1 and thus mimics the mechanistic underpinnings that were previously hypothesised to account for the emergence of the architectonic type principle (Barbas, 1986, 2015; Hilgetag et al., 2016; Dombrowski et al., 2001). The other four sets deviate from this most realistic set in different ways. Sets 2 and 5, with *inverse* and *random* density gradients, respectively, test how the specifics of the neuron density gradient affect connectivity in the presence of planar growth. In set 4, the *static* growth layouts examine how the absence of planar growth affects connectivity if the neuron density distribution remains unchanged. Set 3, with *radial* growth layouts, contrasts planar growth with radial growth, while the final distribution of neuron densities again remains unchanged.

2.4.2 Connection formation

Axons randomly grew across the cortical sheet and stochastically formed synaptic connections (similar to, e.g., Kaiser et al. (2009); also see Kaiser (2017)). Each neuron was assigned one axon terminal, which was initially located at the respective soma position. With each time step of the simulation, the axon extended by a fixed length at a random angle, and the position of the axon terminal changed accordingly.

Once axon terminals left the cortical area which their parent soma was located in, they were free to form a synapse with any neuron soma they encountered. Since both terminals and somata were defined by point-coordinates, a synapse was formed once the axon terminal approached a soma closer than a defined maximal distance. Upon synaptic contact, an axon stopped growing and the now occupied axon terminal remained at the location of the contacted soma for the remainder of time steps. To further increase stochasticity, we imposed a connection probability of 90% on potential synaptic contacts. Thus, in 90% of cases, a synapse successfully formed once the terminal was close enough to a soma, but in a randomly chosen 10% of cases, no synapse formed at this time step and the axon continued to grow. If soma positions changed because the cortical sheet grew, axon terminals (both occupied and unoccupied) were shifted with the cortical area they found themselves in at the time, and synaptic contacts were retained. This procedure of axon growth and synapse formation was not modified across variants of the *in silico* model.

Different parameters of the axon growth process interacted to determine how fast axon terminals made synaptic contacts. This included for example the increase in axon length per time step and the maximal distance for synapse formation. In pilot runs of the simulation, we calibrated the relevant parameters such that after the fixed simulated length of time, most axon terminals (>99.9%) had made synaptic contact and final inter-areal connectivity fell into a range comparable to empirical reports (Felleman and Van Essen, 1991; Beul et al., 2015; Markov et al., 2014a). This calibration resulted in slightly different parameter values for *1D* and *2D* growth modes, but the same values were used in all simulation instances within these growth modes.

2.4.3 Properties of the simulated cortical sheet

From the final state of the simulated cortical sheet, we extracted a number of properties that were analogous to measures used in previous analyses of the mammalian cortex.

First, we collapsed the axonal connections between individual neurons into a simulated connectome, which contained information about the existence of all possible area-wise connections. Thus, we constructed a complete binary connectivity matrix where connections were coded as either absent or present.

Second, we extracted the two relevant structural measures from the final cortical sheet. The first measure was each area's neuron density, and derived from that

the difference in neuron density between area pairs, where density difference = density_{area of origin} - density_{area of termination}. For most analyses, we considered the undirected equivalent, the absolute value of density difference, which indicates the magnitude of the difference in neuron density between two areas. These two measures were equivalent to measures of architectonic differentiation previously used in studies examining mammalian cortical connectivity, such as neuron density difference (e.g. Hilgetag et al., 2016), the log-ratio of neuron densities (Section 3.3), or difference in architectonic type, which is an ordinal measure of architectonic differentiation (e.g. Hilgetag and Grant, 2010; Hilgetag et al., 2016). The second measure was the spatial proximity between pairs of areas, which we calculated as the Euclidean distance between areas' centres of mass. This measure was equivalent to measures of spatial proximity we used in previous empirical studies (e.g. Hilgetag et al., 2016; Section 3.3). Since distance is an undirected measure, each analysis that included distance required the use of the undirected measure of neuron density difference, its absolute value.

2.4.4 Analyses

For each of the 100 instances that were simulated for each growth layout, we performed the analyses described below and aggregated results across instances. For the simulations and analyses we used Matlab (The MathWorks, Inc., Natick, MA, USA).

Relative frequency of present connections

To gain an overview of how present and absent connections were distributed across the range of possible absolute density differences and distances, we computed the relative frequency of present connections, similarly to our analyses of connectivity in the cat and macaque cortex. To do this, we divided the range of each structural measure in up to 10 bins and computed the fraction of present connections in each bin as relative frequency = number of present connections / (number of present connections + number of absent connections). For distance, we always used 10 bins. For absolute neuron density difference, we used 10 bins where possible, but we had to chose a lower number of bins if the particular growth layout had been implemented with a small number of area neuron density tiers. This was for example the case in

the *2D 4origins* growth layout, where the exponential increase in the number of areas with each growth event caused us to restrict the simulation to four growth events, and thus four different levels of neuron density. To assess whether there was a systematic relation between the relative frequency of present connections and the respective structural measure, we then computed Spearman rank correlations of the computed fractions across all bins. We show the resulting distribution of correlation coefficients ρ and report median ρ - and p-values averaged across simulation instances. To determine whether the rank correlation was consistently significant across instances, we computed a left-tailed sign test for each growth layout. Specifically, we tested whether the group of 100 p-values obtained from the rank correlations for each instance had a median value smaller than a significance threshold, $\alpha_{\text{Spearman}} = 0.05$. We considered the sign test significant below $\alpha_{\text{sign}} = 0.05$, and in these cases rejected the null-hypothesis that the median of the group of p-values was not smaller than α_{Spearman} . For the sign test, we report the test statistic z and the corresponding p-value.

Prediction of simulated connectivity data

To assess how well density difference and distance accounted for the simulated inter-areal connectivity, we performed logistic regression analyses, a classification algorithm for distinction between two classes. That is, we endeavoured to predict the existence of simulated connections from the structural properties of the corresponding simulated cortical sheet. We considered four combinations of predicting factors: First, a null model which included only a constant and amounted to chance performance. Second and third, we further included either absolute density difference or distance as predicting factors. Thus, we constructed two models with two predicting factors each, testing the effect of each individual structural measure on classification performance. In a fourth model, we included all three predicting factors, that is, a constant and both structural measures, testing their joint classification performance. Prior to inclusion, both structural measures were transformed to z-scores, that is, we subtracted the respective mean and then divided by the respective standard deviation. To evaluate how much each predicting factor contributed to classification performance, we computed McFadden's Pseudo $R^2 = \log\text{-likelihood}_{\text{model}} / \log\text{-likelihood}_{\text{null model}}$. The log-likelihood for each model captures how well its predictions correspond to the actual data, with larger values indicating a better correspondence. McFadden's Pseudo R^2 thus indicates how much better prediction performance becomes with the inclusion of further predicting factors, relative to chance performance. Values of

McFadden's Pseudo R^2 of 0.10 and above were considered a moderate increase in prediction performance, values of 0.15 and above were considered adequate, and values from 0.20 on were considered a very high increase in prediction performance (McFadden, 1979).

Area degree

We assessed one topological property of areas, their degree, which we found to be related to architectonic differentiation in the cat and macaque cortex (Sections 3.2 and 3.3). Area degree indicates how many connections are maintained by an area, and we computed it as the sum of afferent and efferent connections for each area. Since degree is not a relational property and hence applies to a single area and not a pair of areas, we related it to neuron density but not to spatial proximity. Analogous to our previous analyses, we computed a Spearman rank correlation between area degree and neuron density to assess whether there was a relation between the two. We show the resulting distribution of correlation coefficients ρ and report median ρ - and p-values averaged across simulation instances. To determine whether the rank correlation was consistently significant across instances, we computed a left-tailed sign test for each growth layout, as described above for relative connection frequencies. The same significance thresholds applied here.

Prediction of empirical connectivity data

To assess how well the relationships between simulated connectivity and simulated structural measures translated to empirically observed relations in the mammalian cortex, we used classifiers trained on the simulated data to predict empirical connectivity data. To this end, we used the two data sets of ipsilateral cortico-cortical connectivity (i.e., connections within a hemisphere) which we also used for our analyses of empirical data in the cat and the macaque cortex. These were the most extensive and up-to-date connectivity data sets available for the macaque (Markov et al., 2014a) and cat cortex (Scannell et al., 1995), acquired using retrograde tract-tracing experiments. Here, we considered these connectivity data as a binary measure of connection existence. For both data sets, measures of architectonic differentiation and spatial proximity were available. In the macaque, we used the absolute log-ratio of neuron density and Euclidean distance between areas as the equivalents of the

absolute density difference and Euclidean distance obtained from the simulations and included 1128 empirical data points in our analyses. In the cat, these measures were represented by the absolute difference in architectonic type, an ordinal ranking of areas by architectonic differentiation, and the border distance between areas, which quantifies the shortest distance between two areas based on a given parcellation of the cortex. Here, we included 954 empirical data points in our analyses. To be able to apply the two simulated structural measures to the empirical measures despite their different scales, we transformed all three pairs of structural measures (simulated, macaque, cat) to z-scores by subtracting the respective mean and then dividing by the respective standard deviation.

For each instance of each growth layout, we trained a classifier to predict simulated connection existence from the z-scores of simulated relative architectonic differentiation (i.e., absolute density difference) and spatial proximity (i.e., distance), using a support vector machine with a linear kernel function and the assumption of uniform prior probabilities for the two learned classes (as described in Section 2.3.4.2 for classification of connection existence in the macaque cortex). We then applied the trained classifier to the z-scores of empirical relative architectonic differentiation (i.e., absolute log-ratio of neuron density and absolute type difference, respectively) and spatial proximity (i.e., Euclidean distance and border distance, respectively), separately for the macaque and the cat, and obtained posterior probabilities that a connection was present, p_{present} . Similarly to the procedure followed in the linear discriminant analysis for the cat cortex and the classification by the support vector machine classifier in the macaque cortex, we then used two classification rules, derived from a common threshold probability $p_{\text{threshold}}$, to label empirical data points as either absent or present. We assigned the status ‘present’ to all empirical connections whose posterior probability exceeded the threshold probability, that is, data points with $p_{\text{present}} > p_{\text{threshold}}$. Alternatively, we assigned the status ‘absent’ to all empirical connections whose posterior probability was sufficiently low, that is, data points with $p_{\text{present}} < 1 - p_{\text{threshold}}$. These two rules excluded a range of posterior probabilities where classification was not confident enough to warrant a prediction, which entailed that not all empirical connections were assigned a predicted label for each simulation instance. Additionally to the measures that we used to quantify prediction performance, we therefore report the fraction of available empirical data points that were actually classified. To mitigate influences of any one threshold probability, we considered ten threshold probabilities, increasing $p_{\text{threshold}}$ in step sizes of 0.025 from $p_{\text{threshold}} = 0.750$ to $p_{\text{threshold}} = 0.975$, and report results averaged across thresholds for each simulation instance.

Again, we assessed prediction performance through two measures, accuracy and

the Youden index J . We calculated these measures at each threshold probability and report results averaged across all ten thresholds. Accuracy was computed as the fraction of predictions that were correct, that is, $\text{accuracy} = \text{number of correct predictions} / (\text{number of correct predictions} + \text{number of incorrect predictions})$. The Youden index J (Youden, 1950; Fluss et al., 2005) is a more comprehensive summary measure which takes into account both sensitivity (true positive rate) and specificity (true negative rate), with $J = \text{sensitivity} + \text{specificity} - 1$. As in our analyses of empirical data, values of the Youden index below 0.25 were considered to indicate negligible classification performance, values of 0.25 and above were considered weak performance, values of 0.40 and above were considered moderate performance, and values of J above 0.50 were considered to indicate good classification performance.

We show the distribution of resulting mean values of accuracy and Youden index across the ten threshold probabilities, and report the median values of these distributions across the 100 instances for each growth layout. In the following, we describe the procedure that we followed to validate the two classification performance measures, assessing how they compared against chance performance. An overview is provided in Figure 2.4. Within each simulation instance, we performed a permutation analysis at each threshold probability to determine how the accuracy or Youden index at this threshold compared to chance performance. To this end, we randomly permuted the labels of the empirical data points, so that there was no association any more between the predictive variables and connection existence, and then applied the classification procedure again, computing accuracy and Youden index to quantify chance performance. We repeated this for 100 permutations of the data labels, so that, for both measures, we obtained a distribution of values that represented chance performance at each threshold probability. To test whether the corresponding classification performance measure was likely to be from this chance distribution, we first fit the chance performance distribution to a normal distribution, obtaining an inferred mean value and standard deviation. We then performed a two-tailed z-test, which tests whether a particular value comes from a population with a particular mean, which in this case was the fitted distribution of performance measures obtained from the permutation analysis. If the test was significant at $\alpha_{z\text{-test}} = 0.05$, we rejected the null hypothesis that the actual performance measure at the given threshold probability came from the fitted distribution of chance performance. Since the z-statistic was never smaller than 0 if the p-value was below $\alpha_{z\text{-test}}$, we then inferred that the actual performance was better than chance performance at a given threshold probability. We then averaged the p-values obtained from the z-tests across thresholds by computing their median. Thus, for each growth layout, we obtained distributions of 100 (one per instance) mean performance measures and

2.4. Simulating the development of cortico-cortical connections: Existence of connections

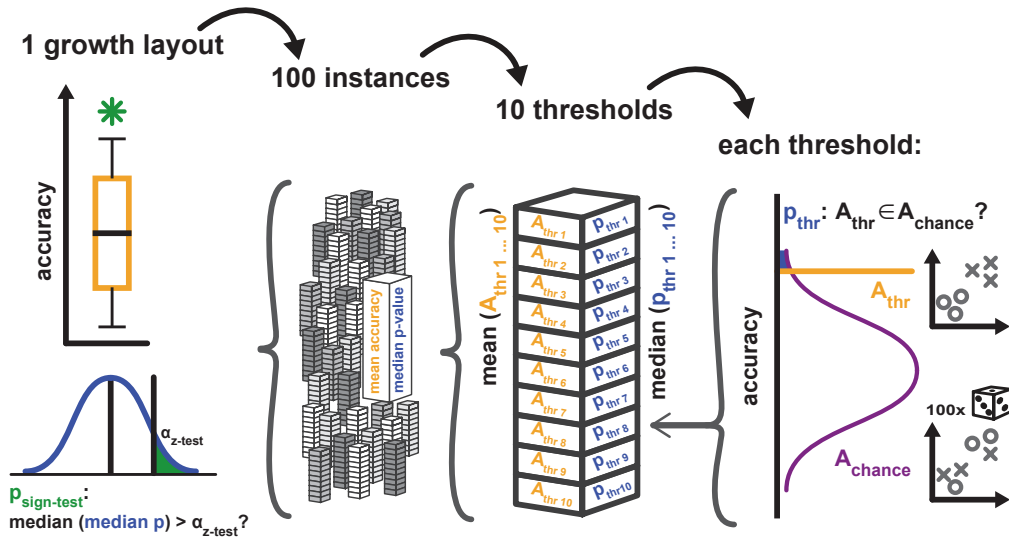


Figure 2.4: Validation procedure for measures of simulation-to-empirical classification performance. The figure illustrates the general procedure for assessing the performance of the classification of empirical data from the cat and macaque cortex by classifiers that were trained on simulated data. We computed median measures of classification performance for each growth layout and compared these measures against chance performance, as assessed by a permutation analysis. Specifically, for each of the 21 growth layouts shown in Figure 3.25 and Supplementary Table D.13, 100 instances were simulated. For each instance, classification was performed using 10 different classification threshold probabilities. For each threshold probability, a simulation-trained classifier assigned labels to the empirical data, resulting in an accuracy value A_{thr} . Additionally, a distribution of chance performance accuracies, A_{chance} , was generated by classifying 100 times from randomly permuted non-sensical labels. A z-test quantified the probability that A_{thr} was an element of the distribution of A_{chance} . The corresponding p-value p_{thr} was used for further calculations. For each simulation instance, classification performance from all 10 threshold probabilities was averaged, resulting in one mean accuracy value and one median value of p_{thr} per instance, thus amounting to a total of 100 values each per growth layout. Figure 3.25 shows the distribution of mean accuracy values from these 100 instances, and indicates the median accuracy. The indication of significance in Figure 3.25 refers to the p-value obtained from a sign-test which assessed whether the median of the distribution of median values of p_{thr} was larger than the chosen significance threshold α_{z-test} of 0.05 (with a small value of $p_{sign-test}$ indicating that p_{thr} was very unlikely to be larger than α_{z-test}). Supplementary Table D.13 includes the median accuracy, median z-test p-value and the result of the sign-test. Shown here for accuracy, the procedure was analogous for the Youden index J , which is shown in Figure 3.26 and Supplementary Table D.13.

as many associated median p-values validating them against chance performance.

To determine whether these median p-values were consistently significant across instances, we computed a left-tailed sign test for each growth layout. Specifically, we tested whether the group of 100 median p-values obtained from the z-tests at each threshold for each instance had a median value smaller than $\alpha_{z\text{-test}}$. We considered the sign test significant at $\alpha_{\text{sign}} = 0.05$, and in these cases rejected the null-hypothesis that the median of the group of p-values was not smaller than $\alpha_{z\text{-test}}$. For the sign test, we report the test statistic z and the corresponding p-value for each growth layout.

Finally, to assess how the two classification performance measures accuracy and Youden index were affected by the number of origins independent of growth mode and the considered species, we computed a three-way analysis of variance on the performance measures from growth layouts with a *realistically oriented density gradient* (which were the only ones where number of origins ever differed from two). We included three factors: ‘species’, with the levels macaque and cat; ‘growth mode’, with the levels *1D 1row*, *1D 2rows* and *2D*; and ‘number of origins’, with the levels 1, 2 and 3 or 4 (for *1D* and *2D* growth modes, respectively). We report the F-statistic and associated p-value for each factor and considered a main effect significant at $\alpha_{\text{ANOVA}} = 0.05$. To examine the main effect of ‘number of origins’ in more detail, we estimated marginal mean values from the analysis of variance model. These reflect a model estimate of the mean value for each level of ‘number of origins’ across all levels of the remaining factors. We subsequently performed *post-hoc* comparisons between these model estimates of marginal mean values, which revealed specific differences between levels. The *post-hoc* comparisons were Bonferroni-corrected for multiple tests and considered significant at an adjusted threshold of $\alpha_{\text{adj}} = 0.05/3 = 0.0167$.

This section has been published in Beul et al. (2018).

2.5 Simulating the development of cortico-cortical connections: Laminar patterns of connection origins

In the first set of simulation experiments described in the preceding, we investigated how realistic patterns of connection existence could arise. To address the emergence of another crucial property of cortico-cortical connections, the distribution of connection origins across cortical layers, we expanded our *in silico* model and performed a

second set of simulation experiments.

With the model expansion, we did not alter the main characteristics of the *in silico* model. Briefly, on a two-dimensional plane, neuron somata developed and were assigned to cortical areas. Neurons belonging to a single area grew simultaneously, with sets of areas growing sequentially. Cortical areas were designed to be of the same size but to exhibit a range of neuron densities (i.e., number of neurons per area), therefore neuron numbers differed between areas. The specifics of where and when neuron somata developed were aligned to empirical neurodevelopmental findings. In this second set of simulation experiments, we employed the model settings that were previously shown to yield the most realistic connectivity and that corresponded most closely to observations of actual cortical development in mammals. Specifically, our *in silico* model was set to grow expansively around two neurogenetic origins, such that more recently formed areas separated earlier formed areas, increasing the spatial distance between them over time. Moreover, it was set to have a positive correlation between time of neurogenesis and neuron density, such that the earliest formed areas had the lowest neuron density and the areas that developed last had the highest neuron density.

Each neuron had one axon which grew by a specific length, at a random angle, at each time step. Once the axon tip came sufficiently close to a neuron soma, a connection was formed. Connection formation thus happened concurrently with neuron development and can be characterised as stochastic.

2.5.1 Model expansion

To probe the origin patterns of cortico-cortical projections across cortical layers, we extended the previously used *in silico* model by a radial component, assigning the neuron somata to one of three laminar compartments (layer 1, supragranular compartment, infragranular compartment). The cortical sheet remained implemented in two dimensions, since we did not intend to model the growing out of axons towards the white matter or the laminar patterns of projection terminations. As we did previously, we evaluated the existence of projections between cortical areas. Additionally, we considered how the origins of projections were distributed across laminar compartments. Similarly to empirical studies, we report the fraction of projection neurons (for a given projection) which originated in the supragranular compartment, $N_{SG}\%$.

At the baseline setting, the neuron density of an area's supragranular compartment

was equal to the density of the infragranular compartment. Since there are generally few neurons in layer 1 (Marin-Padilla and Marin-Padilla, 1982; Gabbott and Somogyi, 1986), we chose a lower density for layer 1 and specified layer 1 neuron density as 15% of infragranular compartment density. Moreover, since layer 1 is mainly a target for long-range projections (reviewed in Larkum, 2013), we included layer 1 neurons in the *in silico* model only as connection targets, meaning they could form synapses with approaching axon tips, but they did not grow out axons themselves.

Features implemented to modulate laminar projection patterns

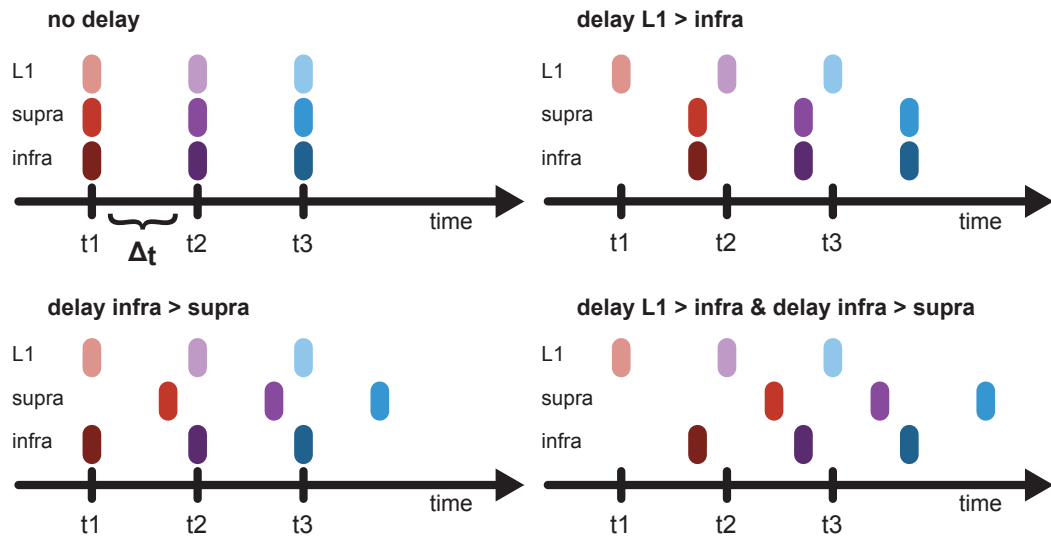
We introduced four features that possibly affect how the origins of projections are distributed across laminar compartments and included these features in the *in silico* model individually or in conjunction (Figure 2.5). Three of these features changed the spatio-temporal pattern of neurogenesis, affecting where and when neurons developed. The fourth feature, in contrast, changed properties of the neurons themselves.

The first two features were temporal delays between the laminar compartments. *In vivo*, cortical neurons develop in an inside-out pattern (with the exception of layer 1 neurons, which develop first), where earlier born neurons come to reside in the lower cortical layers and later born neurons migrate upwards and become positioned successively closer towards layer 1 (Sidman et al., 1959; Angevine and Sidman, 1961; Rakic, 1974; Caviness, 1982). To simulate this radial gradient in time of neurogenesis within areas, we introduced two delay parameters, one for the delay between layer 1 and infragranular compartment neurons and a second for the delay between infragranular compartment neurons and supragranular compartment neurons. When one or both of the delay features were included in the *in silico* model, whole areas did not grow simultaneously any more, but instead laminar compartments appeared on the cortical sheet sequentially, with all the neurons of a laminar compartment appearing simultaneously.

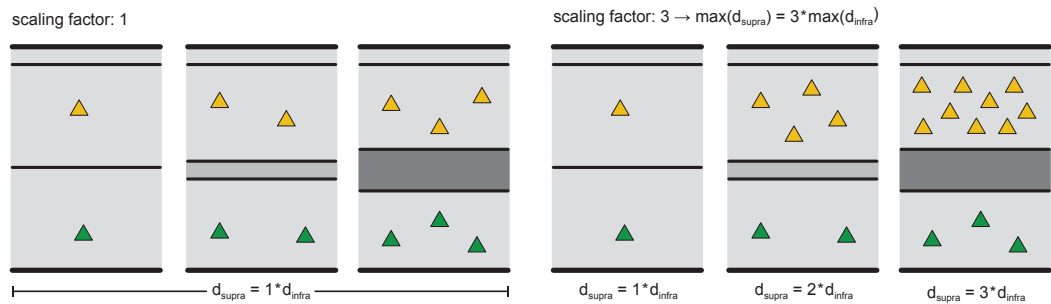
The third feature we introduced was a scaling of the neuron density of the supragranular compartment. In the mammalian cortex, increases in overall neuron density across areas tend to be mediated mostly by increases in supragranular neuron density (Finlay and Darlington, 1995; Charvet and Finlay, 2014). We therefore introduced a parameter that modified how much denser the supragranular compartment became relative to the infragranular compartment. While it left the variation in infragranular compartment density across areas unchanged from the baseline setting, this

2.5. Simulating the development of cortico-cortical connections: Laminar patterns of connection origins

A delay infragranular and supragranular compartment growth



B neuron density scaling



C axon elongation scaling

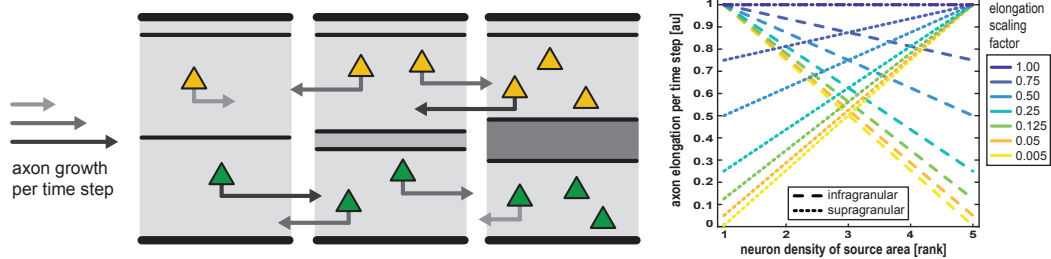


Figure 2.5: Features of the expanded in silico model.

2.5. Simulating the development of cortico-cortical connections: Laminar patterns of connection origins

Figure 2.5: Features of the expanded *in silico* model. **(A)** Delay in the growth of laminar compartments. Without a delay in compartment growth (no delay), all laminar compartments of a given area grow at one single time point. After the growth interval, Δt , the next area appears. If growth of the infragranular compartment is delayed relative to layer 1 (delay $L1 > \text{infra}$), the infragranular compartment grows a fraction of the growth interval after layer 1, while the supragranular compartment appears simultaneously with the infragranular compartment. If growth of the supragranular compartment is delayed (delay $\text{infra} > \text{supra}$), it grows a fraction of the growth interval after layer 1 and the infragranular compartment, both of which appear simultaneously. If both compartments are delayed (delay $L1 > \text{infra}$ & delay $\text{infra} > \text{supra}$), layer 1 appears first, followed by the infragranular compartment and finally the supragranular compartment. **(B)** Scaling in the neuron density of the supragranular compartment. With a scaling factor for supragranular density larger than 1, the ratio of supragranular neuron density to infragranular neuron density becomes larger as infragranular neuron density increases across areas. Additionally, as the scaling factor becomes larger, the divergence between low-density and high-density areas in their ratio of supragranular to infragranular neuron density increases. **(C)** Scaling in axon elongation. We modified how much longer axons became at each time step according to both the laminar compartments of the neuron somata and the architectonic differentiation of the area the neuron somata were positioned in. Axon elongation was gradually adjusted to shrink to a minimum value (light grey arrow), with the ratio of minimum elongation to baseline elongation given by the elongation scaling factor (see color scale). As the scaling factor became smaller, the divergence in elongation values became larger. We implemented two opposing gradients: elongation values in the infragranular compartment (dashed lines) became shorter with increasing source area neuron density, while elongation values in the supragranular compartment (dotted lines) became longer with increasing source area neuron density. At a scaling factor of 1, all neurons, regardless of laminar compartment or source area neuron density, shared the same elongation value (appears as dash-dotted line).

parameter determined to which level the relative density of laminar compartments increased for the highest infragranular compartment density. Supragranular compartment density was always equal to infragranular compartment density for the lowest infragranular compartment density and scaled up linearly in between these two extremes (areas of lowest to highest infragranular compartment density). For example, at baseline (i.e., with a supragranular compartment density scaling parameter value of 1), supragranular compartment density would be equal to infragranular compartment density for all areas. At a parameter value of 3, however, the density of the supragranular compartment would be three times the infragranular compartment density for the areas with the highest infragranular compartment density, while it would be double the infragranular compartment density for the areas with an infragranular compartment density halfway between lowest and highest infragranular compartment density.

The fourth feature, axon elongation scaling, did not affect spatio-temporal patterns of neurogenesis but modified properties of individual neurons while leaving their time and place of origin unchanged. As architectonic differentiation changes, so do prop-

2.5. Simulating the development of cortico-cortical connections: Laminar patterns of connection origins

erties of individual neurons, for example in morphological and physiological aspects (Schmidt et al., 2018a; Section 3.4). One striking phenomenon is externopyramidization (Sanides, 1962, 1970): the relative sizes of cells in the laminar compartments shift with architectonic differentiation. Less differentiated areas tend to have their larger neurons in infragranular layers, but cells become more equal in size between infra- and supragranular layers for more differentiated areas, while very strongly differentiated areas, finally, tend to have their largest neurons in the supragranular layers. Evidence that larger cells are able to maintain longer connections (reviewed in Goulas et al., 2018) indicates that cell-intrinsic properties play a role in shaping connectivity, even though the question of causality still remains. To generate differences in the likelihood that neurons will form long-range connections which arise from properties inherent to the neurons, we varied the elongation of axons, changing the distance they grow per time step, in a manner similar to the observed relative cell sizes. Neurons with larger axon elongation were predisposed towards longer connections, because they traversed a larger distance per time step and were therefore more likely to have travelled further before encountering a connection target, relative to neurons with shorter axon elongation. In particular, we set a default distance that axons travel per time step, and introduced a minimum distance that the slowest neurons were limited to. In between these two extremes, we varied the distance that an axon travelled per time step according to the neuron density of its area, changing the axon elongation of infragranular and supragranular neurons in a complementary way. Specifically, the default value of axon elongation was assigned to infragranular compartment neurons in the areas with the lowest neuron density as well as to the supragranular compartment neurons in the areas with the highest neuron density, while the minimum value of axon elongation was assigned to supragranular compartment neurons in the areas with the lowest neuron density as well as the infragranular compartment neurons in the areas with the highest neuron density. As the parameter value for the minimum travelled distance decreased, the divergence between the neurons with shortest and longest axon elongation increased. At baseline, the minimum axon elongation was equal to the default axon elongation, and hence axons elongation was equal for all infra- and supragranular neurons and constant across all source area densities. Independent of whether the elongation of axons within a given time period is actually a relevant factor *in vivo*, this manipulation represents one of many possible ways to implement, *in silico*, differences in cell-intrinsic properties that covary with architectonic differentiation and that account for the fact that infragranular and supragranular compartments can contain neurons with markedly different characteristics (Song and Moyer, 2018; Kroon et al., 2019).

We implemented each of the four features at a range of parameter values to systematically evaluate the sensitivity of the outcome measures of interest to variation in the respective property of the *in silico* model. 50 instances of each model implementation were simulated. Since we considered the baseline setting, seven parameter values for each of the two temporal delays, four parameter values for the scaling of supragranular compartment density and six parameter values for the differences in cell-intrinsic properties, we simulated a total of 1250 instances to probe the features individually. In addition, we simulated at least 20 instances each to probe (at a reduced range of parameter values) all pair-wise feature combinations as well as the simultaneous implementation of all four features.

2.5.2 Analyses of laminar patterns

For each simulation instance, we evaluated the resulting connectivity. As mentioned above, we assessed the projections between areas with respect to the distribution of projection origins across laminar compartments, computing which fraction of the neurons that constituted a projection originated in the supragranular compartment, $N_{SG}\%$. The main observation from empirical studies that we set out to replicate was a positive correlation between this supragranular contribution and the relative differentiation of connected areas (Barbas, 1986, 2015; García-Cabezas et al., 2019; Hilgetag et al., 2019). Therefore, we correlated the $N_{SG}\%$ values and neuron density differences, computed as $\text{density}_{\text{source area}} - \text{density}_{\text{target area}}$, between connected areas that were obtained from the *in silico* model instances, computing Spearman rank correlation coefficients ρ . Since $N_{SG}\%$ is a fraction, its value is quite volatile for very weak projections. As previously done in empirical studies, we therefore applied a threshold to projections strengths prior to computing $N_{SG}\%$ (Barbas et al., 2005). We only included projections with a minimum of 10 constituting axons in the analyses. To determine whether the correlation coefficient was consistently significant across the distribution resulting from all 50 instances of a model implementation, we computed a left-tailed sign test. Specifically, we tested whether the group of 50 p-values obtained from the rank correlations for each instance had a median value smaller than a significance threshold, $\alpha_{\text{Spearman}} = 0.05$. We considered the sign test significant below $\alpha_{\text{sign}} = 0.05$, and in these cases rejected the null-hypothesis that the median of the group of p-values was not smaller than α_{Spearman} .

2.5.3 Analyses of connection existence

In our first set of simulation experiments, addressing connection existence, the two most comprehensive measures that we report are the correlation between area neuron density and the number of connections an area maintains (area degree) as well as the classification performance that a classifier which was trained on simulated networks reached when it was applied to empirical data. We wanted to monitor whether the features we introduced in our expanded *in silico* model changed the simulated networks with respect to these overarching properties that concern the existence of connections. Therefore, we also evaluated the two measures correlation of neuron density with area degree and simulation-to-empirical classification performance for all implementations of the *in silico* model. We assessed them as described above (Section 2.4.4). Briefly, for the correlation between neuron density and area degree we report Spearman rank correlation coefficients ρ and tested the distribution of correlation coefficients across instances of a given model implementation for significance using a left-tailed sign test as described above for the correlation between $N_{SG}\%$ and neuron density differences. To assess simulation-to-empirical classification performance for each simulation instance, we first trained a linear support vector machine to classify projection existence (absent or present) from the z-scores of simulated relative architectonic differentiation (i.e., absolute difference in neuron density) and spatial proximity (i.e., distance) of area pairs. In a second step we used this classifier to classify projection existence in two empirical data sets, from the cat (Scannell et al., 1995) and the macaque (Markov et al., 2014a) cortex. To quantify classification performance, we report the Youden index J (Youden, 1950; Fluss et al., 2005), a comprehensive summary measure which takes into account both sensitivity (true positive rate) and specificity (true negative rate), and measures how well a binary classifier operates above chance level with $J = 0$ indicating chance performance and $J = 1$ indicating perfect classification. Also here, we considered values of J above 0.40 to indicate moderate classification performance and values of above 0.50 to indicate good performance. In a third step, we validated the Youden index, assessing how it compared against chance performance by performing permutation analyses. Similar to the other measures of interest, we show the distribution of resulting values of J across all 50 instances of a model implementation.

This section has been submitted for peer-review in Beul and Hilgetag (2019b).

Chapter three

Results

3.1 Intrinsic circuitry varies with architectonic differentiation

The composition of the cortex changes across areas, such that different cell populations are present and they are arranged in characteristic laminar patterns, as reflected in measures of architectonic differentiation. This change in the structural substrate of cortical connectivity is expected to affect intrinsic as well as extrinsic connectivity, given that distinct complements of elements are available to be connected. Here, we present a tentative intrinsic circuitry of the agranular cortex in rodents, which differs from intrinsic circuitry as described in the striate cortex.

Figure 3.1 summarises our review of the available literature on intrinsic interlaminar circuitry in the agranular frontal cortex of the rodent brain and puts it in comparison to a recent rendering of the intrinsic circuitry in striate cortex. Excitatory-to-excitatory connections from L2/3 to L5 have clearly been demonstrated in rat agranular frontal cortex by measuring excitatory postsynaptic currents (EPSC) in monosynaptically coupled pyramidal neurons in L5, induced by stimulation in L2/3 (Kang, 1995; Otsuka and Kawaguchi, 2008, 2009, 2011; Hirai et al., 2012). One of these paired recording studies (Otsuka and Kawaguchi, 2009) additionally demonstrated the existence of excitatory-to-inhibitory connections from L2/3 to L5, a finding also reported by Apicella and colleagues (2012) in mouse motor cortex. The experiments of Hirai and colleagues (2012) showed that reciprocal connections to the excitatory-to-excitatory connections from L2/3 to L5 exist from L5 pyramidal cells to L2/3

3.1. Intrinsic circuitry varies with architectonic differentiation

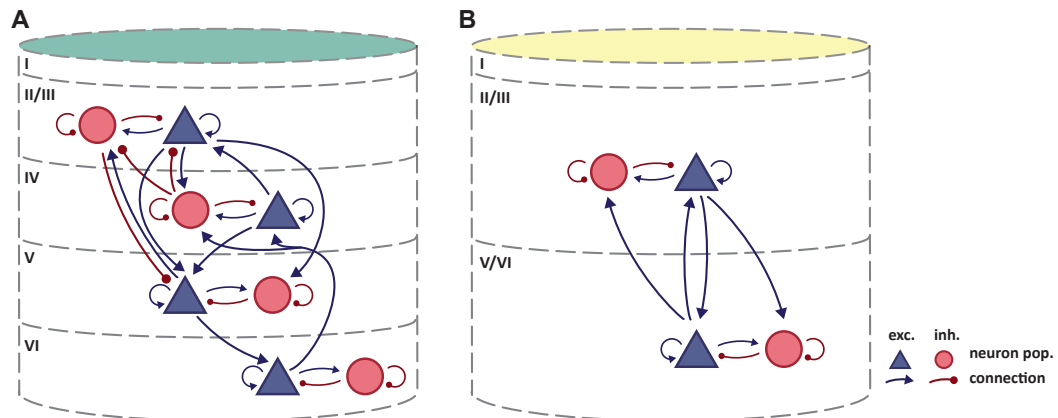


Figure 3.1: Intrinsic circuitry in the mammalian cortex. **(A)** Intrinsic circuitry in granular cat striate cortex. Adapted from Potjans and Diesmann (2014) who largely based their diagram on Binzegger and colleagues (2004). **(B)** Tentative scheme of intrinsic circuitry in agranular rodent frontal cortex. Intralaminar connectivity in agranular cortex is similar to that in granular cortex, but interlaminar connectivity differs. Column colours follow the colour coding of architectonic differentiation in Figure 1.1: yellow-weakly differentiated cortex to dark green-strongly differentiated cortex.

pyramidal cells. This observation is confirmed in medial entorhinal cortex of the rat (van Haeften et al., 2003), which can be considered agranular since its layer 4 ('lamina dissecans') is mainly acellular (Andersen et al., 2007). The microscopy study of van Haeften and colleagues (2003) traced the processes of pyramidal cells in the deep layers ramifying in superficial layers, and identified the synaptic contacts made by those neurons. The analysis revealed excitatory-to-excitatory, as well as excitatory-to-inhibitory, connections from deep to superficial layers.

Considering the trend of weakening inhibitory-to-excitatory connectivity in architectonically less differentiated areas (Kätzel et al., 2011, see Section 1.2.2), we consider it likely that there exists no substantial interlaminar inhibition of excitatory neurons in rodent agranular frontal cortex, which is reflected in our tentative circuit diagram. The study by van Haeften and colleagues (2003) in medial entorhinal cortex, which reports an absence of inhibitory-to-excitatory synapses from deep to superficial layers, supports the same conclusion. Van Haeften and colleagues furthermore report that only a small percentage of the observed synapses could potentially be classified as inhibitory-to-inhibitory, thus giving little evidence for such a connection from deep to superficial layers. Considering the reciprocal inhibitory-to-inhibitory connection from superficial to deep layers, we could find no studies reporting either on the absence or presence of such a connection. In the circuit diagram, we did not include connections which could only be inferred from exclusively morphological results (e.g. Kawaguchi, 1993, 1995; Kawaguchi and Kubota, 1997; Kubota et al., 2011), since we

3.2. Comparison of the architectonic type principle, distance model and hierarchical model in the cat cortex

did not consider data on the spatial spread of axon collaterals sufficiently reliable to demonstrate a functional connection, given that synapse formation has been shown to be highly specific (e.g. Kozloski et al., 2001; Brown and Hestrin, 2009). For these reasons, Figure 3.1B indicates no inhibitory interlaminar connections, although the validity of this assessment of course remains contingent upon further experimental data.

By contrast, there is abundant evidence for rich intralaminar connectivity including excitatory-to-inhibitory and inhibitory-to-excitatory connections (Kang, 1995; Somogyi et al., 1998; Kawaguchi and Kondo, 2002; Barthó et al., 2004; Otsuka and Kawaguchi, 2009; Fino and Yuste, 2011; Kätzel et al., 2011). Therefore, we assumed a stereotypical pattern of connectivity within deep and superficial layers as illustrated in Figure 3.1B.

The intrinsic circuitry we have sketched here thus comprises interlaminar excitatory connections that connect neuronal populations from both upper and lower layers to excitatory as well as inhibitory neuron populations in the complementary cortical layers. Within upper and lower layers, intralaminar connections reciprocally connect excitatory and inhibitory neuron populations. This intrinsic interlaminar circuitry is strikingly similar to the simplified original circuit diagram for the striate cortex of Douglas and colleagues (1989), and allows for recurrent excitation and inhibition. These physiological interactions were inferred to underlie essential computational mechanisms in striate cortex (Douglas et al., 1995; Douglas and Martin, 2007a, 2009). The microcircuitry as we sketch it here should accordingly be able to support elemental neural functions, such as the amplification of weak inputs through positive feedback or gain control and signal normalisation through negative feedback.

This section has been published in Beul and Hilgetag (2015).

3.2 Comparison of the architectonic type principle, distance model and hierarchical model in the cat cortex

To test the architectonic type principle, the distance model, and the hierarchical model of cortical organisation in the cat cortex, we first assessed how informative they were regarding the presence or absence of connections between cortical areas, putting a special focus on the possibility of predicting connectivity. We then explored how architectonic differentiation may relate to topological properties of cortical

connectivity, such as membership in a ‘rich-club’ hub module or area degree. Finally, shifting perspective to further properties of the cortical connectome, we examined whether laminar projection patterns were well explained by difference in architectonic type.

3.2.1 Relationship of projection existence to structural measures

We evaluated the association among qualitative projection strength and the variables border distance, Δ_{dist} , architectonic type difference, Δ_{type} , and hierarchical level difference, Δ_{level} . Figure 3.2 shows the distribution of present projections for each structural measure. It also depicts the cumulative percentage of present projections, where, for each structural measure, the cumulative percentage at each value was calculated as the sum of the number of present projections found up to this value, divided by the total number of present projections and multiplied by one hundred.

About 75 % of present connections were found within values of $\Delta_{\text{dist}} = 1\text{--}3$ (of the range 1–6 possible in the used cortical parcellation; Figure 3.2A), within $|\Delta_{\text{type}}| = 0\text{--}1$ (of the range 0–4 possible between the 5 types; Figure 3.2B), or within $|\Delta_{\text{level}}| = 0\text{--}5$ (of the range 0–10 occurring in this data set or 0–13 possible in the employed hierarchy; Figure 3.2C). That is, the great majority of existing connections were short range and between areas of relatively similar intrinsic architecture and hierarchical position.

Rank correlation analyses revealed no significant relationship between Δ_{dist} and $|\Delta_{\text{type}}|$ ($\rho = 0.06$, $p > 0.05$, Figure 3.3A), or between Δ_{dist} and $|\Delta_{\text{level}}|$ ($\rho = 0.04$, $p > 0.05$, Figure 3.3B), suggesting that Δ_{dist} was a largely independent factor. However, there was a strong correlation between Δ_{type} and Δ_{level} ($\rho = -0.63$, $p < 0.001$, Figure 3.3C), which we discuss below (Section 4.1.1).

Relative projection frequencies (i.e., relative proportions of present connections) were maximally negatively correlated with both Δ_{dist} ($\rho = -1.00$, $p < 0.01$, Figure 3.4A) and $|\Delta_{\text{type}}|$ ($\rho = -1.00$, $p < 0.05$, Figure 3.4B). This monotonic decline for both factors indicates that the more distant or the more architectonically dissimilar cortical areas are, the fewer projections are present between them. The results did not change substantially when the analyses were conducted only on the subset of 308 projections for which Δ_{level} was available (Δ_{dist} : $\rho = -1.0$, $p < 0.05$, $|\Delta_{\text{type}}|$: $\rho = -1.00$, $p < 0.05$). By contrast, the relative proportion of present projections was not correlated with $|\Delta_{\text{level}}|$ ($\rho = -0.36$, $p > 0.05$, Figure 3.4C), indicating that the level difference between areas within the hierarchy proposed by Scannell and colleagues (1995) does

3.2. Comparison of the architectonic type principle, distance model and hierarchical model in the cat cortex

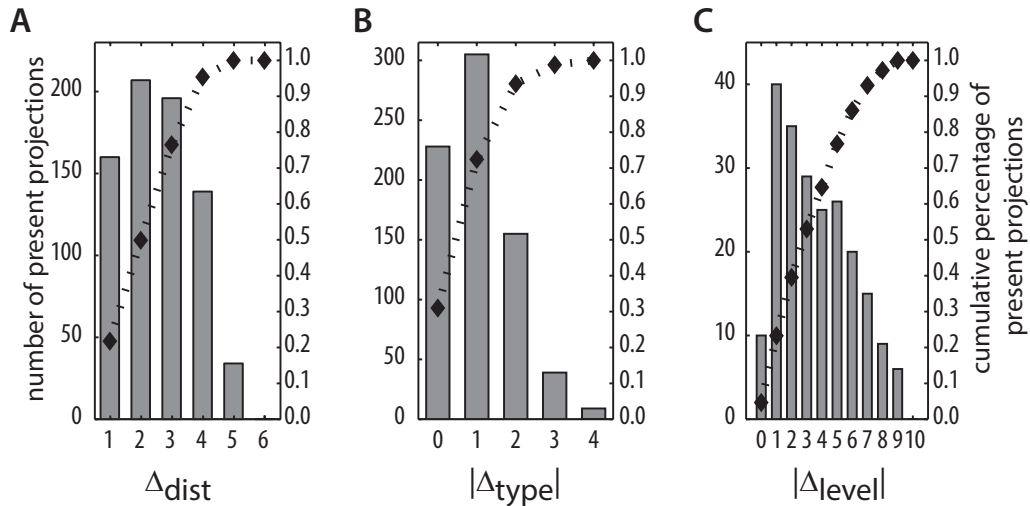


Figure 3.2: Cumulative percentages of present projections in the cat cortex. For each structural measure, the absolute number of present projections is shown for each of its values (bars, left axis). Additionally, the cumulative percentage of present projections is indicated (diamonds, right axis). **(A)** Border distance Δ_{dist} . **(B)** Absolute architectonic type difference $|\Delta_{type}|$. **(C)** Absolute hierarchical level difference $|\Delta_{level}|$.

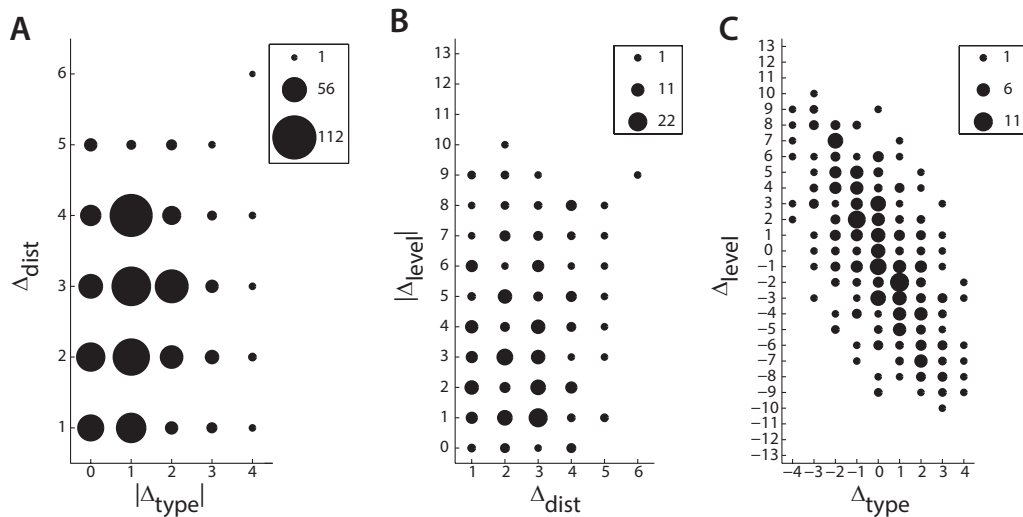


Figure 3.3: Interrelations of structural measures in the cat cortex. **(A)** Distance Δ_{dist} was not correlated with absolute architectonic type difference $|\Delta_{type}|$ or **(B)** with absolute hierarchical level difference $|\Delta_{level}|$. **(C)** Architectonic type difference Δ_{type} and hierarchical level difference Δ_{level} were strongly correlated. Marker size indicates number of projections.

3.2. Comparison of the architectonic type principle, distance model and hierarchical model in the cat cortex

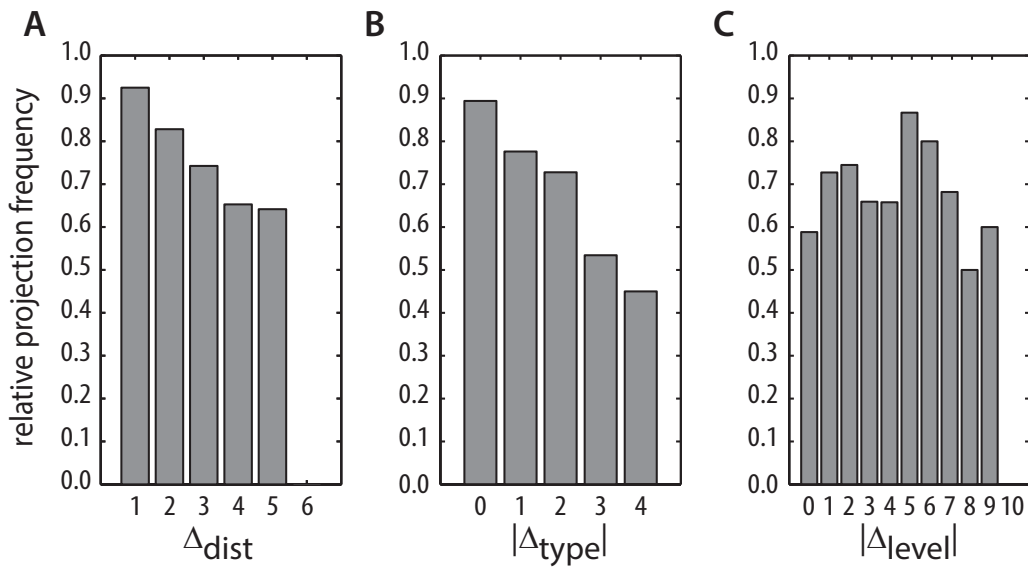


Figure 3.4: Correlation of structural measures with relative frequencies of present projections in the cat cortex. **(A), (B)** Distance Δ_{dist} and absolute architectonic type difference $|\Delta_{\text{type}}|$ were negatively correlated with relative projection frequency. **(C)** Absolute hierarchical level difference $|\Delta_{\text{level}}|$ was not correlated with relative projection frequency.

not contain information about whether two areas are connected by an anatomical projection. Such a correlation was also absent for an alternative hierarchical ranking described by Hilgetag and colleagues (2000b) (see Section 2.2.4).

3.2.2 Combining architectonic type difference and border distance allows the classification of connection existence

We performed a linear discriminant analysis to distinguish between present and absent projections by their associated $|\Delta_{\text{type}}|$ and Δ_{dist} . The linear discriminant analysis assigned a significant contribution to classification performance to both measures, with standardised canonical discrimination function coefficients of 0.95 and 0.71 for $|\Delta_{\text{type}}|$ and Δ_{dist} , respectively. Figure 3.5A depicts the posterior probabilities that resulted from the linear discriminant analysis across the predictive variable space. Projections were confidently labelled as ‘present’ ($p_{\text{present}} \geq 0.75$) if both $|\Delta_{\text{type}}|$ and Δ_{dist} were in their lower range, that is $|\Delta_{\text{type}}| < 2$ and $\Delta_{\text{dist}} \leq 3$, and as ‘absent’ ($p_{\text{present}} \leq 0.25$) if the measures were in their upper range of $|\Delta_{\text{type}}| > 2$ and $\Delta_{\text{dist}} \geq 4$. From the posterior probabilities we made predictions about the existence of connections using different classification thresholds for the assignment of connections into

3.2. Comparison of the architectonic type principle, distance model and hierarchical model in the cat cortex

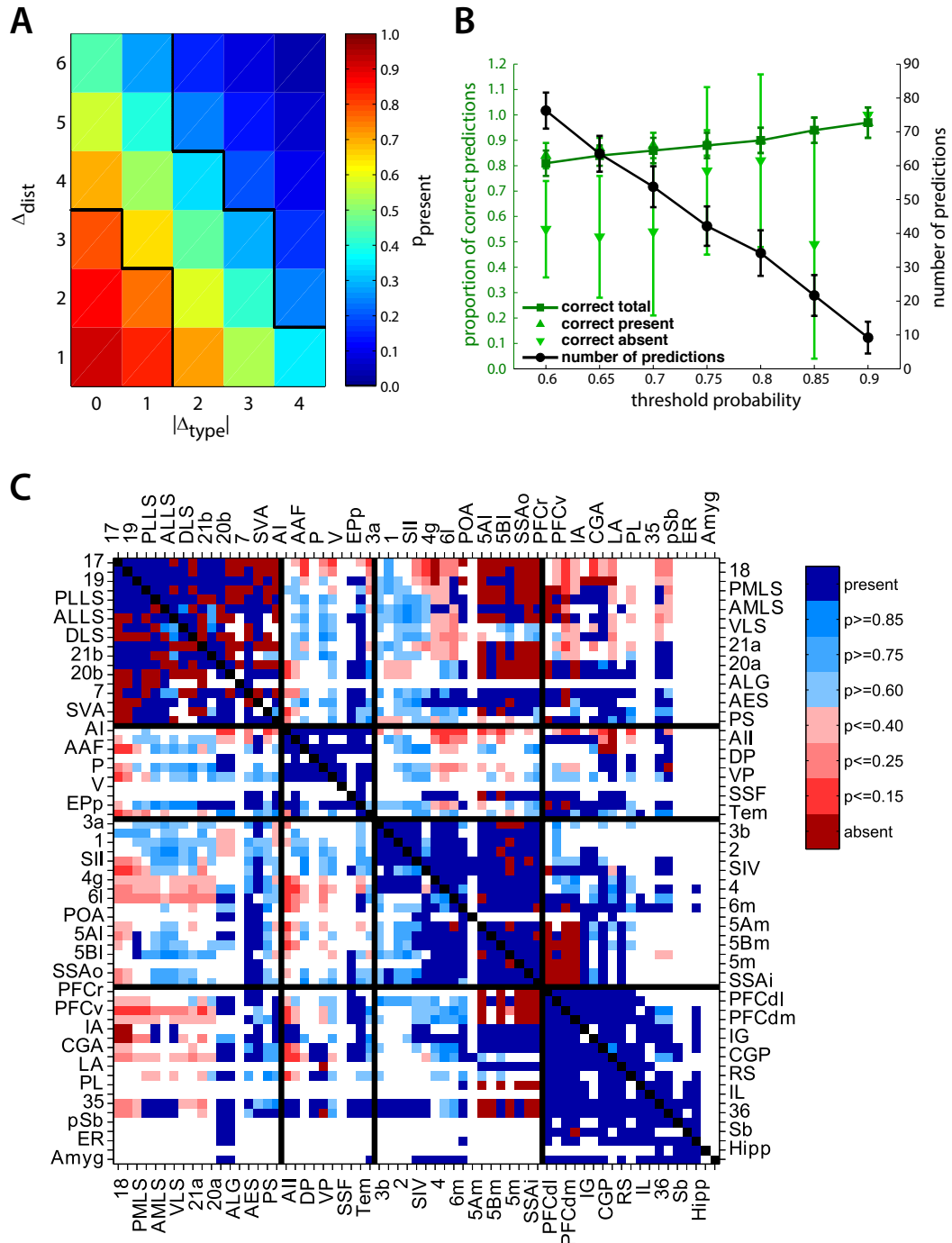


Figure 3.5: Results of linear discriminant analysis. **(A)** Posterior probabilities for presence of projections across the predictive variable space. Black borders enclose ranges of $p_{\text{present}} > 0.75$ and $p_{\text{present}} < 0.25$. **(B)** Results of cross-validation at different prediction thresholds. Mean prediction accuracy for projections that were predicted to be present and absent (light green) as well as overall mean prediction accuracy (dark green) are shown. Mean number of predictions at each threshold is shown in black. Error bars indicate standard deviations. **(C)** Matrix of cortico-cortical connections in the cat, adapted from Scannell and colleagues (1995). Projections of known status are coded dark red (absent) and dark blue (present). Additionally, predicted connectivity for 926 unexamined projections

3.2. Comparison of the architectonic type principle, distance model and hierarchical model in the cat cortex

Figure 3.5: (cont.) is indicated. Projections predicted to be absent are shown in lighter reds, predictions predicted to be present are shown in lighter blues. Colour saturation indicates how conservative a prediction threshold a particular prediction survived. White cells are unexamined connections for which no prediction has been made. The diagonal of intra-areal connections has been marked black. Projections' source regions are arranged on the vertical axis, target regions are arranged on the horizontal axis. Abbreviations as in Supplementary Table D.1. Note that area labels are split across left/top and right/bottom axes.

the categories 'present' and 'absent'. Figure 3.5B shows the cross-validated prediction accuracy of our model within the test sets across the used range of classification thresholds. Prediction accuracy increased as thresholds became more conservative, while at the same time the number of connections that were predicted decreased. A sensible choice for the classification threshold appeared to be $p_{\text{present}} = 0.75$ and $p_{\text{absent}} = 0.25$ for 'present' and 'absent' connections, respectively. In this case the classification accuracy for both prediction categories exceeded 75%, while the number of predictions remained substantial. These results illustrate how the combination of the two independent factors of absolute architectonic type difference and distance allowed us to confidently determine, for the subset of cortical connections that link cortical areas of appropriate $|\Delta_{\text{type}}|$ and Δ_{dist} , whether two cortical areas were connected. We therefore applied the posterior probabilities resulting from the model to predict the existence of connections that have not yet been investigated. Figure 3.5C depicts the classification of 926 as yet unexamined projections between cat cortical areas, where the classification threshold surpassed by the predicted connections is indicated by cell colour saturation. At a classification threshold of 0.75 for present connections and 0.25 for absent connections, we made predictions about the existence of 418 unknown connections.

3.2.3 Relation of architecture with connection topology

Modules of cortical areas

The 11 cortical areas considered to constitute a 'rich-club' hub module by Zamora-López and colleagues (2010) had significantly lower architectonic types than all the remaining areas not belonging to the 'rich-club' (hub-module areas: median = 1.5, non-hub-module areas: median = 3; $W = 146.5$, $z = -2.6$, $p = 0.01$, Figure 3.6A). Furthermore, the modality-specific clusters differed in their architectonic type medians (visual cluster: median = 3, auditory cluster: median = 3, somatosensory

3.2. Comparison of the architectonic type principle, distance model and hierarchical model in the cat cortex

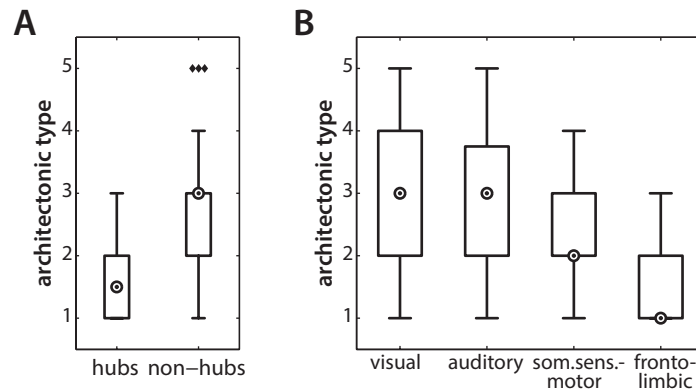


Figure 3.6: Distribution of architectonic types across modules of cortical areas in the cat cortex. **(A)** Hub-module areas had a lower median architectonic type than non-hub-module areas. **(B)** Architectonic type gradually decreased across four anatomical modules of cortical areas. Markers inside circles indicate median degree, diamonds indicate outliers.

cluster: median = 2, fronto-limbic cluster: median = 1; $H(3) = 11.1, p < 0.05$, Figure 3.6B). *Post hoc* tests, Bonferroni-corrected for multiple comparisons (resulting in $\alpha_{\text{adj}} = 0.0008$), revealed that the visual cluster had a higher median architectonic type than the fronto-limbic cluster ($W = 255.0, z = 2.7, p = 0.0006$); all other pairwise differences in architectonic type between the four modality-specific clusters were not significant after correcting for multiple comparisons. However, architectonic type decreased gradually from the visual to the auditory, then to somatosensory and finally to the fronto-limbic cortices ($JT = -2.0, p < 0.05$).

Area degree and weighted area degree

The node degree (number of maintained projections) of cortical areas was negatively correlated with their architectonic type ($\rho = -0.53, p < 0.001$, Figure 3.7A), such that areas with lower architectonic differentiation had more connections. However, the weighted area degree (connection strength or density) of cortical areas was not correlated with their architectonic type ($\rho = 0.004, p > 0.05$, Figure 3.7B). When calculated separately for projections of each ordinal projection strength, the correlation with architectonic type remained unaffected for sparse ($\rho = -0.49, p < 0.001$) and intermediate ($\rho = -0.50, p < 0.001$) projections, but disappeared for dense projections ($\rho = 0.06, p > 0.05$), thus explaining the lack of an overall correlation between architectonic type and weighted area degree.

3.2. Comparison of the architectonic type principle, distance model and hierarchical model in the cat cortex

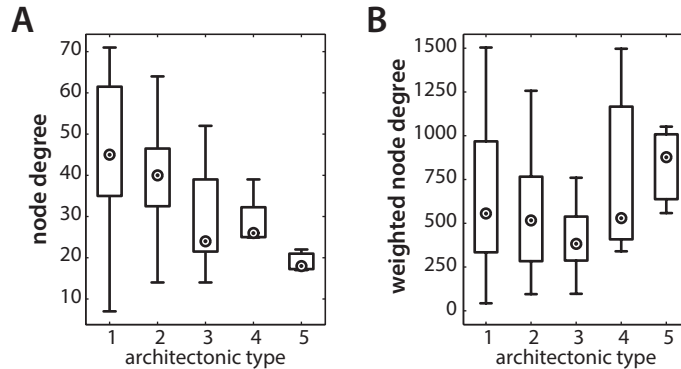


Figure 3.7: Degree distribution of cortical areas in the cat cortex. **(A)** Node degree of cortical areas across architectonic types. **(B)** Weighted node degree of cortical areas across architectonic types. Area degree was correlated with architectonic type, while weighted area degree was not. Markers inside circles indicate median degree.

We present this remarkable observation in a different form in Figure 3.8, which depicts the mean number of dense, intermediate and sparse projections averaged across areas of a given architectonic type. This representation underlines that the number of dense projections remains roughly constant, while the number of intermediate and sparse projections decreases notably with architectonic type, as revealed by the above correlation analyses.

Since the hub-module areas were originally identified, in part, by their very large number of connections and were found to be concentrated at the low end of the architectonic differentiation spectrum, it is possible that the ‘rich-club’ module was mainly responsible for the strong association between high area degree and low architectonic type. To examine this possibility, we repeated the analyses with the ‘rich-club’ areas excluded. While this procedure had a quantitative impact, reducing the strength of the correlations, the relationship between low architectonic differentiation and high area degree remained significant ($\rho = -0.41$, $p < 0.01$), and there was no qualitative effect on the lack of correlation with weighted area degree ($\rho = 0.29$, $p > 0.05$).

We observed an unexpected correlation between architectonic type and the total number of projections studied for a cortical area (comprising projections found to be absent as well as projections found to be present) ($\rho = -0.40$, $p < 0.01$). This effect raises the possibility that the correlation of area degree with architectonic type was a result of unequally distributed sampling efforts. However, it needs to be considered what impact additional data could have on the results. If all remaining unknown projections were to be examined, only a proportion of them would be found present. We verified that, if this proportion was equal across all architectonic types,

3.2. Comparison of the architectonic type principle, distance model and hierarchical model in the cat cortex

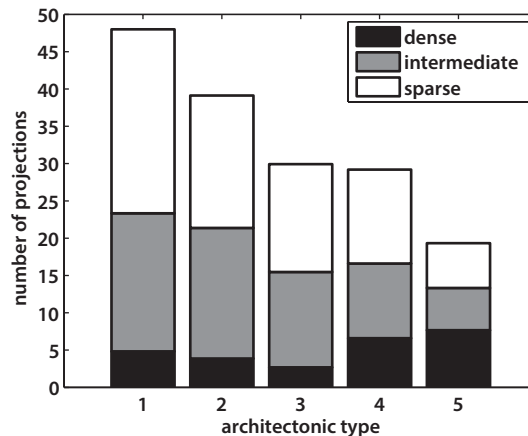


Figure 3.8: Mean number of projections across architectonic types in the cat cortex. Means for ordinal projection strengths are indicated separately for each architectonic type. The maximal standard deviation across all architectonic types is 5 for the number of dense projections, 7 for the number of intermediate projections, and 9 for the number of sparse projections.

the correlation we observed between node degree and architectonic type would remain moderate and significant up to an added proportion of present projections of 87%. In the current data set, 77% of examined projections were found to be present, whereas cortical connectivity levels have previously been estimated to reach about 50% (Felleman and Van Essen, 1991) or 66% (Markov et al., 2014a). Thus, even assuming the uncommonly high connectivity level of the examined data set (which likely reflects a lack of probing for absent projections in the literature, rather than a genuinely increased proportion of present projections), a uniform increase of present projections would still yield a correlation between area degree and architectonic type of $\rho = -0.37, p < 0.01$. A perhaps more probable proportion of present projections, such as 60%, would result in a correlation of $\rho = -0.44, p < 0.01$. Thus, notwithstanding the possible undersampling of areas of high architectonic type, our results suggest that areas of lower architectonic type are more frequently interconnected within the cortical connectome, and regardless of whether or not they are members of the ‘rich-club’ hub module.

3.2.4 Connection range

The connection distance profiles of cortical areas varied across architectonic types. When we compared aggregate connection ranges for all areas of a given architectonic type across all five types, we found a positive relation for the proportion of short

3.2. Comparison of the architectonic type principle, distance model and hierarchical model in the cat cortex

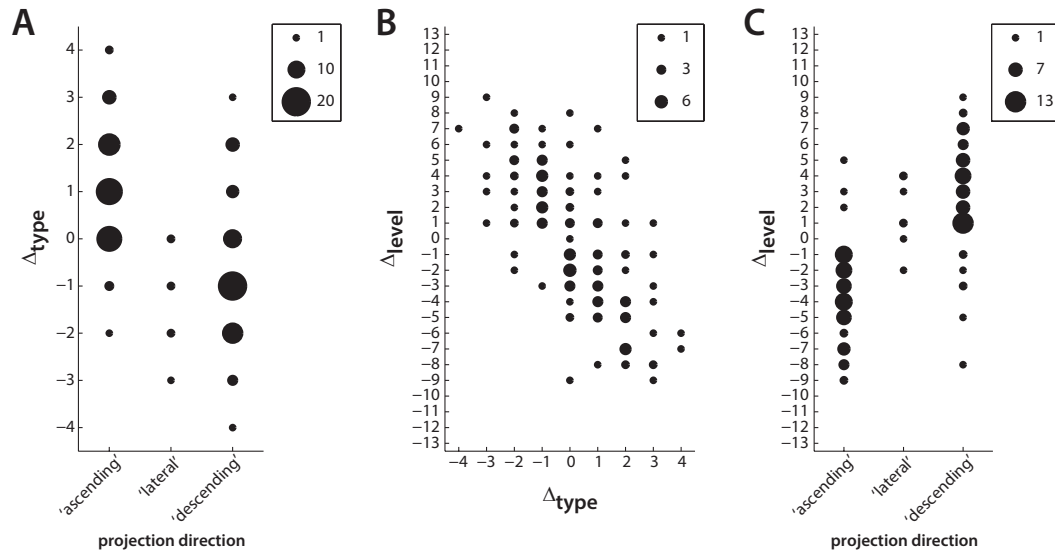


Figure 3.9: Correlation of structural measures with assigned directionalities of projections. **(A)** Architectonic type difference Δ_{type} was strongly correlated with projection directions and **(B)** hierarchical level difference Δ_{level} . **(C)** Hierarchical level difference Δ_{level} was strongly correlated with projection directions. Marker size indicates number of projections.

projections, such that areas of a higher architectonic type had higher proportions of short-range connections than areas of a lower architectonic type ($JT = 3.1, p < 0.01$). We also found an inverse relation between architectonic type and the proportion of long projections, such that areas of a lower architectonic type had a higher proportion of long projections than areas of a higher architectonic type ($JT = -2.9, p < 0.01$). For example, the average proportions of short- versus long-range connections for areas of the highest architectonic differentiation (type 5) were 65% and 9%, respectively, compared to 45% and 25% for those of the lowest differentiation (type 1).

3.2.5 Laminar projection profiles

We investigated the relationship between the laminar projection patterns of connections, as coded in their assigned directions of ‘ascending’, ‘lateral’, and ‘descending’, and the associated Δ_{type} , as well as Δ_{level} . The Δ_{type} was strongly correlated with both projection direction ($\rho = -0.53, p < 0.001$, Figure 3.9A) and Δ_{level} ($\rho = -0.73, p < 0.001$, Figure 3.9B, compare also Figure 3.3C). Projection direction was also strongly correlated with Δ_{level} ($\rho = 0.74, p < 0.001$, Figure 3.9C), which was to be expected, as the hierarchical arrangements, and therefore the level differences, were

derived from the projection directions in the first place. Results did not change if all projections classified as less reliable by Scannell and colleagues (1995) were excluded from the analysis.

This section has been published in Beul et al. (2015).

3.3 Comparison of the architectonic type principle, the distance model and the thickness model in the macaque cortex

To assess the architectonic type principle, the distance model and the thickness model in the adult macaque cortex, we examined the association between the macaque cortical connectome and three structural measures of the macaque cerebral cortex: architectonic differentiation quantified by neuron density; spatial proximity quantified by Euclidean distance; and cortical thickness. We tested how well each of the three structural measures was related to the existence and the laminar patterns of projection origins between cortical areas, and could predict the presence or absence of projections. We also probed the extent to which the structural measures accounted for laminar projection patterns and whether they were linked to topological properties of brain regions.

3.3.1 Relations among structural measures

To quantify relative structural similarity across the cortex, we computed, for all pairs of connected areas, the difference in neuron density or cortical thickness as measured on a log scale. That is, structural (dis-)similarities were expressed as log-ratios, while spatial proximity was quantified by Euclidean distance between areas. The structural measures associated with the cortico-cortical projections were not completely independent. We found a moderate correlation between the undirected neuron density ratio and the Euclidean distance of area pairs ($r = 0.47$, $p < 0.001$), whereas the correlation of Euclidean distance with the undirected thickness ratio was significant but of negligible magnitude ($r = 0.12$, $p < 0.001$). In contrast, neuron density ratio and thickness ratio were strongly negatively correlated ($r = -0.76$,

3.3. Comparison of the architectonic type principle, the distance model and the thickness model in the macaque cortex

$p < 0.001$), an association which results from a strong inverse correlation between the neuron density and thickness of brain areas ($r = -0.69$, $p < 0.001$).

3.3.2 Relationship of projection existence to structural measures

We used three different approaches to explore how the three structural measures of neuron density, cortical thickness and distance relate to the absence and presence of projections.

In an initial comparison, we found that connected areas were closer or more similar than non-connected areas for all three structural measures (mean $|\log\text{-ratio}_{\text{density}}|$ (absent) = 0.49, mean $|\log\text{-ratio}_{\text{density}}|$ (present) = 0.24, $t(1126) = 13.8$, $p < 0.001$; mean distance(absent) = 32.9 mm, mean distance(present) = 25.7 mm, $t(2608) = 15.1$, $p < 0.001$; mean $|\log\text{-ratio}_{\text{thickness}}|$ (absent) = 0.20, mean $|\log\text{-ratio}_{\text{thickness}}|$ (present) = 0.14, $t(2608) = 11.5$, $p < 0.001$). This effect was largest for the neuron density ratio (effect sizes: $|\log\text{-ratio}_{\text{density}}|$: $r = 0.38$, distance: $r = 0.28$, $|\log\text{-ratio}_{\text{thickness}}|$: $r = 0.22$). Results did not change if Welch's t-test was applied, which does not assume equal variances across groups.

Then, to assess the distribution of absent and present projections across the three structural measures in more detail, we plotted the relative frequency of present projections across neuron density ratio and Euclidean distance in comparison to the absolute numbers of absent and present projections (Figure 3.10). For all structural measures, present projections became relatively less frequent with increasing distance or structural dissimilarity of two potentially connected areas, as also shown by a rank correlation coefficient, ρ , of the relative frequencies ($|\log\text{-ratio}_{\text{density}}|$: $\rho = -1.00$, $p < 0.001$; distance: $\rho = -0.98$, $p < 0.001$; $|\log\text{-ratio}_{\text{thickness}}|$: $\rho = -0.93$, $p < 0.01$).

3.3.3 Combining neuron density ratio and Euclidean distance allows the classification of connection existence

Finally, to exploit the association of the structural measures with the existence of cortico-cortical connections, we used them to classify projections as either absent or present. We predicted projection presence or absence, using a support vector machine classifier, based on all seven possible combinations of the three structural measures (each measure individually, three pairwise combinations of the measures, and the simultaneous inclusion of all three measures).

3.3. Comparison of the architectonic type principle, the distance model and the thickness model in the macaque cortex

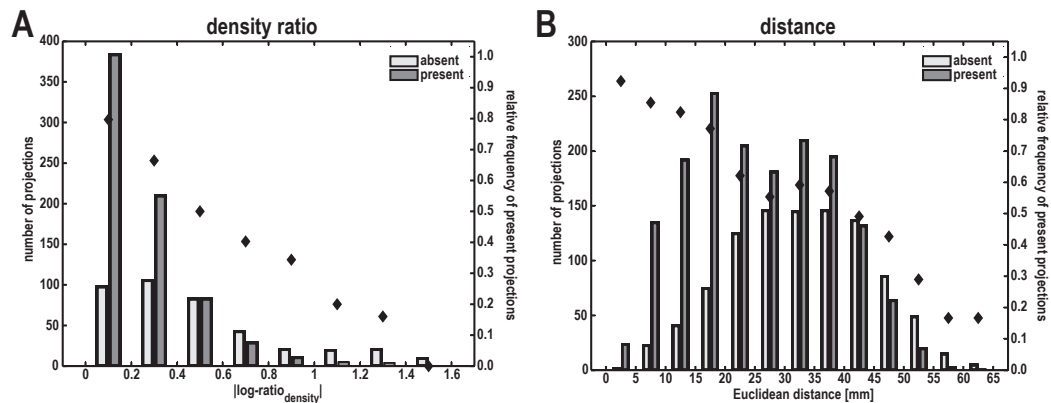


Figure 3.10: Comparison of neuron density similarity and distance for projection frequency. Distribution of absent and present projections across **(A)** neuron density ratio and **(B)** Euclidean distance. Absolute numbers of absent and present projections (bars) are depicted alongside the corresponding relative frequency of present projections (diamonds).

The best classification performance among the six combinations of one or two measures was obtained from the combination of the log-ratio of neuron density (i.e., density similarity) with Euclidean distance. This pairing was superior to all other combinations; its accuracy, precision and negative predictive value were not exceeded at comparable thresholds, and overall performance as quantified by the mean Youden index J was worse for all other combinations (mean \pm standard deviation: $J(|\log\text{-ratio}_{\text{density}}| \& \text{distance}) = 0.75 \pm 0.04$; $J(\text{distance} \& |\log\text{-ratio}_{\text{thickness}}|) = 0.51 \pm 0.13$; $J(|\log\text{-ratio}_{\text{density}}| \& |\log\text{-ratio}_{\text{thickness}}|) = 0.11 \pm 0.03$; $J(|\log\text{-ratio}_{\text{density}}|) = 0.0 \pm 0.0$; $J(\text{distance}) = 0.07 \pm 0.03$; $J(|\log\text{-ratio}_{\text{thickness}}|)$: no predictions at thresholds above $p_{\text{present}} = 0.775$; see Supplementary Figure C.1 for the underlying distribution of true positive rate and false positive rate and Supplementary Figure C.2 for a detailed depiction of the Youden index J across all thresholds). Including all three structural measures as predictive variables did not improve classification accuracy or overall performance as assessed by the mean Youden index ($J(|\log\text{-ratio}_{\text{density}}| \& \text{distance} \& |\log\text{-ratio}_{\text{thickness}}|) = 0.76 \pm 0.04$, Figure 3.11C). A Kruskal-Wallis-test showed that the distributions of the Youden index J were significantly different between the combinations of the structural measures ($H = 549.2$, $p < 0.001$). *Post hoc* tests (Bonferroni-corrected for multiple comparisons) revealed that the distributions of the combination of the log-ratio of neuron density and Euclidean distance ('density, distance') and the combination of the log-ratio of neuron density, Euclidean distance and the log-ratio of thickness ('density, distance, thickness') were not significantly different from each other ($p > 0.05$), while the combination of the log-ratio of neuron density and Euclidean distance had a higher mean J than all other combinations ($p < 0.01$ for all pair-wise tests).

3.3. Comparison of the architectonic type principle, the distance model and the thickness model in the macaque cortex

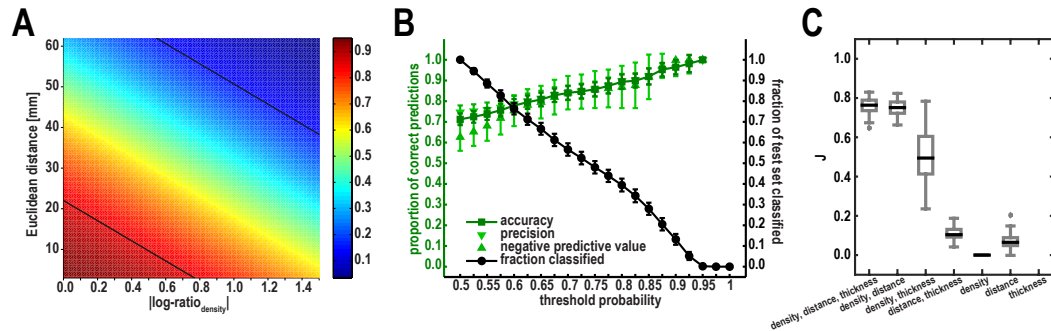


Figure 3.11: Classification of projection existence in the macaque cortex from neuron density similarity and Euclidean distance. **(A)** Posterior probability of a projection being present resulting from training the support vector machine classifier on all projections. Black lines are positioned at $p_{\text{present}} = 0.85$ and $p_{\text{present}} = 0.15$. Also see Supplementary Table D.3 for predictions made about unsampled projections at these thresholds. **(B)** Cross-validated classification performance at different thresholds. Mean prediction accuracy for projections that were predicted to be present and absent (light green) as well as overall mean prediction accuracy (dark green) are shown. Also shown is the fraction of the test set that was classified at each threshold (black). Error bars indicate standard deviations. **(C)** Youden index J for all combinations of structural measures. Distribution of mean J across thresholds $p_{\text{present}} = 0.85$ to $p_{\text{present}} = 1.00$ for all 100 rounds of cross-validation. Boxplots indicate median (text) by a black bar and outliers by grey circles.

According to these results, we adopted the combination of the absolute log-ratio of neuron density and Euclidean distance as predictive variables for our probabilistic model. Figure 3.11A depicts the posterior probability for a projection to be present across the predictive variable space for this feature combination. Cross-validated classification performance across the evaluated thresholds is shown in the remainder of Figure 3.11. As shown in Figure 3.11B, classification accuracy quickly exceeded 80%, with a sizable fraction of the test set being classified. At higher thresholds, accuracy notably surpassed 90%, although this was accompanied by a decrease in the fraction of classified observations. As shown in Supplementary Figure C.1, higher thresholds were associated with a consistent decrease in the rate of false positive predictions at an overall high rate of true positive predictions, resulting in a favourable Youden index J (Figure 3.11C).

Classification performance at all thresholds reliably exceeded chance performance as assessed by a permutation analysis. The permutation analysis revealed a classification performance from nonsensical labels that showed a relatively uniform accuracy of about 65% across tested thresholds. True positive rate and false positive rate equalled 1 across all thresholds, resulting in a Youden index $J = 0.0 \pm 0.0$ for all thresholds.

Using the posterior probabilities obtained by the trained classifier (Figure 3.11A), we were able to make predictions about the status of projections between area pairs that

3.3. Comparison of the architectonic type principle, the distance model and the thickness model in the macaque cortex

were considered as unknown in the considered data set (Markov et al., 2014a). We classified unknown projections at the threshold $p_{\text{threshold}} = 0.85$, as indicated by the black lines in Figure 3.11A. Projections predicted to be absent or present are listed in Supplementary Table D.3.

3.3.4 Relation of architecture with connection topology

We found that nodal network properties of cortical areas were related to the areas' architectonic differentiation. Specifically, areas belonging to the structural network core had lower neuron density than non-core areas ($t(22) = 2.9$, $p < 0.01$, $r = 0.52$, Figure 3.12A). Note that the difference in density between non-core and core areas remained significant if the outlier in the non-core areas (which is area V1) was removed. Given that a major defining feature of core areas is their high degree (i.e., the large total number of connections), we tested whether this observation was indicative of a general relationship between architectonic differentiation and the connectivity of areas. This analysis revealed that neuron density was strongly correlated with areal degree of connectivity ($r = -0.60$, $p < 0.01$, Figure 3.12B). Note that this correlation remained significant if a rank correlation was computed instead, removing differences in magnitude ($\rho = -0.47$, $p = 0.019$). The correlation reached the significance threshold if the data point in the lower right of Figure 3.12B (area V1, same data point as the outlier in Figure 3.12A) was removed ($r = -0.41$, $p = 0.0509$).

Additionally, we tested whether the same relationships could be observed for cortical thickness. Here the results were inconsistent. While cortical thickness did not differ between core and non-core areas ($t(27) = -2.0$, $p > 0.05$, $r = 0.35$), thickness was moderately correlated with the area degree of cortical areas ($r = 0.38$, $p < 0.05$).

Furthermore, we compared the neuron density and cortical thickness of five structural network modules that are related to spatial and functional sub-divisions of the cortex (specifically, comprising frontal, temporal, somato-motor, parieto-motor and occipito-temporal regions). These modules or clusters are characterised by denser structural connectivity within than between the modules (Hilgetag et al., 2000a). Module assignments were reported by Goulas and colleagues (2014b), who delineated the modules for the edge-complete subgraph of the 29 injected cortical areas (i.e., 29×29 cortical areas) (Markov et al., 2014a) using a spectral decomposition algorithm. We found that the network modules differed in their neuron density ($H = 13.7$, $p < .01$), but not in their cortical thickness ($H = 7.2$, $p > 0.05$). *Post hoc* tests, Bonferroni-corrected for multiple comparisons, revealed that the frontal module had a lower

3.3. Comparison of the architectonic type principle, the distance model and the thickness model in the macaque cortex

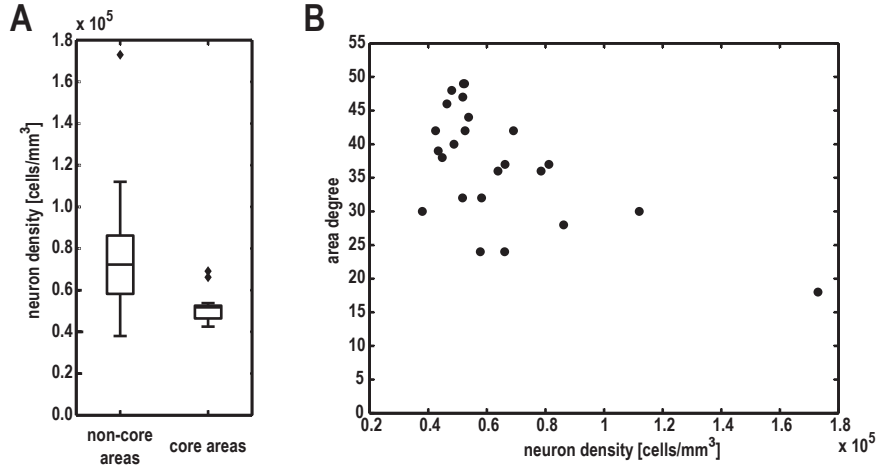


Figure 3.12: Variation of topological properties with neuron density in the macaque cortex. **(A)** Areas that were identified as belonging to a structural core network by Ercsey-Ravasz and colleagues (2013) had a significantly lower neuron density than non-core areas. **(B)** The number of connections maintained by an area (area degree) decreased with increasing neuron density.

neuron density than the occipito-temporal module ($t(13) = -3.8$, $p = 0.002$, $r = 0.73$, with a corrected significance threshold of $\alpha_{\text{adj}} = 0.005$); all other pairwise differences in neuron density between the modules were not significant after correcting for multiple comparisons.

3.3.5 Laminar patterns of projection origins

We observed a strong correlation between the fraction of labelled neurons originating in supragranular layers ($N_{\text{SG}}\%$) and $\log\text{-ratio}_{\text{density}}$ ($r = 0.59$, $p < 0.001$, Figure 3.13A), as well as a moderate correlation between $N_{\text{SG}}\%$ and $\log\text{-ratio}_{\text{thickness}}$ ($r = -0.42$, $p < 0.001$, Figure 3.13B). Given the strong correlation between the neuron density ratio and cortical thickness ratio, we computed a partial correlation of $N_{\text{SG}}\%$, $\log\text{-ratio}_{\text{density}}$, and $\log\text{-ratio}_{\text{thickness}}$ to assess the relative contribution of each variable. The partial correlation revealed that the correlation between thickness ratio and laminar patterns was mainly driven by the neuron density ratio, since the correlation did not reach significance when controlled for neuron density similarity ($r = 0.06$, $p > 0.05$). In contrast, the correlation between the neuron density ratio and laminar patterns was still significant when controlled for the cortical thickness ratio ($r = 0.43$, $p < 0.001$). Additionally, both $N_{\text{SG}}\%$ ($r = 0.09$, $p > 0.05$, Figure 3.13C) and $|N_{\text{SG}}\%|$ ($r = 0.003$, $p > 0.05$, Figure 3.13D) were independent of distance. Thus, the only

3.4. Neuron density is a better predictor of cortico-cortical connectivity than cellular morphological measures

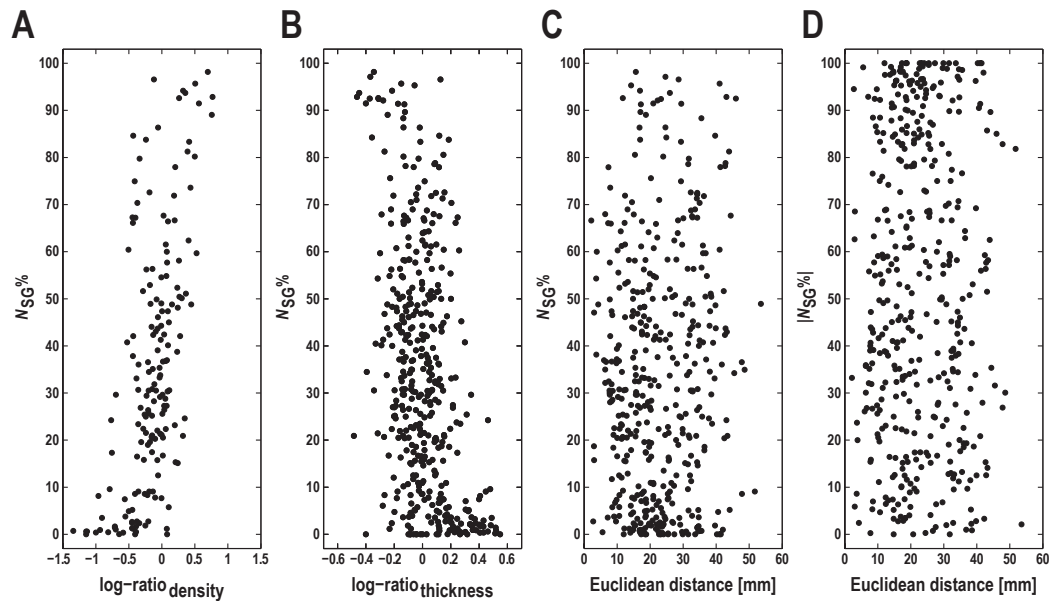


Figure 3.13: Variation of laminar patterns of projection origins with structural measures in the macaque cortex. The fraction of labelled projection neurons originating from supra-granular layers, $N_{SG}\%$, was strongly correlated with $\log\text{-ratio}_{density}$ (A) and moderately correlated with $\log\text{-ratio}_{thickness}$ (B). Neither $N_{SG}\%$ nor $|N_{SG}\%|$ was correlated with Euclidean distance (C,D).

structural measure that was systematically associated with laminar projection patterns was the architectonic similarity of linked areas.

Results did not change qualitatively if a less conservative threshold of 10 constituting neurons (instead of 20 neurons) was applied to determine which projections were excluded from the analyses to guard against unreliable information about the laminar distribution of projection origins.

This section has been published in Beul et al. (2017).

3.4 Neuron density is a better predictor of cortico-cortical connectivity than cellular morphological measures

Recent studies have suggested that inter-areal connectivity may be related to a variety of macroscopic as well as microscopic architectonic features of cortical areas. However, it is unclear how these features are inter-dependent and which of them

3.4. Neuron density is a better predictor of cortico-cortical connectivity than cellular morphological measures

	Neuron density		Soma size		Spine count		Spine density	
	<i>r</i>	p-value	<i>r</i>	p-value	<i>r</i>	p-value	<i>r</i>	p-value
Soma size	-0.63	0.0005	-	-	-	-	-	-
Spine count	-0.54	0.0028	0.56	0.0016	-	-	-	-
Spine density	-0.51	0.0056	0.46	0.0130	0.91	<.0001	-	-
Dendritic tree size	-0.57	0.0012	0.55	0.0017	0.57	0.0005	0.32	0.0679

Table 3.1: Correlation between structural measures in the macaque cortex. Pearson correlation coefficients *r* and associated *p*-values for correlations between neuron density and the morphological measures. Bonferroni correction for multiple tests results in an adjusted significance threshold of $\alpha_{adj} = 0.05/10 = 0.005$.

most strongly and fundamentally relate to structural cortico-cortical connectivity. We systematically investigated the relation of a range of microscopic and macroscopic architectonic features of cortical organisation, namely layer 3 pyramidal cell soma cross section, dendritic synapse count, dendritic synapse density and dendritic tree size as well as area neuron density, to multiple properties of cortico-cortical connectivity. In addition, we included spatial proximity, quantified as geodesic distance, as a sixth structural measure. Importantly, relationships were investigated by multi-variate analyses to account for the interrelations of features.

3.4.1 Macroscopic and microscopic morphological measures are interrelated

The macroscopic and microscopic morphological measures were strongly correlated with each other, with the possible exception of dendritic spine density. When the standard significance threshold of $\alpha = 0.05$ was applied, all correlations but one (dendritic spine density with dendritic tree size) were statistically significant. Using a Bonferroni correction for multiple tests resulted in an adjusted significance threshold of $\alpha_{adj} = 0.05/10 = 0.005$. Under this criterion, the significance of all but two correlations remained unaffected. Only the correlation of dendritic spine density with neuron density and with soma cross section lost statistical significance. Table 3.1 summarises these results. Since the morphological measures presented such strong interrelations, we chose our methods of analysis accordingly in the following assessment of connectivity features, relying on procedures that took all measures into account conjointly.

3.4. Neuron density is a better predictor of cortico-cortical connectivity than cellular morphological measures

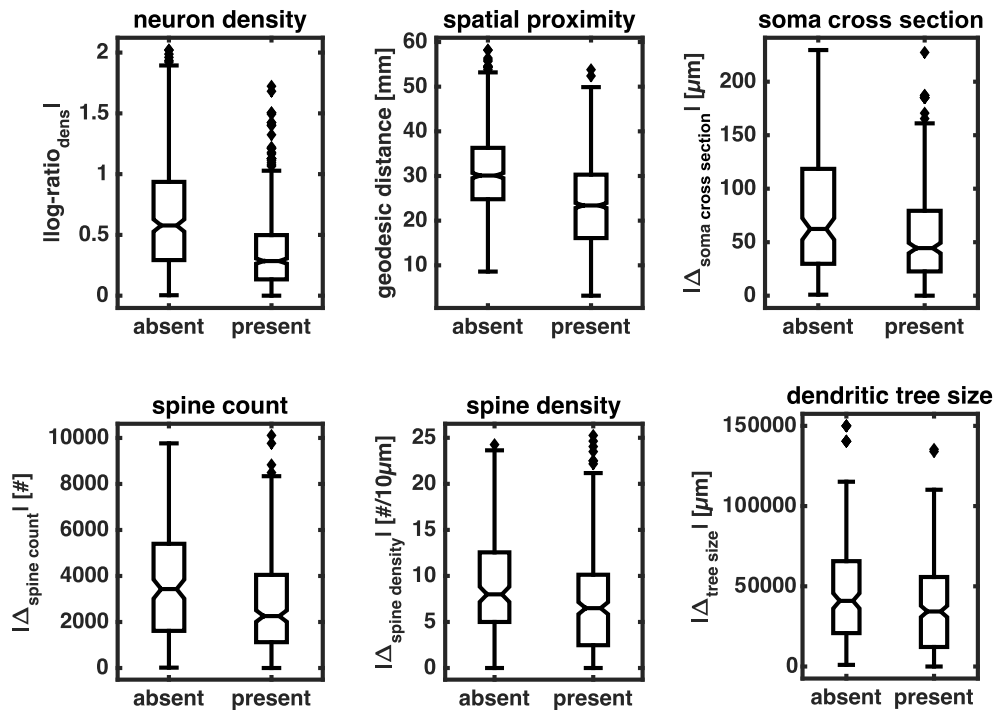


Figure 3.14: Relative structural measures differ between connected and unconnected pairs of areas in the macaque cortex. Box plots show distributions of absolute values of relative structural measures for area pairs without (absent) and with (present) a linking projection. Indicated are median (line), interquartile range (box), data range (whiskers) and outliers (diamonds, outside of 2.7 standard deviations). See Table 3.2 for a summary.

3.4.2 Neuron density is most consistently related to the existence of projections

To assess whether the six structural measures were distributed differently across absent and present projections, we computed independent samples t-tests, using the undirected, absolute values of the structural measures (Figure 3.14, Table 3.2). These showed that connected cortical areas had smaller neuron density ratios than areas that were not linked. Similarly, linked areas were separated by smaller distances than unconnected areas. The differences between areas in the four morphological measures were also smaller if areas were connected than if no connection had been found. Of all the tested structural measures, effect size was largest for neuron density ratio.

To explore these differences in structural measures in more detail, we used multivariate logistic regression analyses to probe how well the structural measures could account for the existence of projections (Figure 3.15, Table 3.3). First, we tested

3.4. Neuron density is a better predictor of cortico-cortical connectivity than cellular morphological measures

	Absent projections		Present projections		t-statistic	p-value	Effect size r
	Mean	Group size	Mean	Group size			
Area-based measures							
log-ratio _{density}	0.67	402	0.35	726	$t_{(1126)} = 14.1$	<.001	0.39
geodesic distance [mm]	30.9	995	23.4	1615	$t_{(2608)} = 20.2$	<.001	0.37
Cellular morphological measures							
Δ soma size [μm^2]	71.7	190	59.0	332	$t_{(520)} = 2.8$	0.005	0.12
Δ spine count [#]	3525	205	2743	339	$t_{(542)} = 4.2$	<.001	0.18
Δ spine density [#/ $10\mu\text{m}$]	8.9	205	7.4	339	$t_{(542)} = 3.0$	0.003	0.13
Δ tree size [μm^2]	48420	220	38060	374	$t_{(592)} = 3.8$	<.001	0.15

Table 3.2: Structural measures in connected and unconnected pairs of areas in the macaque cortex. Absolute values of relative structural measures are averaged across area pairs without (absent) and with (present) a linking projection. T-statistics, p-values and effect size r are results of two-tailed independent samples t-tests comparing the two respective distributions for equal means. See Figure 3.14 for box plots of the underlying distributions.

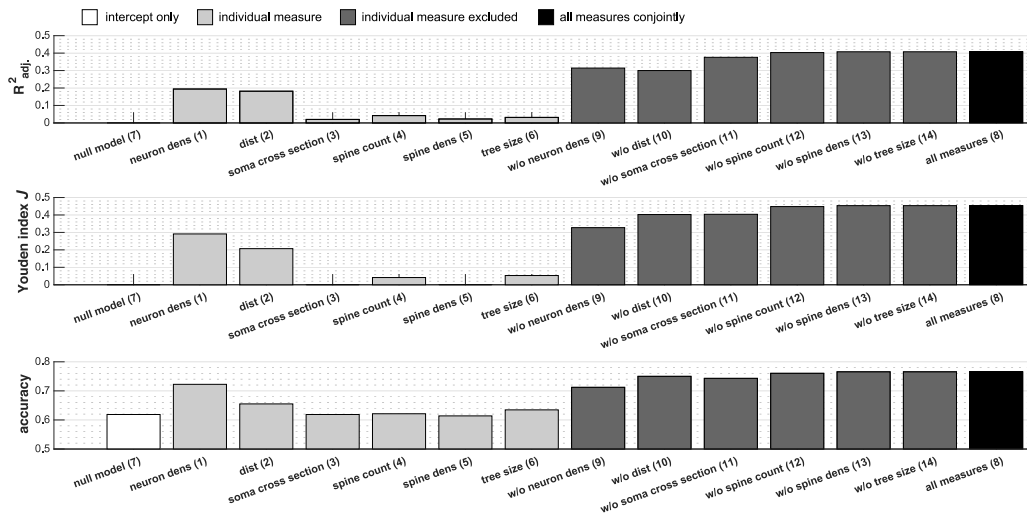


Figure 3.15: Classification of connection existence by logistic regression in the macaque cortex. Projection existence was classified using logistic regression analyses, which included different combinations of the structural measures as covariates. The classification performance measures adjusted R^2 , Youden index J and prediction accuracy are depicted for all logistic regressions. See Table 3.3 for regression coefficients and test statistics of all regression analyses. Enumeration corresponds to Table 3.3.

3.4. Neuron density is a better predictor of cortico-cortical connectivity than cellular morphological measures

	Regression covariate	t-statistic	p-value	R ² _{adj}	J	accuracy	# observations	
Covariates included individually								
(1)	 log-ratio_{density} 	-0.81	-11.6	0.0000	0.194	0.291	0.723	1128
(2)	geodesic distance	-0.86	-17.5	0.0000	0.182	0.207	0.655	2610
(3)	 Δsoma size 	-0.25	-2.8	0.0057	0.020	-0.018	0.619	522
(4)	 Δspine count 	-0.39	-4.1	0.0000	0.042	0.041	0.621	544
(5)	 Δspine density 	-0.28	-3.0	0.0028	0.022	-0.001	0.614	544
(6)	 Δtree size 	-0.33	-3.7	0.0002	0.032	0.053	0.635	594
(7)	intercept	0.48	12.0	0.0000	0.000	0.000	0.619	2610
(8) Covariates included simultaneously								
	 log-ratio_{density} 	-0.74	-4.7	0.0000	0.408	0.453	0.766	384
	geodesic distance	-0.90	-5.8	0.0000				
	 Δsoma size 	0.54	3.2	0.0016				
	Δspine count	-0.34	-1.3	0.1798				
	Δspine density	-0.01	0.0	0.9667				
	Δtree size	0.00	0.0	0.9833				
(9) log-ratio_{density} excluded								
	geodesic distance	-1.06	-8.4	0.0000	0.314	0.327	0.712	476
	Δsoma size	0.19	1.5	0.1333				
	Δspine count	0.06	0.3	0.7728				
	Δspine density	-0.36	-1.9	0.0550				
	 Δtree size 	-0.29	-2.3	0.0229				
(10) geodesic distance excluded								
	 log-ratio_{density} 	-1.00	-7.0	0.0000	0.300	0.403	0.750	384
	 Δsoma size 	0.36	2.5	0.0133				
	 Δspine count 	-0.58	-2.4	0.0144				
	Δspine density	0.14	0.7	0.4903				
	Δtree size	0.07	0.5	0.6181				
(11) Δsoma size excluded								
	 log-ratio_{density} 	-0.46	-3.6	0.0003	0.376	0.404	0.743	432
	geodesic distance	-0.85	-6.2	0.0000				
	Δspine count	-0.20	-0.9	0.3561				
	Δspine density	0.01	0.0	0.9606				
	Δtree size	-0.09	-0.6	0.5549				
(12) Δspine count excluded								
	 log-ratio_{density} 	-0.72	-4.6	0.0000	0.403	0.448	0.760	384
	geodesic distance	-0.92	-6.1	0.0000				
	 Δsoma size 	0.50	3.0	0.0025				
	Δspine density	-0.23	-1.5	0.1232				
	Δtree size	-0.09	-0.6	0.5514				
(13) Δspine density excluded								
	 log-ratio_{density} 	-0.74	-4.7	0.0000	0.408	0.453	0.766	384
	geodesic distance	-0.90	-5.9	0.0000				

Table 3.3: Classification of connection existence by logistic regression.

3.4. Neuron density is a better predictor of cortico-cortical connectivity than cellular morphological measures

		Regression			R^2_{adj}	J	accuracy	# observations
	covariate	t-statistic	p-value					
(13)	$\Delta_{\text{soma size}}$	0.54	3.2	0.0015				
cont.	$\Delta_{\text{spine count}}$	-0.35	-2.0	0.0407				
	$ \Delta_{\text{tree size}} $	0.01	0.0	0.9695				
(14)	$\Delta_{\text{tree size}}$ excluded							
	$\log\text{-ratio}_{\text{density}}$	-0.74	-4.9	0.0000	0.408	0.453	0.766	384
	geodesic distance	-0.90	-5.9	0.0000				
	$\Delta_{\text{soma size}}$	0.54	3.2	0.0016				
	$ \Delta_{\text{spine count}} $	-0.34	-1.5	0.1424				
	$ \Delta_{\text{spine density}} $	-0.01	-0.1	0.9581				

Table 3.3: Classification of connection existence by logistic regression (cont.). We performed logistic regression analyses (enumerated in brackets), each including a different set of the structural measures as covariates and connectivity (grouped into 'absent' and 'present' connections) as the dependent variable. Bold-faced covariates significantly contributed to classification performance as indicated by the p-value. Across all regression analyses, absolute neuron density ratio, geodesic distance and absolute soma cross section difference emerged as meaningful predictors.

each structural measure individually (logistic regressions 1–6), computing logistic regressions with either absolute neuron density ratio, geodesic distance, absolute soma cross section difference, absolute spine count difference, absolute spine density difference, or absolute dendritic tree size difference as the only covariate (plus an intercept term). We also computed a null model that contained only the intercept term (logistic regression 7) and represented chance performance. Second, we included all six measures in conjunction as covariates (logistic regression 8). Third, we removed each measure separately from the conjoint set of covariates (logistic regressions 9–14), so that we computed six logistic regressions with five of the six structural measures as covariates. We assessed model classification performance through the adjusted generalised R^2 , the Youden index J , and prediction accuracy. As presented in Table 3.3, each measure contributed significantly (as indicated by the p-value) to the model performance if it was the only covariate. However, all three performance measures (R^2 , J and accuracy) indicated that classification performance was essentially at chance level for all four cellular morphological measures. Both the neuron density ratio and geodesic distance reached weak classification performance on their own, as indicated by R^2 and J . Accuracy was slightly above chance performance (logistic regression 7) for geodesic distance and clearly above chance performance for the neuron density ratio.

Furthermore, if all measures were included as covariates simultaneously, both macroscopic area-based measures (i.e., neuron density ratio and geodesic distance) con-

3.4. *Neuron density is a better predictor of cortico-cortical connectivity than cellular morphological measures*

tributed significantly to the model performance, while the only cellular morphological measure that remained significant was soma cross section difference. Model performance increased to moderate levels as indicated by all three performance measures. From the overall analysis of model performance, the neuron density ratio emerged as the most important predictive factor for projection existence. This was indicated by the fact that the decline in model performance was largest for the exclusion of neuron density ratio (9), compared to the exclusion of the other five measures (10–14). Logistic regressions 10 and 11 demonstrated that geodesic distance and soma cross section difference also added meaningful information regarding the existence of projections. The other three cellular morphological measures did not contribute any additional information, as can be seen in logistic regressions 12 to 14, where model performance was essentially identical to the full model, although either spine count difference, spine density difference or dendritic tree size difference were excluded. These observations support our conclusion that neuron density was the structural measure that principally related to the existence of connections.

3.4.3 Distance and dendritic tree size are related to projection strength

The strength of cortical projections has been shown to diminish with greater distance of the connected areas (e.g. Ercsey-Ravasz et al., 2013). In a next step, we related all area-based macroscopic as well as cell-based microscopic measures to the strength of projections, $\ln(\text{FLNe})$, using the undirected, absolute values of the structural measures. Figure 3.16 and Table 3.4 show that each measure individually was weakly to moderately correlated with projection strength, with the exception of the absolute soma cross section difference. The strongest correlation was found for geodesic distance. For the absolute neuron density ratio, the negative correlation coefficient signified that areas that were similar in their neuron density (i.e., with a small absolute density ratio) were linked by stronger projections than areas that were less similar in their density (i.e., with a large absolute density ratio). Since most measures were correlated with each other, we entered all measures into a partial Pearson correlation to assess their relative contribution to projection strength while the other measures were controlled for. As shown in Table 3.4, when all other measures were controlled for, geodesic distance and absolute dendritic tree size difference retained their correlation to projection strength, with the respective correlation coefficients even gaining slightly in magnitude. The third measure that was significantly correlated with projection strength in the partial correlation was the absolute soma cross section difference. Neuron density ratio and spine count

3.4. Neuron density is a better predictor of cortico-cortical connectivity than cellular morphological measures

FLNe	Individual correlation		Partial correlation	
	r	p-value	r	p-value
$ \log\text{-ratio}_{\text{density}} $	-0.25	<0.0001	-0.08	0.2158
geodesic distance	-0.49	<0.0001	-0.53	<0.0001
$ \Delta_{\text{soma size}} $	-0.10	0.0787	0.14	0.0319
$ \Delta_{\text{spine count}} $	-0.17	0.0014	0.00	0.9716
$ \Delta_{\text{spine density}} $	-0.12	0.0332	-0.13	0.0527
$ \Delta_{\text{tree size}} $	-0.13	0.0094	-0.19	0.0028
ranked strength	ρ	p-value	ρ	p-value
ranked $ \log\text{-ratio}_{\text{density}} $	0.24	<0.0001	0.11	0.0800
ranked geodesic distance	0.51	<0.0001	0.52	<0.0001
ranked $ \Delta_{\text{soma size}} $	0.17	0.0019	-0.12	0.0656
ranked $ \Delta_{\text{spine count}} $	0.15	0.0050	-0.01	0.8921
ranked $ \Delta_{\text{spine density}} $	0.12	0.0256	0.13	0.0533
ranked $ \Delta_{\text{tree size}} $	0.17	0.0013	0.18	0.0047

Table 3.4: Correlation between projection strength and structural measures in the macaque cortex. Pearson correlation coefficients r and associated p -values for correlations between projection strength, expressed either as $\ln(\text{FLNe})$ or as ranked strengths, and absolute values of relative structural measures or ranked absolute values of relative structural measures. Correlations were assessed both for each measure independently (individual correlation) and while accounting for all other five measures (partial correlation). See Figure 3.16 for scatter plots of the underlying distributions.

difference did not correlate with projection strength if all measures were considered simultaneously. The correlation of spine density difference was close to remaining significant; the magnitude, however, was very weak. These results were mirrored in our analysis of ranked projection strength (Figure 3.16, Table 3.4), where we ranked both the strength of projections (i.e., incoming projections were ordered from strongest to weakest) and the difference measures per target area. Again, all measures were significantly correlated with projection strength if considered individually. The strongest association was again observed for geodesic distance. However, if all other measures were accounted for in a partial correlation, only ranked geodesic distance and the ranked absolute dendritic tree size difference remained significant. All significant correlation coefficients were positive, indicating that weaker projections (with higher rank numbers) were associated with larger absolute differences in the structural measures (with higher rank numbers) between connected areas.

3.4. Neuron density is a better predictor of cortico-cortical connectivity than cellular morphological measures

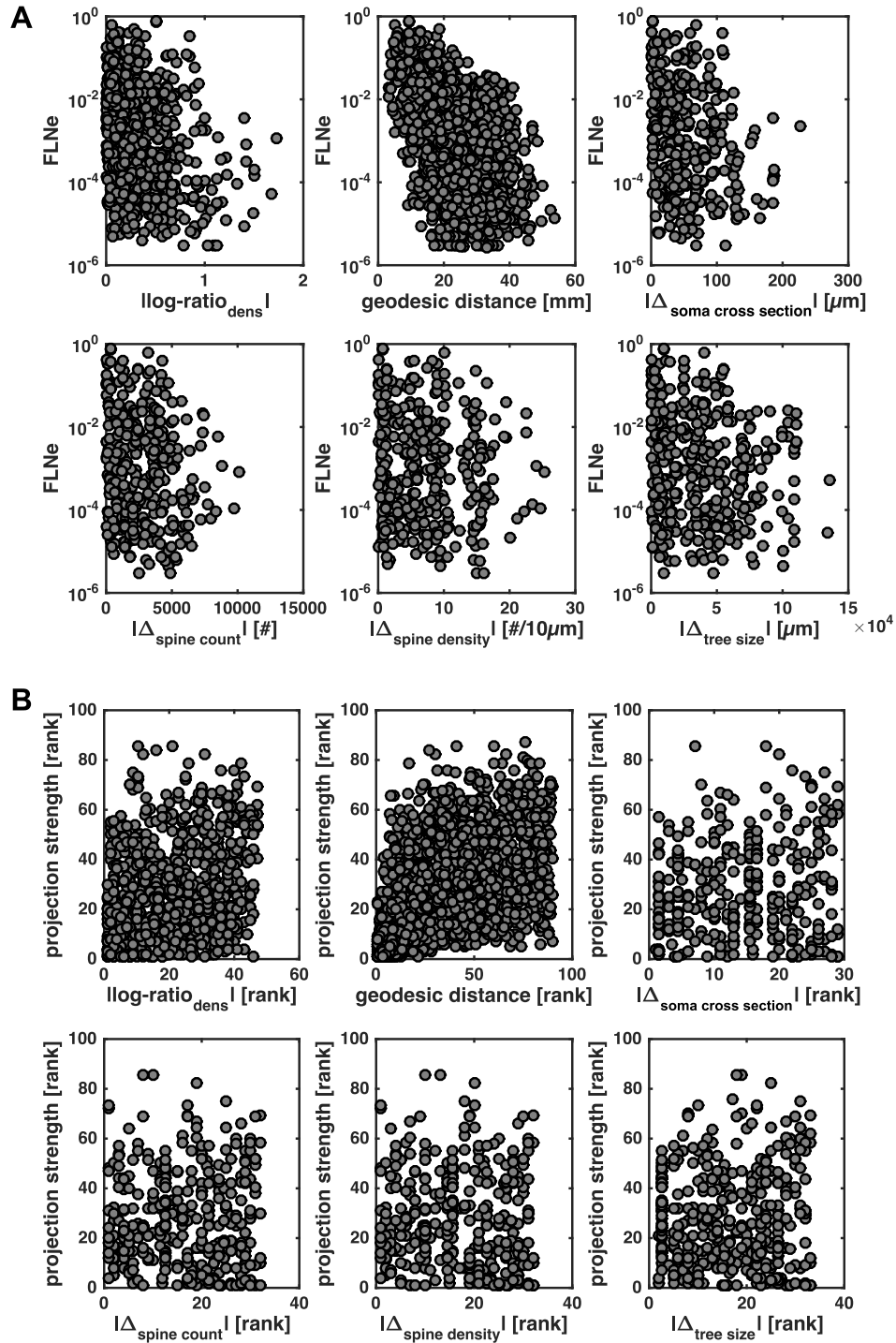


Figure 3.16: Projection strength varies with relative structural measures in the macaque cortex. **(A)** Projection strength for individual projections, FLNe, is shown across absolute values of relative structural measures. **(B)** Ranked projection strength of individual projections is shown across ranked absolute values of relative structural measures. See Table 3.4 for correlation statistics.

3.4.4 Neuron density is consistently related to laminar patterns of projection origins

Our analyses of the extensive projection origin data provided by Chaudhuri and colleagues (2015) show that neuron density is consistently related to the laminar pattern of cortico-cortical projection origins. As seen from Figure 3.17 and Table 3.5, all directed measures were weakly to moderately correlated with the laminar pattern of projection origins expressed as supragranular contribution, $N_{SG}\%$. For the neuron density ratio, the positive correlation coefficient indicated that projections from less dense areas to denser areas had a more infragranular origin, while projections from denser to less dense areas had predominantly supragranular origins. For the cellular morphological measures, the negative correlation coefficient indicated the reverse relationship. However, in a partial Pearson correlation of $N_{SG}\%$ with all measures, except geodesic distance, only neuron density ratio and spine count difference retained significance. Although the p-value of the correlation with soma cross section difference was below the significance threshold, the correlation coefficient changed its sign while remaining at a weak magnitude, indicating that the correlation was volatile and not reliable. Geodesic distance, an undirected measure, was tested for a correlation with an indicator of deviation from bilaminar projection patterns, $|N_{SG}\%|$. This correlation only reached a weak magnitude. To test the effect of additionally controlling the partial Pearson correlation for geodesic distance, we computed a partial Pearson correlation of $|N_{SG}\%|$ with geodesic distance as well as the absolute values of the other five structural measures. Here, absolute neuron density ratio was the only measure that remained significant, retaining its moderate magnitude. In conclusion, the variable found to be significantly and most strongly associated with the laminar pattern of projections across all variations of correlating the structural measures was the neuron density ratio.

3.4.5 Neuron density is correlated with area degree

Since we previously observed that architectonic differentiation related to the topological network property of area degree, we assessed the extent to which this was also true for the four cellular morphological measures. We decided to perform no further analyses of rich-club versus periphery nodes here, because our prior analyses showed that the observed differences in architectonic differentiation between the two sets of areas generalised to the relation between architectonic differentiation and area

3.4. Neuron density is a better predictor of cortico-cortical connectivity than cellular morphological measures

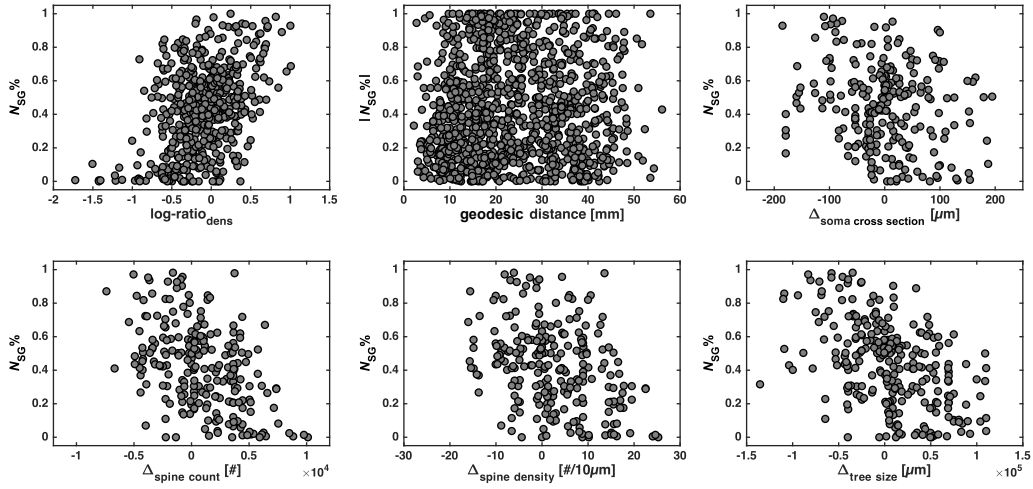


Figure 3.17: Laminar projection patterns vary with relative structural measures in the macaque cortex. Fraction of supragranularly labelled neurons for individual projections, $N_{SG}\%$, is shown across relative structural measures. Note that for geodesic distance, the measure of deviation from columnar laminar patterns, $|N_{SG}\%|$, is shown instead. See Table 3.5 for correlation statistics.

	Individual correlation with $N_{SG}\%$		Partial correlation with $N_{SG}\%$		Partial correlation with $ N_{SG}\% $	
	r	p-value	r	p-value	r	p-value
$ \log\text{-ratio}_{\text{dens}} $	0.43	<.0001	0.40	<.0001	$ \log\text{-ratio}_{\text{dens}} $	0.38 <.0001
geodesic distance*	0.12	0.0001	-/-	-/-	geodesic distance*	-0.07 0.3651
$ \Delta_{\text{soma size}} $	-0.21	0.0009	0.20	0.0090	$ \Delta_{\text{soma size}} $	-0.03 0.7406
$ \Delta_{\text{spine count}} $	-0.47	<.0001	-0.18	0.0206	$ \Delta_{\text{spine count}} $	0.09 0.2708
$ \Delta_{\text{spine density}} $	-0.35	<.0001	0.08	0.2910	$ \Delta_{\text{spine density}} $	0.07 0.3658
$ \Delta_{\text{tree size}} $	-0.47	<.0001	-0.11	0.1428	$ \Delta_{\text{tree size}} $	0.02 0.7975

Table 3.5: Correlation between laminar projection patterns and structural measures in the macaque cortex. Pearson correlation coefficients r and associated p -values for correlations between $N_{SG}\%$ and relative structural measures are reported. Correlations were assessed both for each measure independently (individual correlation with $N_{SG}\%$) and while accounting for four other measures (partial correlation with $N_{SG}\%$). Geodesic distance could not be correlated with $N_{SG}\%$, because it is an undirected measure. Instead, the individual correlation of geodesic distance with laminar patterns (marked ‘*’) was computed using $|N_{SG}\%|$, which indicates deviation from bilaminar projection patterns. Accordingly, we also computed a partial correlation accounting for all six structural measures at once, which had to include the absolute values of the relative structural measures (partial correlation with $|N_{SG}\%|$). See Figure 3.17 for scatter plots of the underlying distributions.

3.4. Neuron density is a better predictor of cortico-cortical connectivity than cellular morphological measures

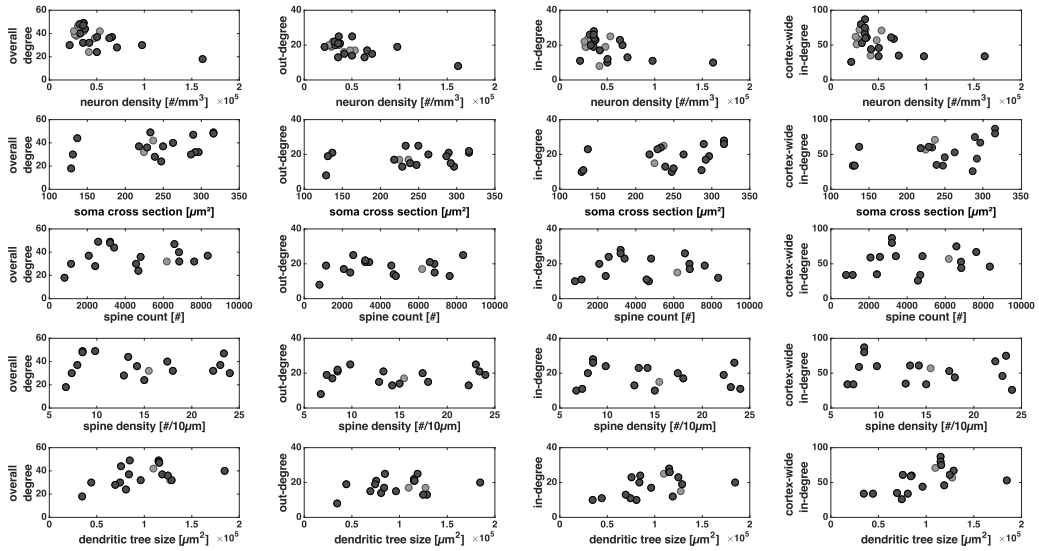


Figure 3.18: Area degree varies with structural measures in the macaque cortex. The number of projections an area maintains, area degree, is shown across structural measures for each area. Depicted are overall degree, out-degree and in-degree on the 29×29 edge-complete subgraph, as well as cortex-wide in-degree. See Table 3.6 for correlation statistics. All data points (black and grey) were considered in the individual correlations reported there, while only black data points were considered in the partial correlation.

degree that we analyse here.

As done previously (Scholtens et al., 2014; Section 3.3), we examined the correlation of structural measures with overall area degree, the number of connections a cortical region maintains (within the 29×29 edge-complete subgraph). We tested five of the six measures. Spatial proximity was excluded, because geodesic distance is inherently relational and cannot be related to a measure pertaining to a single area. Figure 3.18 and Table 3.6 show that of the five tested measures, only neuron density was significantly correlated with overall area degree (this correlation of neuron density was reported already in Section 3.3), although the correlation of dendritic tree size with overall degree was very close to significant. Using a Bonferroni correction for multiple tests resulted in an adjusted significance threshold of $\alpha_{\text{adj}} = 0.05/5 = 0.01$. Neuron density remained significantly correlated with overall area degree also under this criterion. Similarly, in a partial Pearson correlation, only neuron density was significantly correlated with overall area degree, at a strong magnitude.

In addition to overall area degree, we also considered incoming and outgoing connections separately as in-degree and out-degree (Figure 3.18, Table 3.6). The only measure that was correlated with out-degree (within the 29×29 edge-complete subgraph), either individually or in a partial correlation, was neuron density, at a

3.4. Neuron density is a better predictor of cortico-cortical connectivity than cellular morphological measures

	Individual correlation		Partial correlation	
	<i>r</i>	p-value	<i>r</i>	p-value
Overall degree (29x29)				
Neuron density	-0.60	0.0020	-0.66	0.0202
Soma size	0.39	0.1078	-0.16	0.6124
Spine count	0.12	0.6557	-0.07	0.8181
Spine density	-0.03	0.9127	-0.27	0.3901
Dendritic tree size	0.47	0.0515	0.30	0.3403
Out-degree (29x29)				
Neuron density	-0.61	0.0014	-0.64	0.0260
Soma size	0.25	0.3104	-0.30	0.3497
Spine count	0.16	0.5319	0.02	0.9616
Spine density	0.12	0.6348	-0.13	0.6802
Dendritic tree size	0.28	0.2628	0.01	0.9784
In-degree (29x29)				
Neuron density	-0.44	0.0297	-0.44	0.1494
Soma size	0.38	0.1166	0.03	0.9170
Spine count	0.05	0.8434	-0.11	0.7262
Spine density	-0.13	0.6101	-0.26	0.4087
Dendritic tree size	0.47	0.0484	0.39	0.2129
In-degree (cortex-wide)				
Neuron density	-0.41	0.0452	-0.27	0.3999
Soma size	0.43	0.0769	0.19	0.5509
Spine count	0.15	0.5538	0.07	0.8209
Spine density	-0.11	0.6749	-0.36	0.2442
Dendritic tree size	0.53	0.0240	0.28	0.3771

Table 3.6: Correlation between area degree and structural measures in the macaque cortex. Pearson correlation coefficients *r* and associated *p*-values for correlations between the structural measures for each area and overall area degree (total number of maintained connections), out-degree, in-degree or cortex-wide in-degree. Correlations were assessed both for each measure independently (individual correlation) and while accounting for the other four measures (partial correlation). Geodesic distance could not be included because it is a relational property which is not defined for individual areas. Bonferroni correction for multiple tests results in an adjusted significance threshold of $\alpha_{adj} = 0.05/5 = 0.01$ for the individual correlations. See Figure 3.18 for scatter plots of the underlying distributions.

strong magnitude, mirroring the results for overall area degree. In-degree (both within the 29×29 edge-complete subgraph and cortex-wide across all 91 areas in the M132 parcellation) was moderately to strongly and significantly correlated with both neuron density and dendritic tree size if the measures were correlated individually. However, in a partial correlation no correlation remained significant. Both neuron density and dendritic tree size retained correlation coefficients of moderate magnitudes, however.

3.4.6 Discarding very weak projections does not affect observed relationships

To exclude the possibility that the reported results were mainly driven by very weak projections that are potentially spurious, we repeated all analyses with a smaller connectivity data set, from which projections that did not have at least five constituent axons were excluded (Supplementary Tables D.5 through D.8). All analyses reported in these supplementary tables were performed in the same way as the corresponding main analyses (see Tables 3.2 through 3.4, and 3.6), but on a reduced connectivity data set. Results corresponding to Table 3.1 are not presented here, because the structural measures did not change through applying a cutoff to the connectivity data set. Results corresponding to Table 3.5 are not presented here, because we applied a cutoff of 20 constituent axons to the connectivity data set in the main analyses of laminar projection patterns and no further connections were excluded by the lower threshold of five constituent axons. None of the reported results was affected substantially by excluding very weak projections, and the same conclusions can be drawn as from the main analyses.

This section has been published in Beul and Hilgetag (2019a).

3.5 The architectonic type principle captures laminar projection patterns early in development

It has been suggested that the architectonic type principle arises in ontogenesis, hence it would be expected that it can already be observed in early stages of cortical development. Here, we explore the extent to which the architectonic type principle is already applicable to laminar patterns of projection origins in immature states of cortical development. To assess whether laminar patterns of projection origins were correlated with relative architectonic differentiation of connected areas in the immature cortex of the macaque monkey, we combined five different resources providing measures of laminar projection patterns (Kennedy et al., 1989; Batardi re et al., 2002; Chaudhuri et al., 2015; Magrou et al., 2018) and architectonic differentiation (Hilgetag et al., 2016).

We considered two measures of architectonic differentiation, specifically architectonic type and neuron density. As mentioned previously, architectonic type is an ordinal

3.5. *The architectonic type principle captures laminar projection patterns early in development*

measure of differentiation based on a cortical area's overall appearance in different types of tissue stains, while neuron density is measured stereologically and has been shown to be a very distinctive marker (Dombrowski et al., 2001; Section 3.4). Both measures are strongly correlated with each other (in the sample of areas considered in the analyses presented here, Spearman rank correlation coefficient $\rho = 0.96$, $p = 3.9e-8$). Architectonic type was available for all considered areas, and neuron density was available for all 4 areas considered by Kennedy and colleagues (1989), for 10 of the 11 areas considered by Batardière and colleagues (2002), as well as for 14 of the 20 areas considered by Magrou and colleagues (2018). We report results for both measures to present a more comprehensive set of observations that is more robust against possible shortcomings of a particular measure.

3.5.1 Immature projection patterns correlate with adult differentiation measures

When immature (i.e., prenatal and neonatal) laminar patterns of projection origins were compared to their eventual adult composition, a clear correspondence could be observed, such that the bias in origin layers found in the immature cortex largely persisted in the adult cortex (Figure 3.19A, Supplementary Table D.10). Consistent with this observation, immature patterns of laminar origins were strongly correlated with the difference in architectonic differentiation between connected areas (Figure 3.19B,C, Supplementary Table D.10). For comparison, we also show the relation between adult $N_{SG}\%$ -values and difference in architectonic differentiation in these panels. Note that the slope of the regression lines becomes steeper for adult laminar patterns compared to immature patterns, indicating that an initial asymmetry in laminar contribution becomes more pronounced with maturation. The relation between immature and adult $N_{SG}\%$ -values becomes even clearer in Figure 3.19D and Figure 3.19E (also see Supplementary Table D.10), though, which show that the amount of remodelling which a projection undergoes from the immature to the adult state was also correlated with the connected areas' relative architectonic differentiation. This implies that later processes serve to refine a projection's laminar origins further towards a laminar bias that was already present from the outset.

3.5. The architectonic type principle captures laminar projection patterns early in development

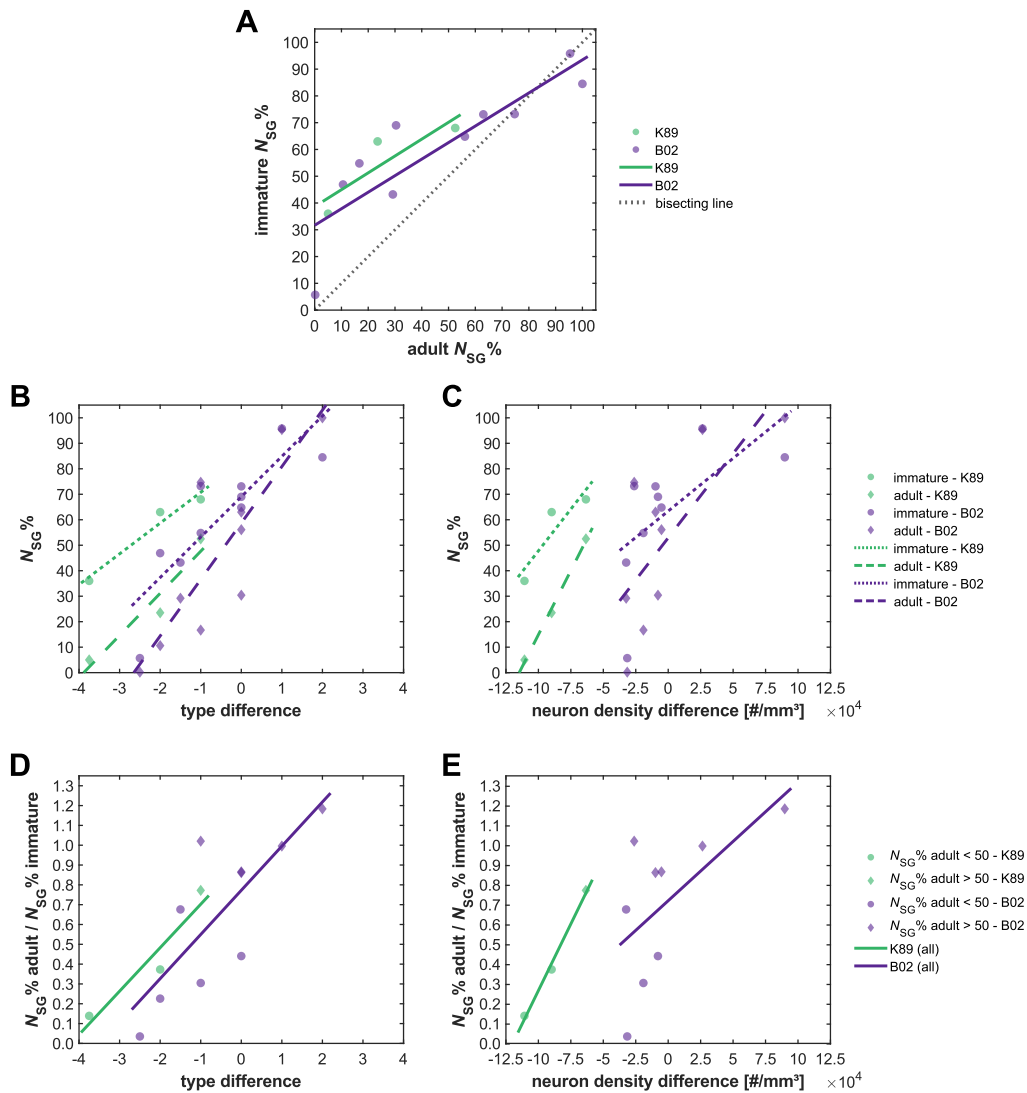


Figure 3.19: Lamina projection patterns in immature macaque cortex. Contribution of supragranularly labelled neurons ($N_{SG}\%$) to projections targeting areas V1 (K89, neonatal) and V4 (B02, fetal) in the immature macaque cortex. **(A)** Immature $N_{SG}\%$ in relation to the respective adult $N_{SG}\%$. **(B)** $N_{SG}\%$ for both immature and adult cortex in relation to architectonic differentiation measured as difference in architectonic type, where $\text{type difference} = \text{type}_{\text{source area}} - \text{type}_{\text{target area}}$. **(C)** $N_{SG}\%$ for both immature and adult cortex in relation to architectonic differentiation measured as difference in neuron density, where $\text{neuron density difference} = \text{density}_{\text{source area}} - \text{density}_{\text{target area}}$. **(D)** Fraction of supragranularly labelled projection neurons observed in the immature cortex that remains in the adult cortex in relation to difference in architectonic type. **(E)** Fraction of supragranularly labelled projection neurons observed in the immature cortex that remains in the adult cortex in relation to difference in neuron density. Generally, the supragranular contribution declines with maturation. That is, in **(D)** and **(E)**, the value of adult $N_{SG}\%$ divided by immature $N_{SG}\%$ is below 1 for most areas. Projection data from K89 (Kennedy et al., 1989) and B02 (Batardière et al., 2002).

3.5.2 Loss of visual input does not substantially alter the gradient of projection patterns

The supragranular contribution to projections in enucleated infant monkeys was strongly correlated with the respective supragranular contribution in intact adult monkeys, especially if connections from highly perturbed area V1 (cf. detailed descriptions in Magrou et al., 2018) were excluded (Figure 3.20A, Supplementary Table D.11). However, there was a tendency towards higher supragranular contribution in the enucleated infants (as most data points are above the bisecting line), especially for projections to area V2. Indeed, a permutation test showed the median change in $N_{SG}\%$ (i.e., enucleated $N_{SG}\%$ - intact $N_{SG}\%$) to be larger for injections in V2 than in V4 ($p = 0.01$, 10^4 permutations). Since the tracer was injected at different ages for projections to V2 and V4, the higher supragranular contribution could be explained by differences in maturation: V2 was injected earlier (at postnatal day 16) than V4 (at postnatal month 10), which may have caused the $N_{SG}\%$ values of projections targeting V4 to be more similar to the intact adult $N_{SG}\%$ values. This hypothesis is in line with the generally higher $N_{SG}\%$ values observed for the prenatal and neonate injections reported by Batardière and colleagues (2002) and Kennedy and colleagues (1989). In principle, a comparison with neonatal projection patterns in intact monkeys would have been preferable to a comparison to adult patterns, but these data are not available for the projections between areas reported by Magrou and colleagues (2018). As it is, it might be argued that the projection patterns after enucleation were even less affected than it appeared here, since the laminar patterns would likely undergo further postnatal changes, similar to the change already observed for injections in the neonatal and the infant cortex. Extrapolating from our analyses in the previous section, a general decline in supragranular contribution with maturation seems realistic, which would increase the correspondence between the $N_{SG}\%$ -values of intact adults and enucleated infants once they matured to adults.

Despite the drastic effects of enucleation on the organisation of the primary visual cortex, the gradual changes in laminar projection patterns that have been reported to align with the relative architectonic differentiation of connected areas could also be observed in enucleated infant monkeys (Figure 3.20B,C, Supplementary Table D.11). The laminar patterns of projections were strongly correlated with the relative architectonic differentiation of two connected areas, both when it was measured as difference in architectonic type and as difference in neuron density. Thus, despite possible changes in projection patterns, the previously observed relation between laminar patterns and relative differentiation still held even after complete loss of visual input. In line with the drastic changes to the organisation of V1 (cf. Magrou

3.6. Mechanistic underpinnings of the architectonic type principle explored by simulation experiments: Existence of connections

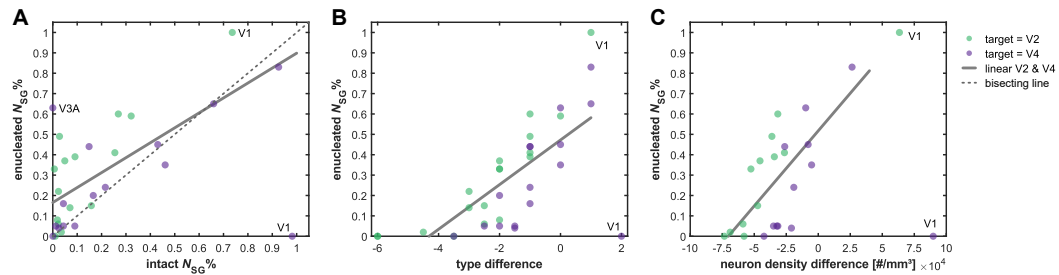


Figure 3.20: Laminar projection patterns in the macaque cortex after enucleation. Contribution of supragranularly labelled neurons ($N_{SG}\%$) to projections targeting areas V2 and V4 in the cortex of enucleated macaque monkeys. **(A)** $N_{SG}\%$ after enucleation in relation to the respective $N_{SG}\%$ in intact monkeys. **(B)** $N_{SG}\%$ after enucleation in relation to architectonic differentiation measured as difference in architectonic type, where type difference = $type_{source\ area} - type_{target\ area}$. **(C)** $N_{SG}\%$ after enucleation in relation to architectonic differentiation measured as difference in neuron density, where neuron density difference = $density_{source\ area} - density_{target\ area}$. Data from V2 and V4 were pooled for correlations and linear regression. Projections originating in V1 were excluded from the linear regression because V1 was affected very strongly by the enucleation and the resulting $N_{SG}\%$ -values are outliers. Projection data from Chaudhuri and colleagues (2015) and Magrou and colleagues (2018).

et al., 2018), projections from V1 appeared to be altered most strongly. While the correlation of supragranular contribution with architectonic type difference or neuron density became stronger if V1 data points were excluded, it was strong and significant even if they were included. This implies, that the establishment of regular laminar projections patterns is largely independent of typical sensory input, with the possible exception of the directly perturbed areas.

3.6 Mechanistic underpinnings of the architectonic type principle explored by simulation experiments: Existence of connections

We explored possible mechanisms that might underlie the emergence of the architectonic type principle in the mammalian cortex using an *in silico* model of cortical development. To this end, we simulated the growth of cortico-cortical connections between areas of different neuron density according to a constant set of growth rules. We evaluated how closely the simulated connectivity corresponded to empirical observations made in mammalian connectomes, when the physical substrate of the connections, that is, the simulated cortical sheet, developed along different spatio-

3.6. Mechanistic underpinnings of the architectonic type principle explored by simulation experiments: Existence of connections

temporal trajectories. To this end, we systematically varied the settings of our *in silico* model to construct a number of variants, which we refer to as spatio-temporal growth layouts (see Figure 1.3, Figure 2.3 and Table 2.1 for an overview). We considered five sets of growth layouts: (1: *realistically oriented density gradient*) planar growth of the cortical sheet, such that cortical areas were added around neurogenetic origins, with new areas having an increasingly higher neuron density (i.e., neuron density increased with distance from a point of origin); (2: *inverse density gradient*) planar growth of the cortical sheet, such that cortical areas were added around neurogenetic origins, but with new areas having increasingly lower neuron density (i.e., neuron density decreased with distance from a point of origin); (3: *radial*) no planar growth of cortical areas on the fringes of the cortical sheet, but gradual addition of neurons at a constant rate across the cortical sheet, which resulted in an ordered gradient of area neuron density that was the same as in sets 1 and 4; (4: *static*) no planar growth of cortical areas, but the same final gradient of area neuron density as in sets 1 and 3; (5: *random*) planar growth of the cortical sheet, such that cortical areas were added around neurogenetic origins, but with no ordered gradient of area neuron density, instead neuron density varied randomly between locations on the cortical sheet. For all five sets, we implemented three growth modes: (*1D 1row*) one-dimensional growth implemented with one row of areas; (*1D 2rows*) one-dimensional growth implemented with two rows of areas; and (*2D*) two-dimensional growth. For all five sets, all three growth modes were implemented with planar growth around two neurogenetic origins. For set 1 (*realistically oriented density gradient*), we additionally implemented each growth mode with one neurogenetic origin as well as three (*1D* growth) or four (*2D* growth) neurogenetic origins. Thus, in total, we considered 21 growth layouts, grouped into five sets according to the spatio-temporal trajectory the cortical sheet traversed.

We first present some general statistics of the simulated connectivity and then go on to characterise how well the relationship between connectivity and the two factors of (relative) neuron density and spatial distance corresponded to previously published empirical observations for the different growth layouts. Finally, we assess how well the different growth layouts predicted empirical connectivity, as an indication of how realistic the simulated connectivity was for a given growth layout (Figure 2.4 provides an outline of this procedure). Table 3.7 gives an overview of all results.

3.6. Mechanistic underpinnings of the architectonic type principle explored by simulation experiments: Existence of connections

set	growth mode	# origins	connectivity between areas of similar neuron density	classification of connections: simulation from simulation	number of connections	classification of connections: empirical from simulation	
						accuracy	Youden index J
realistically oriented gradient	1D 1 row	1	✓	✓	✓	?	✓
	1D 2 rows	1	✓	✓	✓	?	✓
	2D	1	✓	✓	✗	✓	✗
	1D 1 row	2	✓	✓	✓	✓	✓
	1D 2 rows	2	✓	✓	✓	✓	✓
	2D	2	✓	✓	✗	✓	✓
	1D 1 row	3	✓	✓	✓	✓	✓
	1D 2 rows	3	✓	✓	✓	✓	✓
inverse gradient	1D 1 row	2	✓	?	✗	?	?
	1D 2 rows	2	✓	?	✗	✗	✗
	2D	2	✓	?	✗	?	✗
radial	1D 1 row	2	✗	✗	✗	?	✗
	1D 2 rows	2	?	✗	✗	?	✗
	2D	2	✓	✗	✗	✗	✗
static	1D 1 row	2	✗	✗	✗	✗	✗
	1D 2 rows	2	✗	✗	✗	✗	✗
	2D	2	✓	✗	✗	✓	✗
random	1D 1 row	2	✗	✗	✗	?	✗
	1D 2 rows	2	✗	✗	✗	?	✗
	2D	2	✓	✗	✗	✗	✗
corresponding measure			correlation of relative connection frequency vs density difference	McFadden's Pseudo R ² for density difference	correlation of area degree vs density	classification of connection existence in cat and macaque cortex: accuracy	Youden index J

Table 3.7: Summary of correspondence between simulation results and empirical observations. This table provides an estimate of the extent to which the connectivity resulting from each growth layout corresponds to expectations derived from empirically observed phenomena. ✓: good correspondence, ?: inconclusive, ✗: no close correspondence.

3.6.1 Connection statistics

The cortico-cortical networks resulting from the simulations showed realistic levels of overall connectivity, with between 39% and 66% of possible connections present (Figure 3.21A, Supplementary Table D.12). Previously, between 50% and 77% of connections were reported to be present in the macaque and cat cortex (Felleman and Van Essen, 1991; Markov et al., 2014a; Section 3.2). Some 2D growth layouts reached higher levels of connectivity, with up to 87% of possible connections present. This connection density translated into several hundreds of inter-areal connections (Figure 3.21B, Supplementary Table D.12), with between 250 and 400 connections for growth mode *1D 1row* and between 900 and 1500 connections for growth mode *1D 2rows*. Due to the large number of areas, connection numbers were much higher for 2D growth layouts, between 8000 and 18600.

3.6.2 Contributions of distance and density difference to connectivity patterns

We first checked how well the simulated networks corresponded to the empirical observation that a larger fraction of connections is present between regions that are more similar in neuron density, as suggested by the architectonic type principle, and spatially closer to each other. To this end, we computed the relative frequency of present connections (Figure 3.22, Supplementary Table D.12). We then examined how well both factors, absolute density difference and distance, enabled the reconstruction of the simulated networks using logistic regression. Specifically, we assessed these relations by computing McFadden's Pseudo R^2 statistic, which provides a measure of the increase in the model log-likelihood with inclusion of either or both factors compared to a null model (Figure 3.23, Supplementary Table D.12).

Relative frequency of present connections

In general, connections were more likely to be present across smaller distances (Figure 3.22, Supplementary Figure C.4). The relative frequency of present connections was very strongly negatively correlated with the distance between areas. The correlation was significant for all growth layouts, except for the *2D 1origin* growth layout. This effect was due to very weak connections being formed across even

3.6. Mechanistic underpinnings of the architectonic type principle explored by simulation experiments: Existence of connections

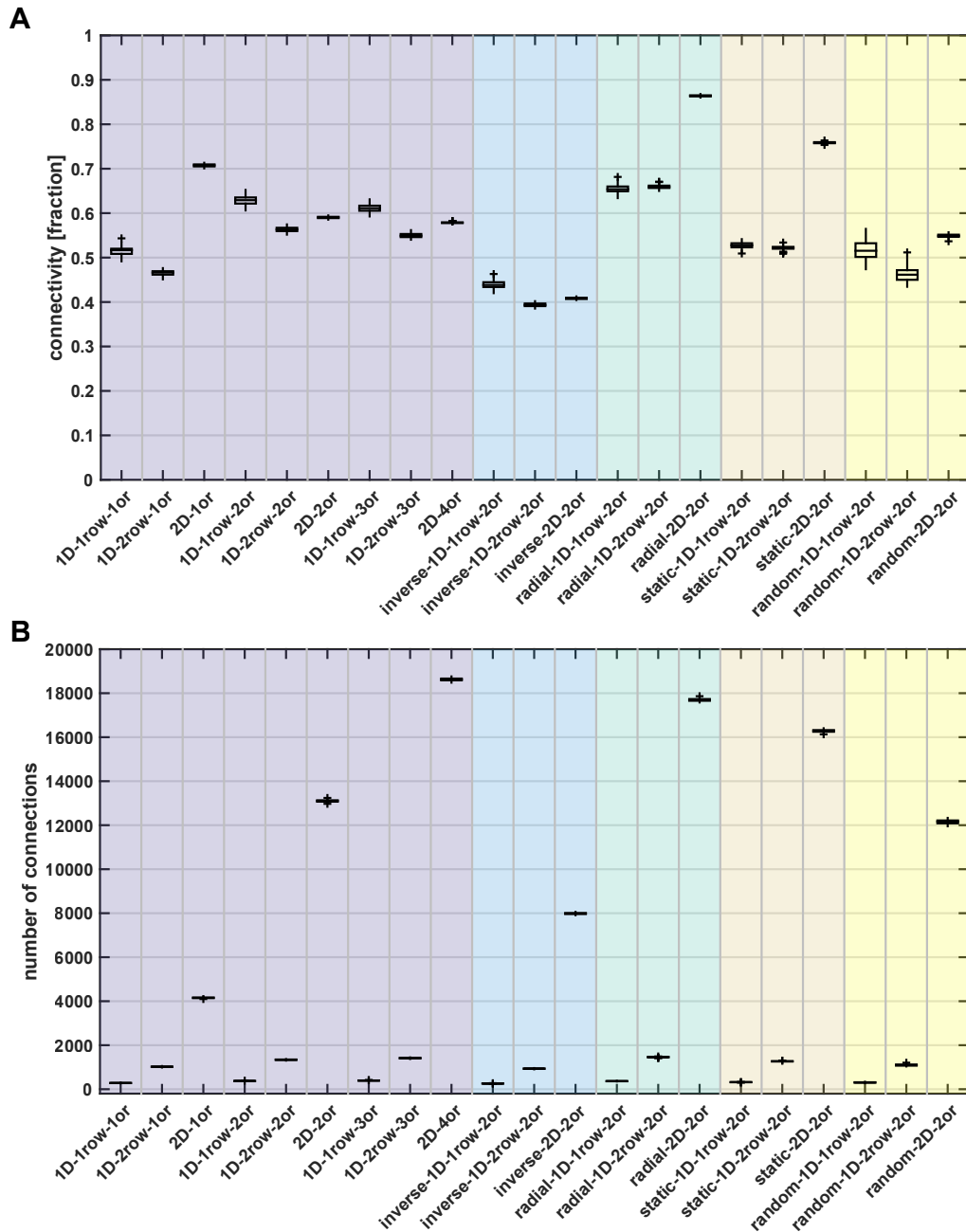


Figure 3.21: Connection statistics of simulation experiments. **(A)** Percentage of connected areas, shown as the fraction of possible connections that are present in the final simulated network. **(B)** Total number of connections among all areas. Box plots show distribution across 100 simulation instances per growth layout, indicating median (line), interquartile range (box), data range (whiskers) and outliers (crosses, outside of 2.7 standard deviations). See Supplementary Table D.12 for a summary. Abbreviations and background colours as in Table 2.1.

3.6. Mechanistic underpinnings of the architectonic type principle explored by simulation experiments: Existence of connections

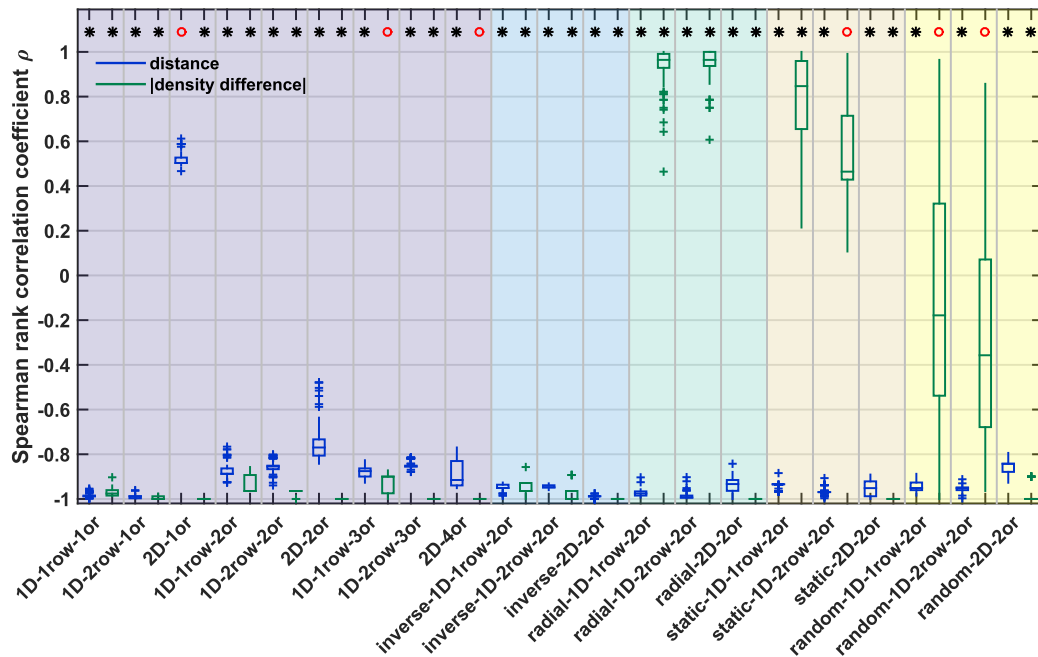


Figure 3.22: Correlation of distance and absolute density difference with relative connection frequency *in silico*. Spearman rank correlation coefficients are provided for the correlation between relative connection frequency and distance (blue) or absolute density difference (green). A sign test was used to test whether the distribution of associated Spearman rank correlation p -values had a median value smaller than $\alpha = 0.05$. The result of the sign test is indicated on top; black star: median $p < 0.05$, red circle: median $p \geq 0.05$. See Supplementary Figure C.4 for representative plots of the correlation for individual simulation instances. Box plots show distribution across 100 simulation instances per growth layout, indicating median (line), interquartile range (box), data range (whiskers) and outliers (crosses, outside of 2.7 standard deviations). See Supplementary Table D.12 for a summary. Abbreviations and background colours as in Table 2.1.

the longest distances in this growth layout, which resulted in a moderate positive correlation that did not reach significance. However, also for this growth layout, the correlation became strongly negative and significant if connections with fewer than 10 constituent axons were excluded, in line with previous treatment of empirical data (Barbas et al., 2005).

In contrast, the correlation of relative connection frequency with absolute density difference was not uniform across all growth layouts. For *1D random*, *static* and *radial* growth layouts, the absolute density difference was not significantly or else positively correlated with relative connection frequency. For *2D* growth layouts, however, the correlation was negative and significant for all three of those sets.

Conversely, the absolute density difference was very strongly negatively correlated with relative projection frequency for all growth layouts with oriented growth (i.e.,

3.6. Mechanistic underpinnings of the architectonic type principle explored by simulation experiments: Existence of connections

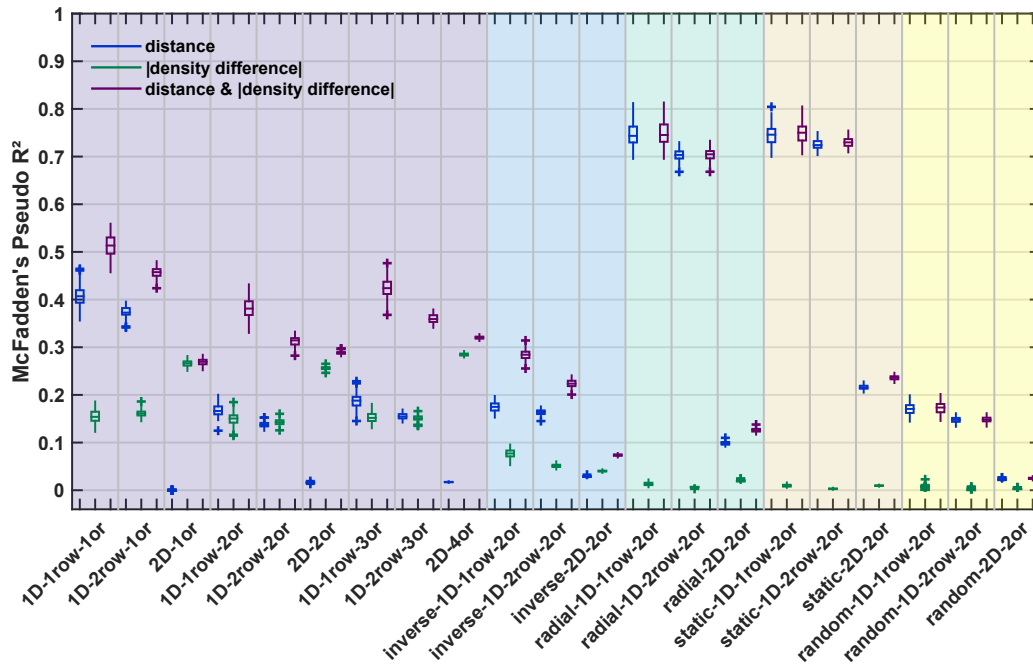


Figure 3.23: Logistic regression performance for classification of simulation data from simulation data. Within each growth layout, a logistic regression was performed to classify connection existence from three sets of factors: distance (blue), absolute density difference (green), or distance as well as absolute density difference simultaneously (purple). To assess whether classification performance was better than chance, McFadden's Pseudo R^2 was computed against performance of a null-model, where a constant was the only factor included in the logistic regression. Box plots show distribution across 100 simulation instances per growth layout, indicating median (line), interquartile range (box), data range (whiskers) and outliers (crosses, outside of 2.7 standard deviations). See Supplementary Table D.12 for a summary. Abbreviations and background colours as in Table 2.1.

realistically oriented density gradient and inverse gradient). The only exceptions here were the *1D 1row 3origins* growth layout and the *2D 4origins* growth layout. For reasons of computational efficiency, these layouts were implemented with only five and four density difference tiers, respectively. For the *1D 1row 3origins* growth layout, the deviation of relative connection frequency from a perfect negative correlation in one of the five tiers was, therefore, sufficient to render the rank correlation insignificant, with a p-value of 0.083. Similarly, for the *2D 4origins* growth layout, the minimal p-value that could be obtained from a rank correlation across the four tiers was 0.083, which is not low enough to reach significance. However, the correlation coefficients for both growth layouts consistently indicated a very strong to perfect negative correlation (cf. also Supplementary Figure C.4).

Logistic regression

When we predicted connection existence using logistic regression analyses, the inclusion of distance as a predicting factor markedly increased prediction performance as compared to the constant-only null model, with median McFadden's Pseudo R^2 values of at least 0.14 (Figure 3.23). This was not true for the 2D growth layouts with planar growth of the cortical sheet (i.e., the *static* and *radial 2D* growth layouts are excepted here), where distance did not markedly increase prediction performance compared to the constant-only null model, with median McFadden's Pseudo R^2 values of at most 0.03. For the *radial 2D* growth layout, distance performed intermediately with a median McFadden's Pseudo R^2 value of 0.10, indicating moderate performance. Absolute density difference as the only predictive factor did not increase prediction performance compared to the constant-only null model for all *random*, *static* and *radial* growth layouts, with median McFadden's Pseudo R^2 values below 0.03. However, inclusion of absolute density difference led to an increase in prediction performance for the growth layouts with oriented growth. For the growth layouts with a *realistically oriented density gradient*, the performance increase was moderate to very high, with median McFadden's Pseudo R^2 values between 0.14 and 0.28. For growth layouts with an *inverse density gradient*, in contrast, the performance increase was very small, with median McFadden's Pseudo R^2 values between 0.04 and 0.08.

Including distance and absolute density difference jointly as predictors for the logistic regression led to a moderate to very high increase in prediction performance compared to the constant-only null model, with median McFadden's Pseudo R^2 values of at least 0.13, but mostly above 0.20 and up to 0.75. The only exceptions to this finding were the *random* and the *inverse 2D* growth layouts, which did not reach median McFadden's Pseudo R^2 of 0.10.

In summary, a logistic regression analysis adequately allowed to predict connection existence from distance and absolute density difference for the overwhelming majority of growth layouts. This result was to be expected given the rules of connection growth that governed the formation of the simulated networks. The notable dissociation that could be observed in the separate prediction from distance and density difference was that distance markedly contributed to prediction performance for most growth layouts, while the contribution of density difference was more specific. Namely, density difference most strongly predicted connection existence for the layouts with oriented growth of the cortical sheet and a *realistically oriented density gradient*.

3.6. Mechanistic underpinnings of the architectonic type principle explored by simulation experiments: Existence of connections

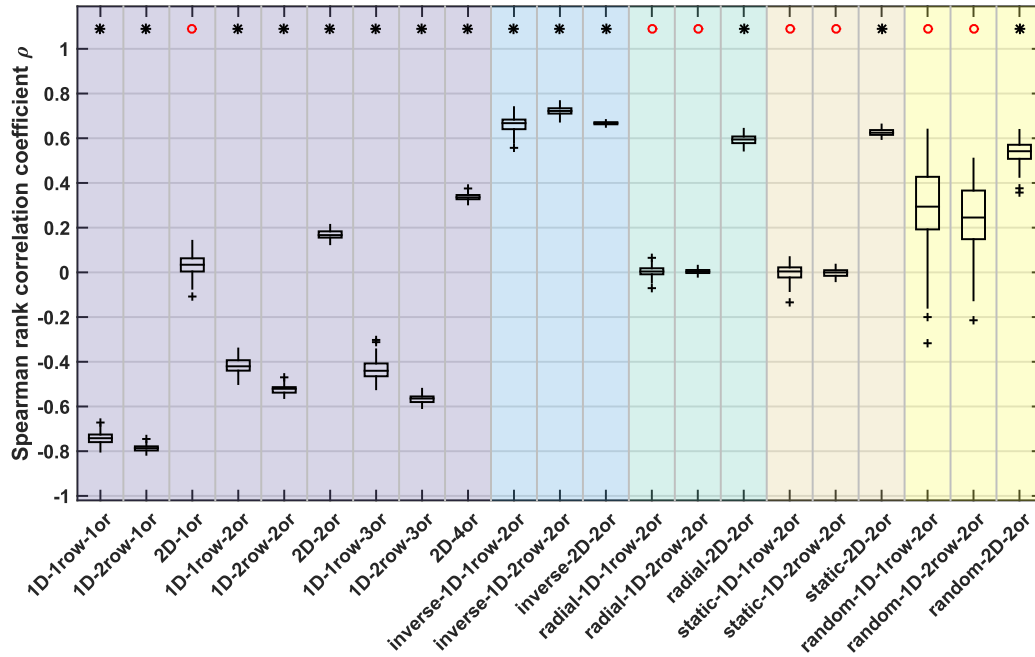


Figure 3.24: Correlation of area degree with neuron density in silico. Spearman rank correlation coefficients for the correlation between area degree (number of connections) and area neuron density. A sign test was used to test whether the distribution of associated Spearman rank correlation p -values had a median value smaller than $\alpha = 0.05$. The result of the sign test is indicated on top; black star: median $p < 0.05$, red circle: median $p \geq 0.05$. See Supplementary Figure C.5 for representative plots of the correlation for individual simulation instances. Box plots show distribution across 100 simulation instances per growth layout, indicating median (line), interquartile range (box), data range (whiskers) and outliers (crosses, outside of 2.7 standard deviations). See Supplementary Table D.12 for a summary. Abbreviations and background colours as in Table 2.1.

3.6.3 Number of connections per area

Another property of the simulated networks that we compared to empirical observations was area degree (i.e., the number of connections per area). We previously reported that, in biological cortical networks, the number of connections maintained by an area is negatively correlated with the area's architectonic differentiation (Sections 3.3 and 3.4). Here, we show an analogous analysis for the simulated networks (Figure 3.24, Supplementary Table D.12, Supplementary Figure C.5). For *random*, *static* and *radial* growth layouts, area degree was not significantly correlated with neuron density, with the exception of 2D growth layouts, which showed a positive and significant correlation in each case.

Growth layouts with *realistically oriented density gradients* showed a strongly negative, significant correlation between area degree and neuron density, with median correla-

3.6. Mechanistic underpinnings of the architectonic type principle explored by simulation experiments: Existence of connections

tion coefficients between -0.42 and -0.79 for both *1D* growth modes. Conversely, for growth layouts with an *inverse density gradient*, area degree was strongly positively correlated with neuron density. For *2D* growth along a *realistically oriented density gradient*, the observed effect was more variable. Correlation coefficients were of weak to moderate magnitude, and the correlation was not significant for *2D* growth around one origin (*2D 1origin*: median $\rho = 0.03$, median $p > 0.05$; *2D 2origins*: median $\rho = 0.17$, median $p < 0.05$; *2D 4origins*: median $\rho = 0.34$, median $p < 0.05$). This observation was in contrast to the strongly positive and significant correlations observed for the *2D* growth layouts without oriented growth, where median correlation coefficients were larger than 0.50 (*random 2D*: median $\rho = 0.54$; *static 2D*: median $\rho = 0.62$; *radial 2D*: median $\rho = 0.59$). We, therefore, concluded that the effect of oriented growth along a *realistically oriented density gradient* on area degree, as observed for both *1D* growth modes, persisted in the *2D* growth mode, but that it was not strong enough to completely abolish the tendency for a positive correlation between area degree and neuron density inherent to the *2D* growth layouts, instead only diminishing the positive correlation.

In summary, the empirically observed negative correlation between area degree and neuron density was only reproduced for the growth layouts with a *realistically oriented density gradient*. We cannot rule out that there existed a minor contribution of geometric centrality to this relationship. However, taking into account the results for the *radial* and *static* growth layouts made clear that such an effect, if there was any in the *realistically oriented density gradient* growth layouts, could only be secondary. Without expansive, planar growth, there is no temporal advantage helping earlier-formed areas to accrue more connections. Any negative correlation between neuron density and area degree would, thus, be caused by geometric centrality. Figure 3.24 illustrates that no such correlation arises for the *radial* and *static* growth layouts, where instead area degree appears to vary randomly with neuron density.

3.6.4 Prediction of empirical connection existence from simulated networks

In the previous sections, we showed that empirically observed regularities, particularly a close relationship between connection existence and the two factors of relative neuron density and spatial distance, could be reproduced *in silico*. We further characterised how well the simulation captured this phenomenon by predicting empirical connectivity using classifiers trained on the simulated networks. Classification performance was used as a measure of how well the properties of the artificially generated

3.6. Mechanistic underpinnings of the architectonic type principle explored by simulation experiments: Existence of connections

networks reflected the characteristics of empirical brain networks, in particular, the macaque and cat cortical connectomes. We report two measures of classification performance, accuracy and the Youden index, J . Accuracy was calculated as the percentage of predictions that were correct, while the Youden index is a summary measure that takes into account both the rate of true positives and the rate of true negatives and indicates divergence from chance performance.

As seen from Figure 3.25 and Figure 3.26, classification performance was generally higher for the macaque connectome than for the cat connectome. However, the described differences between growth layouts held for both species. We also provide the fraction of the available empirical connections that were classified in each species (Figure 3.27, Supplementary Table D.13). Generally, between 30% and 60% of the empirical connections were classified, with some growth layouts reaching up to 86%. However, for some growth layouts, nearly no empirical connections reached posterior probabilities of at least 0.75 (the minimal threshold applied for assigning a predicted label), and, thus, very low fractions of the available empirical connections were classified. Specifically, this applied to *random* growth layouts (median fraction classified between <0.01 and 0.14) and the *inverse 2D* growth layout (median fraction classified macaque: 0.08, cat: 0.05). The overall low posterior probabilities for these growth layouts and the resulting small fraction of classified empirical connections already suggested that the properties of those layouts did not correspond well to the properties of the empirical networks. This impression was corroborated by the classification performance measures (see below).

Accuracy

While classification accuracy is not a comprehensive measure to quantify classification performance, we included it to provide an overall impression of prediction quality. As seen in Figure 3.25 and Supplementary Table D.13, accuracy for most growth layouts surpassed chance performance, as assessed by a permutation analysis. Only the *random* and *radial 2D* growth layouts did not consistently reach better-than-chance accuracy. For classification of macaque connectivity, median accuracies that were better than chance ranged between 0.64 and 0.88, while the range of median accuracy for classification of cat connectivity was between 0.50 and 0.90. Comparing the different growth layouts, accuracy was generally higher for layouts with a *realistically oriented density gradient* than for *random*, *static*, *radial* or *inverse* growth layouts. The accuracies obtained for *realistically oriented density gradient* growth layouts compared well to the accuracies we reported for the classification of empirical connectivity from

3.6. Mechanistic underpinnings of the architectonic type principle explored by simulation experiments: Existence of connections

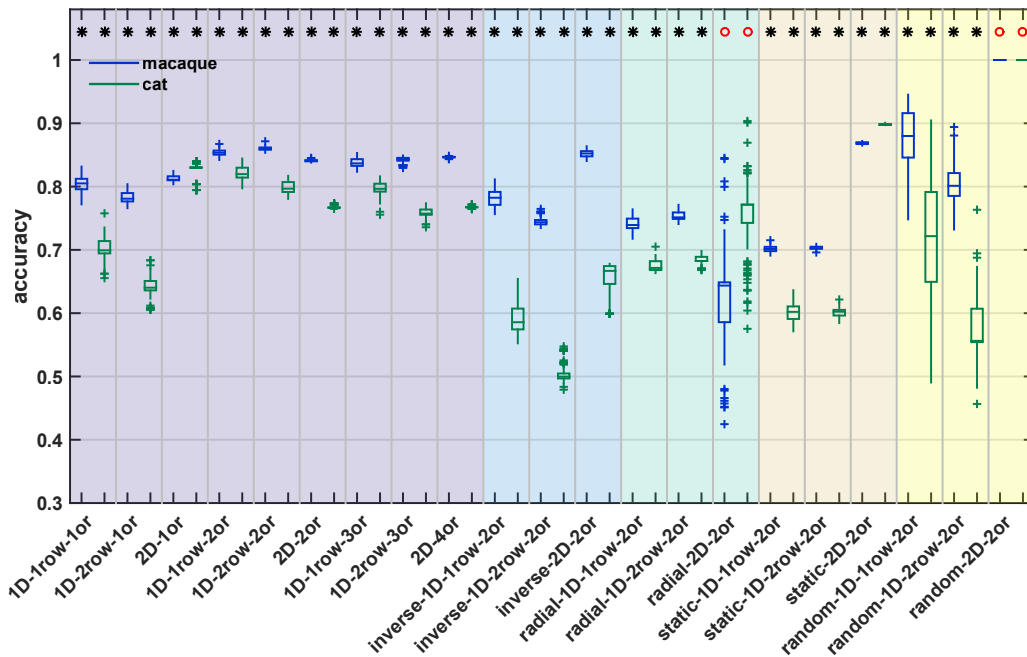


Figure 3.25: Classification accuracy for prediction of empirical connection existence from simulation data. A classifier was trained to predict connection existence of a simulated network from the associated distance and absolute density difference. Classification accuracy for predicting existence of connections in two species (macaque, blue; cat, green) by this classifier is shown. Accuracy was determined at each classification threshold (see Section 2.4.4.4); here, we show mean accuracy across thresholds 0.750 to 0.975. Whether classification accuracy was better than chance was assessed by a permutation test, where classification accuracy was calculated for prediction from randomly permuted labels and a z-test was performed. A sign test was used to test whether the distribution of associated z-test p-values had a median value smaller than $\alpha = 0.05$. The result of the sign test is indicated on top; black star: performance better than chance with median $p < 0.05$, red circle: performance not better than chance with median $p \geq 0.05$. Box plots show distribution across 100 simulation instances per growth layout, indicating median (line), interquartile range (box), data range (whiskers) and outliers (crosses, outside of 2.7 standard deviations). See Supplementary Table D.13 for a summary. Abbreviations and background colours as in Table 2.1.

the corresponding empirical structural measures, which were between 0.85 and 0.99 for the thresholds used here (cat: Section 3.2; macaque: Section 3.3). The better performance of *realistically oriented density gradient* growth layouts was especially apparent if corresponding layouts were compared, for instance, in the macaque, the *random 1D 2rows* growth layout (median accuracy = 0.80) with the *realistically oriented density gradient 1D 2rows 2origins* growth layout (median accuracy = 0.86). Exceptions were, in the macaque, the *random 1D 1row* growth layout and the *inverse 2D* growth layout, as well as, in the macaque and in the cat, the *static 2D* growth layout, all of which had higher accuracy than the corresponding *realistically oriented*

3.6. Mechanistic underpinnings of the architectonic type principle explored by simulation experiments: Existence of connections

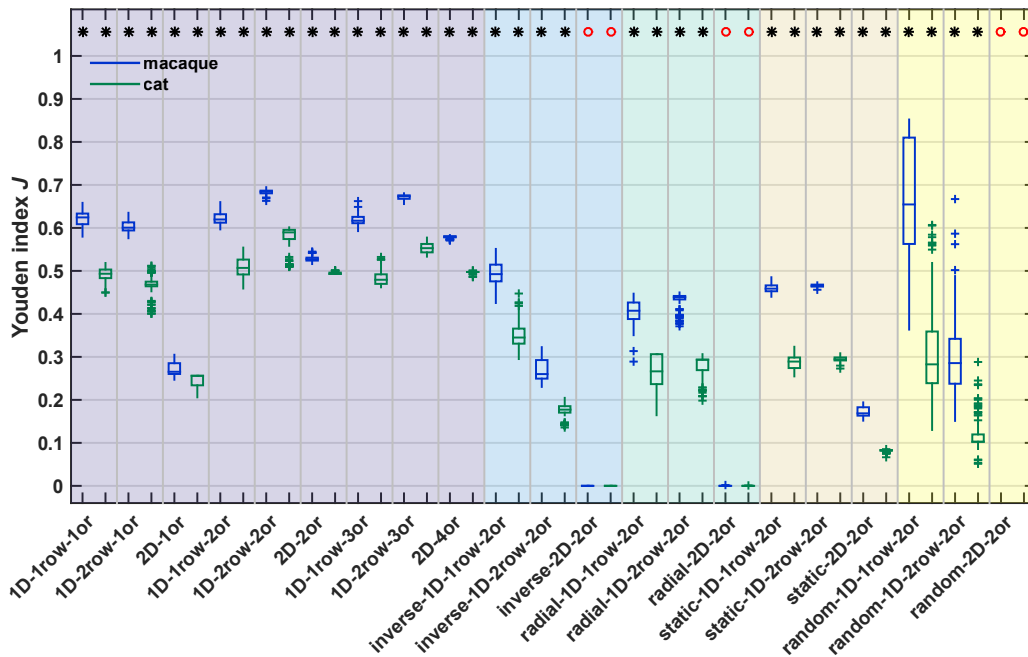


Figure 3.26: Youden index for prediction of empirical connection existence from simulation data. A classifier was trained to predict connection existence of a simulated network from the associated distance and absolute density difference. Youden index J for predicting existence of connections in two species (macaque, blue; cat, green) by this classifier is shown. Youden index J was determined at each classification threshold (see Section 2.4.4.4); here, we show mean J across thresholds 0.750 to 0.975. Whether the Youden index was better than chance was assessed by a permutation test, where J was calculated for prediction from randomly permuted labels and a z-test was performed. A sign test was used to test whether the distribution of associated z-test p-values had a median value smaller than $\alpha = 0.05$. The result of the sign test is indicated on top; black star: performance better than chance with median $p < 0.05$, red circle: performance not better than chance with median $p \geq 0.05$. Box plots show distribution across 100 simulation instances per growth layout, indicating median (line), interquartile range (box), data range (whiskers) and outliers (crosses, outside of 2.7 standard deviations). See Supplementary Table D.13 for a summary. Abbreviations and background colours as in Table 2.1.

growth layout. However, all three growth layouts appeared inferior when their Youden index was considered (see below). Specifically, the *random 1D 1row* growth layout was very variable in terms of both accuracy and Youden index of classification performance, in contrast to the narrow distributions obtained for the *realistically oriented density gradient 1D 1row 2origins* growth layout. The *inverse 2D* growth layout reached a high accuracy for the prediction of macaque connectivity, but the Youden index showed that this did not lead to an overall prediction performance that was better than chance. Finally, for the prediction of both macaque and cat connectivity, the Youden index for the *static 2D* growth layout was below 0.20, indicating low overall prediction performance even though the obtained accuracies

3.6. Mechanistic underpinnings of the architectonic type principle explored by simulation experiments: Existence of connections

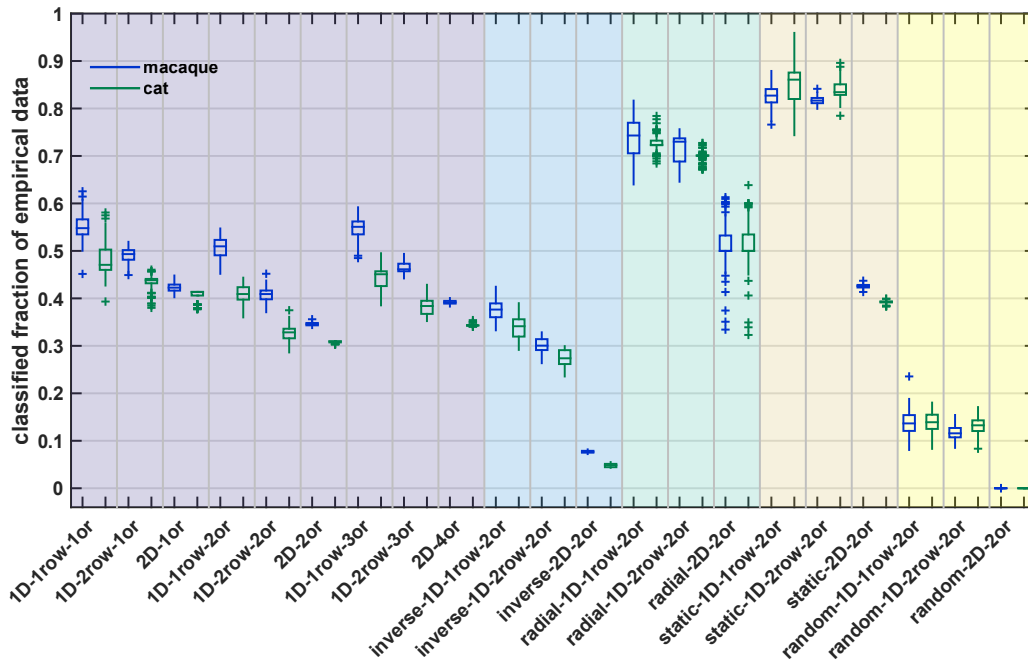


Figure 3.27: Percentage of empirical connectivity data that were classified from simulation data. A classifier was trained to predict connection existence of a simulated network from the associated distance and absolute density difference. This classifier was then used to predict connection existence in two species (macaque, blue; cat, green). Here, we show which fraction of the empirical data set was classified. This fraction differs across classification thresholds (see Section 2.4.4.4); here, we show the mean fraction across thresholds 0.750 to 0.975. Box plots show distribution across 100 simulation instances per growth layout, indicating median (line), interquartile range (box), data range (whiskers) and outliers (crosses, outside of 2.7 standard deviations). See Supplementary Table D.13 for a summary. Abbreviations and background colours as in Table 2.1.

were very high.

Youden index

The Youden index J is a helpful summary measure of overall classification performance and affords a clear distinction between growth layouts. As seen in Figure 3.26 and Supplementary Table D.13, for most growth layouts J surpassed chance performance, as assessed by a permutation analysis. Exceptions here were the *random*, *radial* and *inverse 2D* growth layouts. Across the growth layouts with better-than-chance performance, classification performance ranged from poor to good, generally being somewhat higher for classification of the macaque connectome than for classification of the cat connectome. The highest values of J were reached for the

3.6. Mechanistic underpinnings of the architectonic type principle explored by simulation experiments: Existence of connections

layouts with growth along a *realistically oriented density gradient*. In both species, performance for these growth layouts was moderate to good (macaque: median $J = 0.53$ – 0.68 , cat: median $J = 0.47$ – 0.59). The only exception here was the *2D 1origin* growth layout, which reached only weak classification performance (macaque: median $J = 0.27$, cat: median $J = 0.26$). For the macaque, this performance compares well to the values of J that we previously reported for the classification of empirical connectivity from the corresponding empirical structural measures, where J equalled 0.75 for the classification thresholds 0.85 through 1.00 (Section 3.3). Inclusion of the thresholds 0.75 and 0.80 would lower that value somewhat (cf. Supplementary Figure C.2).

Classification performance for the remaining growth layouts, namely the *random*, *static*, *radial* and *inverse* layouts, was low to moderate (median J macaque: generally < 0.49 , median J cat: < 0.35). The difference to growth along a *realistically oriented density gradient* was particularly apparent if corresponding layouts were compared. Growth layouts that reached moderate performance were the *static*, *radial* and *inverse 1D* growth layouts in the macaque. Their median J was still notably smaller than the median J value of the corresponding layout with growth along a *realistically oriented density gradient* (*1D 1row 2origins*: 0.62 , *1D 2rows 2origins*: 0.68 ; *static 1D 1row*: 0.46 , *static 1D 2rows*: 0.47 ; *radial 1D 1row*: 0.41 , *radial 1D 2rows*: 0.44 ; *inverse 1D 1row*: 0.49 , *inverse 1D 2rows*: 0.26 ; all values are for the macaque; cf. Supplementary Table D.13). The only exception to these observations was the *random 1D 1row* growth layout. In the macaque, this growth layout reached a median J of 0.65 . However, the Youden index was also distributed very broadly, with a range of 0.36 to 0.85 , indicating that classification performance was not consistently good, but volatile and strongly dependent on the particular random neuron density patterns emerging in a given simulation instance.

Classification performance varied with number of simulated growth origins

To assess differences in classification performance in more detail, we compared the layouts with growth along a *realistically oriented density gradient* among each other. Table 3.8 shows the results of a three-way analysis of variance for both accuracy and Youden index among the nine growth layouts of set 1. We included the factors ‘species’ (macaque, cat), ‘growth mode’ (*1D 1row*, *1D 2rows*, *2D*) and ‘number of origins’ (1, 2, 3/4). For both accuracy and Youden index, the main effects of these three factors were significant. We performed *post-hoc* comparisons to describe the effect of the number of origins in more detail. As can be seen from Table 3.9, the

3.6. Mechanistic underpinnings of the architectonic type principle explored by simulation experiments: Existence of connections

Factor	Accuracy					Youden index J				
	Sum Sq.	d.f.	Mean Sq.	F	Prob>F	Sum Sq.	d.f.	Mean Sq.	F	Prob>F
species	2.00	1	2.00	1847.0	0	4.40	1	4.40	1283.7	0
origins	1.24	2	0.62	572.8	0	5.52	2	2.76	804.0	0
growth mode	0.28	2	0.14	128.7	0	8.03	2	4.02	1170.7	0
Error	1.94	1794	0.00			6.15	1794	0.00		
Total	5.46	1799				24.11	1799			

Table 3.8: Analysis of variance on classification performance of realistically oriented density gradient growth layouts. A three-way analysis of variance was performed for both classification accuracy (see Figure 3.25, Supplementary Table D.13) and Youden index J (see Figure 3.26, Supplementary Table D.13), testing for effects of the factors ‘species’, ‘number of origins’, and ‘growth mode’. Sum Sq., Sum of squares; d.f., degrees of freedom; Mean Sq., mean squares = Sum.Sq. / d.f.

	Accuracy		Youden index J	
	estimated mean	standard error est. mean	estimated mean	standard error est. mean
model estimates				
1 origin	0.762	0.0013	0.450	0.0024
2 origins	0.824	0.0013	0.568	0.0024
3/4 origins	0.808	0.0013	0.567	0.0024
post-hoc comparisons				
	difference est. means	p-value difference est.	difference est. means	p-value difference est.
1 vs 2	-0.066	0	-0.118	0
1 vs 3/4	-0.046	0	-0.117	0
2 vs 3/4	0.016	0	0.001	1

Table 3.9: Post-hoc comparisons for classification performance of realistically oriented density gradient growth layouts. Post-hoc comparisons were computed to assess how classification accuracy and Youden index J were affected by the factor ‘number of origins’ in the analysis of variance model. The upper section shows the marginal means estimated from the analysis of variance model. The lower section shows the results of the post-hoc tests for differences between the estimated means.

comparisons showed that classification performance increased as the number of origins changed from one to two, but did not markedly increase further with addition of a third or fourth origin. In fact, for accuracy, there even was a slight decrease in the model estimate for three or four origins compared to two origins. This suggests that the network properties generated by growth around two origins were closer to empirical reality than those of networks grown around one origin, while a third or fourth origin did not further improve correspondence.

This section has been published in Beul et al. (2018).

3.7 Mechanistic underpinnings of the architectonic type principle explored by simulation experiments: Laminar patterns of connection origins

Building on the results presented in the preceding section, which demonstrated that realistic assumptions about neurogenesis, successive tissue growth and stochastic connection formation could interact to produce patterns of connection existence that were similar to empirically observed cortico-cortical connectivity, we expanded our *in silico* model to address the emergence of laminar patterns of projection origins.

We systematically explored the effects of including three features affecting spatio-temporal patterns of neurogenesis, and one feature affecting cell-intrinsic properties, on the laminar patterns of projection origins in the *in silico* model of the developing cortical sheet.

3.7.1 At baseline settings, supragranular contribution was not correlated with relative differentiation

When none of these four features was included in the model, that is, it was implemented at baseline settings, there was no correlation between the relative density of connected areas and the supragranular contribution to the projection linking them (Figure 3.28). Instead, for source areas of all neuron densities and connections across all density differences, the distributions of the contribution from the supragranular

3.7. Mechanistic underpinnings of the architectonic type principle explored by simulation experiments: Laminar patterns of connection origins

compartment ($N_{SG}\%$) were similar, with a mean around 50% and about equal variances (cf. Supplementary Figure C.6A), indicating that there was no preferential connection formation of either laminar compartment across areas or density differences. Moreover, the extension of the *in silico* model by laminar compartments did not affect the characteristics of inter-areal connection existence (i.e., considering only the binary status of connections as absent or present) reported previously for the *in silico* model (Section 3.6). We still observed a negative correlation between the neuron density of areas and the number of connections they maintain (area degree) (cf. Supplementary Figure C.7), consistent with empirical observations (Sections 3.2 and 3.3). The application of classifiers, which were trained on the simulated networks to predict connection existence from relative differentiation and spatial proximity, to empirical data also resulted in the good classification performance reported previously (cf. Supplementary Figure C.8), indicating that our expanded *in silico* model captured *in vivo* relationships between architecture, spatial proximity and connectivity.

3.7.2 Delay in infragranular compartment growth did not affect laminar projection patterns

When the *in silico* model implementation included a delay between the time of origin of the layer 1 compartment and the infragranular compartment (with the supragranular compartment being formed at the same time as the infragranular compartment), we did not observe changes in the laminar patterns of projection origins relative to the implementation of the model at baseline settings (Figure 3.28A, Supplementary Figure C.6B). However, at very long delays, both the magnitude of the negative correlation of area density with area degree (Supplementary Figure C.7A) and the simulation-to-empirical classification performance (Supplementary Figure C.8A) decreased, indicating that the simulated network became less similar to empirical connectomes with respect to characteristics of connection existence.

3.7. Mechanistic underpinnings of the architectonic type principle explored by simulation experiments: Laminar patterns of connection origins

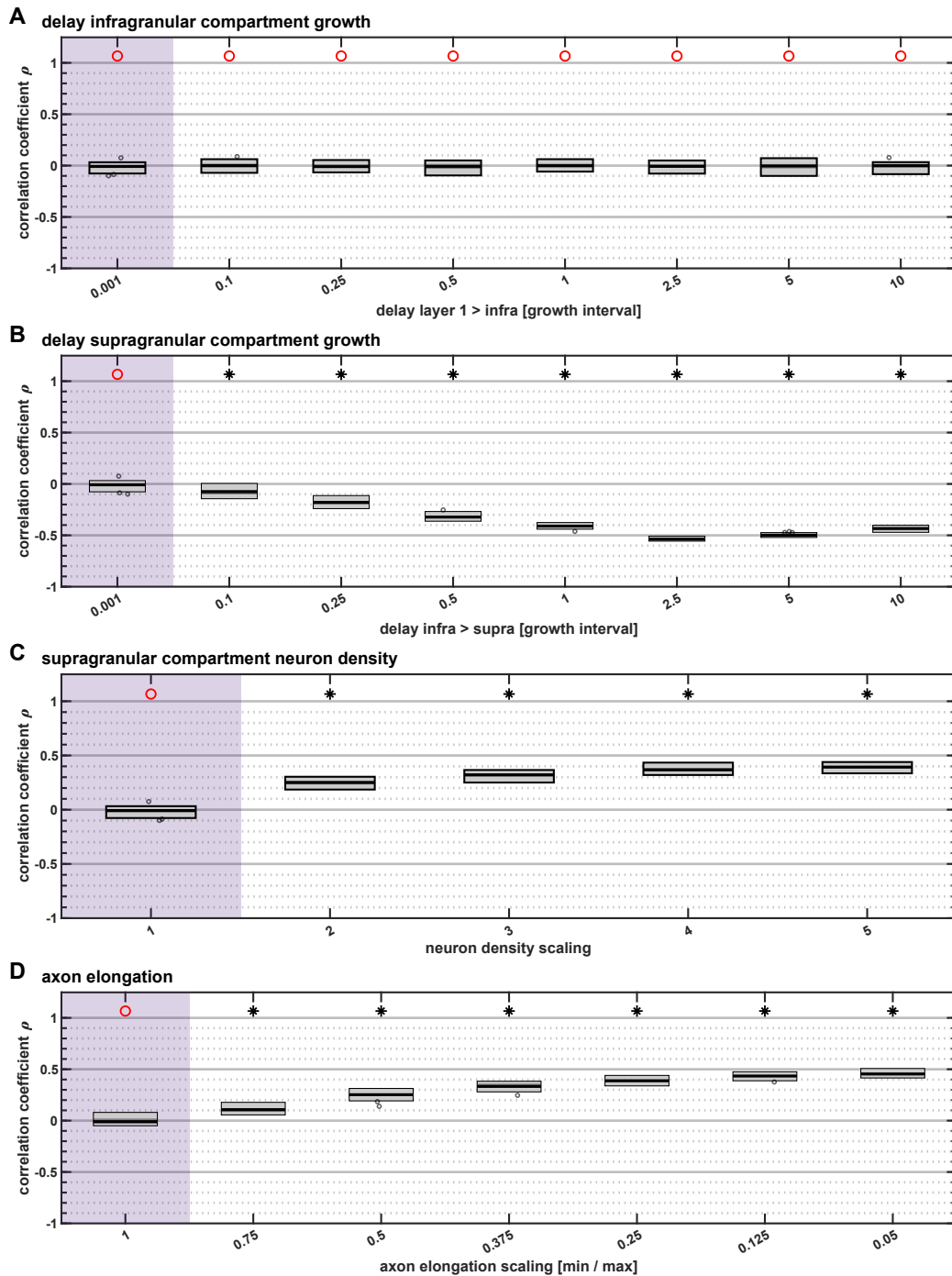


Figure 3.28: Correlation of supragranular contribution with neuron density difference *in silico*. Spearman rank correlation coefficients for the correlation between the supragranular contribution of a projection and the neuron density difference between the connected areas. We used a sign test to determine whether the distribution of associated Spearman rank correlation p -values had a median value smaller than $\alpha = 0.05$. The result of the sign test is indicated on top; black star: median $p < 0.05$, red circle: median $p \geq 0.05$. **(A)** Delays in infragranular compartment growth did not affect the correlation. **(B)** As the growth of the supragranular compartment was increasingly delayed, a negative correlation

Figure 3.28: (cont.) between supragranular contribution and density difference emerged. **(C)** An increase in the density of the supragranular compartment relative to the infragranular compartment resulted in a positive correlation. **(D)** As the axon elongation scaling factor decreased and elongation values diverged, a positive correlation emerged. Box plots show distribution across 50 simulation instances per implementation, indicating median (line), interquartile range (dark grey box), data range (light grey box) and outliers (circles, outside of 2.7 standard deviations). Parameter values that correspond to baseline (i.e., with no feature implemented), are highlighted in purple.

3.7.3 Delay in supragranular compartment growth resulted in negative correlation of supragranular contribution with relative differentiation

Inclusion of a delay between the growth of the infragranular compartment and the supragranular compartment substantially changed the laminar patterns of projection origins, resulting in a negative correlation between the relative density of connected areas and the supragranular compartment contribution to projections (Figure 3.28B). The longer the time became between the formation of the infragranular compartment and the formation of the supragranular compartment of areas, the stronger this negative correlation became. Moreover, at longer delays, the magnitude of the negative correlation of area density with area degree (Supplementary Figure C.7B) as well as the simulation-to-empirical classification performance (Supplementary Figure C.8B) decreased, again indicating that the simulated network became less similar to empirical connectomes with respect to characteristics of connection existence.

Unequal opportunities to connect affected laminar projection patterns

To explore how the negative correlation between density difference and supragranular compartment contribution emerged as the temporal delay between the compartments increased, we considered the distributions of $N_{SG}\%$ values for source areas of different neuron densities and connections across different density differences (Supplementary Figure C.6C). As the delay increased, the distributions changed from their uniform appearance at baseline settings and became strongly skewed. At the longest delays, the supragranular contribution from areas of low neuron density increased as they connected to areas of successively higher neuron density (i.e., as the density difference to the target area became smaller), with connections to areas of similar neuron density constituted largely by infragranular compartment neurons. In contrast, this pattern shifted for areas of high neuron density, where connections to areas of similar

3.7. Mechanistic underpinnings of the architectonic type principle explored by simulation experiments: Laminar patterns of connection origins

neuron density arose evenly from both the infragranular and the supragranular compartment while connections to areas of lower neuron density became successively more dominated by the infragranular compartment as the density difference to the target area increased. We suggest that these changes in laminar patterns of projection origins arose from consequences of the delay in supragranular compartment growth as follows: Neurons in areas of lower neuron density, which were the first to appear on the cortical sheet, started connecting relatively early, while not all target areas were available, and therefore connected more frequently to areas of similar neuron density. But at longer delays, this applied only to the infragranular compartment, because the supragranular compartments in areas of lower neuron density grew after a large portion of the cortical sheet had already appeared, affording them the opportunity to connect across a wide range of density differences. Hence, in low-density areas, connections to higher-density areas (i.e., across larger negative density differences) originated predominantly in the supragranular compartment, while connections to areas with more similar density originated predominantly in the infragranular compartment. This pattern shifted for high-density areas, which grew after the low-density areas. Here, the infragranular compartment neurons had the opportunity to connect to most other areas, which were already present when these neurons appeared. However, at large delays in supragranular compartment growth, these infragranular neuron axons travelled across a cortical sheet that was not populated with supragranular neurons yet, increasing the range the neurons' axons were likely to traverse before encountering a target neuron (relative to baseline settings). Supragranular neurons in high-density areas, in contrast, appeared once all other neurons had grown, making them as likely to encounter target neurons in other areas as at baseline. Thus, in high-density areas, infragranular compartment neurons were more likely to reach areas of less similar neuron density than supragranular neurons, resulting in larger infragranular compartment contribution for connections across relatively large density differences. As these unequal opportunities to connect, which areas of different neuron density and their laminar compartments encountered, combined, they resulted in an overall negative correlation between supragranular compartment contribution and density difference as the delay of supragranular compartment growth increased.

3.7.4 Scaling of supragranular density did not result in representative laminar patterns of projection origins

Another feature that substantially affected the laminar patterns of projection origins was a scaling of the neuron density of the supragranular compartment relative to the infragranular compartment. As the relative density became larger, a successively stronger positive correlation between the relative density of connected areas and the supragranular compartment contribution to projections resulted (Figure 3.28C). The characteristics of connection existence which we considered here, namely the negative correlation of area density with area degree (Supplementary Figure C.7C) as well as the simulation-to-empirical classification performance (Supplementary Figure C.8C), were only negligibly affected by a change in the supragranular compartment neuron density parameter value.

Supragranular contribution increased due to an increase of relative neuron numbers in the supragranular compartment

To identify the source of the positive correlation between density difference and supragranular compartment contribution, which emerged as the relative density of the supragranular compartments increased, we again considered the distributions of $N_{SG}\%$ values for source areas of different neuron densities and connections across different density differences (Supplementary Figure C.6D). As the relative neuron density increased from areas of lower neuron density to areas of higher neuron density, and as this divergence became stronger with an increasing scaling parameter value, the distributions of the $N_{SG}\%$ values shifted upwards, away from the balanced contribution observed at baseline settings and for areas of the lowest neuron density where infragranular and supragranular compartments were of equal neuron density across the whole range of parameter values. However, this effect arose exclusively on the level of source areas. The distribution of $N_{SG}\%$ values was uniform for connections to all target areas (i.e., across all density differences) within source areas of a given neuron density, indicating that the fraction of supragranular contribution was unaffected by relative differentiation between connected areas. Since areas of lower neuron density necessarily formed the connections across the smallest density differences and areas of higher neuron density correspondingly were the source of connections with the largest density differences, the aggregate profile of $N_{SG}\%$ values exhibited a systematic increase of $N_{SG}\%$ with density difference. In sum, the positive correlation observed for model implementations with pronounced differences

3.7. Mechanistic underpinnings of the architectonic type principle explored by simulation experiments: Laminar patterns of connection origins

between relative laminar neuron density across areas resulted from the fact that areas of different neuron density had uniform profiles of $N_{SG}\%$ values for all their connections, which, however, differed between areas. It did not result from a graded pattern of $N_{SG}\%$ values found within any one area.

To demonstrate that the positive correlation was mediated exclusively by the increased number of supragranular neurons, we computed a partial correlation of supragranular compartment contribution with relative neuron density of connected areas while controlling for the ratio of supragranular compartment neurons to total neurons in the source area. In individual correlations with supragranular compartment contribution, both measures (density difference and neuron ratio) exhibited a strong positive correlation (Figure 3.29A). However, if all three measures were included simultaneously in a partial correlation, the correlation between density difference and supragranular contribution was abolished, while the correlation between neuron ratio and supragranular contribution was affected only negligibly (Figure 3.29B). Hence, as the value of the supragranular compartment neuron density scaling parameter became larger, the difference in neuron numbers between infragranular and supragranular compartments increased, and became especially pronounced for areas of higher neuron density. This increase in supragranular neurons accounts for the increase in $N_{SG}\%$ values in the supragranular compartment at higher values of the supragranular density parameter and is the factor that determines the correlation between density difference and supragranular compartment contribution.

***In vivo*, the positive correlation of relative differentiation with laminar patterns of projection origins does not result from a relative increase in supragranular neuron density**

In contrast to the results presented here for our *in silico* model, the positive correlation between supragranular contribution and relative architectonic differentiation of connected areas, which is observed in the mammalian cortex, is not the result of a combination of distributions of supragranular contribution which differ between source areas but are uniform within source areas of a given differentiation. Instead, in the macaque cortex, individual areas across the whole spectrum of architectonic differentiation exhibit the graded pattern of supragranular contribution increase that has been reported for the aggregate connectomes. In Figure 3.29C, we show this in the supragranular contribution to cortico-cortical connections of the macaque brain reported by Chaudhuri and colleagues (2015), with connections grouped according to the architectonic differentiation of the source areas (using the qualitative ranking

3.7. Mechanistic underpinnings of the architectonic type principle explored by simulation experiments: Laminar patterns of connection origins

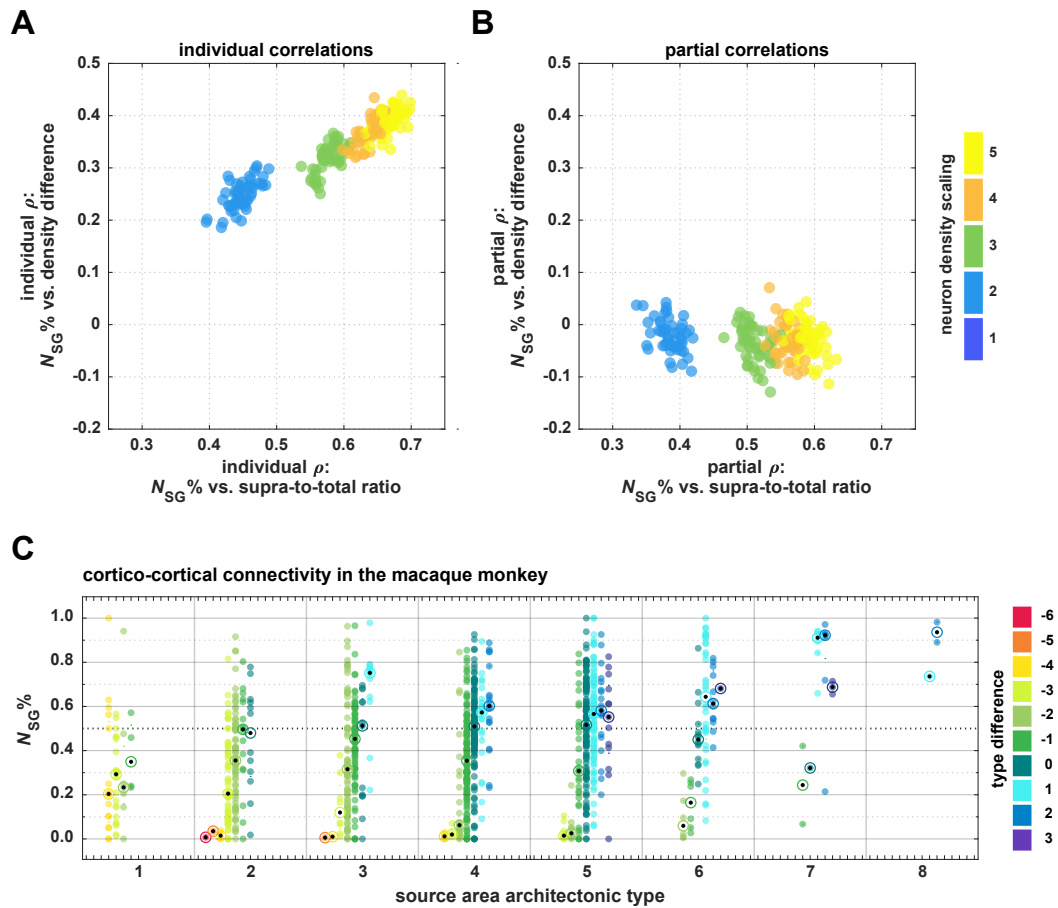


Figure 3.29: Neuron density scaling did not result in realistic laminar patterns of projection origins. **(A, B)** The positive correlation observed for increasing scaling of supragranular compartment neuron density is abolished by controlling for the number of supragranular neurons. **(A)** Individually, both density difference and the ratio of supragranular neurons to total neurons are increasingly correlated with supragranular contribution as the density scaling factor increases. **(B)** However, the correlation of density difference with supragranular contribution decreases to baseline levels when it is included alongside supra-to-total neuron ratio in a partial correlation, while correlation values for supra-to-total neuron ratio are hardly affected by the inclusion of density difference. Note that no correlation coefficients are shown for a scaling factor of 1, the baseline value, because here all supra-to-total ratios are 1 and no correlation can be computed. **(C)** In the macaque monkey, supragranular contribution is distributed across differences in architectonic differentiation (see color scale) in a graded manner even within areas of a particular level of differentiation, contrary to the distributions observed in our simulation experiments (cf. Supplementary Figure C.6C). Projections are grouped according to the architectonic type of their source area and the type difference between the connected areas (see color scale) and for each column a median is indicated (target). $N_{SG}\%$ values from Chaudhuri and colleagues (2015), architectonic type values from Hilgetag and colleagues (2016).

measure of architectonic type, Hilgetag et al., 2016). The profiles of $N_{SG}\%$ values differ markedly from the uniform distributions observed in similar plots of the simulated networks.

3.7.5 Divergence in axon elongation resulted in laminar patterns of projection origins that exhibited the empirically observed relation to relative differentiation

Lastly, we introduced a divergence in the elongation of axons, where distances travelled by axons during each time step differed between infragranular and supragranular compartment neurons and gradually shifted along with neuron density, mirroring the phenomenon of changing relative cell sizes observed across the mammalian cortex (externopyramidization). With increasing divergence in axon elongation, we observed a stronger positive correlation between supragranular contributions to connections and relative differentiation of connected areas (Figure 3.28D). Taking into account the distributions of $N_{SG}\%$ values across connections of varying density difference and for source areas of different neuron density (Supplementary Figure C.6D), it became apparent that the $N_{SG}\%$ values differed according to density difference and moreover became more unequal as the divergence in axon elongations between the slowest and the fastest growing laminar compartments increased. Hence, varying the axon elongation affected the correlation between supragranular compartment contribution and relative differentiation on the level of individual areas, as shown in the macaque monkey (Figure 3.29C), and not only in aggregate across all areas, as shown for the scaling of supragranular compartment neuron density (Supplementary Figure C.6D).

Moreover, the considered characteristics of connection existence, that is, the negative correlation of area density with area degree (Supplementary Figure C.7D) as well as the simulation-to-empirical classification performance (Supplementary Figure C.8D), remained essentially unaffected by the changes in axon elongation.

Spatio-temporal interactions were a necessary condition for the emergence of the positive correlation between laminar patterns and relative differentiation

If the correspondence between time of origin and architectonic differentiation was removed, the effects reported for diverging axon elongations were abolished. This

3.7. Mechanistic underpinnings of the architectonic type principle explored by simulation experiments: Laminar patterns of connection origins

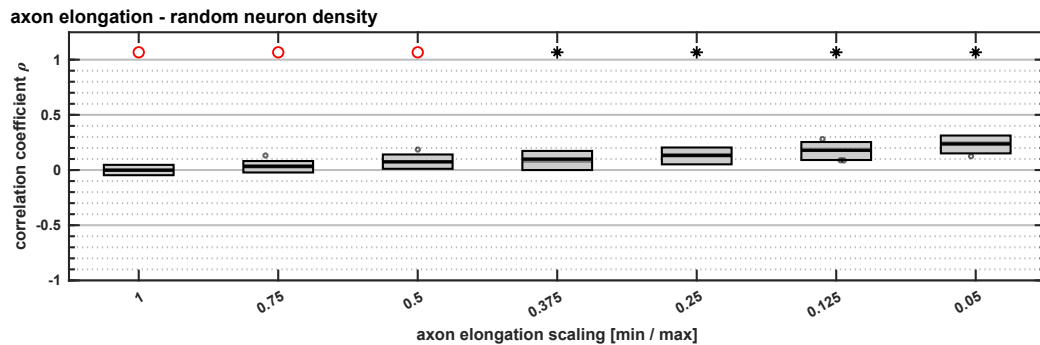


Figure 3.30: Abolishing the ordered neuron density gradient decreased the positive correlation observed for axon elongation scaling. Spearman rank correlation coefficients for the correlation between the supragranular contribution of a projection and the neuron density difference between the connected areas. Here, we implemented the scaling in axon elongation but assigned area neuron densities randomly across times of origin, thus removing the ordered gradient of areas with higher neuron density forming at later points in time that was present in the other implementations. We used a sign test to determine whether the distribution of associated Spearman rank correlation p -values had a median value smaller than $\alpha = 0.05$. The result of the sign test is indicated on top; black star: median $p < 0.05$, red circle: median $p \geq 0.05$. Box plots show distribution across 50 simulation instances per implementation, indicating median (line), interquartile range (dark grey box), data range (light grey box) and outliers (circles, outside of 2.7 standard deviations).

could be concluded from implementations of the *in silico* model in which the neuron density of areas was drawn randomly from the set of neuron densities present in the baseline setting. We simulated 50 instances of such a random variation of area neuron density with time of origin for each parameter value at which we evaluated the feature of axon elongation. Here, as divergence in axon elongation increased, correlation between supragranular compartment contribution and density difference increased slightly, but remained at small magnitudes even for large divergences (Figure 3.30). Moreover, when the neuron density of an area was not correlated with the area's time of neurogenesis, there resulted a positive correlation between neuron density and area degree (Supplementary Figure C.9A), contrary to what has been observed empirically (Sections 3.2 and 3.3). In addition, simulation-to-empirical classification performance was dramatically reduced (Supplementary Figure C.9B) and became quite variable, indicating that it depended strongly on the concrete random layout of neuron densities that was realised in a particular simulation instance.

3.7.6 Combinations of features

If any two of the previously presented features (delay in infragranular compartment growth, delay in supragranular compartment growth, scaling of supragranular compartment neuron density, axon elongation) were combined in the *in silico* model, no unexpected effects emerged from their co-occurrence (Supplementary Figure C.10). Instead, the previously described effects superimposed in a straight-forward manner. Specifically, a delay in supragranular compartment growth resulted in a relative decrease in the correlation between supragranular compartment contribution and relative differentiation, caused by the aforementioned mechanisms. Including a delay in infragranular compartment growth did not modulate the effects caused by the other two features. The inclusion of an increase in the supragranular density scaling parameter value resulted in a relative increase in the correlation between supragranular compartment contribution and relative differentiation, but this correlation was again abolished by controlling for the number of supragranular neurons. Finally, including diverging levels of axon elongation resulted in a relative increase in this correlation. If all four features were implemented simultaneously (Supplementary Figure C.11), the superposition ensued as expected for the three features of delay in supragranular compartment growth, scaling of supragranular compartment neuron density and axon elongation. Again, the effect of supragranular compartment neuron density scaling was abolished by controlling for the number of supragranular neurons. At longer delays in infragranular compartment growth, correlation coefficients were comparatively higher, presenting an effect of this delay that was not observed in the other feature combinations. Given that this effect did not occur in any of the pair-wise feature combinations and was not affected by the scaling in supragranular compartment neuron density (since it persisted regardless of whether the supra-to-total neuron ratio was taken into account), it appears to be specific to the combination of the three features of the two delays and axon elongation. Since including the delay in supragranular compartment growth resulted in a negative correlation between supragranular contribution and relative differentiation, the interaction was not sufficient to increase the correlation coefficient relative to the inclusion of only axon elongation (Figure 3.28D).

This section has been submitted for peer-review in Beul and Hilgetag (2019b).

Chapter **four**

Discussion

We presented extensive evidence corroborating the presence of an architectonic type principle, which integrates cortical architecture and connectivity across the mammalian cortex. In this chapter, we will discuss the results, associated caveats, and their implications.

But first let us return to the question of whether there exists a generic template of intrinsic microcircuitry in the cortex, despite pronounced regional differences in architectonic organisation. The answer depends strongly on how broadly the concept of stereotypy is framed (Silberberg et al., 2002), but even for the cortical region studied most intensely in this context, striate cortex, there exists as yet no consensus on a detailed ‘canonical’ microcircuit. Moreover, differences in circuitry have been reported across the cortex, which are consistent with the changes in the structural substrate in which intrinsic connectivity is embedded. In order to account for these structural differences, we proposed a tentative circuit diagram for the agranular frontal cortex of the rodent brain, an agranular region which is strikingly opposed to striate cortex in its architectonic organisation. Our review of the existing literature points to an intrinsic circuit that features excitatory-to-excitatory and excitatory-to-inhibitory connections from upper layers to lower layers, as well as from lower layers to upper layers (Figure 3.1B), but shows no interlaminar inhibitory-to-inhibitory or inhibitory-to-excitatory connections.

Of course, this synthesis of the available literature has to be appraised cautiously. Our tentative circuit diagram is based on multiple approaches for structural and functional circuit investigation (such as electrophysiological paired recordings using

microstimulation, anatomical tracing experiments, or examination of morphological features using light and electron microscopy), with different caveats and varying levels of reliability. Importantly, the information was drawn from studies whose primary goal was not necessarily the characterisation of interlaminar circuitry. Our circuit diagram is therefore subject to debate and should be modified in the light of future information. In compiling the circuit diagram, we engaged in some common simplifications regarding the anatomical substrate in which the connections are placed. In studying intrinsic circuitry, distinct sublayers are often collapsed, as for example when layers 5A, 5B and 6 are considered collectively as ‘infragranular’ layers. This treatment may be misleading, since different (sub)layers have been shown to be involved in distinct processing circuits (e.g. Lübke and Feldmeyer, 2007). The same caveat holds for the merging of diverse neuron types into the two main classes of inhibitory and excitatory neurons. It discards a wealth of functionally relevant information about morphological and physiological differences between neuron types, as well as about cell type specific connectivity (Kozloski et al., 2001; Silberberg et al., 2002; Thomson and Bannister, 2003; Kampa et al., 2006; Otsuka and Kawaguchi, 2008, 2009, 2011; Brown and Hestrin, 2009; Xu and Callaway, 2009; Apicella et al., 2012; Hirai et al., 2012). Not to disambiguate such significant anatomical features introduces additional uncertainty about the validity of any intrinsic circuit diagram. Moreover, note that a description of general layer-to-layer connectivity within a column, as we propose here, does not necessarily reflect synaptic circuits formed by individual neurons across layers, as, for example, Binzegger and colleagues (2004) have estimated. Thus, there may exist functionally relevant differences between the average laminar interconnections described here and the specific laminar microcircuits formed within these average patterns. A further dimension that is missing from many descriptions of local microcircuitry is an estimation of connection strength. However, with current technology, structural measures of strength, such as the frequency of connections from one cell type onto another or the number of involved synapses and their morphology, can only be obtained by arduous manual labour. Moreover, the translation of structural into functional strength, as expressed by the amplitude of evoked postsynaptic currents, is opaque: number, size, morphology and position of synapses matter, as do numerous molecular mechanisms regulating synaptic function at both the pre- and postsynaptic site. In addition, the impact of evoked currents on postsynaptic cell function depends on many further factors. All these aspects are not static, but can potentially change on short time scales (Squire et al., 2008; Buonomano and Maass, 2009; Dityatev et al., 2010; Eroglu and Barres, 2010; Silver, 2010; Ribault et al., 2011; Arnsten et al., 2012; Camiré and Topolnik, 2012; Caroni et al., 2012; Cortés-Mendoza et al.,

2013; Dallérac et al., 2013; Vitureira and Goda, 2013; Chevaleyre and Piskorowski, 2014).

In summary, although the proposed intrinsic circuitry for agranular cortex is still speculative, the issue we address remains crucial (Marcus et al., 2014). There has to be variation in intrinsic circuitry across the cerebral cortex, because the composition of the cortex is not uniform, but highly variable on a number of dimensions. We are convinced that a better understanding of the intrinsic cortical circuitry is essential for an improved comprehension of its physiology, and has to take into account differences in the cortical structural substrate. We hope that we have provided a starting point for discussion which will lead to the synthesis of new insights from available data or further experimental efforts to elucidate circuitry outside of striate cortex, taking structural variation into consideration.

This section has been published in Beul and Hilgetag (2015).

4.1 The architectonic type principle captures cortico-cortical connectivity across mammalian cortices

Cortico-cortical connectivity, which is neither random nor regular, exhibits a strikingly complex organisation. We assessed the extent to which different structural measures are associated with cortico-cortical connectivity, to gain insights into the principles underlying its organisation. To this end, we used two extensive data sets of anatomical tract-tracing experiments, performed in the cat (Scannell et al., 1995) and the macaque monkey (Markov et al., 2014a).

We considered four structural measures: the architectonic differentiation of cortical areas; distances between areas; the thickness of cortical areas (only in the macaque cortex); and their positions in an anatomical hierarchy (Felleman and Van Essen, 1991; Scannell et al., 1995) (only in the cat cortex). There were five main findings: First, the relative architectonic differentiation of areas contained significant information about several aspects of inter-areal cortico-cortical connectivity, including the existence of projections and their laminar patterns. Second, the spatial separation of areas across the cortical sheet also contained information about whether connections are present or not. Therefore, a combination of the two structural measures of relative differentiation and spatial distance allowed us to classify the existence of connections in the data sets with high accuracy. Third, the relative position of cat

cortical areas in previously suggested hierarchical orderings was not informative about their inter-areal connectivity. Fourth, differences in thickness between macaque cortical areas, while smaller between connected than between unconnected area pairs, did not provide information about connectivity beyond what could be inferred from relative architectonic differentiation. Lastly, the architectonic differentiation of areas was related to two of their topological properties. These were their membership in a densely connected ‘rich-club’ hub module or network core, as well as the number of projections maintained by different areas (area degree).

Thus, architectonic differentiation was the structural measure that related most consistently and strongly to the investigated features of cortico-cortical connectivity. Figure 4.1 summarises this finding and displays all present projections that were included in the analyses. Areas are arranged according to their architectonic differentiation, and projections are colour-coded according to the architectonic similarity of the connected areas. The dominance of projections linking architectonically similar areas is quite apparent. Moreover, it is noticeable that hub-module and structural core areas are clustered at the lower end of the architectonic differentiation scale, as are areas with a relatively large number of connections (marked by their larger node size).

4.1.1 Relationship among structural measures

Since we draw inferences about the relative merits of different structural measures, their interrelations need to be considered. The degree to which relative architectonic differentiation and spatial proximity covary is not immediately evident. While we observed a moderate correlation of neuron density ratio and Euclidean distance in the sample of areas we considered in the macaque cortex, in the data set we considered in the cat cortex, the absolute architectonic type difference and border distance of area pairs were not correlated. Architectonic differentiation frequently changes gradually across the cortical surface of cats (Hassler and Muhs-Clement, 1964; Sanides and Hoffmann, 1969) and primates (Sanides, 1970; Barbas and Pandya, 1989; Zilles and Amunts, 2012b), which intertwines relative architectonic differentiation with the spatial distance between areas. However, the gradual change in architectonic differentiation repeats multiple times across the cortical sheet, for instance, between primary and more remote ‘association’ areas within modules. In our approach, we assessed the proximity of areas along all spatial directions, not just along a select axis (e.g., caudal to rostral), obscuring potential correlations for specific spatial gradients of architectonic differentiation. The resulting mixed results regarding their correlation

4.1. The architectonic type principle captures cortico-cortical connectivity across mammalian cortices

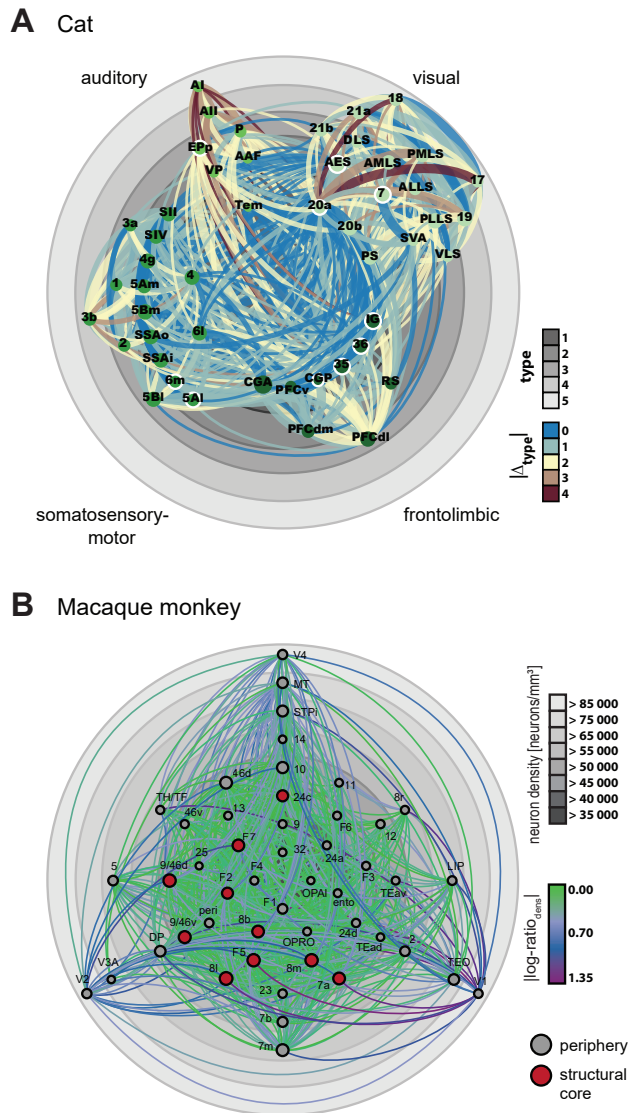


Figure 4.1: The architectonic basis of the mammalian connectome. **(A)** Cat cortical connectome based on architectonic type gradients. All present projections between cortical areas for which an architectonic type was defined (49 of 65 areas) are displayed. Circles correspond to architectonic types, cortical areas are placed accordingly. Architectonic type increases from center to periphery. Projections are colour-coded according to the absolute architectonic type difference of the connected areas. Ordinal projection strength (sparse, intermediate, or dense) is coded by increasing projection width. Nodes are grouped and colour-coded according to anatomical modules as indicated. Node sizes indicate the areas' (unweighted) degree. Hub-module areas, as classified by Zamora-López and colleagues (2010), are marked by a white outline. **(B)** Macaque cortical connectome based on neuron density gradients. Grey circles correspond to periphery; cortical areas are positioned accordingly (cf. Figure 2.2). Present projections between cortical areas are displayed colour-coded according to absolute neuron density ratios of the connected areas from green (small ratios) via blue to purple (large ratios). Node sizes indicate the areas' degree (i.e., number of connections). Areas belonging to a structural core, as classified by Ercsey-Ravasz and colleagues (2013), are filled in red. Abbreviations as in Markov et al. (2014a).

thus indicates that the two measures of relative architectonic differentiation and spatial proximity capture largely independent structural aspects at the global cortical level, justifying our treatment of them as independent variables. Moreover, spatial proximity and hierarchical level difference were not correlated in the cat cortex data set, indicating that they, too, describe independent aspects of cortical organisation.

In contrast, relative architectonic differentiation and hierarchical level difference were found to be interdependent factors. This association arises inevitably from the fact that relative architectonic differentiation and laminar patterns are strongly correlated and that cortical hierarchies are constructed from the laminar patterns, so that differences in hierarchical levels actually emerge from the strong relationship between architectonic differentiation and laminar projection patterns.

Lastly, cortical thickness has been reported to be inversely related to neuron density in the primate cortex (von Economo, 1927), and also in our data set these two measures were negatively correlated. Thus, these two structural measures are not independent dimensions of cortical organisation.

Because of these possible interrelations between the structural measures, we designed our analyses, particularly our use of classification procedures, in such a way that they were able to account for potential interdependencies.

4.1.2 Connection existence can be classified based on architectonic differentiation and spatial proximity

We found that the structural measures differed markedly between pairs of cortical areas, depending on whether they were connected or unconnected. We capitalised on this association to classify the existence of projections based on the differences in structural measures between potentially connected areas. Integrating architectonic similarity and spatial proximity in predictive models made it possible to determine whether two areas would be connected with high accuracy (Figure 3.5B, Figure 3.11B). The classifiers trained in the cat and macaque cortex showed that a connection was most likely to exist between areas that are similar in their architectonic differentiation and spatially close (Figure 3.5A, Figure 3.11A). While there was considerable uncertainty about the status of projections between cortical areas possessing combinations of intermediate differences in architectonic differentiation and intermediate spatial distance, we were able to derive predictions for the existence of as yet unstudied projections between cortical areas which fall into those ranges of relative architectonic differentiation and spatial proximity which were confidently associated

with either absence or presence of projections. We used the trained classifiers to make predictions about the status of unsampled projections (Figure 3.5C, Supplementary Table D.3), which provides an opportunity to compare our models' performance with future experimental results, allowing further model validation. For example, the data sets currently contain insufficient information to resolve the question of which of the structural measures dominates in cases of opposing predictions. Classification from alternative feature combinations in the macaque cortex revealed that, when the three structural measures were used as single predictors, architectonic similarity yielded the highest maximum Youden index J compared to spatial proximity or thickness similarity on their own (Supplementary Figure C.2B). This suggests that the performance of the predictive model hinged predominantly on architectonic similarity and to a lesser extent on spatial proximity. While thickness similarity also correlated with the relative frequency of present projections, including this feature into our predictive model did not improve classification performance. Furthermore, even though the relative thickness of brain areas was strongly correlated with the areas' relative neuron density, substituting density similarity for thickness similarity led to a considerable decrease in our model's predictive power.

Our models predict symmetric connectivity, that is, connections from areas of weak to areas of strong differentiation are expected to be as likely as connections from strong to weak differentiation. This prediction disregards the possibility that mechanisms may exist which preferentially mediate connections of one direction over the other, thus leading to asymmetric connectivity profiles. Furthermore, the data sets provided an unequal sampling of the predictive variable space, which may have biased the resulting models.

Nonetheless, the predictive models also revealed that, although the likelihood of a connection decreased across large differences in architectonic differentiation or long distances, this effect was mitigated if areas were spatially very close or respectively very similar in their architectonic differentiation. Thus, although connections were relatively less likely to exist between spatially remote areas, they did occur preferentially when distance was compensated for by similar architectonic differentiation. Axonal wiring costs are a major constraint on structural connectivity (Bullmore and Sporns, 2012) but are not strictly minimised in neural networks (Bullmore and Sporns, 2009; Chen et al., 2006; Kaiser and Hilgetag, 2006), since connections across longer distances can provide network shortcuts that boost efficiency from a functional perspective. In the presented results, we did not explore the impact of potential functional constraints, such as topological path length (which may be related to functional efficiency), on connectivity features. Naturally, our approach for classifying the existence of connections could be augmented by considering additional functional or

topological properties that have been explored previously (Jouve et al., 1998; Costa et al., 2007). Incorporating a broader range of factors could potentially enable us to reproduce features of cortico-cortical connectivity that are not resolved by our models in their current form, such as modularity and hub features, which have been suggested to result from a combination of spatial and topological properties (Chen et al., 2013).

Notwithstanding possible additions to the predictive models, our results highlight architectonic differentiation as a key factor for predicting the occurrence of costly connections between spatially remote areas.

4.1.3 Topological features are related to architectonic differentiation

Topological features of areas, such as their degree, have implications for their interaction with other areas in cortical networks. We found that areas belonging to the core or hub-module of the network of cortico-cortical connections were of weaker architectonic differentiation than areas in the periphery (Figure 3.12A, Figure 3.6A). This finding complements the observation that there are differences in several aspects of regional cellular morphology (e.g., dendritic tree size) between core and periphery areas (Scholtens et al., 2014). One of the main defining features of core areas is their exceptionally large number of connections (Hagmann et al., 2008; Harriger et al., 2012). Therefore, we assessed whether there exists a direct relationship between architectonic differentiation and area degree (i.e., the number of connections maintained by an area), without interposing the classification into core or hub-module and periphery areas. This analysis revealed a strong general relationship between area degree and architectonic differentiation across the entire cortex in the cat and the macaque, where areas of weaker differentiation possessed a larger number of connections (Figure 3.12B, Figure 3.7A), consistent with previous findings (Barbas and Pandya, 1989). Moreover, a similar association has been observed in the human brain, where less differentiated agranular or dysgranular areas had the highest amount of functional connectivity (Wylie et al., 2015).

More specifically, in the cat cortex, areas of a lower type appeared to possess a larger number of sparse and intermediate projections added to a backbone of dense connections which remained uniform across areas of all architectonic types (Figure 3.8). In contrast to architectonic differentiation, cortical thickness in the macaque cortex showed an inconsistent and weaker relationship to membership in the structural network core and area degree.

Shifting focus to the levels of architectonic differentiation which are present in the different modules that have been identified in the cat and the macaque cortex, we found variation in architectonic differentiation across modules. Specifically, we observed the weakest differentiation in the fronto-limbic module and the strongest differentiation in the visual module (Figure 3.6B). It has been suggested that network modules in the cortex result from a combination of spatial and topological properties (Chen et al., 2013). Our findings suggest that architectonic differentiation may be another factor in the formation of structural modules.

The differences observed in average level of architectonic differentiation in different cortical modules may partly explain their strong intra-modular connections—since minimal differences in architectonic differentiation were associated with dense connectivity between areas—and ultimately the separation of cortico-cortical connections into modular subnetworks linking areas of different sensory and motor functions. However, the actual mechanisms leading to the formation of cortical modules are still unresolved (Kaiser and Hilgetag, 2007).

Finally, in the cat cortex, we also found a relationship between the architectonic differentiation and the connection distances profile of areas, such that areas of a lower architectonic type had larger proportions of long connections and smaller proportions of short connections than observed in areas of a higher architectonic type. Thus, areas of weaker architectonic differentiation appear to be more widely interlinked with other brain regions, both in terms of their number of connections and in terms of the spatial range of their connections, compared to regions of stronger architectonic differentiation which typically correspond to the primary sensory and immediately neighbouring areas of each major uni-modal module.

4.1.4 Methodological considerations

The presented findings hinge on the reliability of the data sets and analyses employed. Since, in the cat cortex, we considered data on cortico-cortical connectivity that were collated across a large number of studies, aspects of the execution as well as the collation of tract-tracing experiments need to be considered. Moreover, we used multiple measures of cortical structure, each associated with similar questions concerning their reliability.

Data sets of adult cortico-cortical connectivity

We highly value the data set of cortico-cortical connectivity in the macaque monkey by Markov and colleagues (2014a), because the tract-tracing studies have been performed to a high technical standard. Moreover, results from the considerable number of injections can be combined easily, since experimental variables have been controlled very closely across injections.

In contrast, for the cat cortex, the most comprehensive and detailed data set of cortico-cortical connectivity that is available (Scannell et al., 1995), is a collation of results from a wide range of experimental conditions. The data set derives from anatomical studies published between 1968 and 1991 using intracellular transport of tracers. While this methodology usually enables the unambiguous detection of direct inter-areal connections, tracing studies are subject to technical caveats, which affect especially older results. For example, tracer uptake in fibres of passage can lead to false-positive results, while false-negative results can be caused by unsatisfactory tracer uptake, transport and/or detection (reviewed in, e.g., Heimer and Robards, 1981; Lanciego and Wouterlood, 2011). The data set could therefore diverge from the actual pattern of connectivity especially by erroneous ‘absences’ of projections, which cannot be detected in a single tracing experiment. Notwithstanding these limitations, tract-tracing remains the gold-standard technique for evaluating structural connections, and the caveats associated with older studies do not detract from the data set’s unique coverage of the cat cortex.

Another potential limitation of this connectivity data set is the adequacy of the specific cortical parcellation scheme used by the data collators, since alternative subdivisions have been proposed for all regions of cat cortex to that adopted by Scannell and colleagues (1995), which we followed here. The determination of area boundaries directly relates to connectivity patterns, with subtle differences in the latter often used to demarcate borders between neighbouring areas. However, global organisational aspects of brain networks appear to be relatively robust to different parcellation schemes (de Reus and van den Heuvel, 2013). The collators also necessarily averaged connectivity across areas, thus masking any inhomogeneities within and between them, such as possible differences in selective connectivity strengths between areas of the visual module containing ‘over-representations’ of central versus peripheral or of upper versus lower fields, or between tonotopic and non-tonotopic areas of auditory cortex. A further related question concerns the validity of the criteria used by the collators to assess relative inter-areal connection strengths (including apparent ‘absences’) across tract-tracing experiments that used techniques with differing sensitivities. While we acknowledge that future resolution

of these matters may result in changes to our connectional summary (Figure 4.1), we do not expect them to obscure the systematic properties of the global cortical connectome that we have identified.

We further note that, because both connectivity data set contains information exclusively about ipsilateral cortico-cortical connections, our findings provide no insight into principles governing the connectivity across the cortical hemispheres.

Structural measures

Architectonic differentiation We employed two ways to quantify the structural measure of architectonic differentiation, namely an ordinal ranking into architectonic types and the quantitative empirical measure of neuron density. One caveat applying to our architectonic type classification is that architectonic differentiation of the mammalian cerebral cortex likely forms a gradual continuum (Sanides and Hoffmann, 1969; Sanides, 1970), as do laminar projection patterns, even though they have been grouped into ordinal classes (e.g. Grant and Hilgetag, 2005). Therefore, a measure objectively capturing gradual transitions across the cortex would be more faithful than the discrete architectonic types we assigned to brain regions. One such measure is neural density, but unlike for the macaque cortex, such stereologically measured neuron density data were not available for a significant part of the cat cortex. However, neuron densities across cortical layers have previously been reported to vary systematically between areas classified into architectonic types by the criteria used here (Dombrowski et al., 2001). We are confident, therefore, that our discrete architectonic type classification captured genuine and relevant effects of architectonic differentiation.

Is it justified, then, to assume that neuron density suitably reflects overall architectonic differentiation? Even though it is a measure of but one aspect of cytoarchitecture, we argue that it is, indeed, the most comprehensive individual measure indicative of architectonic differentiation that has been objectively quantified for a considerable number of species and cortical areas. Other crucial features of cytoarchitecture include the number and distinctiveness of cortical layers and the relative width and granularity of layer 4. Additionally, features that cannot be observed in cytoarchitecture, for example myeloarchitectonic properties, contribute to a fuller characterisation of cortical differentiation (see Barbas and García-Cabezas, 2015). However, many of these aspects are difficult to quantify. Moreover, there exists no consistent, objective framework for integrating these measures into a one-dimensional

ranking of architectonic differentiation. In practice, therefore, estimates of the overall differentiation of brain areas were usually obtained by subjective expert categorisations, resulting in the assignment of areas to architectonic types, as we also made use of. In contrast, neuron density can be determined objectively using unbiased stereologic methods. In a comparison of multiple quantitative features of cortical architecture, neuron density turned out to be the most discriminating parameter for identifying cortical areas in the primate prefrontal cortex (Dombrowski et al., 2001). The features included in that analysis comprised cortical thickness, and density of different cell markers, including neurons, glia, and neurons labelled with calbindin, calretinin or parvalbumin, and their respective laminar distributions. Thus, neuron density is a well established, characteristic measure for quantifying architectonic differentiation of cortical areas.

Spatial proximity We quantified spatial proximity using three different measures of spatial distance: border distance, Euclidean distance, and geodesic distance. All three measures have in common that they only approximate actual lengths of projections. This is due to two factors: First, we used generic measures of the distance between cortical areas, not measures associated with specific projections observed in tract-tracing experiments (which could only measure distance for present projections, but not absent ones, in any case). Second, even if projections lengths were attempted to be measured in tract-tracing experiments, it is technically very challenging to reconstruct the trajectories of individual axons through the brain for a large number of tracing experiments. Since no such measures of projection lengths were available for either the cat or the macaque cortex, we therefore employed pragmatic estimates of the distance between cortical regions which we assume to correlate strongly with actual projection lengths.

In the cat cortex, we used the ordinal measure of border distance to quantify the spatial separation of areas, rather than an interval measure such as Euclidean or geodesic distance. This was mainly due to the fact that for the cat cortex, there is currently no detailed three-dimensional atlas available which quantifies the absolute distance between the mass centres of all areas. To obtain all the Euclidean or geodesic area separations in the absence of such reliable information would thus have necessitated a number of unsubstantiated assumptions, whereas the use of border distance requires fewer constraints. Border distances are, however, potentially distorted by unequal area sizes and do not account for the actual projection lengths, as axons run under gyri and/or around sulci between their origins and destinations. Despite these complications, border distance generally correlates strongly with Euclidean and geodesic distance where these latter are known (e.g., in the macaque cortex, border

distance with Euclidean distance: $\rho = 0.57, p = 0$; border distance with geodesic distance: $\rho = 0.66, p = 4e-323$).

Cortical thickness Lastly, to quantify the thickness of cortical areas, we used measurements of cortical thickness obtained from structural MRI in one macaque monkey. The MRI measures provided coverage of all cortical areas, and agreed well with the corresponding microscopic thickness measurements from histological sections (cf. Section 2.2.2). This finding is in line with similar agreements between histological and MRI-based thickness measures seen for cortical regions of the human brain (Scholtens et al., 2015). Therefore, the thickness measurements were considered reliable, despite the small sample size. Reliability was further strengthened by averaging thickness values for corresponding regions of the left and right hemisphere.

4.1.5 **Connectivity is not optimised solely for minimal wiring**

We showed that spatial proximity is one structural measure that is reliably associated with the existence of connections, and strongly relates to the strength of connections. Spatial proximity did not capture how strongly the laminar distribution of projection origins deviated from a columnar pattern. We found that, in the cat and macaque cortex, pairs of areas are less frequently interconnected, the further they are separated across the cortical surface. This result is consistent with a large number of studies that investigated constraints of brain connectivity and found neural wiring length to be of critical importance (Bullmore and Sporns, 2012). However, we also observed that a significant portion of longer projections was in fact present, mostly when a large spatial distance was counterbalanced by a small difference in architectonic differentiation. Hence, brain connectivity does not appear to be exclusively optimised with respect to physical wiring length, because trade-offs exist, for instance, with minimal topological path length (Kaiser and Hilgetag, 2006; Bullmore and Sporns, 2009). Thus, individually, the distance model appears useful mainly as a predictor of the numerical neuron strength (high versus low) of connections.

4.1.6 **Cortical thickness is not a suitable predictor of connectivity**

While thickness measures have the advantage of being accessible non-invasively using MRI in humans, their relation to other anatomical features and to structural

connectivity remains unclear. Our findings suggest that, while cortical thickness may show similarities to neuron density in its variability across the cerebral cortex, it is an imperfect surrogate and does not capture the fundamental aspects of brain networks that can be delineated from architectonic differentiation.

4.1.7 A cortical hierarchy is not a suitable predictor of connectivity

In the cat cortex, hierarchical level difference was strongly correlated with the assigned ‘hierarchical’ direction of projections (Figure 3.9B). But this finding is neither surprising nor instructive, as the anatomical hierarchy had been constructed from these connection orientations in the first place (Scannell et al., 1995), so that the correlation between the two variables was based on a circular approach. Concerning the absence or presence of projections, the relative position of two areas within the hierarchical ordering was uninformative (Figure 3.4C), with areas on adjacent levels of the hierarchy being no more frequently interconnected than those separated by more levels. This finding is contrary to the common understanding of hierarchical cortical schemes (Felleman and Van Essen, 1991). It also resonates with several other shortcomings of hierarchical processing schemes, such as their failure to account for the level-skipping nature of many cortico-cortical (and thalamo-cortical) pathways (Symonds and Rosenquist, 1984; Goldman-Rakic, 1988; Mountcastle, 1995; Hilgetag et al., 2000b; Petroni et al., 2001) or physiological features of cortical processing, in terms of near-synchronous response latencies (Nowak and Bullier, 1997; Schmolesky et al., 1998) and similarities in receptive field size and complexity for the same stimulus (Hegd  and Van Essen, 2007) at ‘lower’ and ‘higher’ hierarchical levels. Moreover, an optimal hierarchy has hitherto proven elusive, as large numbers of different orderings comply equally well with the constraints provided by the anatomical data (Hilgetag et al., 1996, 2000a). While the great laminar regularity of inter-areal projection patterns is certainly intriguing, it remains open for discussion whether elaborate schemes for ordering brain areas hierarchically are fundamentally helpful for understanding cortical organisation (Hegd  and Felleman, 2007; Markov et al., 2013b).

4.1.8 The architectonic type principle is further corroborated

Previous studies, which were restricted largely to fronto-limbic regions of macaque monkey cortex (Barbas, 1986; Barbas and Rempel-Clower, 1997; Rempel-Clower and Barbas, 2000; Barbas et al., 2005) or to the visual module in the cat (Hilgetag and Grant, 2010), have demonstrated strong associations between architectonic differentiation and laminar connectivity. Here, we reported that the laminar projection patterns across the whole cat and macaque cortex were very well accounted for by architectonic similarity. In contrast, there was no systematic relationship between laminar patterns of projection origins and either distance or cortical thickness in the macaque cortex, when the correlation with relative architectonic differentiation was accounted for. Moreover, the associations reported between architectonic differentiation and connection existence as well as topological properties of areas suggest that several features of cortico-cortical connectivity can largely be accounted for by the underlying architectonic properties of the cerebral cortex. Specifically, the relative architectonic differentiation of the cortex provides an essential scaffold for explaining the organisation of structural brain networks.

Both in the cat and the macaque cortex, architectonic similarity integrated with spatial proximity was highly predictive of the existence of connections between area pairs. This close association of cortical architecture with connectivity was observed for areas distributed across the entire cortical surface, and was not contingent on grouping the areas into functional or anatomical modules of any kind. Furthermore, an inverse relationship between the architectonic differentiation and the connection degree of areas was observed in both species, such that areas of weaker differentiation have more connections. Highly connected areas are often hubs or members of a functionally prominent rich-club, occupying a topologically special position within networks of structural connections (e.g. Harriger et al., 2012; van den Heuvel and Sporns, 2013a). Moreover, weakly differentiated areas likely differ from more strongly differentiated areas in their intrinsic circuitry and signal processing properties (cf. Section 3.1). Hence, this observation is indicative of differences in the functional roles performed by areas across the spectrum of architectonic differentiation.

In summary, there is excellent correspondence of findings across two mammalian species and across the entire cerebral cortex. Furthermore, these findings were recently paralleled in the mouse cortex (Goulas et al., 2017). Analyses of comprehensive global cortico-cortical connectivity thus closely mirror previous findings across a number of cortical systems and connection targets, including the contralateral hemisphere and the amygdala, in several species (Barbas, 1986; Barbas and Rempel-Clower,

4.2. Compared to measures of neuron morphology, neuron density is a superior indicator of connectivity features

1997; Rempel-Clower and Barbas, 2000; Dombrowski et al., 2001; Barbas et al., 2005; Medalla and Barbas, 2006; Ghashghaei et al., 2007; Medalla et al., 2007; Hilgetag and Grant, 2010; Hilgetag et al., 2016; Goulas et al., 2017). Our findings, therefore, show that the architectonic type principle extends across species and from the local, intra-modal level to the global organisation of the cerebral cortex as a whole. Combined with evidence from previous studies, our findings suggest that the reported association between architectonic differentiation of cortical areas and features of the inter-areal brain network reflects general organisational principles underlying the formation and maintenance of connections in the mammalian cortex.

Parts of this section have been published in Beul et al. (2015) and Beul et al. (2017).

4.2 Compared to measures of neuron morphology, neuron density is a superior indicator of connectivity features

The extent to which cortical architecture determines the organisation of structural connectivity in the cerebral cortex has been examined from a variety of macroscopic and microscopic perspectives (Hilgetag and Grant, 2010; Scholtens et al., 2014; Hilgetag et al., 2016) (for a review see Barbas, 2015). In Section 3.4, we explored the relative explanatory power of six structural measures with regard to the organisation of cortico-cortical connections in the macaque cortex. These architectonic measures were examined individually in previous reports (Scholtens et al., 2014; Hilgetag et al., 2016; Section 3.3) and fall into two broad categories: The first group consists of the macroscopic measures of architectonic differentiation, measured as neuron density, and spatial proximity, measured as geodesic distance. The second group comprises the microscopic cellular morphological measures of soma cross section, total dendritic spine count, peak dendritic spine density, and dendritic tree size, all measured in L3 cortical pyramidal neurons. We considered these measures in conjunction, to assess how they relate to each other as well as to establish which of them carried the most weight for explaining fundamental organisational aspects of the macaque cortical connectome.

We found that all morphological measures were strongly correlated with neuron density as well as mostly interrelated among each other (Table 3.1). Moreover, all six structural measures diverged depending on whether areas were linked by a projection or not (Figure 3.14, Table 3.2). This finding raised the question of whether all of these

4.2. Compared to measures of neuron morphology, neuron density is a superior indicator of connectivity features

measures contribute equally to the discrimination of cortico-cortical connectivity, or whether some of them are redundant, being dependent on other factors, and supply no additional information. Systematic analysis by multivariate logistic regression analyses (Figure 3.15, Table 3.3) revealed that of the six measures, only three carried significant information allowing the prediction of projection existence. These were neuron density, geodesic distance and L3 pyramidal cell soma cross section. The other three cellular morphological measures did not add any information. Of the three significant predictive factors, neuron density emerged as the most relevant factor, reaching the best classification performance on its own and resulting in the largest decline in classification performance if excluded. This finding suggests that neuron density was the most informative of the five neural measures regarding the existence of projections, and arguably even the most informative of all six structural measures.

We further found that, even if all other structural measures were controlled for, geodesic distance was strongly and dendritic tree size difference was weakly correlated with projection strength (Table 3.4). This is in line with previous reports showing projection strength to decline as distance between connected areas increases (Ercsey-Ravasz et al., 2013; Markov et al., 2013b).

Additionally, the laminar patterns of projection origins were correlated with the neuron density ratio (Figure 3.17, Table 3.5), but they were not correlated as strongly or as consistently with the other five measures. This corroborates previous findings on the importance of architectonic differentiation regarding the laminar distribution of projecting neurons (e.g. Barbas, 1986; Beul et al., 2015; Hilgetag et al., 2016). Figure 4.2 illustrates the observed patterns of projection origins in the context of the five neural measures. Furthermore, the observed lack of a meaningful correlation between laminar projection patterns and spatial proximity directly contradicts the hypothesis that physical distance has a crucial role in affecting laminar patterns (Salin and Bullier, 1995).

Moreover, neuron density was the only structural measure that was correlated with the topological measure of overall area degree, that is, the number of afferent and efferent connections of cortical areas (Figure 3.18, 3.6). Considering in-degree and out-degree separately revealed a strong negative correlation between out-degree and neuron density, even if all other measures were controlled for. That is, areas of weaker differentiation tended to innervate more areas than more strongly differentiated areas, which would allow the former to supply modulatory input to a large part of the cortex. For in-degree, we observed a moderate to strong correlation with both neuron density and dendritic tree size, both within the edge-complete 29×29 subgraph and cortex-wide, if the measures were considered individually. These

4.2. Compared to measures of neuron morphology, neuron density is a superior indicator of connectivity features

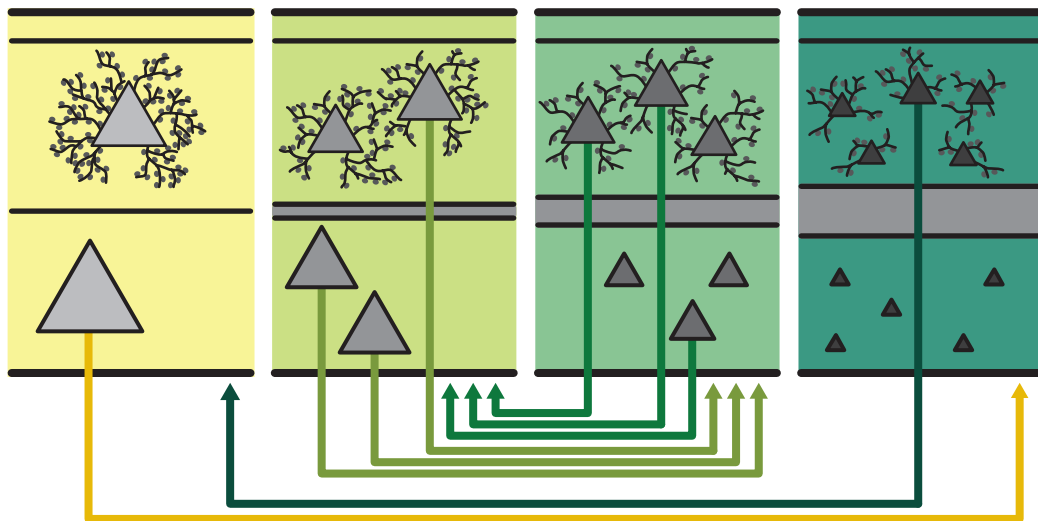


Figure 4.2: Projection patterns in the context of cortical structural variation. Both macroscopic and microscopic structural measures exhibit concurrent and spatially ordered changes across the cortex. Such cortical gradients have been described for many properties of the cortical sheet (e.g. Abbie, 1940; Sanides, 1962; Zilles and Palomero-Gallagher, 2017), and are closely tied to the organisation of structural and functional connections (cf. Figure 4.3). Here we find that less architectonically differentiated cortical areas (agranular, yellow) are characterised by lower neuron density and more elaborate morphology of layer 3 pyramidal cells than more strongly differentiated areas (eulaminate, dark green), with gradual changes across the spectrum (light green, medium green). Specifically, as shown in Table 3.1, higher neuron density correlates with smaller cross section of the soma and smaller size of the dendritic tree as well as with lower total spine count and lower peak spine density. Laminar patterns of projection origin are indicated as observed in this report (cf. Table 3.5) and consistent with the architectonic type principle of cortical connectivity (Barbas, 1986, 2015). Connections between areas of similar architectonic differentiation show a bilaminar projection origin pattern (light green to medium green, medium green to light green), while connections between areas of distinct differentiation show a skewed unilaminar projection pattern, with projections originating predominantly in the infragranular or supragranular layers (yellow to dark green, representing agranular to eulaminate projections, and dark green to yellow, representing eulaminate to agranular projections).

4.2. Compared to measures of neuron morphology, neuron density is a superior indicator of connectivity features

correlations were not robust enough to remain significant if all other measures were controlled for. This could be due to an actual lack of a relationship with in-degree, or, alternatively, added noise from the other three cellular morphological measures (which were not significantly correlated with in-degree individually) could have made a relationship indiscernible. In the latter case, areas of weaker differentiation as well as areas with larger dendritic tree sizes would tend to be targeted by more projections. This observation would be in line with less differentiated areas being set up for the integration of sensory inputs over a relatively large part of the cortex and for meta-processing (e.g. Goldman-Rakic, 1988; Buckner and Krienen, 2013). Moreover, to accommodate a larger number of incoming afferents, more dendritic space might be necessary.

Regardless of their interpretation, the results for in-degree within the edge-complete 29×29 subgraph were very similar to the results for cortex-wide in-degree. This observation corroborates a previous proposition (Ercsey-Ravasz et al., 2013) stating that the edge-complete 29×29 subgraph, whose constituent areas were widely distributed within the complete set of 91 cortical areas, is representative of the cortex-wide full network of inter-areal connections. Our analysis of in-degree, thus, indicates that the results for overall degree as well as out-degree, which took into account only connections within the 29×29 subgraph, reflect genuine cortex-wide relationships between the structural measures and area degree.

In summary, our analyses indicate that, while the cellular morphological measures and the area-based measure neuron density are closely related, neuron density is a more essential predictor of three of the four tested basic features of cortico-cortical connectivity (projection existence, laminar projection patterns and area degree) than the cellular morphological measures. Thus, our analyses unify various previous reports that related different aspects of cortical architecture to each other as well as to features of cortical connectivity. This finding is consistent with previous reports which demonstrated that neuron density provided a more characteristic ‘fingerprint’ of the architectonic differentiation of cortical areas than other architectonic measures (Dombrowski et al., 2001), as well as with reports showing that a close relation between architectonic differentiation and cortico-cortical connectivity could also be observed in different mammalian species such as the cat (Hilgetag and Grant, 2010; Section 3.2), the mouse (Rubinov et al., 2015; Goulas et al., 2017), and humans (van den Heuvel et al., 2015).

4.2.1 Limitations of the explanatory power of the cellular measures

The present results show that a characteristic indicator of the overall degree of architectonic differentiation, neuron density, is well suited to account for structural connections within the global, macro-scale cortical connectome of the primate. In contrast, more fine-grained structural aspects of the cortex, such as the cellular morphological features considered here, convey less information on the connective features of areas, appearing as derivative properties determined mostly by overall regional differentiation. However, it should be noted, that the considered morphological measures were solely acquired in supragranular cortical layer 3 and characterise only pyramidal neurons. Hence, these measures were not designed to comprehensively capture the intrinsic architectonic organisation of cortical areas. Considering such inherent differences between the measures, it is plausible that neuron density, as an overall characterisation of area architecture, correlates better with the areas' macroscopic connectivity properties, as found. If a more detailed characterisation of cellular morphology was available, for example through equivalent morphological measures obtained from the infragranular layers, the morphology might be captured by a summary measure (e.g., ratios across different laminar compartments) which could be used to characterise overall cortical architecture. Such a more detailed characterisation of cellular morphology might then correlate with macroscopic properties of the connectome as well as neuron density. Moreover, it will be interesting to see how such findings might vary across the spectrum of mammalian cortical organisation, considering that the degree to which architectonic gradients exist within the cortex of a species is variable across mammals (Goulas et al., 2018, 2019a).

4.2.2 Developmental mechanisms may regulate the covariation of architectonic measures

Systematic, joint variation of different features of cellular morphology has been observed between cortical regions within mammalian species. In primates, a higher number and higher density of spines and more complex dendritic arbors have been reported in prefrontal cortices compared to motor or sensory cortices (Elston, 2003, 2007; Elston et al., 2011a; Bianchi et al., 2013). In mouse cortex, spine density in the prelimbic and infralimbic fields is twice as high as in other cortex (Ballesteros-Yáñez et al., 2010), and spine size varies across the cortex (Benavides-Piccione et al., 2002). Here, we have shown that these gradual changes in cell morphology are

4.2. Compared to measures of neuron morphology, neuron density is a superior indicator of connectivity features

aligned with the overall degree of architectonic differentiation observed in cortical areas, by reporting a negative relationship between architectonic differentiation and morphological complexity. Figure 4.2 gives an overview of the observed relations between the five structural measures. Cortical gradients, that is, concurrent and spatially ordered changes across the cortical sheet, have been described for these and multiple other macroscopic and microscopic structural measures (e.g. Abbie, 1940; Sanides, 1962; Zilles and Palomero-Gallagher, 2017), and are closely related to the organisation of structural and functional connections across the cortex (see Section 4.2.3 below). Moreover, it has been noted that variation in both cellular architecture and neuron numbers is well aligned with developmental gradients (Charvet and Finlay, 2014; Charvet et al., 2015). This link has been corroborated by findings in the human cortex, which directly traced the systematic architectonic variation of the cortex to the timing of development (Barbas and García-Cabezas, 2016). Thus, multiple dimensions of cellular morphology appear to be tightly coupled, matching the overall degree of area differentiation as well as variation in developmental timing. Together, these observations point towards a precise orchestration of cell specification during ontogenesis, such that morphological, microscopic features of neurons and the macroscopic architectonic differentiation of an area as a whole grow attuned.

Additionally, physical self-organisation may play a role in shaping the covariation of morphological measures and overall architectonic differentiation, which is determined by spatio-temporal developmental gradients. Assuming that neurons and neuropil are packed into the available cortical volume as tightly as possible, thus approximating maximum volume packing (e.g., Chklovskii et al., 2002), the cellular morphological features would be expected to co-vary with neuron density, similar to what is observed. In particular, a higher density of neurons would be accompanied by smaller somata, less extensive dendritic arborisation, and potentially dendrites that are less spiny. Indeed, in the present study we report a negative correlation between neuron density and soma cross section. However, this finding does not necessarily provide evidence for a general inverse relationship between neuron density and the size of neuronal somata. Beyond the questions of which neuronal populations were evaluated for cellular features and how soma cross section was measured, aspects other than variations in neuron density are expected to affect soma size. These aspects include, for example, the phenomenon of externopyramidization (Sanides, 1962; Goulas et al., 2018), which describes a systematic shift across the cortex in relative soma size, from the largest projection neurons being located in infragranular layers of mostly less dense internopyramidal areas to the largest neurons being located in supragranular layers of neuronally dense externopyramidal areas. However, the effect of externopyramidization on soma size specifically in layer 3, where the

4.2. *Compared to measures of neuron morphology, neuron density is a superior indicator of connectivity features*

presently used morphological data were acquired, is difficult to ascertain. Moreover, the general hypothesis of a gradual decrease of overall soma size with increasing architectonic differentiation needs to be reconciled with specific contradictory observations. For example, many cells observed in the posterior orbitofrontal cortex of the macaque monkey are noticeably smaller than cells observed in the secondary somatosensory cortex (Barbas, 1986, their Figure 2).

4.2.3 Local cortical architecture, features of cortico-cortical connections and areas' functional roles are tightly interrelated

It appears that local cortical architecture and connection features of a cortical area, as well as an area's functional role within the cortical network, are tightly interrelated (Figure 4.3).

Connection features and functional roles

First, laminar projection patterns place origins and terminations in laminar microenvironments which are appropriate for the type of information exchange that occurs between the respective pairs of cortical areas. As noted before, the observed anatomical distinctions between laminar patterns of projections connecting areas of varying relative differentiation likely reflect differences in information processing (e.g. Barone et al., 1995). Specifically, projections that propagate information towards more abstract and multi-modal processing regions show a different laminar composition than projections that feed back the results of information integration to areas closer to the sensory periphery, affecting behaviour by modulating information processing (reviewed in Batardière et al., 1998; Buckner and Krienen, 2013; Harris and Shepherd, 2015). These anatomical distinctions are accompanied by differences in electrophysiological signatures associated with the respective pathways (Bastos et al., 2015). Moreover, neurons in infragranular and supragranular layers have been shown to possess different physiological (Lagae et al., 1989; Nowak et al., 1995; Raiguel et al., 1995) as well as histochemical (Hof et al., 1996, 1997) characteristics. These observations are functionally relevant, since even small variations in cell-intrinsic properties can induce substantial differences in the computations performed by otherwise similar circuits (Harris and Shepherd, 2015). A large body of work on hierarchical predictive coding integrates aspects of connectivity such as

4.2. Compared to measures of neuron morphology, neuron density is a superior indicator of connectivity features

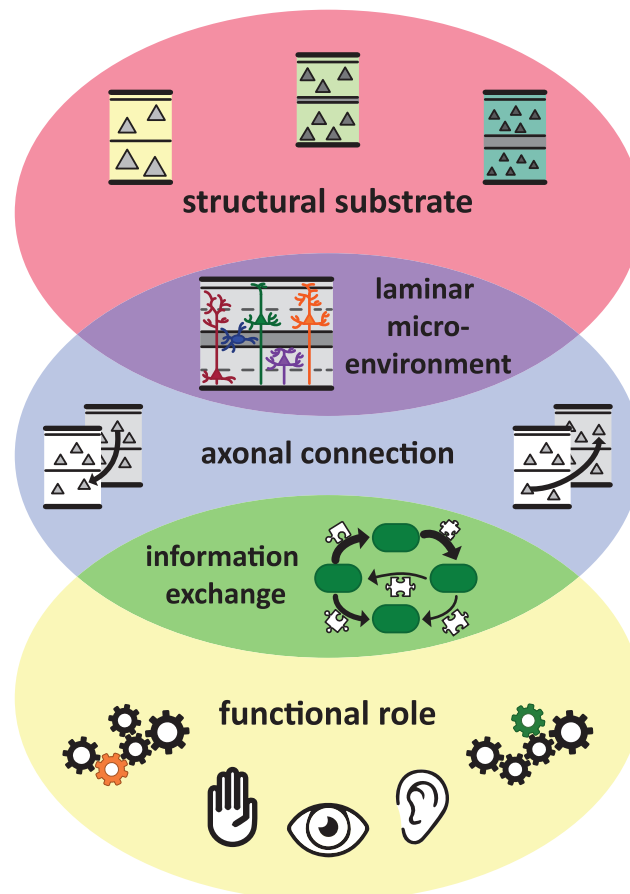


Figure 4.3: Structure and function of brain areas and connections are interlinked. Connections create functions of brain areas and functional interactions among brain areas from the structural substrate of the brain, particularly the cortical sheet. In particular, areas are linked through connections which have a laminar composition that is appropriate for the laminar microenvironment within the respective areas and the type of information exchange between these areas. Thus, local cortical architecture, the connection features of a cortical area, and an area's functional role within the cortical network are tightly intertwined. See Section 4.2.3 for an elaboration of the links between these three aspects.

4.2. Compared to measures of neuron morphology, neuron density is a superior indicator of connectivity features

intrinsic, local microcircuitry, laminar projection patterns and oscillatory signatures of pathways to explain the perception of sensory signals (e.g. Bastos et al., 2012; Friston et al., 2015; Shipp, 2016). The modulation of information processing is accomplished through precisely targeted inputs (reviewed in Larkum, 2013), so that exerting a modulatory effect does not require an accumulation of incoming connections, but can be achieved by relatively weak inputs. This situation is in contrast to driving inputs delivered by feedforward projections that originate predominantly in supragranular layers. In a comparison of feedforward and feedback projections that were similar in their absolute deviation from bilaminar projection patterns (i.e., $|N_{SG\%}|$), feedforward projections were reported to be stronger than feedback projections (Markov et al., 2013b), illustrating diverging requirements for driving and modulating influences. Similarly, feedforward projections terminating in middle cortical layers were shown to have larger boutons, and hence potentially stronger drive, than projections terminating outside the middle layers (Germuska et al., 2006). Moreover, the stronger, driving effect of feedforward projections is counterbalanced by their more pronounced capacity to elicit inhibition, as reported by D'Souza and colleagues (2016), who have shown that the fraction of inhibitory targets is larger for feedforward than feedback projections. Connection features thus correspond well to the functional roles of connected areas.

Functional roles and cortical architecture

Second, in a complementary way, the intrinsic processing capabilities of cortical areas are, to a large extent, determined by local characteristics of cellular morphology, as detailed in Section 2.2.1.2. Cellular morphological properties and the functional roles of cortical areas, thus, also appear attuned to each other.

Cortical architecture and connection features

Finally, the relation between cortical architecture and connection features completes the three interacting aspects. The observations integrated into the architectonic type principle extensively describe this interrelation. Moreover, the dependence of cortical connections on relative architectonic differentiation formalised in the architectonic type principle affords deeper insight into multiple aspects of the organisation of cortical connectivity (reviewed in Barbas, 2015; Hilgetag et al., 2016). For example,

4.2. Compared to measures of neuron morphology, neuron density is a superior indicator of connectivity features

the arrangement of areas by relative differentiation is consistent with onset latencies in the visual system (Petroni et al., 2001) and an ordering of areas inferred from their functional interactions in different frequency bands (Bastos et al., 2015). Laminar projection patterns indicate that areas of weak differentiation feed back information to more strongly differentiated areas (Barbas, 1986; Barbas and Rempel-Clower, 1997), placing them in a central position in the cortical network. This observation is consistent with their involvement in the default mode network (Raichle, 2011) as well as a suggested link to functional conscious access (Dehaene et al., 1998, 2011). The architectonic type principle also pertains to disruptions of specific pathways in diseases, for example autism (Zikopoulos and Barbas, 2010, 2013).

In summary, the strong correlation between the laminar origins of inter-areal projections and relative architectonic differentiation is closely intertwined with the functional relevance of a given projection. It reflects the seamless integration of the functional interplay of areas with local morphological properties and their associated intrinsic processing capabilities.

4.2.4 Neuron density is a powerful predictor of connectivity features

Cortical architecture has been shown to relate to fundamental aspects of the organisation of cortico-cortical connections (Barbas, 1986; Barbas and Rempel-Clower, 1997; Barbas et al., 2005; Medalla and Barbas, 2006; Hilgetag and Grant, 2010; Barbas, 2015; Hilgetag et al., 2016) and appears integral for understanding cortical connectivity. However, not all structural measures are equally informative on connectivity, as we have shown in conjoint analyses of multiple macro- and microscopic properties here, and as has been reported previously (Dombrowski et al., 2001; Hilgetag et al., 2016). We found that neuron density, a basic and classic (Brodmann, 1909) macroscopic indicator of overall architectonic differentiation of cortical areas, was more consistently related to multiple features of macaque cortico-cortical connectivity than four microscopic measures of cell morphology. These cellular measures, moreover, were themselves closely related to neuron density. Thus, it can be speculated whether these microscopic properties are developmentally attuned to the overall architectonic differentiation of the cortex. Such an alignment might result from neurodevelopmental mechanisms combining genetic determination of regionally specific gradients with processes of physical self-organisation, such as maximum volume packing, resulting in trade-offs between cell density and cell size as well as cellular complexity. Neuron density, thus, is a fundamental feature which links the macroscale and microscale architectonic and connectional organisation

of cortical areas and allows integrating the overall architectonic differentiation of areas with features of cellular morphology as well as with the existence and laminar characteristics of cortico-cortical connections. This insight may be a significant step towards the development of advanced across-scales models of cortical organisation and function.

This section has been published in Beul and Hilgetag (2019a).

4.3 The architectonic type principle is already applicable in the developing cortex

An explanation for the strong relationship between architectonic differentiation and connectivity features of cortical areas is likely to be found in ontogeny. The development of the regional architectonic structure may be associated with the establishment of the connections of an area. One possible mechanism might draw on the relative timing of the emergence of areas, where areas that appear earlier might have the opportunity to connect more widely (Dombrowski et al., 2001). Indeed, a similar process has been suggested to explain the degree distribution of single neurons in *Caenorhabditis elegans* (Varier and Kaiser, 2011; Towlson et al., 2013). The systematic architectonic variation of the cortex, which is at the core of the architectonic type principle, has recently been shown (in humans) to originate in cortical development (Barbas and García-Cabezas, 2016). Barbas and García-Cabezas (2016) also directly linked connectivity of the prefrontal cortex to its time of origin, thus providing strong support for the hypothesis that relative timing of area formation is a crucial determinant of cortical connectivity.

It remains unclear, however, by which mechanisms the relationship between architectonic differentiation and connectivity, which is the crucial component of the architectonic type principle, emerges in the developing brain. Compelling suggestions might result from exploring at which point in time the associations can first be observed. In Section 3.5, we report that the laminar patterns of projection origins, which have been shown to be closely associated with the relative architectonic differentiation of cortical areas, are already correlated with (eventual adult) architectonic differentiation in the immature macaque cortex. This has consistently been observed in intact fetal and neonate macaque monkeys as well as in enucleated infant macaque monkeys. Hence, it appears that the processes that determine which

4.3. The architectonic type principle is already applicable in the developing cortex

layers a projection originates from occur early in development, and are relatively robust to severe changes like the loss of sensory input. Since we report that laminar projection patterns are consistent with the architectonic type principle soon after their establishment, processes that occur later during ontogenesis appear to play a smaller role in the emergence of the architectonic type principle. This applies, for example, to processes such as pruning, activity-dependent remodelling or selective apoptosis in the different layers across the cortical gradient. These phenomena may serve to further refine the laminar patterns of projection origins, but do not appear to have a crucial role in determining their overall bias towards infra- or supragranular origin.

These observations about immature laminar patterns can inform attempts to explain how the architectonic type principle may arise during development. Since early, robust processes appear to be sufficient for its emergence, later processes could likely be omitted from a mechanistic explanation without losing much explanatory power. That is, a mechanism that takes into account only early processes but disregards later processes should still be able to generate laminar patterns that do not diverge too much from empirical observations. It has previously been hypothesised that spatio-temporal interactions in a forming cortical sheet could give rise to connectivity that is consistent with the architectonic type principle (Barbas, 1986; Barbas and García-Cabezas, 2016; Hilgetag et al., 2016). The fact that immature projection patterns are already consistent with the architectonic type principle, as presented here, implies that such spatio-temporal interactions may be sufficient to generate the typically observed laminar patterns of projection origins. If the underlying neurogenetic processes can be captured adequately, this link could be demonstrated *in silico*.

To sum up, we draw two main conclusions from the presented results (Figure 4.4). First, we show that already in the prenatal and neonatal cortex, the laminar patterns of projection origins correlate with the architectonic differentiation observed in the adult cortex, and that these laminar patterns are not substantially altered by complete loss of visual input. Second, it appears that the initially present biases in laminar projections patterns are progressively strengthened by later developmental processes. During this sharpening of laminar specificity, the amount of change that projections undergo in their supragranular contribution varies concurrently with the relative architectonic differentiation of the connected areas (Figure 4.4C). These findings have implications for the organisation of structural connectivity, indicating that early neurogenetic processes are sufficient to establish typical laminar projection patterns during brain development. We have previously suggested that the architectonic type principle results from spatio-temporal interactions in the forming

4.3. The architectonic type principle is already applicable in the developing cortex

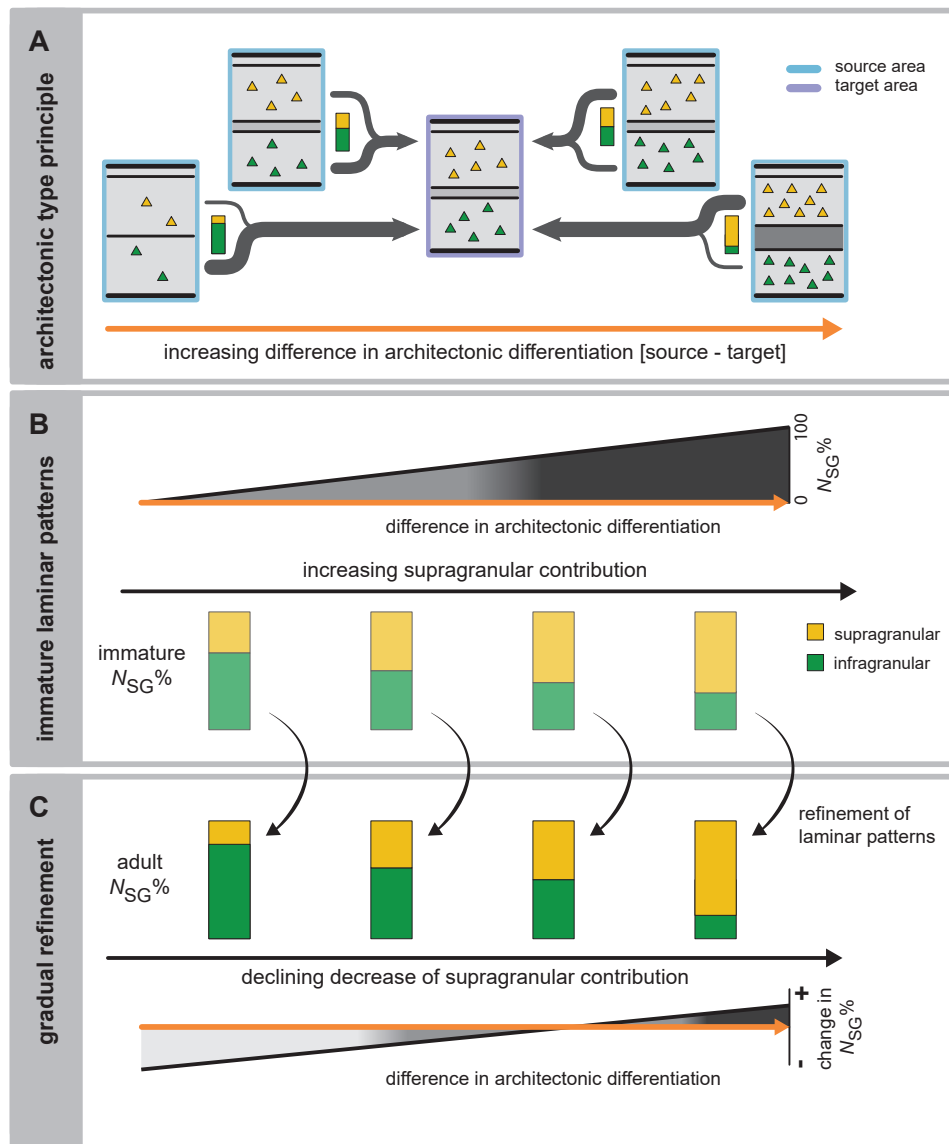


Figure 4.4: Summary of changes in laminar projection patterns. As the source area of a projection becomes more differentiated than the target area, the two areas' relative architectonic differentiation increases from a negative to a positive value. **(A)** The architectonic type principle describes how imbalances in the laminar origins of projection neurons vary along this gradient of relative differentiation. **(B)** We show that, already in the immature cortex, it can be observed that the contribution of supragranular neurons to a given projection is stronger, the more differentiated the source area is relative to the target area (immature $N_{SG}\%$) (cf. Figure 3.19B,C). **(C)** This pattern becomes more pronounced as the initially formed projections are refined by later developmental processes (adult $N_{SG}\%$). Specifically, we observed that this refinement appears to be proportional to the relative differentiation of connected areas. While the supragranular contribution to projections mainly decreases, the magnitude of this decrease changes concurrently with relative differentiation and eventually reverses into an increase in supragranular contribution. This results in the progressive strengthening of initially present biases in laminar projection patterns (cf. Figure 3.19D,E).

brain. This mechanism is consistent with the determination of laminar patterns through early neurogenetic processes. Hence, our findings on immature laminar patterns of projection origins strengthen the support for this mechanistic explanation of how the architectonic type principle emerges during ontogenesis.

Parts of this section have been published in Beul et al. (2017).

4.4 Possible mechanistic underpinnings of the architectonic type principle

So how does the architectonic type principle emerge? The findings demonstrating its applicability in the immature macaque cortex, discussed in the preceding section, point towards early neurodevelopmental processes. The interaction of spatial and temporal aspects of neurogenesis has been suggested to underlie the emergence of the architectonic type principle, and we set up an *in silico* model of cortical development to probe this hypothesis.

By performing comprehensive computational simulation experiments of how the network of inter-areal connections may develop during ontogenesis, we addressed the question of how cortico-cortical structural connections come to be closely related to the architectonic differentiation of the underlying structural substrate, an empirical observation made in multiple species (Barbas, 1986; Barbas and Rempel-Clower, 1997; Rempel-Clower and Barbas, 2000; Dombrowski et al., 2001; Barbas et al., 2005; Medalla and Barbas, 2006; Ghashghaei et al., 2007; Medalla et al., 2007; Hilgetag and Grant, 2010; Hilgetag et al., 2016; Goulas et al., 2017). The main component of our *in silico* model was a developing two-dimensional cortical sheet, gradually populated by neurons. To assess potential explanatory mechanisms, we varied the spatio-temporal trajectory of this simulated corticogenesis. The rules governing axon outgrowth and connection formation, by contrast, were kept fixed across all variants of simulated corticogenesis, so that the differences in outcome measures between spatio-temporal growth trajectories were introduced exclusively by the specifics of when and where neurons were generated.

As discussed in the preceding section, the architectonic type principle is already applicable to laminar patterns of projection origins at early stages of development. Therefore, we limited our exploration to features that would affect patterns of connectivity early in development and disregarded later occurring processes such

as regressive events and activity-dependent remodelling of projections. This is consistent with observations showing that the mouse brain can form in a typical manner, including initial connectivity, independent of synaptic transmission (Verhage et al., 2000).

To allow for straightforward interpretation of the simulation results, we applied network measures that were used in previous empirical studies, which allowed us to perform analyses on the simulated connectomes in the same way as we did on the empirical connectomes. Accordingly, the two characteristics of areas that were considered in the analyses of the final simulated network of inter-areal connections were their final position on the two-dimensional cortical sheet relative to other areas, measured as Euclidean distance, and their neuron density, which functioned as a surrogate for overall architectonic differentiation. Neuron density was expressed relative to the densities of other areas, that is, as density difference, for most analyses. We treated the existence of connections between areas as binary, that is, connections were considered as either absent or present.

4.4.1 Spatio-temporal growth trajectories determine essential properties of the final connectome

In a first set of simulation experiments, which addressed how patterns of connection existence could emerge, we considered different spatio-temporal trajectories of how neurons populated the simulated cortical sheet. To recapitulate, simulated corticogenesis proceeded according to five different sets of growth rules, with three to nine specific implementations per set (a total of 21 different growth layouts). These five sets were (1: *realistically oriented density gradient*) planar, expansive growth of the cortical sheet, with newer areas having successively higher neuron density; (2: *inverse gradient*) planar, expansive growth of the cortical sheet, with newer areas having successively lower neuron density; (3: *radial*) instead of planar growth, neurons started to populate all areas simultaneously and were added at a constant rate across the whole cortical sheet until each area reached its predetermined complement of neurons, with a final neuron density gradient identical to sets 1 and 4; (4: *static*) all neurons of the cortical sheet formed simultaneously, with a neuron density gradient identical to the final gradient of sets 1 and 3; (5: *random*) planar, expansive growth of the cortical sheet, with no ordered gradient of area neuron density around the two origins. To exclude effects specific to any particular implementation of these sets of growth rules, we considered three growth modes for each set: one-dimensional growth with one row of areas, one-dimensional growth

4.4. Possible mechanistic underpinnings of the architectonic type principle

with two rows of areas, and two-dimensional growth. For set 1, with a *realistically oriented density gradient*, we considered growth around one origin and three or four origins (for one-dimensional and two-dimensional growth modes, respectively) additionally to the growth around two origins that was used in all five sets.

These distinct spatio-temporal trajectories of cortical sheet growth led to considerable differences in the properties of the generated networks of structural connections. See Table 3.7 for an overall assessment of the results. While all growth layouts exhibited a clear decline in the relative frequency of present projections across larger distances, this measure correlated with absolute density difference only for a subset of growth layouts (Figure 3.22). Particularly, there was no consistent relationship for the *random*, *static* and *radial* growth layouts, while for oriented growth, both along a *realistically oriented density gradient* and along an *inverse gradient*, the relative frequency of present connections decreased with larger absolute density differences between areas.

A more precise assessment of the extent to which distance and density difference determined connection existence was obtained by predicting simulated connectivity using logistic regression analysis. Here, a similar picture as for relative connection frequency emerged from comparing McFadden's Pseudo R^2 values across growth layouts (Figure 3.23). Distance was a better-than-chance predictor of connection existence for most growth layouts, as shown by the performance increase compared to a constant-only null model that is measured by McFadden's Pseudo R^2 . In contrast, inclusion of absolute density difference increased prediction performance only for the layouts with oriented growth (both along *realistically oriented* and *inverse density gradients*), but not for the *random*, *static* or *radial* growth layouts.

Finally, the growth layouts differed in whether neuron density correlated with area degree (Figure 3.24). As before, for *random*, *static* and *radial* growth layouts, there was no consistent effect of neuron density on the measure of interest, in this case area degree. In contrast, there was a significant correlation with neuron density for layouts with oriented growth. This correlation was negative, as observed empirically, for growth layouts with a *realistically oriented density gradient*, but positive for growth layouts with an *inverse density gradient*.

In combination, these results demonstrate that the relation between cortico-cortical connections and neuron density, which is one crucial feature of the physical substrate in which connections are embedded, is strongly influenced by the precise spatio-temporal trajectory of cortex growth, which coincides with the time of connection formation. By manipulating where and when areas of varying neuron density were generated, we could observe a change in the extent to which connections of the

simulated network were accounted for by the two factors of spatial proximity on the fully formed cortical sheet and the relative neuron density, indicating relative architectonic differentiation of areas.

4.4.2 Realistic network properties emerge from empirically grounded growth trajectories

As described above, the extent to which spatial proximity and relative neuron density determined simulated connectivity strongly depended on the specific spatio-temporal trajectory of the simulated growth of the cortical sheet. Growth layouts that more closely mirrored the biological developmental trajectory of the mammalian cortical sheet led to closer correspondence of the simulation results with empirical observations on adult connectivity. This finding became particularly apparent when we predicted empirical connectivity in two different mammalian species, cat and macaque, from regularities that were extracted from the simulated connectivity generated by the different growth layouts. Applying the regularities that emerged in our simulations to empirical data afforded a strong test of whether the simulations adequately captured ontogenetic processes and produced realistic networks. Our results showed that both of the aspects that were manipulated across growth layouts (i.e., the temporal trajectory of area growth as well as the direction of the neuron density gradient) were relevant for how well simulated connectivity allowed to predict empirical connectivity (Figure 3.25 and Figure 3.26). First, we observed that growth layouts in which areas appeared successively around origins of neurogenesis (i.e., the *realistically oriented density gradient* growth layouts), were much better able to predict empirical connectivity than growth layouts with the same final neuron density gradient, but without the observed link between time of origin and neuron density (i.e., *static* and *radial* growth layouts). Second, in the presence of planar growth around origins, the direction of the neuron density gradient was crucial. This finding was indicated by the large decrease in prediction performance when comparing the *realistically oriented density gradient* growth layouts with the *random* and *inverse density gradient* layouts. These sets of growth layouts both followed the same time course of cortical sheet expansion as the *realistically oriented density gradient*, but with no relationship between time of origin and neuron density or a negative correlation between time of origin and neuron density, which contradicts the empirically observed positive correlation of time of origin with neuron density. Hence, the extent to which neuron density is well suited as a predictor of connectivity could be due to it reflecting neurodevelopmental time windows.

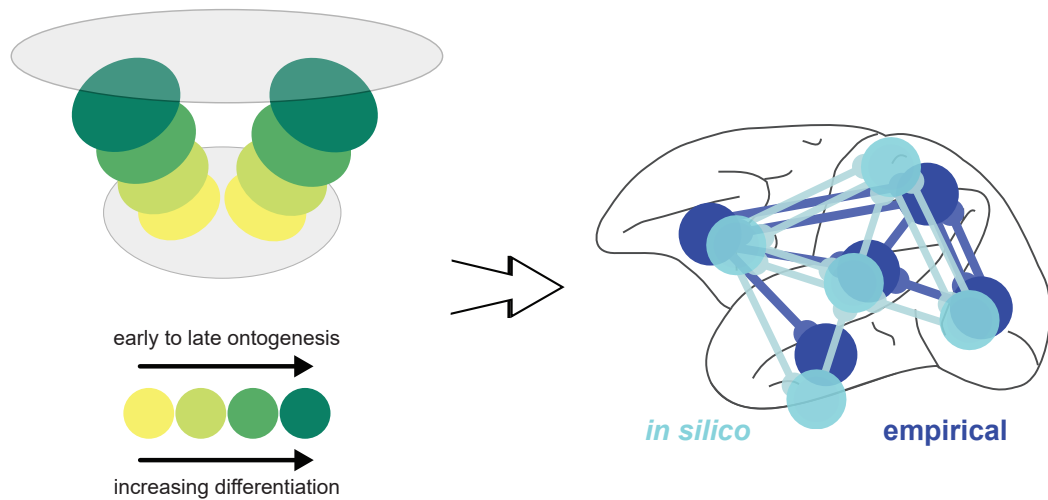


Figure 4.5: Number and relation of neurogenetic and architectonic gradients. A synthesis of the simulation results presented here indicates that the presence of two origins of neurogenesis, resulting in two neurogenetic (temporal) and architectonic gradients is necessary for the closer correspondence of the *in silico* model to the empirical relations between connectivity and architectonic differentiation. Importantly, the empirically observed relations are replicated *in silico* only if the less-to-more differentiated architectonic gradients align with early-to-late ontogenetic gradients. Hence, the suggested mechanism is consistent with correspondence of neurogenesis and architectonic differentiation (Dombrowski et al., 2001; Barbas and García-Cabezas, 2016; Goulas et al., 2017) and a dual origin of the cerebral cortex (Sanides, 1962; Pandya et al., 2015).

Third, our analyses revealed that the number of neurogenetic origins, around which new areas grew, influenced the correspondence of simulated connectivity to empirical connectivity (Table 3.8 and Table 3.9). Growth around two origins arguably led to the best prediction performance: it was superior to growth around one origin for both accuracy and Youden index, and performed better than growth around three or four origins in terms of accuracy. For the Youden index, this performance difference was present, but too small to be meaningful or statistically significant. Thus, while correspondence between simulated and empirical connectivity clearly increased with the addition of a second origin of neurogenesis, there was at the very least no further performance increase with the addition of a third or fourth origin. Fourth, we observed that the overall level of prediction performance for the *realistically oriented density gradient* growth layouts was quite high, indicating that they afforded a good correspondence with empirical connectivity not only relative to the other growth layouts, but also in absolute terms. Therefore, a dual origin of neurogenesis and the resulting architectonic gradients arguably are necessary components of a developmental mechanism that can generate connectivity for which empirically observed relations hold (Figure 4.5). These findings stress the importance

4.4. Possible mechanistic underpinnings of the architectonic type principle

of the theory of the dual origin of the cerebral cortex (Sanides, 1962; Pandya et al., 2015) and the presence of multiple gradients of neurogenesis (Smart, 1984; Bayer and Altman, 1991), for the configuration of connectivity in the adult cortex.

Collectively, the presented results suggest that planar growth of the cortical sheet around two origins of neurogenesis as well as a systematic increase in neuron density with later time of origin are crucial determinants of the development of realistic cortico-cortical structural connections. Conversely, assuming that connection formation is a stochastic process with few constraints, as simulated here, the assumptions underlying the spatio-temporal growth trajectories of the *random*, *static*, *radial* and *inverse* growth layouts were shown not to mirror actual principles of cortical organisation.

4.4.3 Simulation results validate the mechanistic explanations hypothesised to underlie the architectonic type principle

With the postulation of the architectonic type principle it was suggested that a close relationship between cortico-cortical connections and architectonic differentiation of the cortex might arise from the timing of neurogenesis (Barbas, 1986), a process that occurs in close temporal proximity to the formation of connections. Specifically, it has been hypothesised that the relative time of generation of areas of different neuron densities affords them with different opportunities to connect with each other, thus imposing constraints on stochastically formed connections (Barbas, 2015; Hilgetag et al., 2016). This mechanism would be in line with findings in *Caenorhabditis elegans* (Varier and Kaiser, 2011) and rat cortex (Bayer and Altman, 1987). Moreover, a previous computational study demonstrated that topological features, such as modular connectivity, may arise from the growth of connectivity within developmental time windows (Kaiser and Hilgetag, 2007). Thus, the main premise of our simulation experiments, that spatio-temporal interactions in the forming cortex determine connectivity, has long been under consideration. Here, we provide the first systematic exploration of the possible mechanistic underpinnings of the architectonic type principle. We simulated multiple combinations of spatio-temporal growth trajectories of the cortical sheet and neuron density gradients, to probe from which of the combinations realistic connectivity emerged. Our results showed that, indeed, of the wide variety of examined spatio-temporal growth trajectories, the variant of the *in silico* model that led to the best correspondence with empirical observations was the one that was based on the same assumptions as the mechanism proposed to underlie the realisation of the architectonic type principle. Hence, the

4.4. Possible mechanistic underpinnings of the architectonic type principle

underlying assumption that differences in neuron density correspond to distinct time windows was not refuted in the model, and neuron density carried predictive power with respect to connectivity features only if such a relation between density and neurogenetic timing held. Our systematic simulation experiments, thus, distinctly corroborate the previously hypothesised mechanistic underpinnings of the architectonic type principle and contribute a conceptualisation that can be scrutinised for similarities with, and distinctions from, actual ontogenetic processes. This approach opens up the possibility of characterising in more detail how correlations between the structure of the cortex and cortical connections emerge, because all aspects of the process are observable. Further refinement of the simulation, for example by introducing species-specific histogenetic time courses, will enable the exploration of species differences or potentially the demonstration of invariance to changes in some aspects of ontogenesis. Another factor that could be probed is how robust the emergence of realistic connectivity is against changes in absolute neuron density, which varies considerably across species (Charvet and Finlay, 2014; DeFelipe, 2011).

Temporal proximity during neurogenesis appears to be fundamental to the emergence of the architectonic type principle

From our simulations, it appears that temporal proximity of areas during neurogenesis underlies the positive relationship between similar neuron density and high connection probability. The close correlation between time of origin and architectonic differentiation described empirically (see Section 1.6.1.2) leads to a derivative correlation between temporal proximity of neurogenetic time windows and relative differentiation of cortical areas. Independent of this correlation, on a cortical sheet that expands around the origins of neurogenesis, areas with closer neurogenetic time windows tend to be spatially closer as well. Assuming that connection formation is a stochastic process, which implies that connection probability declines with spatial distance, this relationship between temporal and spatial proximity leads to a higher connection probability between areas that are generated during nearby time windows. Temporal proximity during neurogenesis would, thus, be the common antecedent determining both relative architectonic differentiation and connection probability, while those two factors would only be indirectly related. Temporal proximity, however, is difficult to measure, and it is, therefore, no surprise that the correlation between its two direct consequences has been empirically observed first. This chain of reasoning reveals how our modulation of the relationship between temporal proximity during neurogenesis and relative architectonic differentiation in

4.4. Possible mechanistic underpinnings of the architectonic type principle

the considered growth layouts could have caused the vastly different outcomes in connectivity that we report.

Spatial proximity of areas in the adult cortex is a distorted measure

In our simulations, we observed a relationship between the spatial proximity of areas and their likelihood to be connected, which appears to be an epiphenomenon of stochastic connection growth within a physically embedded system (cf. Kaiser et al., 2009; Lim and Kaiser, 2015). Distance is an inherent property of a spatially embedded system that cannot be removed from the implementation of spatial growth. However, in our simulation of cortical growth, the final distance between areas was not always an accurate measure of their distance during the time period of connection formation, which would be the factor that mattered principally for determining the likelihood by which two areas became connected. Since this distance during cortical sheet growth is correlated with the areas' final distance, there was also a correlation between final spatial proximity and connection probability. But this correlation does not genuinely describe the dependency of the stochastic growth process on distance, because inter-areal distance was not static, as implied by this measure of final distance. The distance measure relevant here, namely distance at the time of connection formation, would be challenging to measure empirically. Therefore, relying on measures of final, adult distance and assuming a strong correlation between the two distance measures appears as a pragmatic strategy for empirical analyses.

4.4.4 Simulating the development of laminar projection patterns

The simulation experiments discussed so far were designed to allow for the analysis of connection existence, that is, whether a possible connection between a pair of areas is present or absent in the final network. Naturally, axonal connections have many further properties beyond their simple existence; one prominent feature being the laminar distribution of the projection neurons' somata and axon terminals in the areas of origin and termination, respectively. Laminar patterns of projection origins and terminations are very well captured by the architectonic type principle (reviewed in, e.g., Barbas, 2007, 2015; Hilgetag et al., 2019), as has been demonstrated extensively in different species and cortical systems. These conspicuous regularities most likely arise from fundamental developmental mechanisms, since they are ubiquitous and

4.4. Possible mechanistic underpinnings of the architectonic type principle

quite robust. This aspect becomes strikingly apparent in reeler mutant mice, where laminar connectivity patterns are largely correct (Devor et al., 1975; Caviness and Yorke, 1976; Caviness and Frost, 1983) (shortly reviewed in Caviness et al., 2008), despite a systematic inversion (to ‘inside-out’) of neurons’ final laminar positions relative to the regular order that neurons typically assume according to their time of origin (‘outside-in’) (Caviness, 1982; Devor et al., 1975; Caviness and Sidman, 1972, 1973; Caviness, 1976; Harsan et al., 2013). However, the precise mechanisms through which laminar projection patterns become established are still under investigation.

Correspondingly, it remains unclear how the close association between laminar patterns and relative differentiation emerges, which is a central observation that is captured by the architectonic type principle. Since detailed observations of developmental events, which could answer this question, are difficult to obtain, simulation experiments are the most feasible way to systematically evaluate hypotheses about the mechanisms that underlie the emergence of the architectonic type principle. Therefore, we performed a second set of simulation experiments, building on the results from the first set, which demonstrated that realistic assumptions about the spatio-temporal patterns of neurogenesis could lead to simulated networks that complied with the regularities that are described by the architectonic type principle in the mammalian cortex with respect to the existence of connections between areas. We extended this *in silico* model by laminar compartments to probe not only the existence of connections, but also the distribution of the connecting neurons across layers, that is, the laminar patterns of projection origins. Moreover, we introduced four features, three of which changed the spatio-temporal patterns of neurogenesis: a delay in the growth of the infragranular compartment (relative to layer 1), a delay in the growth of the supragranular compartment (relative to the infragranular compartment) and a scaling in the relative neuron density of the supragranular compartment. The fourth feature, in contrast, affected cell-intrinsic properties by changing the axon elongation per time step according to a neuron’s laminar compartment and an area’s architectonic differentiation. By varying the strength (i.e., the parameter value) with which each of the four features was included in the *in silico* model, we tested the sensitivity of the laminar projection patterns to a given parameter.

Spatio-temporal interactions could not be shown to produce empirically observed patterns of laminar projection origins

Including the three spatio-temporal features in the *in silico* model did not induce the simulated networks to exhibit the empirically observed patterns of projections origins.

4.4. Possible mechanistic underpinnings of the architectonic type principle

A delay in the growth of the infragranular compartment did not affect the laminar patterns at all (Figure 3.28A), while a delay in the growth of the supragranular compartment resulted in a negative correlation between supragranular contribution to connections and relative differentiation (Figure 3.28B), which is the opposite of what has been observed in the mammalian cortex. This negative correlation indicated that areas of lower density formed their connections increasingly from the supragranular compartment the more pronounced the difference in neuron density to the target area became, while areas of higher density formed their connections increasingly from the infragranular compartment the larger the difference in neuron density became. This effect was due to unequal opportunities to connect encountered by neurons in the infragranular and supragranular compartments of lower density and higher density areas. A combination of both delays, which is the model implementation that most closely resembles the radial gradient of neurogenesis observed *in vivo*, did not result in unexpected effects. Instead, the effects of both delays superimposed without any interactions. Since the delay in infragranular compartment growth did not affect laminar patterns of origins, this means that the results for a combination of both delays were indistinguishable from the results obtained from including the delay in supragranular compartment growth individually (Supplementary Figure C.10A).

Although including a scaling of supragranular compartment neuron density did result in a positive correlation between supragranular contribution and relative differentiation for larger parameter values (Figure 3.28C), this correlation was not accompanied by a graded distribution of supragranular contributions across density differences between connected areas (Supplementary Figure C.6D). Instead, source areas of each neuron density level formed their connections at a characteristic supragranular contribution, which did not differ for connections across different density differences. The positive correlation emerging overall thus results from the fact that by definition areas of lower neuron density form projections across the smallest neuron density differences and areas of highest density form projections across the largest neuron density differences. This composite correlation is in stark contrast to the patterns of supragranular contribution that have been observed empirically, where areas of each level of architectonic differentiation exhibit a graded pattern of supragranular contributions that varies with the difference in architectonic differentiation to the target area (Figure 3.29C). Moreover, the aggregate positive correlation could be abolished by controlling for the ratio of supragranular neurons to total neurons in the source area (Figure 3.29B). This implies that the shifts that occurred to the distributions of supragranular compartment contribution for each level of source area neuron density (which were uniform across density differences) was caused by the preponderance of supragranular compartment neurons compared to infragranular

compartment neurons at larger values of the supragranular compartment neuron density scaling parameter.

Summing up, in our simulation experiments it was not sufficient to modify spatio-temporal patterns of neurogenesis in order to produce simulated networks in which the origins of connections were distributed across laminar compartments in a manner that was similar to the patterns observed empirically in the mammalian cortex.

Differences in cell-intrinsic properties that were linked to architectonic differentiation produced realistic patterns of projection origins

As a fourth feature, we introduced graded differences in a property that was intrinsic to individual neurons, namely the elongation of their axon per time step. This property was changed in accordance with an area's neuron density, such that the divergence in axon elongation between the neurons in the infragranular and in the supragranular compartment varied systematically along the gradient of architectonic differentiation (represented by neuron density). Similar to the changes in relative cell size between the infragranular layers and the supragranular layers that have been described as externopyramidization (Sanides, 1962, 1970) and that also vary systematically with architectonic differentiation (reviewed in Goulas et al., 2018), we varied the relative levels of axon elongation across laminar compartments and areas. At larger levels of divergence a positive correlation between supragranular compartment contributions and relative differentiation emerged (Figure 3.28D). This correlation mirrored empirically observed patterns of supragranular compartment contributions, as it was realised across connections of differing density differences already at the level of individual areas (Supplementary Figure C.6D). Moreover, for the emergence of this positive correlation, the spatio-temporal patterns of neurogenesis, which were previously identified to be sufficient for the emergence of realistic patterns of connection existence, had to be present. When the underlying relationship of time of origin to areas' neuron density (i.e., higher density with later time of origin) was removed, the positive correlation between relative architectonic differentiation and supragranular contribution was largely abolished (Figure 3.30).

Thus, in our simulation experiments, differences in cell-intrinsic properties that varied with architectonic differentiation and spatio-temporal patterns of neurogenesis interacted, allowing the formation of simulated networks that exhibited a relationship of laminar patterns of connection origins to relative differentiation of connected areas which resembled their relationship observed in the mammalian cortex (Figure 4.6).

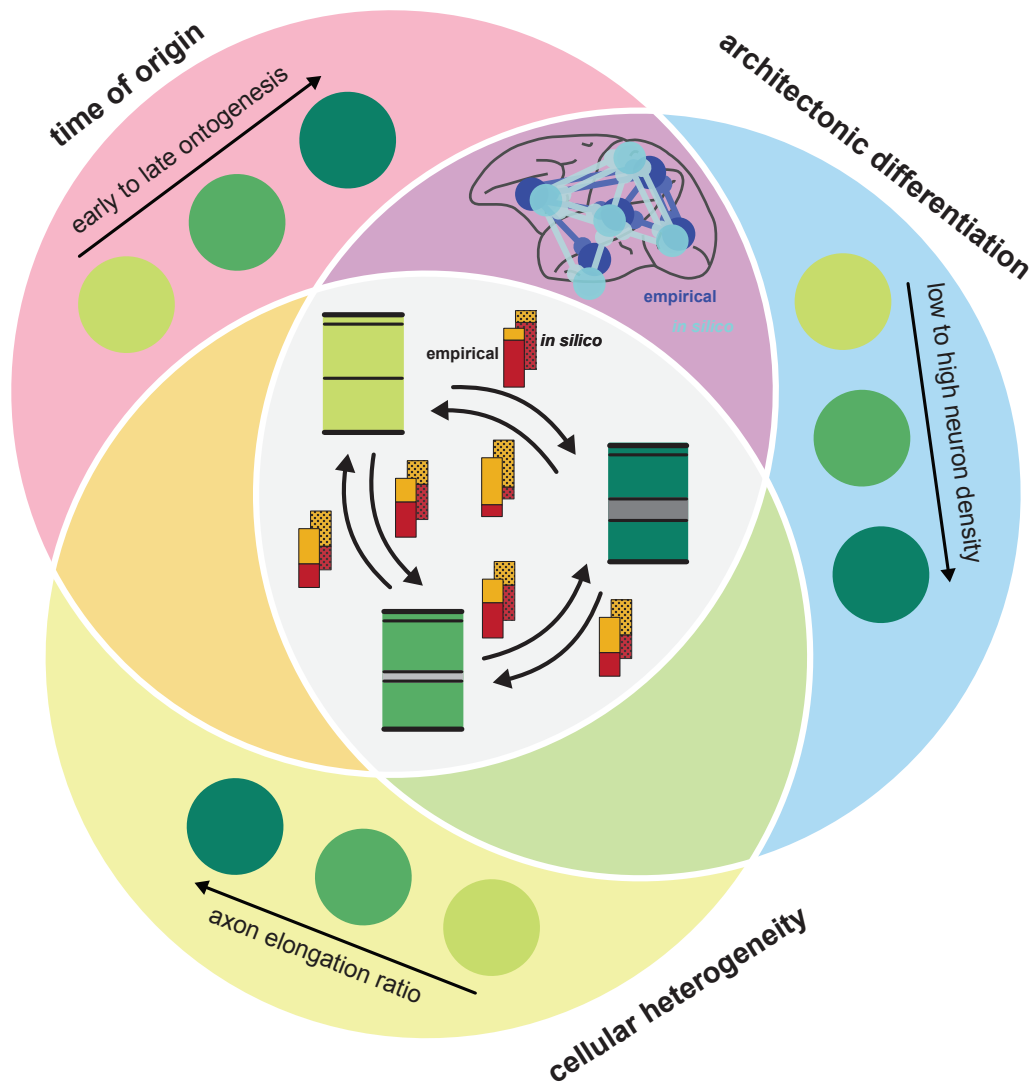


Figure 4.6: Realistic laminar patterns can arise from an interaction of spatio-temporal gradients in neurogenesis with gradients in cell-intrinsic properties. Our *in silico* model of the developing cortical sheet included three properties of areas which changed gradually. These were time of origin (red), architectonic differentiation (blue) and cellular heterogeneity, changing the balance of axon elongation in the infragranular compared to the supragranular compartment (yellow). Axon elongation values changed gradually, from larger in the infragranular compartment to larger in the supragranular compartment, yielding an increasing ratio of the supragranular to infragranular value. While realistic patterns of connection existence can arise from an alignment of the two gradients of time of origin and architectonic differentiation (purple), the inclusion of a gradient in the cell-intrinsic property of axon elongation, which was aligned to the gradient of architectonic differentiation, was crucial for the emergence of realistic laminar patterns of projection origins (grey). Bars indicate laminar contributions to projections, with red representing contribution from the infragranular compartment and orange representing contribution from the supragranular compartment. Solid colors indicate empirically observed relationships, captured by the architectonic type principle, while dotted colors indicate simulated patterns.

Differences in cellular properties *in silico* and *in vivo*

From our simulation experiments it appears that the establishment of laminar patterns of projection origins does not easily arise from spatio-temporal interactions in the developing cortical sheet. More specific assumptions about developmental processes were necessary for our *in silico* model to generate realistic laminar projection patterns. By modifying the cell-intrinsic property of axon elongation, we introduced differences between individual neurons, which were modelled to vary systematically with the architectonic differentiation of areas and which also modified properties of infragranular compartment neurons and supragranular compartment neurons separately. This approach is consistent with a wealth of observations in the mammalian cortex, demonstrating that many properties of neurons vary both with architectonic differentiation and laminar position. For example, myelination, cellular markers of synaptic stability and plasticity, cellular morphological properties, the distribution and density of neurotransmitter receptors as well as the density of neurons expressing parvalbumin and calbindin have all been described to change across the spectrum of architectonic differentiation (Dombrowski et al., 2001; Nieuwenhuys et al., 2015; García-Cabezas et al., 2017; Zilles and Palomero-Gallagher, 2017; Burt et al., 2018; Holley et al., 2018)(Section 3.4). Similarly, the expression of many transcription factors and neurotransmitter receptors as well as the distribution of neurons expressing proteins such as parvalbumin, calbindin, calretinin and latexin have been shown to vary across cortical layers (Dombrowski et al., 2001; Bai et al., 2004; Guy and Staiger, 2017; Palomero-Gallagher and Zilles, 2017; Popovitchenko and Rasin, 2017; Zilles and Palomero-Gallagher, 2017), as have physiological (Lagae et al., 1989; Nowak et al., 1995; Raiguel et al., 1995; Song and Moyer, 2018) and histochemical properties of pyramidal neurons (Hof et al., 1996, 1997). Moreover, there is ample evidence that axons are guided by attractants and repellants both on large spatial scales, for example during the establishment of contralateral or cortico-spinal projections (Morales and Kania, 2017; Stoeckli, 2017; Chédotal, 2019), and on small spatial scales, for example during the specification of laminar projection targets (Bolz et al., 1990; Castellani and Bolz, 1997; Sanes and Yamagata, 1999; Kageyama and Yamamori, 2013). These processes are affected by a multitude of diffusible and membrane-bound molecules (Tessier-Lavigne and Goodman, 1996), and an additional layer of complexity is added by the fact that the same guidance molecule can have opposing effects on different neurons, depending on the receptor complement that is expressed by the guided neurons (Bagnard et al., 1998; Castellani et al., 1998). Given this large range in spatial scales documented for axon guidance mechanisms, it appears plausible that similar mechanisms could cover the whole

4.4. Possible mechanistic underpinnings of the architectonic type principle

range of spatial scales, that is, also the mesoscopic, medium spatial scale of ipsilateral cortico-cortical connectivity, thus affecting laminar patterns of projection origins.

Our implementation of differences in cellular properties assumed the existence of two opposing trends in axon elongation, which changed in opposite directions along the spectrum of architectonic differentiation in the infragranular and supragranular compartments. It is conceivable that gene expression patterns across the mammalian cortex could, in a similar manner, mediate differences in axon elongation and thereby the growth speed of axons across the differentiation spectrum and cortical layers, and hence, that our chosen experimental manipulation would mirror an actual mechanism occurring in the mammalian brain. However, this is not the premise under which we interpreted our *in silico* model. Rather, we wanted to probe how the pattern of two opposing gradients, varying the properties of neurons along the gradient of architectonic differentiation separately in the two laminar compartments, affected laminar patterns of projection origins. Unspecific axon outgrowth, following the pattern of shifting relative cell sizes described as externopyramidization, was but one of many possible cellular properties to investigate. Other possibilities are for example the susceptibility of neurons to axon guidance mechanisms. Based on the fact that architectonic differentiation goes along with marked differences in the presence and laminar distribution of specific cell types and gene expression patterns, as described above, such axon guidance could operate both on a general level, affecting axons' attractedness to or repulsion from areas based on their degree of architectonic differentiation, and on a more specific level, affecting projection patterns towards specific neuron populations.

Although the assumption of two opposing gradients in the infragranular and supragranular compartments may appear strong at first, it is plausible when considering related experimental observations. Concerted changes in macroscopic and microscopic architectonic features mirroring architectonic differentiation are pervasive in the adult mammalian cortex, as described in the preceding. It has been demonstrated that common gene expression signatures can distinguish neuron subtypes and regional identity, which supports a transcriptional basis for differences in cortical cytoarchitecture (Lake et al., 2016; Nowakowski et al., 2017; Mickelsen et al., 2019). Obviously, these gradients arise from developmental mechanisms (García-Cabezas et al., 2019). For example, the time point at which a neuron is formed is flagged by markers of embryonic age and impacts the trajectory of differentiation the neuron follows (Telley et al., 2019). The existence of similar gradients prior to the finalisation of adult levels of differentiation is difficult to observe experimentally, but does not appear contentious. Is it plausible, then, that two opposing gradients should exist in the infragranular and the supragranular layers? Distinct molecular mechanisms have

4.4. Possible mechanistic underpinnings of the architectonic type principle

been identified that are crucial in the specification of infragranular and supragranular neurons (reviewed in Kennedy and Dehay, 2012). Moreover, infragranular and supragranular neurons have been reported to exhibit diverging developmental time courses (Barone et al., 1995; Batardière et al., 1998, 2002), for example in the modification of their spatial divergence or whether they display waiting periods. These observations demonstrate that the two laminar compartments are sufficiently dissociated in their specification to support opposing gradients, for example in their sensitivity to axon guidance molecules, across the architectonic differentiation spectrum. Interestingly, from an evolutionary perspective, more differentiated areas are newer than less differentiated areas (Pandya et al., 2015; García-Cabezas et al., 2019), and increased differentiation is mediated by lengthening developmental schedules, which result in an increase in neuron complement especially in the supragranular layers (Finlay and Darlington, 1995; Charvet and Finlay, 2014). This specific expansion would have opened up the supragranular neurons as a new substrate for connecting newly specified areas and for modification independent of pre-existing circuits involving infragranular neurons. Indeed, the increased prominence of supragranular layers has been suggested to be one of the crucial substrates for evolutionary adaptation in primates (Harris and Shepherd, 2015).

4.4.5 Limitations and future extensions

Our results illustrate how a mechanism linking the temporal order of neurogenesis across the cortex with the architectonic differentiation of areas could come to shape cortico-cortical connectivity such that it resembles the empirically observed connectivity of mammalian connectomes. However, simulation experiments, as performed here, can only assess whether a suggested mechanism is feasible in principle, and explore what its essential components might be. That is, such computational experiments put a candidate mechanism to the test and allow drawing some inferences about possible (and, importantly, impossible) ingredients, but they do not establish biological facts by themselves. Ultimately, only empirical observation of the ontogenesis of the cortex can establish how this developmental process unfolds. The possibility cannot be excluded that there may exist an unrelated mechanism working through features not considered here, which could cause the phenotype of interest, in our case the close relation between architectonic differentiation and connectivity. Generally, incorporating more empirical anchor points in a model gives the conclusions of a simulation study more significance. To triangulate a likely solution to the developmental puzzle of how axonal connections are organised, it is necessary to

4.4. Possible mechanistic underpinnings of the architectonic type principle

constrain potential mechanisms by as many observable features as possible. More processes that shape connectivity could be included in our *in silico* model of cortical development, such as waiting periods for connection formation, a differential ability of cortical layers to retain connections (possibly linked to externopyramidization), the pruning of established connections, or the action of signalling molecules in attracting and repelling axons during connection formation. By integrating such phenomena, further insights could be gained into the emergence of connection features such as laminar patterns of projection origins and terminations or projection strengths.

We constrained our *in silico* model to represent a single cerebral hemisphere, hence our results only apply to ipsilateral, intra-hemispheric connections. Contralateral, inter-hemispheric axonal connections have also been reported to be well represented by the architectonic type principle (Barbas et al., 2005; Goulas et al., 2017), although at generally lower connection strengths. The *in silico* model could be expanded by a second hemisphere which develops simultaneously. Since similar types of cortex in the two hemispheres would be formed at nearby points in time, but further apart in space, this setup would be expected to lead to the observed pattern of architectonic type principle-consistent, but weaker, connectivity if the principle holds that spatio-temporal interactions govern patterns of connection existence.

We modelled the developing cortex as a two-dimensional sheet, across which axons grew until they met a target soma and formed a connection. In reality, the mammalian cortical sheet is not flat, but becomes at least curved, and often intricately folded, during corticogenesis. Moreover, axons are not positioned exclusively within the grey matter, but instead cover large distances through the white matter. These shortcuts between distant points on the cortical sheet imply that representing projection length as Euclidean distance between points on a flat cortical sheet is not accurate. Yet, regardless of how the concurrent processes of neurogenesis, axon formation and cortical folding affect each other (Hilgetag and Barbas, 2006; Zilles et al., 2013), measuring the precise lengths of projections in the adult cortex has so far not been straightforward. Hence, approximate measures have been employed, such as border distance on a cortical parcellation, Euclidean distance in three-dimensional space, or geodesic distance which accounts for some of projections' confinement to white matter tracts. Euclidean distance on the simulated two-dimensional cortical sheet may, therefore, be a suitable surrogate measure for these approximate empirical measures. In line with this assumption, if cortical folding had a strong impact on our prediction of empirical data, it would be expected that performance in the less folded cat cortex would be better than in the more strongly folded macaque cortex. As this was not the case, we suspect that cortical folding and the resulting changes in projection lengths do not dramatically alter the spatio-temporal interactions which

4.4. Possible mechanistic underpinnings of the architectonic type principle

we hypothesise link architectonic differentiation and cortical connectivity. To further test this expectation, it would be interesting to predict connectivity data from a wider range of species, such as lissencephalic rodents and humans, whose cortex is even more strongly folded than the macaque cortex.

Lastly, applying the classifier which was trained on simulated network data to predict empirical connectivity data resulted in better prediction performance for the macaque cortex than the cat cortex. Ultimately, there might be two reasons for this finding: Either the architectonic type principle characterises connectivity better in one of these species than the other, or the empirical measures that were used more faithfully capture the true structure in one of the species.

Regarding the first possibility, adherence to the architectonic type principle might not be as pronounced in the smaller cat cortex, where both distances are shorter and therefore less distinctive, and there is less variation in total neuron number within the cortex due to a shortened neurogenetic interval (Charvet et al., 2015). This is in line with previous findings demonstrating a less pronounced alignment of architectonic differentiation and connectivity for the rodent cortex, where the divergence in architectonic differentiation is not as strong as in the cat or macaque cortex (Goulas et al., 2019b). Moreover, we observed an impact of spatial size on the predictive power of spatial proximity when we simulated the formation of cortical sheets of varying sizes (Supplementary Figure C.12). As the spatial dimensions of the cortical sheet increased, and irrespective of whether that expansion was accompanied by an increase in the number of cortical areas, the contribution of spatial distance to the classification of connection existence increased. This supports the hypothesis that larger physical size allows spatial proximity to become more distinctive, as it can vary across a larger range than in a small cortical sheet.

Regarding the second possible reason, the structural measures from which we predicted connectivity were more detailed in the macaque cortex (neuron density and Euclidean distance) than in the cat cortex (architectonic type and border distance). Further experiments are therefore required to distinguish between these two explanations. Indeed, it would be intriguing to expand the prediction of empirical connectivity data from simulated networks to other species, preferably to mammals whose cortex is on either side of cat and macaque on the scales of size and degree of architectonic differentiation. Just as for assessing the impact of cortical folding, rodents and humans would be good candidates to identify the source of the observed difference in prediction performance.

Simulating laminar patterns in more detail

Our simulation experiments evaluated the laminar patterns of projection origins, but did not address how projection terminations were distributed across cortical layers. Termination patterns have also been shown to relate to relative differentiation of connected areas (Barbas and Rempel-Clower, 1997; Hilgetag et al., 2016) and thus fall within the scope of the architectonic type principle. Further simulation experiments could probe which mechanisms possibly mediate their specification.

To address the distribution of both projection origins and terminations across cortical layers in even more detail, there are potential modifications of the stochastic formation of connections to be considered. First, the pruning of connections during later stages of development (Innocenti and Price, 2005) was not taken into account in the presented simulation experiments. Laminar projection patterns may conceivably be affected by selective elimination of some axon branches but not others (O'Leary and Koester, 1993; Price et al., 2006). Moreover, it has been observed that the time course of connection formation is not the same for all types of cells. Callosal projection neurons can reach their target areas without actually invading the grey matter, instead remaining in the white matter for a waiting period of days (Wise and Jones, 1976; Ivy et al., 1979; Schwartz and Goldman-Rakic, 1991). Similarly, waiting periods below the grey matter have been described for infragranular neurons projecting to area V4 from multiple areas in the ipsilateral hemisphere in macaques (Batardière et al., 2002). In contrast, supragranular neurons in the same tract-tracing experiments were found to invade the grey matter early, but many of them formed only transient projections that were subsequently eliminated. More generally, these and similar tract-tracing experiments have been interpreted to demonstrate different developmental profiles for axon outgrowth and connection formation in infra- and supragranular neurons (Barone et al., 1995; Batardière et al., 1998, 2002; Berezovskii et al., 2011). In 'feedback' pathways, which according to the architectonic type principle can be conceptualised as projecting towards a relatively more differentiated area, extensive remodelling of laminar projection patterns until long after birth has been observed in a number of species (mouse, cat, macaque, human) and target areas (Price and Blakemore, 1985; Kennedy et al., 1989; Kato et al., 1991; Meissirel et al., 1991; Burkhalter, 1993; Price et al., 1994; Barone et al., 1995; Batardière et al., 1998, 2002; Berezovskii et al., 2011; Khalil and Levitt, 2014). This remodelling has been linked to activity-dependent maturation of pathways and the emergence of more refined perceptual capabilities (Barone et al., 1995; Dong et al., 2004; Khalil and Levitt, 2014) (reviewed in, e.g., Polleux, 2005; Buckner and Krienen, 2013). This observation suggests that not all factors contributing to adult laminar projection

4.4. Possible mechanistic underpinnings of the architectonic type principle

patterns may be accessible in simulation experiments with time frames that are restricted to corticogenesis and initial axon outgrowth.

A further potential determining factor in the establishment of laminar projection patterns that warrants exploration is the possibility of genetic specification. To tie in with the previous discussion of axon guidance mechanisms, genetically encoded factors are very likely to play some role in the establishment of laminar projection patterns. It has been shown that the eventual projection fate is often acquired even prior to neuron migration (Jensen and Killackey, 1984; McConnell, 1988; Polleux et al., 2001) and that initial establishment of connectivity is largely independent of synaptic activity (Verhage et al., 2000). Guidance molecules and their receptors are often expressed in a cell-type specific manner, with many guidance molecules having dual actions depending on the type of receptor they bind to (Castellani and Bolz, 1997; Bagnard et al., 1998; Castellani et al., 1998; Kolodkin and Tessier-Lavigne, 2011; Seiradake et al., 2016; Morales and Kania, 2017; Stoeckli, 2017), enlarging the range of potential interactions. For example, Castellani and colleagues (1998) found that the membrane-bound protein Ephrin-A5 functioned as a repulsive axonal guidance signal in neurons destined to migrate to layer 2/3, while acting as a 'branch-promoting' signal in neurons destined for layer 6.

These combinations of guidance molecules and receptors have been shown to strongly constrain local, intra-areal connectivity (Bolz and Castellani, 1997; Castellani and Bolz, 1997). The same principle may apply to longer-range, inter-areal connections. The expression of guidance molecules and receptors is mediated by transcription factors, whose spatially and temporally fine-tuned expression gives rise to distinct cell types with diverse morphological and connectional properties and distinct functions. For example, corticofugal projection identity is mediated by the transcription factors encoded by genes such as *Fezf2* and *Ctip2* (reviewed in, e.g., Molyneaux et al., 2007; Gaspard and Vanderhaeghen, 2011). The effect of *Fezf2* expression is not only permissive, but also causal, as forced expression of *Fezf2* in progenitors destined for upper layers can induce these cells to atypically project to the pons (Chen et al., 2005). Another example of the genetic specification of a broad class of projection neurons are callosally projecting neurons, of which there are both upper and lower layer populations. Expression of different genes such as *Satb2*, *Hspb3* and *Lpl* appears to generally specify callosal projection neurons (Alcamo et al., 2008; Molyneaux et al., 2009), while there are also genes specific to either upper or lower layer callosal projection neurons (e.g., *Dkk3*, *Nectin-3* or *Plexin-D1* (Molyneaux et al., 2009)).

Thus, numerous layer-specific transcription factors and neurotrophins have been described, which afford a precise targeting of specific layers or even cell types and cellular compartments (reviewed in, e.g., Sanes and Yamagata, 1999; Kageyama

and Yamamori, 2013). Co-culture experiments using cortical explants have shown that appropriate laminar position of axon terminals can be retained outside of the ontogenetic growth environment, that is, in the absence of regular temporal and spatial relationships. Accurate laminar specificity has been demonstrated, for example, for thalamo-cortical, geniculate-cortical, and cortico-spinal connections in co-culture (reviewed in, e.g., Sanes and Yamagata, 1999). Similarly, connections formed in co-culture of rat visual cortex explants were shown to conform to organotypic laminar distributions (Bolz et al., 1990; Yamamoto et al., 1992). Castellani and Bolz (1997) elegantly demonstrated that organotypic and cell type specific projection patterns could be induced by membrane-associated factors through both induction and prevention of axon ingrowth and branching.

Since there is evidence for the genetic specification of anatomical projection patterns at small (intrinsic, intra-areal circuits) and large (e.g., corticofugal versus callosal projections) spatial scales, projections at intermediate spatial scales, such as cortico-cortical inter-areal projections, are not likely to be an exception from this mode of connection organisation. For example, it has been shown that while the white matter of the spinal cord is generally permissive for cortical axon growth, innervation of sections of the spinal grey matter is specific and topographically correct (Stanfield and O'Leary, 1985; O'Leary and Stanfield, 1986; Kuang and Kalil, 1994; Kuang et al., 1994). These observations support our conclusion that laminar projection patterns may not be entirely explicable by spatio-temporal interactions in the forming tissue, but are regulated by more prescriptive determinants. Including pertinent aspects of axon guidance in *in silico* models of the developing cortex may enable the generation of realistic laminar projection patterns, with respect to both the position of projection origins as well as projection terminations.

4.4.6 Realistic networks of inter-areal connections can be generated from an *in silico* model realising spatio-temporal interactions in the forming tissue

The architectonic type principle conceptualises structural connections between brain areas in terms of their relative architectonic differentiation, providing a mammalian-general principle for the organisation of cortico-cortical connections (Barbas, 2015; García-Cabezas et al., 2019; Hilgetag et al., 2019). How the empirically observed relationship between cortical architecture and features of connectivity emerges has not yet been elucidated by empirical developmental studies, but it has been suggested

to result from spatio-temporal interactions during neurogenesis (Barbas, 1986; Dombrowski et al., 2001; Barbas, 2015; Hilgetag et al., 2016). We demonstrated *in silico* that, given an empirically grounded relationship between the time of formation of areas and their architectonic differentiation (of which neuron density is a very good surrogate measure), spatio-temporal interactions between forming cortical areas were sufficient to give rise to patterns of connection existence that conformed to the architectonic type principle, as it has been observed in mammalian cortico-cortical connectivity.

We further expanded our *in silico* model of the developing cortical sheet to include laminar compartments and probed which factors might shape the laminar patterns of projection origins. Our results indicate that while the emergence of typical laminar patterns is indeed affected by spatio-temporal interactions during neurogenesis, the specifics of where and when neurons are formed are not the exclusive determinants of laminar patterns. A further specification of neuron identity, varying a cell-intrinsic property across the gradient of architectonic differentiation, was sufficient to enable our *in silico* model to generate realistic laminar patterns of projection origins. This suggests that future research should consider the intricacies of how neuron identity is specified developmentally, to identify the mechanistic underpinnings of the architectonic type principle and thereby advance our understanding of how connectivity in the mammalian cortex is organised.

Parts of this section have been published in Beul et al. (2018) and Beul and Hilgetag (2019a) and submitted for peer-review in Beul and Hilgetag (2019b).

4.5 Conclusions

We examined empirical and simulated data to gain insights into the organisation of cortico-cortical connections in the mammalian cortex. Our analyses corroborate the existence of a fundamental organising principle, the architectonic type principle, and support the hypothesis that this principle emerges from spatio-temporal interactions in the developing brain during ontogenesis.

4.5.1 Architecture and intrinsic connectivity vary across the cortex

Based on regularities in the intrinsic microcircuitry of cortical areas, variants of a ‘canonical’ cortical microcircuit have been proposed and widely adopted, particularly in computational neuroscience and neuroinformatics. However, this circuit is founded on striate cortex, which manifests perhaps the most extreme instance of cortical organisation, in terms of a very high density of cells in highly differentiated cortical layers. Most other cortical regions have a less well differentiated architecture, with the gradient in differentiation ranging from the very dense eulaminate primary cortical areas to the other extreme of dysgranular and agranular areas of low density and poor laminar differentiation. It is unlikely for the patterns of inter- and intra-laminar connections to be uniform in spite of strong variations in their physical substrate. This assumption is corroborated by reports of divergence in intrinsic circuitry across the cortex. Consequently, it remains an important goal to define local microcircuits for a variety of cortical types, in particular, agranular cortical regions. As a counterpoint to the striate microcircuit, which may be anchored in an exceptional architecture, we outlined a tentative microcircuit for agranular cortex. The circuit is based on a synthesis of the available literature on the local microcircuitry in agranular cortical areas of the rodent brain, investigated by anatomical and electrophysiological approaches. A central observation of these investigations is a weakening of interlaminar inhibition as cortical architecture becomes less differentiated. Thus, our study of agranular microcircuitry revealed deviations from the well-known ‘canonical’ microcircuit established for striate cortex, suggesting variations in intrinsic circuitry across the cortex that are functionally relevant.

4.5.2 The architectonic type principle comprehensively accounts for features of connectivity in the mammalian cortex

Architectonic differentiation, which encompasses characteristic differences of local cortical organisation (Zilles and Amunts, 2012b), has previously been shown to account for laminar patterns of cortico-cortical connections (e.g. Barbas, 1986; Barbas and Rempel-Clower, 1997). It is the central measure of cortical structure upon which the architectonic type principle is based, which links structural connections to the architectonic differentiation of cortical areas (reviewed in Barbas, 2015; García-Cabezas et al., 2019; Hilgetag et al., 2019). Our studies assessed models of cortico-cortical connectivity in the adult cat and macaque cortex across a more

comprehensive set of cortical areas and more functional modules than previous studies. Our findings underscore the significance of architectonic differentiation as a fundamental factor that captures multiple aspects of the organisation of cortico-cortical connectivity. This conclusion is based on the observations that architectonic differentiation of cortical areas is closely associated with the presence or absence of connections, with the number of connections of a cortical area, as well as with the laminar patterns of present connections. By contrast, other structural measures, such as spatial proximity, cortical thickness (in the macaque) and hierarchical level (in the cat), are not that consistently related to connection features.

Moreover, we directly compared the extent to which neuron density, spatial proximity and four measures of cellular morphology in layer 3 pyramidal neurons (i.e., soma cross section, spine count, peak spine density and dendritic tree size) were associated with cortico-cortical connectivity in the macaque cortex. The classical architectonic measure of neuron density most strongly and consistently related to essential features of cortical connectivity (specifically, the existence of projections and their laminar patterns, as well as area degree), and in conjoint analyses largely abolished effects of cellular morphological measures. These observations imply that neuron density and the considered measures of cellular morphology contain redundant information, with neuron density capturing most of the regularities that can be extracted from all of the four morphological measures. These results confirm neuron density as a central architectonic indicator of the primate cerebral cortex that is closely related to essential aspects of structural connectivity and is also highly indicative of further aspects of the architectonic organisation of cortical areas, such as the considered cellular morphological measures. Neuron density, and by extension architectonic differentiation, therefore integrates several aspects of cortical micro- and macroscopic organisation.

The architectonic type principle was originally developed qualitatively, in the classic studies of Sanides and Pandya (e.g. Pandya and Sanides, 1973), and systematically extended into quantitative studies by Barbas and colleagues, particularly through studies of prefrontal connectivity in the primate, but also of cat and mouse cortex (Barbas, 1986; Barbas and Rempel-Clower, 1997; Rempel-Clower and Barbas, 2000; Barbas et al., 2005; Medalla and Barbas, 2006; Medalla et al., 2007; Hilgetag and Grant, 2010; Goulas et al., 2014c; Hilgetag et al., 2016; Goulas et al., 2017). By exploring this principle for comprehensive connectivity and architectonic data sets in the cat and macaque cortex, we further corroborated the architectonic type principle, which has been developed by experimental and theoretical neuroanatomists over several decades.

To conclude, the applicability of the architectonic type principle across different

mammalian species and cortical systems suggests that it captures fundamental organisational principles underlying the global structural connectivity of the mammalian cerebral cortex. In humans, connections cannot be measured directly by tract-tracing studies for ethical reasons, but brain architecture can be studied *post mortem*. Thus, the likely applicability of the architectonic type principle in humans also has important implications for understanding the structural connectivity of the human brain, since it enables inferences from brain architecture (which can be measured in humans) to structural connectivity (which cannot be measured directly).

4.5.3 The architectonic type principle may emerge from spatio-temporal interactions during brain development

One prominent characteristic of structural connections are the laminar patterns of projection origins, which vary in a graded manner with the relative architectonic differentiation of connected areas in the adult brain. We showed that the architectonic type principle is already applicable to the laminar origins of cortico-cortical projections in the immature cortex of the macaque monkey. We found that prenatal and neonatal laminar patterns correlate with architectonic differentiation, and that the relation of laminar patterns to relative architectonic differentiation of connected areas is not substantially altered by complete loss of visual input. Moreover, we showed that the laminar patterns of projections change with maturation, such that the amount of change in supragranular contribution varies concurrently with the relative architectonic differentiation of the connected areas. Hence, it appears that biases in laminar projection patterns that are present initially become progressively strengthened by later developmental processes. These findings have significance for efforts to understand how structural connectivity is organised, the implication being that early neurogenetic processes during the formation of the brain are sufficient to establish typical laminar projection patterns. This conclusion is in line with mechanistic explanations previously suggested to underlie the emergence of the architectonic type principle and provides constraints for explorations of the fundamental factors that shape structural connectivity in the mammalian brain.

Guided by these results, which demonstrate the applicability of the architectonic type principle already during development, we performed simulations of cortical sheet growth and the concurrent formation of cortico-cortical connections, systematically varying the spatio-temporal trajectory of neurogenesis as well as the relation between architectonic differentiation and time of origin of neural populations. Our results showed that, for realistic assumptions about neurogenesis, successive tissue growth

and stochastic connection formation interacted to produce realistic cortico-cortical connectivity. This finding illustrated the fact that precise targeting of inter-areal connection terminations was not necessary for obtaining a realistic replication of connection existence within a cortical hemisphere. Instead, spatio-temporal interactions within the structural substrate were sufficient if a small number of empirically well-grounded assumptions were met, namely (i) planar, expansive growth of the cortical sheet as neurogenesis progressed, (ii) stronger architectonic differentiation for later neurogenetic time windows, and (iii) stochastic connection formation. We, thus, demonstrated a possible mechanism of how relative architectonic differentiation and connectivity become linked during development. These findings support hypotheses advanced previously about the mechanistic underpinnings of the architectonic type principle (Barbas, 1986; Dombrowski et al., 2001; Barbas, 2015; Hilgetag et al., 2016). Moreover, they point towards a central role of time of neurogenesis, which appears to prescribe both areas' architectonic differentiation and their spatial proximity (which is directly related to their connection probability). The implication is that time of origin could mediate a secondary correlation between relative architectonic differentiation and connection probability, which, in contrast to the two primary correlations, can be observed empirically in the adult cortex.

While these results demonstrated that spatio-temporal interactions between the time and place of neurogenesis could underlie projection existence as observed empirically in the mammalian cortex, and similar simulation experiments point towards a link between spatio-temporal interactions and the distribution of projection strengths (Goulas et al., 2019a), so far, no mechanistic explanation for the emergence of typically observed laminar patterns of projection origins and terminations had been tested. We therefore expanded our *in silico* model of the developing cortical sheet to explore which factors could potentially constrain the development of laminar projection patterns. We showed that manipulations which rely solely on spatio-temporal interactions, namely the relative density of laminar compartments, a delay in the growth of infragranular layers relative to layer 1, and a delay in the growth of supragranular layers relative to infragranular layers, do not result in the striking correlation between supragranular contribution to projections and the relative differentiation of areas that is typically observed in the mammalian cortex. In contrast, we found that if we introduced systematic variation in cell-intrinsic properties, coupling them with architectonic differentiation, the resulting laminar projection patterns closely mirror the empirically observed patterns. We also find that the spatio-temporal interactions posited to occur during neurogenesis are necessary for the formation of the characteristic laminar patterns. Hence, our results indicate that the specification of the laminar patterns of projection origins may result from systematic variation in a number of

cell-intrinsic properties, superimposed on the previously identified spatio-temporal interactions which are sufficient for the emergence of the architectonic type principle on the level of inter-areal connectivity *in silico*.

Thus, although our results arguably point towards fundamental mechanisms that could underlie the emergence of the architectonic type principle, further details of these mechanistic underpinnings remain to be worked out before we can comprehend how all features of cortico-cortical connectivity are determined.

Parts of this section have been published in Beul and Hilgetag (2015), Beul et al. (2015), Beul et al. (2017), Beul et al. (2018) and Beul and Hilgetag (2019a) and submitted for peer-review in Beul and Hilgetag (2019b).

Summary

5.1 English Summary

Structural connections mediate information processing in the brain, synaptically linking neurons across a range of spatial scales. The mammalian cortex exhibits a strikingly complex organisation, both in terms of its architecture, that is, its constituent cellular elements and their arrangement, and in terms of its connectivity, which is neither random nor regular. Untangling the principles that govern the organisation of structural connectivity in the brain, and within the cortex more specifically, is a formidable challenge. One candidate organisational framework is the architectonic type principle, which links structural connections to the architecture of cortical areas. It has previously been reported that regularities of cortico-cortical connections are well captured by the architectonic type principle.

We provide further support for the existence of the architectonic type principle by expanding the scope of empirical investigation. We show that the architectonic type principle is applicable to the entire cat and macaque cortex, and that laminar patterns of projection origins in the macaque cortex are captured by the architectonic type principle both in immature and adult stages. Our findings thus corroborate the architectonic type principle as a fundamental organising principle of cortical connectivity in the mammalian cortex, which is able to integrate cortical characteristics across spatial scales. This has implications for our understanding of functional interactions in the mammalian brain, which are strongly constrained by structural connectivity.

Moreover, the applicability of the architectonic type principle across mammalian species enables inferences about the organisation of connectivity in species where reliable connectivity data are difficult to obtain, as for example humans.

In addition, we explore the mechanistic underpinnings which have been hypothesised to result in the emergence of the architectonic type principle. Through systematic simulation experiments, we demonstrate that patterns of connection existence that are consistent with the architectonic type principle could emerge from simple spatio-temporal interactions in the developing cortex. Specifically, it appears that the time of origin prescribes both areas' architectonic differentiation and the spatial distance between them, and hence their connection probability. Based on these two fundamental associations, time of origin could thereby mediate a secondary correlation between relative architectonic differentiation and connection probability, which can be observed empirically.

However, for the characteristic, empirically observed, laminar patterns of projection origins to emerge, our *in silico* model of the developing cortical sheet needs to include cellular heterogeneity, where cell-intrinsic properties vary systematically along the gradient of architectonic differentiation.

Our results thus suggest that spatio-temporal interactions in a homogeneous developing cortical sheet can be sufficient to shape patterns of connection existence, while more specific constraints govern the establishment of more detailed connectivity features such as laminar projection patterns.

5.2 Deutsche Zusammenfassung

Strukturelle Verbindungen, die Neurone über verschiedene räumliche Skalen synaptisch miteinander in Kontakt treten lassen, sind die physische Grundlage für Informationsverarbeitung im Gehirn. Der Kortex von Säugetieren bildet eine erstaunlich komplexe Organisation aus, sowohl in Bezug auf seine Architektur, also die Charakteristiken und die Anordnung seiner Zellen, als auch bezüglich seiner Konnektivität, die weder zufällig noch regelmäßig ist. Die Prinzipien aufzudecken, die die Organisation struktureller Verbindungen im Gehirn bestimmen, insbesondere im Kortex, ist eine enorme Herausforderung. Ein mögliches erklärendes Modell ist das Prinzip des architektonischen Typs, welches strukturelle Verbindungen zur architektonischen Differenzierung von Arealen in Bezug setzt. Frühere Studien haben gezeigt, dass das Prinzip des architektonischen Typs Regelmäßigkeiten in kortiko-kortikalen

Verbindungen gut repräsentiert.

Wir untermauern die Existenz des Prinzips des architektonischen Typs, indem wir den Umfang empirischer Studien erweitern. Wir zeigen, dass das Prinzip des architektonischen Typs auf Verbindungen im gesamten Kortex der Katze und des Makaken anwendbar ist, sowie, dass die laminaren Muster von Verbindungsursprüngen sowohl im erwachsenen als auch im sich entwickelnden Kortex des Makaken vom Prinzip des architektonischen Typs gut repräsentiert werden. Unsere Ergebnisse bestätigen daher das Prinzip des architektonischen Typs als fundamentales Organisationsprinzip kortikaler Konnektivität in Säugetieren, welches Eigenschaften des Kortex über räumliche Skalen hinweg integriert. Dies hat Auswirkungen auf unser Verständnis funktioneller Interaktionen im Säugetiergehirn, die stark von struktureller Konnektivität bestimmt werden. Außerdem ermöglicht die generelle Anwendbarkeit des Prinzips des architektonischen Typs auf das Säugetiergehirn Rückschlüsse auf die Organisation kortikaler Konnektivität in Spezies, für die zuverlässige Konnektivitätsdaten nur schwer erhoben werden können, wie zum Beispiel den Menschen.

Des Weiteren untersuchen wir mögliche Mechanismen, die zum Auftreten des Prinzips des architektonischen Typs führen könnten. Anhand systematischer Simulationsexperimente demonstrieren wir, dass durch einfache raumzeitliche Interaktionen im sich entwickelnden Kortex Muster von Verbindungsexistenz entstehen können, die dem Prinzip des architektonischen Typs genügen. Aus unseren Simulationen schließen wir, dass der Zeitpunkt, zu dem ein Areal entsteht, sowohl seine architektonische Differenzierung bestimmt, als auch seine räumliche Nähe zu anderen Arealen, und damit die jeweilige Verbindungswahrscheinlichkeit. Diese beiden grundlegenden Zusammenhänge könnten sich überlagern, so dass der Entstehungszeitpunkt von Arealen eine sekundäre Korrelation zwischen relativer architektonischer Differenzierung und Verbindungswahrscheinlichkeit herbeiführt, die empirisch beobachtet werden kann.

Damit jedoch die charakteristischen laminaren Muster von Verbindungsursprüngen auftreten, wie sie empirisch beobachtet werden, muss unser *in silico* Modell des sich entwickelnden Kortex zelluläre Heterogenität beinhalten, wobei sich den Zellen intrinsische Eigenschaften systematisch entlang des Differenzierungsgradienten verändern.

Unsere Ergebnisse deuten demzufolge darauf hin, dass raumzeitliche Interaktionen in einem sich entwickelnden homogenen Kortex ausreichen können, um realistische Muster von Verbindungsexistenz zu formen, während stärkere Einschränkungen die Entstehung detaillierterer Verbindungseigenschaften, wie zum Beispiel laminarer Muster, regulieren.

Bibliography

- A. A. Abbie. Cortical lamination in the Monotremata. *The Journal of Comparative Neurology*, 72(3):429–467, 1940. doi: 10.1002/cne.900720302.
- A. A. Abbie. Cortical lamination in a polyprotodont marsupial, *Perameles nasuta*. *Journal of Comparative Neurology*, 76(3):509–536, 1942. doi: 10.1002/cne.900760310.
- S. Achard, R. Salvador, B. Whitcher, J. Suckling, and E. T. Bullmore. A Resilient, Low-Frequency, Small-World Human Brain Functional Network with Highly Connected Association Cortical Hubs. *The Journal of Neuroscience*, 26(1):63–72, 2006. doi: 10.1523/JNEUROSCI.3874-05.2006.
- E. A. Alcamo, L. Chirivella, M. Dautzenberg, G. Dobрева, I. Fariñas, R. Grosschedl, and S. K. McConnell. *Satb2* Regulates Callosal Projection Neuron Identity in the Developing Cerebral Cortex. *Neuron*, 57(3):364–377, 2008. doi: 10.1016/j.neuron.2007.12.012.
- A. F. Alexander-Bloch, P. E. Vértes, R. Stidd, F. Lalonde, L. Clasen, J. Rapoport, J. Giedd, E. T. Bullmore, and N. Gogtay. The Anatomical Distance of Functional Connections Predicts Brain Network Topology in Health and Schizophrenia. *Cerebral Cortex*, 23(1):127–138, 2013. doi: 10.1093/cercor/bhr388.
- J. R. Alger. The Diffusion Tensor Imaging Toolbox. *The Journal of Neuroscience*, 32(22):7418–7428, 2012. doi: 10.1523/JNEUROSCI.4687-11.2012.
- P. Andersen, R. Morris, and D. G. Amaral, editors. *The Hippocampus Book*. Oxford University Press, New York, USA, 2007. ISBN 978-0-19-510027-3.
- J. B. Angevine and R. L. Sidman. Autoradiographic Study of Cell Migration during Histogenesis of Cerebral Cortex in the Mouse. *Nature*, 192(4804):766–768, 1961. doi: 10.1038/192766b0.
- A. J. Apicella, I. R. Wickersham, H. S. Seung, and G. M. G. Shepherd. Laminarly Orthogonal Excitation of Fast-Spiking and Low-Threshold-Spiking Interneurons in

- Mouse Motor Cortex. *The Journal of Neuroscience*, 32(20):7021–7033, 2012. doi: 10.1523/JNEUROSCI.0011-12.2012.
- A. F. T. Arnsten, M. J. Wang, and C. D. Paspalas. Neuromodulation of Thought: Flexibilities and Vulnerabilities in Prefrontal Cortical Network Synapses. *Neuron*, 76(1):223–239, 2012. doi: 10.1016/j.neuron.2012.08.038.
- D. Bagnard, M. Lohrum, D. Uziel, A. W. Püschel, and J. Bolz. Semaphorins act as attractive and repulsive guidance signals during the development of cortical projections. *Development (Cambridge, England)*, 125(24):5043–5053, 1998.
- W. Z. Bai, M. Ishida, and Y. Arimatsu. Chemically defined feedback connections from infragranular layers of sensory association cortices in the rat. *Neuroscience*, 123(1): 257–267, 2004. doi: 10.1016/j.neuroscience.2003.08.056.
- A. Bailey, B. Ombuki-Berman, and M. Ventresca. Automatic Inference of Hierarchical Graph Models using Genetic Programming with an Application to Cortical Networks. In C. Blum, editor, *Proceedings of the 2013 Genetic and Evolutionary Computation Conference*, volume GECCO 2013, pages 893–900, Amsterdam, Netherlands, 2013. ISBN 978-1-4503-1963-8. doi: 10.1145/2463372.2463498.
- G. Ball, P. Aljabar, S. Zebari, N. Tusor, T. Arichi, N. Merchant, E. C. Robinson, E. Ogunjipe, D. Rueckert, A. D. Edwards, and S. J. Counsell. Rich-club organization of the newborn human brain. *Proceedings of the National Academy of Sciences*, 111(20):7456–7461, 2014. doi: 10.1073/pnas.1324118111.
- I. Ballesteros-Yáñez, R. Benavides-Piccione, G. N. Elston, R. Yuste, and J. DeFelipe. Density and morphology of dendritic spines in mouse neocortex. *Neuroscience*, 138(2):403–409, 2006. doi: 10.1016/j.neuroscience.2005.11.038.
- I. Ballesteros-Yáñez, R. Benavides-Piccione, J.-P. Bourgeois, J.-P. Changeux, and J. DeFelipe. Alterations of cortical pyramidal neurons in mice lacking high-affinity nicotinic receptors. *Proceedings of the National Academy of Sciences*, 107(25): 11567–11572, 2010. doi: 10.1073/pnas.1006269107.
- A. P. Bannister. Inter- and intra-laminar connections of pyramidal cells in the neocortex. *Neuroscience Research*, 53(2):95–103, 2005. doi: 10.1016/j.neures.2005.06.019.
- H. Barbas. Pattern in the laminar origin of corticocortical connections. *The Journal of Comparative Neurology*, 252(3):415–422, 1986. doi: 10.1002/cne.902520310.

- H. Barbas. Flow of information for emotions through temporal and orbitofrontal pathways. *Journal of Anatomy*, 211(2):237–249, 2007. doi: 10.1111/j.1469-7580.2007.00777.x.
- H. Barbas. General Cortical and Special Prefrontal Connections: Principles from Structure to Function. *Annual Review of Neuroscience*, 38(1):269–289, 2015. doi: 10.1146/annurev-neuro-071714-033936.
- H. Barbas and M. Á. García-Cabezas. Motor cortex layer 4: less is more. *Trends in Neurosciences*, 38(5):259–261, 2015. doi: 10.1016/j.tins.2015.03.005.
- H. Barbas and M. Á. García-Cabezas. How the prefrontal executive got its stripes. *Current Opinion in Neurobiology*, 40:125–134, 2016. doi: 10.1016/j.conb.2016.07.003.
- H. Barbas and D. N. Pandya. Architecture and intrinsic connections of the prefrontal cortex in the rhesus monkey. *The Journal of comparative neurology*, 286(3):353–375, 1989. doi: 10.1002/cne.902860306.
- H. Barbas and N. L. Rempel-Clower. Cortical structure predicts the pattern of corticocortical connections. *Cerebral Cortex*, 7(7):635–646, 1997. doi: 10.1093/cercor/7.7.635.
- H. Barbas, C. C. Hilgetag, S. Saha, C. R. Dermon, and J. L. Suski. Parallel organization of contralateral and ipsilateral prefrontal cortical projections in the rhesus monkey. *BMC Neuroscience*, 6:32, 2005. doi: 10.1186/1471-2202-6-32.
- D. L. Barbour and E. M. Callaway. Excitatory local connections of superficial neurons in rat auditory cortex. *The Journal of Neuroscience: The Official Journal of the Society for Neuroscience*, 28(44):11174–11185, 2008. doi: 10.1523/JNEUROSCI.2093-08.2008.
- A. Barnes and F. Polleux. Establishment of axon-dendrite polarity in developing neurons. *Annual Review of Neuroscience*, 32:347–381, 2009. doi: 10.1146/annurev-neuro.31.060407.125536,10.1146/annurev.neuro.31.060407.125536.
- P. Barone, C. Dehay, M. Berland, J. Bullier, and H. Kennedy. Developmental remodeling of primate visual cortical pathways. *Cerebral Cortex*, 5(1):22–38, 1995.
- P. Barone, A. Batardiere, K. Knoblauch, and H. Kennedy. Laminar distribution of neurons in extrastriate areas projecting to visual areas V1 and V4 correlates with the hierarchical rank and indicates the operation of a distance rule. *The Journal of Neuroscience*, 20(9):3263–3281, 2000.

- P. Barthó, H. Hirase, L. Monconduit, M. Zugaro, K. D. Harris, and G. Buzsáki. Characterization of Neocortical Principal Cells and Interneurons by Network Interactions and Extracellular Features. *Journal of Neurophysiology*, 92(1):600–608, 2004. doi: 10.1152/jn.01170.2003.
- D. S. Bassett and E. T. Bullmore. Small-world brain networks. *The Neuroscientist*, 12(6):512–523, 2006. doi: 10.1177/1073858406293182.
- D. S. Bassett, E. T. Bullmore, B. A. Verchinski, V. S. Mattay, D. R. Weinberger, and A. Meyer-Lindenberg. Hierarchical Organization of Human Cortical Networks in Health and Schizophrenia. *The Journal of Neuroscience*, 28(37):9239–9248, 2008. doi: 10.1523/JNEUROSCI.1929-08.2008.
- D. S. Bassett, D. L. Greenfield, A. Meyer-Lindenberg, D. R. Weinberger, S. W. Moore, and E. T. Bullmore. Efficient Physical Embedding of Topologically Complex Information Processing Networks in Brains and Computer Circuits. *PLoS Comput Biol*, 6(4):e1000748, 2010. doi: 10.1371/journal.pcbi.1000748.
- A. M. Bastos, W. M. Usrey, R. A. Adams, G. R. Mangun, P. Fries, and K. J. Friston. Canonical Microcircuits for Predictive Coding. *Neuron*, 76(4):695–711, 2012. doi: 10.1016/j.neuron.2012.10.038.
- A. M. Bastos, J. Vezoli, C. A. Bosman, J.-M. Schoffelen, R. Oostenveld, J. R. Dowdall, P. De Weerd, H. Kennedy, and P. Fries. Visual Areas Exert Feedforward and Feedback Influences through Distinct Frequency Channels. *Neuron*, 85(2):390–401, 2015. doi: 10.1016/j.neuron.2014.12.018.
- A. Batardière, P. Barone, C. Dehay, and H. Kennedy. Area-specific laminar distribution of cortical feedback neurons projecting to cat area 17: Quantitative analysis in the adult and during ontogeny. *The Journal of Comparative Neurology*, 396(4):493–510, 1998. doi: 10.1002/(SICI)1096-9861(19980713)396:4<493::AID-CNE6>3.0.CO;2-X.
- A. Batardière, P. Barone, K. Knoblauch, P. Giroud, M. Berland, A.-M. Dumas, and H. Kennedy. Early Specification of the Hierarchical Organization of Visual Cortical Areas in the Macaque Monkey. *Cerebral Cortex*, 12(5):453–465, 2002. doi: 10.1093/cercor/12.5.453.
- S. A. Bayer and J. Altman. Directions in Neurogenetic Gradients and Patterns of Anatomical Connections in the Telencephalon. *Progress in Neurobiology*, 29:57–106, 1987.

- S. A. Bayer and J. Altman. *Neocortical Development*. Raven Press, New York, USA, 1991. ISBN 0-88167-778-7.
- C. Beaulieu and M. Colonnier. Number of neurons in individual laminae of areas 3b, 4 gamma, and 6a alpha of the cat cerebral cortex: a comparison with major visual areas. *The Journal of Comparative Neurology*, 279(2):228–234, 1989. doi: 10.1002/cne.902790206.
- R. Benavides-Piccione, I. Ballesteros-Yáñez, J. DeFelipe, and R. Yuste. Cortical area and species differences in dendritic spine morphology. *Journal of Neurocytology*, 31(3-5):337–346, 2002.
- V. K. Berezovskii, J. J. Nassi, and R. T. Born. Segregation of feedforward and feedback projections in mouse visual cortex. *The Journal of Comparative Neurology*, 519(18):3672–3683, 2011. doi: 10.1002/cne.22675.
- B. C. Bernhardt, O. M. Klimecki, S. Leiberg, and T. Singer. Structural Covariance Networks of the Dorsal Anterior Insula Predict Females’ Individual Differences in Empathic Responding. *Cerebral Cortex*, 24(8):2189–2198, 2014. doi: 10.1093/cercor/bht072.
- S. F. Beul and C. C. Hilgetag. Towards a “canonical” agranular cortical microcircuit. *Frontiers in Neuroanatomy*, 8:165, 2015. doi: 10.3389/fnana.2014.00165.
- S. F. Beul and C. C. Hilgetag. Neuron density fundamentally relates to architecture and connectivity of the primate cerebral cortex. *NeuroImage*, 189:117051, 2019a. doi: 10.1016/j.neuroimage.2019.01.010.
- S. F. Beul and C. C. Hilgetag. Systematic modelling of the development of laminar projection origins in the cerebral cortex: Interactions of spatio-temporal patterns of neurogenesis and cellular heterogeneity. *Under review*, 2019b.
- S. F. Beul, S. Grant, and C. C. Hilgetag. A predictive model of the cat cortical connectome based on cytoarchitecture and distance. *Brain Structure and Function*, 220(6):3167–3184, 2015. doi: 10.1007/s00429-014-0849-y.
- S. F. Beul, H. Barbas, and C. C. Hilgetag. A Predictive Structural Model of the Primate Connectome. *Scientific Reports*, 7:43176, 2017. doi: 10.1038/srep43176.
- S. F. Beul, A. Goulas, and C. C. Hilgetag. Comprehensive computational modelling of the development of mammalian cortical connectivity underlying an architectonic type principle. *PLoS Computational Biology*, 14(11):e1006550, 2018. doi: 10.1371/journal.pcbi.1006550.

- S. Bianchi, C. D. Stimpson, A. L. Bauernfeind, S. J. Schapiro, W. B. Baze, M. J. McArthur, E. Bronson, W. D. Hopkins, K. Semendeferi, B. Jacobs, P. R. Hof, and C. C. Sherwood. Dendritic Morphology of Pyramidal Neurons in the Chimpanzee Neocortex: Regional Specializations and Comparison to Humans. *Cerebral Cortex*, 23(10):2429–2436, 2013. doi: 10.1093/cercor/bhs239.
- T. Binzegger, R. J. Douglas, and K. A. Martin. A Quantitative Map of the Circuit of Cat Primary Visual Cortex. *The Journal of Neuroscience*, 24(39):8441–8453, 2004. doi: 10.1523/JNEUROSCI.1400-04.2004.
- J. Bolz and V. Castellani. How do wiring molecules specify cortical connections? *Cell and Tissue Research*, 290(2):307–314, 1997. doi: 10.1007/s004410050935.
- J. Bolz, N. Novak, M. Götz, and T. Bonhoeffer. Formation of target-specific neuronal projections in organotypic slice cultures from rat visual cortex. *Nature*, 346(6282): 359–362, 1990. doi: 10.1038/346359a0.
- V. Braitenberg. Brain Size and Number of Neurons: An Exercise in Synthetic Neuroanatomy. *Journal of Computational Neuroscience*, 10(1):71–77, 2001. doi: 10.1023/A:1008920127052.
- V. Braitenberg and A. Schüz. *Cortex: statistics and geometry of neuronal connectivity*. Springer, Berlin; New York, 2nd edition, 1998. ISBN 3-540-63816-4 978-3-540-63816-2.
- K. Brodmann. *Vergleichende Lokalisationslehre der Großhirnrinde in ihren Prinzipien dargestellt auf Grund des Zellenbaues*. Johannes Ambrosius Barth Verlag, Leipzig, 1909.
- S. P. Brown and S. Hestrin. Intracortical circuits of pyramidal neurons reflect their long-range axonal targets. *Nature*, 457(7233):1133–1136, 2009. doi: 10.1038/nature07658.
- R. L. Buckner and F. M. Krienen. The evolution of distributed association networks in the human brain. *Trends in Cognitive Sciences*, 17(12):648–665, 2013. doi: 10.1016/j.tics.2013.09.017.
- E. A. Buffalo, P. Fries, R. Landman, T. J. Buschman, and R. Desimone. Laminar differences in gamma and alpha coherence in the ventral stream. *Proceedings of the National Academy of Sciences*, 108(27):11262–11267, 2011. doi: 10.1073/pnas.1011284108.

- E. T. Bullmore and O. Sporns. Complex brain networks: graph theoretical analysis of structural and functional systems. *Nature Reviews Neuroscience*, 10(3):186–198, 2009. doi: 10.1038/nrn2575.
- E. T. Bullmore and O. Sporns. The economy of brain network organization. *Nature Reviews Neuroscience*, 13:336–349, 2012. doi: 10.1038/nrn3214.
- D. V. Buonomano and W. Maass. State-dependent computations: spatiotemporal processing in cortical networks. *Nature Reviews Neuroscience*, 10(2):113–125, 2009. doi: 10.1038/nrn2558.
- A. Burkhalter. Development of Forward and Feedback Connections between Areas V1 and V2 of Human Visual Cortex. *Cerebral Cortex*, 3(5):476–487, 1993. doi: 10.1093/cercor/3.5.476.
- R. B. Burns and R. A. Burns. Discriminant Analysis. In *Business Research Methods and Statistics Using SPSS*, pages 589–608. SAGE Publications Ltd., London, UK, 2008. ISBN 978-1-4129-4530-1.
- J. B. Burt, M. Demirtaş, W. J. Eckner, N. M. Navejar, J. L. Ji, W. J. Martin, A. Bernacchia, A. Anticevic, and J. D. Murray. Hierarchy of transcriptomic specialization across human cortex captured by structural neuroimaging topography. *Nature Neuroscience*, 21(9):1251, 2018. doi: 10.1038/s41593-018-0195-0.
- G. Buzsáki and K. Mizuseki. The log-dynamic brain: how skewed distributions affect network operations. *Nature Reviews Neuroscience*, 15(4):264–278, 2014. doi: 10.1038/nrn3687.
- D. J. Cahalane, B. Clancy, M. A. Kingsbury, E. Graf, O. Sporns, and B. L. Finlay. Network Structure Implied by Initial Axon Outgrowth in Rodent Cortex: Empirical Measurement and Models. *PLoS ONE*, 6(1):e16113, 2011. doi: 10.1371/journal.pone.0016113.
- D. J. Cahalane, C. J. Charvet, and B. L. Finlay. Systematic, balancing gradients in neuron density and number across the primate isocortex. *Frontiers in Neuroanatomy*, 6:28, 2012. doi: 10.3389/fnana.2012.00028.
- D. J. Cahalane, C. J. Charvet, and B. L. Finlay. Modeling local and cross-species neuron number variations in the cerebral cortex as arising from a common mechanism. *Proceedings of the National Academy of Sciences*, 111(49):17642–17647, 2014. doi: 10.1073/pnas.1409271111.

- S. R. Y. Cajal. *Recollections of My Life*. American Philosophical Society, Philadelphia PA, 1937. p.395. Translated by E. H. Craigie and J. Cano. 1st MIT press paperback edition, 1989.
- O. Camiré and L. Topolnik. Functional compartmentalisation and regulation of postsynaptic Ca²⁺ transients in inhibitory interneurons. *Cell Calcium*, 52(5): 339–346, 2012. doi: 10.1016/j.ceca.2012.05.001.
- C. N. Carlo and C. F. Stevens. Structural uniformity of neocortex, revisited. *Proceedings of the National Academy of Sciences*, 110(4):1488–1493, 2013. doi: 10.1073/pnas.1221398110.
- P. Caroni, F. Donato, and D. Muller. Structural plasticity upon learning: regulation and functions. *Nature Reviews Neuroscience*, 13(7):478–490, 2012. doi: 10.1038/nrn3258.
- V. Castellani and J. Bolz. Membrane-associated molecules regulate the formation of layer-specific cortical circuits. *Proceedings of the National Academy of Sciences*, 94(13):7030–7035, 1997.
- V. Castellani, Y. Yue, P. P. Gao, R. Zhou, and J. Bolz. Dual action of a ligand for Eph receptor tyrosine kinases on specific populations of axons during the development of cortical circuits. *The Journal of Neuroscience: The Official Journal of the Society for Neuroscience*, 18(12):4663–4672, 1998.
- B. Cauli, E. Audinat, B. Lambolez, M. C. Angulo, N. Ropert, K. Tsuzuki, S. Hestrin, and J. Rossier. Molecular and Physiological Diversity of Cortical Nonpyramidal Cells. *The Journal of Neuroscience*, 17(10):3894–3906, 1997.
- V. S. Caviness. Patterns of cell and fiber distribution in the neocortex of the reeler mutant mouse. *The Journal of Comparative Neurology*, 170(4):435–447, 1976. doi: 10.1002/cne.901700404.
- V. S. Caviness. Neocortical histogenesis in normal and reeler mice: A developmental study based upon [3h]thymidine autoradiography. *Developmental Brain Research*, 4(3):293–302, 1982. doi: 10.1016/0165-3806(82)90141-9.
- V. S. Caviness and D. O. Frost. Thalamocortical projections in the reeler mutant mouse. *The Journal of Comparative Neurology*, 219(2):182–202, 1983. doi: 10.1002/cne.902190205.
- V. S. Caviness and R. L. Sidman. Olfactory structures of the forebrain in the reeler mutant mouse. *The Journal of Comparative Neurology*, 145(1):85–104, 1972. doi: 10.1002/cne.901450106.

- V. S. Caviness and R. L. Sidman. Time of origin of corresponding cell classes in the cerebral cortex of normal and reeler mutant mice: An autoradiographic analysis. *The Journal of Comparative Neurology*, 148(2):141–151, 1973. doi: 10.1002/cne.901480202.
- V. S. Caviness and C. H. Yorke. Interhemispheric neocortical connections of the corpus callosum in the reeler mutant mouse: A study based on anterograde and retrograde methods. *The Journal of Comparative Neurology*, 170(4):449–459, 1976. doi: 10.1002/cne.901700405.
- V. S. Caviness, P. G. Bhide, and R. S. Nowakowski. Histogenetic Processes Leading to the Laminated Neocortex: Migration Is Only a Part of the Story. *Developmental Neuroscience*, 30(1-3):82–95, 2008. doi: 10.1159/000109854.
- V. S. Caviness, R. S. Nowakowski, and P. G. Bhide. Neocortical neurogenesis: morphogenetic gradients and beyond. *Trends in Neurosciences*, 32(8):443–450, 2009. doi: 10.1016/j.tins.2009.05.003.
- C. J. Charvet and B. L. Finlay. Evo-devo and the primate isocortex: the central organizing role of intrinsic gradients of neurogenesis. *Brain, Behavior and Evolution*, 84(2):81–92, 2014. doi: 10.1159/000365181.
- C. J. Charvet, D. J. Cahalane, and B. L. Finlay. Systematic, Cross-Cortex Variation in Neuron Numbers in Rodents and Primates. *Cerebral Cortex*, 25(1):147–160, 2015. doi: 10.1093/cercor/bht214.
- R. Chaudhuri, K. Knoblauch, M.-A. Gariel, H. Kennedy, and X.-J. Wang. A Large-Scale Circuit Mechanism for Hierarchical Dynamical Processing in the Primate Cortex. *Neuron*, 88(2):419–431, 2015. doi: 10.1016/j.neuron.2015.09.008.
- A. Chédotal. Roles of axon guidance molecules in neuronal wiring in the developing spinal cord. *Nature Reviews Neuroscience*, 20(7):380, 2019. doi: 10.1038/s41583-019-0168-7.
- B. L. Chen, D. H. Hall, and D. B. Chklovskii. Wiring optimization can relate neuronal structure and function. *Proceedings of the National Academy of Sciences*, 103(12):4723–4728, 2006. doi: 10.1073/pnas.0506806103.
- J.-G. Chen, M.-R. Rašin, K. Y. Kwan, and N. Šestan. Zfp312 is required for subcortical axonal projections and dendritic morphology of deep-layer pyramidal neurons of the cerebral cortex. *Proceedings of the National Academy of Sciences*, 102(49):17792–17797, 2005. doi: 10.1073/pnas.0509032102.

- Y. Chen, S. Wang, C. C. Hilgetag, and C. Zhou. Trade-off between Multiple Constraints Enables Simultaneous Formation of Modules and Hubs in Neural Systems. *PLoS Comput Biol*, 9(3):e1002937, 2013. doi: 10.1371/journal.pcbi.1002937.
- Z. J. Chen, Y. He, P. Rosa-Neto, J. Germann, and A. C. Evans. Revealing Modular Architecture of Human Brain Structural Networks by Using Cortical Thickness from MRI. *Cerebral Cortex*, 18(10):2374–2381, 2008. doi: 10.1093/cercor/bhn003.
- Z. J. Chen, Y. He, P. Rosa-Neto, G. Gong, and A. C. Evans. Age-related alterations in the modular organization of structural cortical network by using cortical thickness from MRI. *NeuroImage*, 56(1):235–245, 2011. doi: 10.1016/j.neuroimage.2011.01.010.
- V. Chevalyere and R. A. Piskorowski. Modulating excitation through plasticity at inhibitory synapses. *Frontiers in Cellular Neuroscience*, 8:93, 2014. doi: 10.3389/fncel.2014.00093.
- V. Colizza, A. Flammini, M. A. Serrano, and A. Vespignani. Detecting rich-club ordering in complex networks. *Nature Physics*, 2(2):110–115, 2006. doi: 10.1038/nphys209.
- G. Collin, O. Sporns, R. C. W. Mandl, and M. P. van den Heuvel. Structural and Functional Aspects Relating to Cost and Benefit of Rich Club Organization in the Human. *Cerebral Cortex*, 24(9):2258–2267, 2014. doi: 10.1093/cercor/bht064.
- C. E. Collins, D. C. Airey, N. A. Young, D. B. Leitch, and J. H. Kaas. Neuron densities vary across and within cortical areas in primates. *Proceedings of the National Academy of Sciences*, 107(36):15927–15932, 2010. doi: 10.1073/pnas.1010356107.
- J. Cortés-Mendoza, S. Díaz de León-Guerrero, G. Pedraza-Alva, and L. Pérez-Martínez. Shaping synaptic plasticity: The role of activity-mediated epigenetic regulation on gene transcription. *International Journal of Developmental Neuroscience*, 31(6): 359–369, 2013. doi: 10.1016/j.ijdevneu.2013.04.003.
- P. J. Coskren, J. I. Luebke, D. Kabaso, S. L. Wearne, A. Yadav, T. Rumbell, P. R. Hof, and C. M. Weaver. Functional consequences of age-related morphologic changes to pyramidal neurons of the rhesus monkey prefrontal cortex. *Journal of computational neuroscience, Journal of computational neuroscience*, 38, 38(2, 2):263, 263–283, 2015. doi: 10.1007/s10827-014-0541-5,10.1007/s10827-014-0541-5.
- L. d. F. Costa, M. Kaiser, and C. C. Hilgetag. Predicting the connectivity of primate cortical networks from topological and spatial node properties. *BMC Systems Biology*, 1(1):16, 2007. doi: 10.1186/1752-0509-1-16.

- N. A. Crossley, A. Mechelli, P. E. Vértes, T. T. Winton-Brown, A. X. Patel, C. E. Ginestet, P. McGuire, and E. T. Bullmore. Cognitive relevance of the community structure of the human brain functional coactivation network. *Proceedings of the National Academy of Sciences*, 110(28):11583–11588, 2013. doi: 10.1073/pnas.1220826110.
- N. A. Crossley, A. Mechelli, J. Scott, F. Carletti, P. T. Fox, P. McGuire, and E. T. Bullmore. The hubs of the human connectome are generally implicated in the anatomy of brain disorders. *Brain: A Journal of Neurology*, 137(Pt 8):2382–2395, 2014. doi: 10.1093/brain/awu132.
- T. J. Cullen, M. A. Walker, S. L. Eastwood, M. M. Esiri, P. J. Harrison, and T. J. Crow. Anomalies of asymmetry of pyramidal cell density and structure in dorsolateral prefrontal cortex in schizophrenia. *The British Journal of Psychiatry*, 188(1):26–31, 2006. doi: 10.1192/bjp.bp.104.008169.
- N. M. da Costa and K. A. C. Martin. Whose cortical column would that be? *Frontiers in Neuroanatomy*, 4:16, 2010. doi: 10.3389/fnana.2010.00016.
- G. Dallérac, O. Chever, and N. Rouach. How do astrocytes shape synaptic transmission? Insights from electrophysiology. *Frontiers in Cellular Neuroscience*, 7:159, 2013. doi: 10.3389/fncel.2013.00159.
- R. A. Dart. The Dual Structure of the Neopallium: its History and Significance. *Journal of Anatomy*, 69(Pt 1):3–19, 1934.
- M. A. de Reus and M. P. van den Heuvel. Rich Club Organization and Intermodule Communication in the Cat Connectome. *The Journal of Neuroscience*, 33(32):12929–12939, 2013. doi: 10.1523/JNEUROSCI.1448-13.2013.
- J. DeFelipe. The evolution of the brain, the human nature of cortical circuits, and intellectual creativity. *Frontiers in Neuroanatomy*, 5:29, 2011. doi: 10.3389/fnana.2011.00029.
- J. DeFelipe, M. C. González-Albo, M. R. Del Río, and G. N. Elston. Distribution and patterns of connectivity of interneurons containing calbindin, calretinin, and parvalbumin in visual areas of the occipital and temporal lobes of the macaque monkey. *The Journal of Comparative Neurology*, 412(3):515–526, 1999. doi: 10.1002/(SICI)1096-9861(19990927)412:3<515::AID-CNE10>3.0.CO;2-1.
- S. Dehaene, M. Kerszberg, and J.-P. Changeux. A neuronal model of a global workspace in effortful cognitive tasks. *Proceedings of the National Academy of Sciences*, 95(24):14529–14534, 1998. doi: 10.1073/pnas.95.24.14529.

- S. Dehaene, J.-P. Changeux, and L. Naccache. The Global Neuronal Workspace Model of Conscious Access: From Neuronal Architectures to Clinical Applications. In S. Dehaene and Y. Christen, editors, *Characterizing Consciousness: From Cognition to the Clinic?*, pages 55–84. Springer, Berlin, Heidelberg, 2011. ISBN 978-3-642-18014-9 978-3-642-18015-6.
- C. Dehay, H. Kennedy, and K. S. Kosik. The Outer Subventricular Zone and Primate-Specific Cortical Complexification. *Neuron*, 85(4):683–694, 2015. doi: 10.1016/j.neuron.2014.12.060.
- M. Devor, V. S. Caviness, and P. Derer. A normally laminated afferent projection to an abnormally laminated cortex: Some olfactory connections in the reeler mouse. *Journal of Comparative Neurology*, 164(4):471–482, 1975. doi: 10.1002/cne.901640406.
- E. Dégenétais, A.-M. Thierry, J. Glowinski, and Y. Gioanni. Electrophysiological Properties of Pyramidal Neurons in the Rat Prefrontal Cortex: An In Vivo Intracellular Recording Study. *Cerebral Cortex*, 12(1):1–16, 2002. doi: 10.1093/cercor/12.1.1.
- A. Dityatev, M. Schachner, and P. Sonderegger. The dual role of the extracellular matrix in synaptic plasticity and homeostasis. *Nature Reviews Neuroscience*, 11(11):735–746, 2010. doi: 10.1038/nrn2898.
- S. M. Dombrowski, C. C. Hilgetag, and H. Barbas. Quantitative Architecture Distinguishes Prefrontal Cortical Systems in the Rhesus Monkey. *Cerebral Cortex*, 11(10):975–988, 2001. doi: 10.1093/cercor/11.10.975.
- A.-L. S. Donahoo and L. J. Richards. Understanding the Mechanisms of Callosal Development Through the Use of Transgenic Mouse Models. *Seminars in Pediatric Neurology*, 16(3):127–142, 2009. doi: 10.1016/j.spen.2009.07.003.
- H. Dong, Q. Wang, K. Valkova, Y. Gonchar, and A. Burkhalter. Experience-dependent development of feedforward and feedback circuits between lower and higher areas of mouse visual cortex. *Vision Research*, 44(28):3389–3400, 2004. doi: 10.1016/j.visres.2004.09.007.
- R. J. Douglas and K. A. C. Martin. A functional microcircuit for cat visual cortex. *The Journal of Physiology*, 440(1):735–769, 1991.
- R. J. Douglas and K. A. C. Martin. Neuronal Circuits of the Neocortex. *Annual Review of Neuroscience*, 27(1):419–451, 2004. doi: 10.1146/annurev.neuro.27.070203.144152.

- R. J. Douglas and K. A. C. Martin. The Butterfly and the Loom. *Brain Research Reviews*, 55(2):314–328, 2007a. doi: 10.1016/j.brainresrev.2007.04.011.
- R. J. Douglas and K. A. C. Martin. Mapping the Matrix: The Ways of Neocortex. *Neuron*, 56(2):226–238, 2007b. doi: 10.1016/j.neuron.2007.10.017.
- R. J. Douglas and K. A. C. Martin. Recurrent neuronal circuits in the neocortex. *Current Biology*, 17(13):R496–R500, 2007c. doi: 10.1016/j.cub.2007.04.024.
- R. J. Douglas and K. A. C. Martin. Inhibition in cortical circuits. *Current Biology*, 19(10):R398–R402, 2009. doi: 10.1016/j.cub.2009.03.003.
- R. J. Douglas, K. A. C. Martin, and D. Whitteridge. A Canonical Microcircuit for Neocortex. *Neural Computation*, 1(4):480–488, 1989. doi: 10.1162/neco.1989.1.4.480.
- R. J. Douglas, C. Koch, M. Mahowald, K. A. C. Martin, and H. H. Suarez. Recurrent excitation in neocortical circuits. *Science*, 269(5226):981–985, 1995. doi: 10.1126/science.7638624.
- R. D. D’Souza, A. M. Meier, P. Bista, Q. Wang, and A. Burkhalter. Recruitment of inhibition and excitation across mouse visual cortex depends on the hierarchy of interconnecting areas. *eLife*, 5:e19332, 2016. doi: 10.7554/eLife.19332.
- J. Du, V. Vegh, and D. C. Reutens. The Laminar Cortex Model: A New Continuum Cortex Model Incorporating Laminar Architecture. *PLoS Comput Biol*, 8(10):e1002733, 2012. doi: 10.1371/journal.pcbi.1002733.
- S. S. Easter, L. S. Ross, and A. Frankfurter. Initial tract formation in the mouse brain. *Journal of Neuroscience*, 13(1):285–299, 1993.
- G. N. Elston. Pyramidal Cells of the Frontal Lobe: All the More Spinous to Think With. *The Journal of Neuroscience*, 20(18):RC95–RC95, 2000.
- G. N. Elston. Cortex, Cognition and the Cell: New Insights into the Pyramidal Neuron and Prefrontal Function. *Cerebral Cortex*, 13(11):1124–1138, 2003. doi: 10.1093/cercor/bhg093.
- G. N. Elston. Specialization of the Neocortical Pyramidal Cell during Primate Evolution. In J. H. Kaas, editor, *Evolution of Nervous Systems*, pages 191–242. Academic Press, Oxford, 2007. ISBN 978-0-12-370878-6.
- G. N. Elston and K. S. Rockland. The Pyramidal Cell of the Sensorimotor Cortex of the Macaque Monkey: Phenotypic Variation. *Cerebral Cortex*, 12(10):1071–1078, 2002. doi: 10.1093/cercor/12.10.1071.

- G. N. Elston and M. G. Rosa. The occipitoparietal pathway of the macaque monkey: comparison of pyramidal cell morphology in layer III of functionally related cortical visual areas. *Cerebral Cortex*, 7(5):432–452, 1997. doi: 10.1093/cercor/7.5.432.
- G. N. Elston and M. G. Rosa. Complex dendritic fields of pyramidal cells in the frontal eye field of the macaque monkey: comparison with parietal areas 7a and LIP. *Neuroreport*, 9(1):127–131, 1998a.
- G. N. Elston and M. G. Rosa. Morphological variation of layer III pyramidal neurones in the occipitotemporal pathway of the macaque monkey visual cortex. *Cerebral Cortex*, 8(3):278–294, 1998b. doi: 10.1093/cercor/8.3.278.
- G. N. Elston, R. Tweedale, and M. G. Rosa. Supragranular pyramidal neurones in the medial posterior parietal cortex of the macaque monkey: morphological heterogeneity in subdivisions of area 7. *NeuroReport*, 10(9):1925–1929, 1999a.
- G. N. Elston, R. Tweedale, and M. G. P. Rosa. Cortical integration in the visual system of the macaque monkey: large-scale morphological differences in the pyramidal neurons in the occipital, parietal and temporal lobes. *Proceedings of the Royal Society of London B: Biological Sciences*, 266(1426):1367–1374, 1999b. doi: 10.1098/rspb.1999.0789.
- G. N. Elston, R. Benavides-Piccione, and J. DeFelipe. The Pyramidal Cell in Cognition: A Comparative Study in Human and Monkey. *The Journal of Neuroscience*, 21(17):RC163–RC163, 2001.
- G. N. Elston, R. Benavides-Piccione, and J. DeFelipe. A Study of Pyramidal Cell Structure in the Cingulate Cortex of the Macaque Monkey with Comparative Notes on Inferotemporal and Primary Visual Cortex. *Cerebral Cortex*, 15(1):64–73, 2005. doi: 10.1093/cercor/bhh109.
- G. N. Elston, T. Oga, and I. Fujita. Spinogenesis and Pruning Scales across Functional Hierarchies. *Journal of Neuroscience*, 29(10):3271–3275, 2009. doi: 10.1523/JNEUROSCI.5216-08.2009.
- G. N. Elston, T. Oga, T. Okamoto, and I. Fujita. Spinogenesis and Pruning from Early Visual Onset to Adulthood: An Intracellular Injection Study of Layer III Pyramidal Cells in the Ventral Visual Cortical Pathway of the Macaque Monkey. *Cerebral Cortex*, 20(6):1398–1408, 2010a. doi: 10.1093/cercor/bhp203.
- G. N. Elston, T. Okamoto, T. Oga, D. Dornan, and I. Fujita. Spinogenesis and pruning in the primary auditory cortex of the macaque monkey (*Macaca fascicularis*): An

- intracellular injection study of layer III pyramidal cells. *Brain Research*, 1316: 35–42, 2010b. doi: 10.1016/j.brainres.2009.12.056.
- G. N. Elston, R. Benavides-Piccione, A. Elston, P. Manger, and J. Defelipe. Pyramidal cells in prefrontal cortex of primates: marked differences in neuronal structure among species. *Frontiers in Neuroanatomy*, 5:2, 2011a. doi: 10.3389/fnana.2011.00002.
- G. N. Elston, T. Oga, T. Okamoto, and I. Fujita. Spinogenesis and pruning in the anterior ventral inferotemporal cortex of the macaque monkey: an intracellular injection study of layer III pyramidal cells. *Frontiers in Neuroanatomy*, 5:42, 2011b. doi: 10.3389/fnana.2011.00042.
- M. Ercsey-Ravasz, N. T. Markov, C. Lamy, D. C. Van Essen, K. Knoblauch, Z. Toroczkai, and H. Kennedy. A Predictive Network Model of Cerebral Cortical Connectivity Based on a Distance Rule. *Neuron*, 80(1):184–197, 2013. doi: 10.1016/j.neuron.2013.07.036.
- C. Eroglu and B. A. Barres. Regulation of synaptic connectivity by glia. *Nature*, 468 (7321):223–231, 2010. doi: 10.1038/nature09612.
- A. C. Evans. Networks of anatomical covariance. *NeuroImage*, 80:489–504, 2013. doi: 10.1016/j.neuroimage.2013.05.054.
- P. Fang, L.-L. Zeng, H. Shen, L. Wang, B. Li, L. Liu, and D. Hu. Increased Cortical-Limbic Anatomical Network Connectivity in Major Depression Revealed by Diffusion Tensor Imaging. *PLoS ONE*, 7(9):e45972, 2012. doi: 10.1371/journal.pone.0045972.
- L. Feldman Barrett and W. K. Simmons. Interoceptive predictions in the brain. *Nature Reviews Neuroscience*, 16(7):419–429, 2015. doi: 10.1038/nrn3950.
- D. Feldmeyer, M. Brecht, F. Helmchen, C. C. H. Petersen, J. F. A. Poulet, J. F. Staiger, H. J. Luhmann, and C. Schwarz. Barrel cortex function. *Progress in Neurobiology*, 103:3–27, 2013. doi: 10.1016/j.pneurobio.2012.11.002.
- D. J. Felleman and D. C. Van Essen. Distributed hierarchical processing in the primate cerebral cortex. *Cerebral Cortex*, 1(1):1–47, 1991. doi: 10.1093/cercor/1.1.1-a.
- B. L. Finlay and R. B. Darlington. Linked regularities in the development and evolution of mammalian brains. *Science*, 268(5217):1578–1584, 1995. doi: 10.1126/science.7777856.

- B. L. Finlay and R. Uchiyama. Developmental mechanisms channeling cortical evolution. *Trends in Neurosciences*, 38(2):69–76, 2015. doi: 10.1016/j.tins.2014.11.004.
- E. Fino and R. Yuste. Dense Inhibitory Connectivity in Neocortex. *Neuron*, 69(6):1188–1203, 2011. doi: 10.1016/j.neuron.2011.02.025.
- R. Fluss, D. Faraggi, and B. Reiser. Estimation of the Youden Index and its Associated Cutoff Point. *Biometrical Journal*, 47(4):458–472, 2005. doi: 10.1002/bimj.200410135.
- K. Friston. The free-energy principle: a unified brain theory? *Nature Reviews Neuroscience*, 11(2):127–138, 2010. doi: 10.1038/nrn2787.
- K. J. Friston, A. M. Bastos, D. Pinotsis, and V. Litvak. LFP and oscillations—what do they tell us? *Current Opinion in Neurobiology*, 31:1–6, 2015. doi: 10.1016/j.conb.2014.05.004.
- P. L. A. Gabbott and P. Somogyi. Quantitative distribution of GABA-immunoreactive neurons in the visual cortex (area 17) of the cat. *Experimental Brain Research*, 61(2):323–331, 1986. doi: 10.1007/BF00239522.
- M. Á. García-Cabezas and H. Barbas. Area 4 has layer IV in adult primates. *European Journal of Neuroscience*, 39(11):1824–1834, 2014. doi: 10.1111/ejn.12585.
- M. Á. García-Cabezas, M. K. P. Joyce, Y. J. John, B. Zikopoulos, and H. Barbas. Mirror trends of plasticity and stability indicators in primate prefrontal cortex. *European Journal of Neuroscience*, 46:2392–2405, 2017. doi: 10.1111/ejn.13706.
- M. Á. García-Cabezas, B. Zikopoulos, and H. Barbas. The Structural Model: a theory linking connections, plasticity, pathology, development and evolution of the cerebral cortex. *Brain Structure and Function*, 2019. doi: 10.1007/s00429-019-01841-9.
- N. Gaspard and P. Vanderhaeghen. Laminar fate specification in the cerebral cortex. *F1000 Biology Reports*, 3(6), 2011. doi: 10.3410/B3-6.
- D. George and J. Hawkins. Towards a mathematical theory of cortical micro-circuits. *PLoS computational biology*, 5(10):e1000532, 2009. doi: 10.1371/journal.pcbi.1000532.
- M. Germuska, S. Saha, J. Fiala, and H. Barbas. Synaptic Distinction of Laminar-specific Prefrontal-temporal Pathways in Primates. *Cerebral Cortex*, 16(6):865–875, 2006. doi: 10.1093/cercor/bhj030.

- H. T. Ghashghaei, C. C. Hilgetag, and H. Barbas. Sequence of information processing for emotions based on the anatomic dialogue between prefrontal cortex and amygdala. *NeuroImage*, 34(3):905–923, 2007. doi: 10.1016/j.neuroimage.2006.09.046.
- C. D. Gilbert and T. N. Wiesel. Functional Organization of the Visual Cortex. *Progress in Brain Research*, 58:209–218, 1983. doi: 10.1016/S0079-6123(08)60022-9.
- J. P. Gilman, M. Medalla, and J. I. Luebke. Area-Specific Features of Pyramidal Neurons—a Comparative Study in Mouse and Rhesus Monkey. *Cerebral Cortex (New York, N.Y.: 1991)*, 27(3):2078–2094, 2017. doi: 10.1093/cercor/bhw062.
- J. Gómez-Gardeñes, G. Zamora-López, Y. Moreno, and A. Arenas. From Modular to Centralized Organization of Synchronization in Functional Areas of the Cat Cerebral Cortex. *PLoS ONE*, 5(8), 2010. doi: 10.1371/journal.pone.0012313.
- D. C. Godlove, A. Maier, G. F. Woodman, and J. D. Schall. Microcircuitry of Agranular Frontal Cortex: Testing the Generality of the Canonical Cortical Microcircuit. *The Journal of Neuroscience*, 34(15):5355–5369, 2014. doi: 10.1523/JNEUROSCI.5127-13.2014.
- N. Gogtay, T. F. Nugent, D. H. Herman, A. Ordonez, D. Greenstein, K. M. Hayashi, L. Clasen, A. W. Toga, J. N. Giedd, J. L. Rapoport, and P. M. Thompson. Dynamic mapping of normal human hippocampal development. *Hippocampus*, 16(8):664–672, 2006. doi: 10.1002/hipo.20193.
- J. Goñi, M. P. v. d. Heuvel, A. Avena-Koenigsberger, N. V. d. Mendizabal, R. F. Betzel, A. Griffa, P. Hagmann, B. Corominas-Murtra, J.-P. Thiran, and O. Sporns. Resting-brain functional connectivity predicted by analytic measures of network communication. *Proceedings of the National Academy of Sciences*, 111(2):833–838, 2014. doi: 10.1073/pnas.1315529111.
- P. S. Goldman-Rakic. Topography of cognition: parallel distributed networks in primate association cortex. *Annual review of neuroscience*, 11(1):137–156, 1988. doi: 10.1146/annurev.ne.11.030188.001033.
- G. Gong, Y. He, Z. J. Chen, and A. C. Evans. Convergence and divergence of thickness correlations with diffusion connections across the human cerebral cortex. *NeuroImage*, 59(2):1239–1248, 2012. doi: 10.1016/j.neuroimage.2011.08.017.
- A. Goulas and C. C. Hilgetag. Cross-species prediction of macroscale connectivity of mammalian cortices. In *Front. Neuroinform. Conference Abstract: Neuroinformatics*

- 2016, Reading, UK, 2016. Frontiers Media SA. doi: 10.3389/conf.fninf.2016.20.00023.
- A. Goulas, M. Bastiani, G. Bezgin, H. B. M. Uylings, A. Roebroek, and P. Stiers. Comparative Analysis of the Macroscale Structural Connectivity in the Macaque and Human Brain. *PLoS Comput Biol*, 10(3):e1003529, 2014a. doi: 10.1371/journal.pcbi.1003529.
- A. Goulas, A. Schaefer, and D. S. Margulies. The strength of weak connections in the macaque cortico-cortical network. *Brain Structure and Function*, 220(5):2939–2951, 2014b. doi: 10.1007/s00429-014-0836-3.
- A. Goulas, H. B. M. Uylings, and P. Stiers. Mapping the Hierarchical Layout of the Structural Network of the Macaque Prefrontal Cortex. *Cerebral Cortex*, 24(5):1178–1194, 2014c. doi: 10.1093/cercor/bhs399.
- A. Goulas, H. B. M. Uylings, and C. C. Hilgetag. Principles of ipsilateral and contralateral cortico-cortical connectivity in the mouse. *Brain Structure and Function*, 222(3):1281–1295, 2017. doi: 10.1007/s00429-016-1277-y.
- A. Goulas, K. Zilles, and C. C. Hilgetag. Cortical Gradients and Laminar Projections in Mammals. *Trends in Neurosciences*, 41(11):775–788, 2018. doi: 10.1016/j.tins.2018.06.003.
- A. Goulas, R. F. Betzel, and C. C. Hilgetag. Spatiotemporal ontogeny of brain wiring. *Science Advances*, 5(6):eaav9694, 2019a. doi: doi.org/10.1101/385369.
- A. Goulas, P. Majka, M. G. Rosa, and C. C. Hilgetag. A blueprint of the mammalian cortical connectome. *PLoS Biology*, 17(3):e2005346, 2019b. doi: 10.1371/journal.pbio.2005346.
- S. Grant and C. C. Hilgetag. Graded classes of cortical connections: quantitative analyses of laminar projections to motion areas of cat extrastriate cortex. *European Journal of Neuroscience*, 22(3):681–696, 2005. doi: 10.1111/j.1460-9568.2005.04232.x.
- A. Griffa, P. S. Baumann, J.-P. Thiran, and P. Hagmann. Structural connectomics in brain diseases. *NeuroImage*, 80:515–526, 2013. doi: 10.1016/j.neuroimage.2013.04.056.
- J. Guy and J. F. Staiger. The Functioning of a Cortex without Layers. *Frontiers in Neuroanatomy*, 11, 2017. doi: 10.3389/fnana.2017.00054.

- S. Habenschuss, Z. Jonke, and W. Maass. Stochastic Computations in Cortical Microcircuit Models. *PLoS Comput Biol*, 9(11):e1003311, 2013. doi: 10.1371/journal.pcbi.1003311.
- S. Haeusler and W. Maass. A Statistical Analysis of Information-Processing Properties of Lamina-Specific Cortical Microcircuit Models. *Cerebral Cortex*, 17(1):149–162, 2007. doi: 10.1093/cercor/bhj132.
- S. Haeusler, K. Schuch, and W. Maass. Motif distribution, dynamical properties, and computational performance of two data-based cortical microcircuit templates. *Journal of Physiology-Paris*, 103(1–2):73–87, 2009. doi: 10.1016/j.jphysparis.2009.05.006.
- P. Hagmann, L. Cammoun, X. Gigandet, R. Meuli, C. J. Honey, V. J. Wedeen, and O. Sporns. Mapping the Structural Core of Human Cerebral Cortex. *PLoS Biol*, 6(7):e159, 2008. doi: 10.1371/journal.pbio.0060159.
- L. Harriger, M. P. van den Heuvel, and O. Sporns. Rich Club Organization of Macaque Cerebral Cortex and Its Role in Network Communication. *PLoS ONE*, 7(9):e46497, 2012. doi: 10.1371/journal.pone.0046497.
- K. D. Harris and G. M. G. Shepherd. The neocortical circuit: themes and variations. *Nature Neuroscience*, 18(2):170–181, 2015. doi: 10.1038/nn.3917.
- L.-A. Harsan, C. Dávid, M. Reisert, S. Schnell, J. Hennig, D. v. Elverfeldt, and J. F. Staiger. Mapping remodeling of thalamocortical projections in the living reeler mouse brain by diffusion tractography. *Proceedings of the National Academy of Sciences*, 110(19):E1797–E1806, 2013. doi: 10.1073/pnas.1218330110.
- R. Hassler and K. Muhs-Clement. Architectonic Construction of the Sensomotor and Parietal Cortex in the Cat. *Journal für Hirnforschung*, 7:377–420, 1964.
- Y. He, Z. J. Chen, and A. C. Evans. Small-World Anatomical Networks in the Human Brain Revealed by Cortical Thickness from MRI. *Cerebral Cortex*, 17(10):2407–2419, 2007. doi: 10.1093/cercor/bhl149.
- J. Hegdé and D. J. Felleman. Reappraising the Functional Implications of the Primate Visual Anatomical Hierarchy. *The Neuroscientist*, 13(5):416–421, 2007. doi: 10.1177/1073858407305201.
- J. Hegdé and D. C. Van Essen. A Comparative Study of Shape Representation in Macaque Visual Areas V2 and V4. *Cerebral Cortex*, 17(5):1100–1116, 2007. doi: 10.1093/cercor/bhl020.

- L. Heimer and M. J. Robards. *Neuroanatomical Tract-tracing Methods*. Plenum Press, New York, USA, 1981. ISBN 978-0-306-40593-8.
- J. Heinzle, K. Hepp, and K. A. C. Martin. A Microcircuit Model of the Frontal Eye Fields. *The Journal of Neuroscience*, 27(35):9341–9353, 2007. doi: 10.1523/JNEUROSCI.0974-07.2007.
- S. Herculano-Houzel, C. Watson, and G. Paxinos. Distribution of neurons in functional areas of the mouse cerebral cortex reveals quantitatively different cortical zones. *Frontiers in Neuroanatomy*, 7:35, 2013. doi: 10.3389/fnana.2013.00035.
- S. P. Hicks and C. J. D’Amato. Cell migrations to the isocortex in the rat. *The Anatomical Record*, 160(3):619–633, 1968. doi: 10.1002/ar.1091600311.
- C. C. Hilgetag and H. Barbas. Role of Mechanical Factors in the Morphology of the Primate Cerebral Cortex. *PLoS Comput Biol*, 2(3):e22, 2006. doi: 10.1371/journal.pcbi.0020022.
- C. C. Hilgetag and S. Grant. Uniformity, specificity and variability of corticocortical connectivity. *Philosophical Transactions of the Royal Society B: Biological Sciences*, 355(1393):7–20, 2000. doi: 10.1098/rstb.2000.0546.
- C. C. Hilgetag and S. Grant. Cytoarchitectural differences are a key determinant of laminar projection origins in the visual cortex. *NeuroImage*, 51(3):1006–1017, 2010. doi: 10.1016/j.neuroimage.2010.03.006.
- C. C. Hilgetag, M. A. O’Neill, and M. P. Young. Indeterminate organization of the visual system. *Science*, 271(5250):776–777, 1996. doi: 10.1126/science.271.5250.776.
- C. C. Hilgetag, G. A. Burns, M. A. O’Neill, J. W. Scannell, and M. P. Young. Anatomical connectivity defines the organization of clusters of cortical areas in the macaque monkey and the cat. *Philosophical Transactions of the Royal Society B: Biological Sciences*, 355(1393):91–110, 2000a. doi: 10.1098/rstb.2000.0551.
- C. C. Hilgetag, M. A. O’Neill, and M. P. Young. Hierarchical organization of macaque and cat cortical sensory systems explored with a novel network processor. *Philosophical Transactions of the Royal Society of London. Series B: Biological Sciences*, 355(1393):71–89, 2000b. doi: 10.1098/rstb.2000.0550.
- C. C. Hilgetag, M. Medalla, S. F. Beul, and H. Barbas. The primate connectome in context: Principles of connections of the cortical visual system. *NeuroImage*, 134: 685–702, 2016. doi: 10.1016/j.neuroimage.2016.04.017.

- C. C. Hilgetag, S. F. Beul, S. J. van Albada, and A. Goulas. An Architectonic Type Principle Integrates Macroscopic Cortico-Cortical Connections with Intrinsic Cortical Circuits of the Primate Brain. *Network Neuroscience*, 3(4):905–923, 2019. doi: 10.1162/netn_a_00100.
- Y. Hirai, M. Morishima, F. Karube, and Y. Kawaguchi. Specialized Cortical Subnetworks Differentially Connect Frontal Cortex to Parahippocampal Areas. *The Journal of Neuroscience*, 32(5):1898–1913, 2012. doi: 10.1523/JNEUROSCI.2810-11.2012.
- P. R. Hof, L. G. Ungerleider, M. J. Webster, R. Gattass, M. M. Adams, C. A. Sailstad, and J. H. Morrison. Neurofilament protein is differentially distributed in subpopulations of corticocortical projection neurons in the macaque monkey visual pathways. *The Journal of Comparative Neurology*, 376(1):112–127, 1996. doi: 10.1002/(SICI)1096-9861(19961202)376:1<112::AID-CNE7>3.0.CO;2-6.
- P. R. Hof, L. G. Ungerleider, M. M. Adams, M. J. Webster, R. Gattass, D. M. Blumberg, and J. H. Morrison. Callosally projecting neurons in the macaque monkey V1/V2 border are enriched in nonphosphorylated neurofilament protein. *Visual Neuroscience*, 14(5):981–987, 1997. doi: 10.1017/S0952523800011688.
- Z. L. Holley, K. M. Bland, Z. O. Casey, C. J. Handwerk, and G. S. Vidal. Cross-Regional Gradient of Dendritic Morphology in Isochronically-Sourced Mouse Supragranular Pyramidal Neurons. *Frontiers in Neuroanatomy*, 12, 2018. doi: 10.3389/fnana.2018.00103.
- G. M. Innocenti and R. Caminiti. Axon diameter relates to synaptic bouton size: structural properties define computationally different types of cortical connections in primates. *Brain Structure and Function*, 222(3):1169–1177, 2017. doi: 10.1007/s00429-016-1266-1.
- G. M. Innocenti and D. J. Price. Exuberance in the development of cortical networks. *Nature Reviews Neuroscience*, 6(12):955–965, 2005. doi: 10.1038/nrn1790.
- G. M. Innocenti, A. Vercelli, and R. Caminiti. The Diameter of Cortical Axons Depends Both on the Area of Origin and Target. *Cerebral Cortex*, 24(8):2178–2188, 2014. doi: 10.1093/cercor/bht070.
- G. O. Ivy, R. M. Akers, and H. P. Killackey. Differential distribution of callosal projection neurons in the neonatal and adult rat. *Brain Research*, 173(3):532–537, 1979. doi: 10.1016/0006-8993(79)90247-6.

- K. F. Jensen and H. P. Killackey. Subcortical projections from ectopic neocortical neurons. *Proceedings of the National Academy of Sciences*, 81(3):964–968, 1984.
- B. Jouve, P. Rosenstiehl, and M. Imbert. A mathematical approach to the connectivity between the cortical visual areas of the macaque monkey. *Cerebral Cortex*, 8(1):28–39, 1998.
- R. Kageyama and T. Yamamori, editors. *Cortical Development - Neural Diversity and Neocortical Organization*. Springer, 2013. ISBN 978-4-431-54495-1.
- M. Kaiser. Mechanisms of Connectome Development. *Trends in Cognitive Sciences*, 21(9):703–717, 2017. doi: 10.1016/j.tics.2017.05.010.
- M. Kaiser and C. C. Hilgetag. Modelling the development of cortical systems networks. *Neurocomputing*, 58-60:297–302, 2004. doi: 10.1016/j.neucom.2004.01.059.
- M. Kaiser and C. C. Hilgetag. Nonoptimal Component Placement, but Short Processing Paths, due to Long-Distance Projections in Neural Systems. *PLoS Computational Biology*, 2(7):e95, 2006. doi: 10.1371/journal.pcbi.0020095.
- M. Kaiser and C. C. Hilgetag. Development of multi-cluster cortical networks by time windows for spatial growth. *Neurocomputing*, 70(10-12):1829–1832, 2007. doi: 10.1016/j.neucom.2006.10.060.
- M. Kaiser, C. C. Hilgetag, and A. van Ooyen. A Simple Rule for Axon Outgrowth and Synaptic Competition Generates Realistic Connection Lengths and Filling Fractions. *Cerebral Cortex*, 19(12):3001–3010, 2009. doi: 10.1093/cercor/bhp071.
- B. M. Kampa, J. J. Letzkus, and G. J. Stuart. Cortical feed-forward networks for binding different streams of sensory information. *Nature Neuroscience*, 9(12):1472–1473, 2006. doi: 10.1038/nn1798.
- Y. Kang. Differential paired pulse depression of non-NMDA and NMDA currents in pyramidal cells of the rat frontal cortex. *The Journal of Neuroscience*, 15(12):8268–8280, 1995.
- S. J. Karlen and L. Krubitzer. Effects of Bilateral Enucleation on the Size of Visual and Nonvisual Areas of the Brain. *Cerebral Cortex (New York, NY)*, 19(6):1360, 2009. doi: 10.1093/cercor/bhn176.
- N. Kato, J. M. R. Ferrer, and D. J. Price. Regressive changes among corticocortical neurons projecting from the lateral suprasylvian cortex to area 18 of the kitten’s visual cortex. *Neuroscience*, 43(2-3):291–306, 1991. doi: 10.1016/0306-4522(91)90294-X.

- Y. Kawaguchi. Groupings of nonpyramidal and pyramidal cells with specific physiological and morphological characteristics in rat frontal cortex. *Journal of Neurophysiology*, 69(2):416–431, 1993.
- Y. Kawaguchi. Physiological subgroups of nonpyramidal cells with specific morphological characteristics in layer II/III of rat frontal cortex. *The Journal of Neuroscience*, 15(4):2638–2655, 1995.
- Y. Kawaguchi and S. Kondo. Parvalbumin, somatostatin and cholecystokinin as chemical markers for specific GABAergic interneuron types in the rat frontal cortex. *Journal of neurocytology*, 31(3-5):277–287, 2002.
- Y. Kawaguchi and Y. Kubota. GABAergic cell subtypes and their synaptic connections in rat frontal cortex. *Cerebral Cortex*, 7(6):476–486, 1997. doi: 10.1093/cercor/7.6.476.
- H. Kennedy and C. Dehay. Chapter 16 - Self-organization and interareal networks in the primate cortex. In M. A. H. a. D. Falk, editor, *Progress in Brain Research*, volume 195 of *Evolution of the Primate Brain*, pages 341–360. Elsevier, 2012.
- H. Kennedy, J. Bullier, and C. Dehay. Transient projection from the superior temporal sulcus to area 17 in the newborn macaque monkey. *Proceedings of the National Academy of Sciences*, 86(20):8093–8097, 1989.
- R. Khalil and J. B. Levitt. Developmental remodeling of corticocortical feedback circuits in ferret visual cortex. *The Journal of comparative neurology*, 522(14):3208–3228, 2014. doi: 10.1002/cne.23591.
- W. R. Klecka. Discriminant Analysis. In *Discriminant Analysis*, number 07-019 in Quantitative Applications in the Social Sciences, page 71. SAGE Publications Ltd., London, UK, 1980. ISBN 0-8039-1491-1.
- A. Kölliker. *Handbuch der Gewebelehre des Menschen*. Engelmann, Leipzig, 1896.
- V. A. Klyachko and C. F. Stevens. Connectivity optimization and the positioning of cortical areas. *Proceedings of the National Academy of Sciences*, 100(13):7937–7941, 2003.
- A. L. Kolodkin and M. Tessier-Lavigne. Mechanisms and Molecules of Neuronal Wiring: A Primer. *Cold Spring Harbor Perspectives in Biology*, 3(6):a001727, 2011. doi: 10.1101/cshperspect.a001727.
- J. Kozloski, F. Hamzei-Sichani, and R. Yuste. Stereotyped Position of Local Synaptic Targets in Neocortex. *Science*, 293(5531):868–872, 2001. doi: 10.1126/science.293.5531.868.

- T. Kroon, E. v. Hugte, L. v. Linge, H. D. Mansvelder, and R. M. Meredith. Early postnatal development of pyramidal neurons across layers of the mouse medial prefrontal cortex. *Scientific Reports*, 9(1):5037, 2019. doi: 10.1038/s41598-019-41661-9.
- D. Kätzel, B. V. Zemelman, C. Buetfering, M. Wölfel, and G. Miesenböck. The columnar and laminar organization of inhibitory connections to neocortical excitatory cells. *Nature Neuroscience*, 14(1):100–107, 2011. doi: 10.1038/nn.2687.
- R. Z. Kuang and K. Kalil. Development of specificity in corticospinal connections by axon collaterals branching selectively into appropriate spinal targets. *Journal of Comparative Neurology*, 344(2):270–282, 1994. doi: 10.1002/cne.903440208.
- R. Z. Kuang, M. Merline, and K. Kalil. Topographic specificity of corticospinal connections formed in explant coculture. *Development*, 120(7):1937–1947, 1994.
- Y. Kubota, N. Shigematsu, F. Karube, A. Sekigawa, S. Kato, N. Yamaguchi, Y. Hirai, M. Morishima, and Y. Kawaguchi. Selective Coexpression of Multiple Chemical Markers Defines Discrete Populations of Neocortical GABAergic Neurons. *Cerebral Cortex*, 21(8):1803–1817, 2011. doi: 10.1093/cercor/bhq252.
- C. la Fougère, S. Grant, A. Kostikov, R. Schirmacher, P. Gravel, H. M. Schipper, A. Reader, A. Evans, and A. Thiel. Where in-vivo imaging meets cytoarchitectonics: The relationship between cortical thickness and neuronal density measured with high-resolution [18f]flumazenil-PET. *NeuroImage*, 56(3):951–960, 2011. doi: 10.1016/j.neuroimage.2010.11.015.
- L. Lagae, B. Gulyas, S. Raiguel, and G. A. Orban. Laminar analysis of motion information processing in macaque V5. *Brain Research*, 496(1-2):361–367, 1989.
- B. B. Lake, R. Ai, G. E. Kaeser, N. S. Salathia, Y. C. Yung, R. Liu, A. Wildberg, D. Gao, H.-L. Fung, S. Chen, R. Vijayaraghavan, J. Wong, A. Chen, X. Sheng, F. Kaper, R. Shen, M. Ronaghi, J.-B. Fan, W. Wang, J. Chun, and K. Zhang. Neuronal subtypes and diversity revealed by single-nucleus RNA sequencing of the human brain. *Science*, 352(6293):1586–1590, 2016. doi: 10.1126/science.aaf1204.
- J. L. Lanciego and F. G. Wouterlood. A half century of experimental neuroanatomical tracing. *Journal of chemical neuroanatomy*, 42(3):157–183, 2011. doi: 10.1016/j.jchemneu.2011.07.001.
- M. Larkum. A cellular mechanism for cortical associations: an organizing principle for the cerebral cortex. *Trends in Neurosciences*, 36(3):141–151, 2013. doi: 10.1016/j.tins.2012.11.006.

- M. E. Larkum, L. S. Petro, R. N. S. Sachdev, and L. Muckli. A Perspective on Cortical Layering and Layer-Spanning Neuronal Elements. *Frontiers in Neuroanatomy*, 12, 2018. doi: 10.3389/fnana.2018.00056.
- S. B. Laughlin and T. J. Sejnowski. Communication in Neuronal Networks. *Science*, 301(5641):1870–1874, 2003. doi: 10.1126/science.1089662.
- S. B. Laughlin, R. R. de Ruyter van Steveninck, and J. C. Anderson. The metabolic cost of neural information. *Nature Neuroscience*, 1(1):36–41, 1998. doi: 10.1038/236.
- S. N. Lawson and P. J. Waddell. Soma neurofilament immunoreactivity is related to cell size and fibre conduction velocity in rat primary sensory neurons. *The Journal of Physiology*, 435(1):41–63, 1991. doi: 10.1113/jphysiol.1991.sp018497.
- J. Lübke and D. Feldmeyer. Excitatory signal flow and connectivity in a cortical column: focus on barrel cortex. *Brain Structure and Function*, 212(1):3–17, 2007. doi: 10.1007/s00429-007-0144-2.
- S. Lefort, C. Tomm, J. C. Floyd Sarria, and C. C. H. Petersen. The Excitatory Neuronal Network of the C2 Barrel Column in Mouse Primary Somatosensory Cortex. *Neuron*, 61(2):301–316, 2009. doi: 10.1016/j.neuron.2008.12.020.
- J. P. Lerch, K. Worsley, W. P. Shaw, D. K. Greenstein, R. K. Lenroot, J. Giedd, and A. C. Evans. Mapping anatomical correlations across cerebral cortex (MACACC) using cortical thickness from MRI. *NeuroImage*, 31(3):993–1003, 2006. doi: 10.1016/j.neuroimage.2006.01.042.
- Y. Li, Y. Liu, J. Li, W. Qin, K. Li, C. Yu, and T. Jiang. Brain Anatomical Network and Intelligence. *PLoS Comput Biol*, 5(5):e1000395, 2009. doi: 10.1371/journal.pcbi.1000395.
- S. Lim and M. Kaiser. Developmental time windows for axon growth influence neuronal network topology. *Biological Cybernetics*, 109(2):275–286, 2015. doi: 10.1007/s00422-014-0641-3.
- R. Lorente de Nó. The Cerebral Cortex: Architecture, Intracortical Connections, Motor Projections. In J. Fulton, editor, *Physiology of the nervous system*, pages 288–330. Oxford University Press, Oxford, 3rd edition, 1949.
- L. Magrou, P. Barone, N. T. Markov, H. P. Killackey, P. Giroud, M. Berland, K. Knoblauch, C. Dehay, and H. Kennedy. How Areal Specification Shapes the Local and Interareal Circuits in a Macaque Model of Congenital Blindness. *Cerebral Cortex*, 28(8):3017–3034, 2018. doi: 10.1093/cercor/bhy125.

- G. Marcus, A. Marblestone, and T. Dean. The atoms of neural computation. *Science*, 346(6209):551–552, 2014. doi: 10.1126/science.1261661.
- M. Marin-Padilla and T. M. Marin-Padilla. Origin, prenatal development and structural organization of layer I of the human cerebral (motor) cortex. *Anatomy and Embryology*, 164(2):161–206, 1982. doi: 10.1007/BF00318504.
- N. T. Markov, P. Misery, A. Falchier, C. Lamy, J. Vezoli, R. Quilodran, M. A. Gariel, P. Giroud, M. M. Ercsey-Ravasz, L. J. Pilaz, C. Huissoud, P. Barone, C. Dehay, Z. Toroczkai, D. C. Van Essen, H. Kennedy, and K. Knoblauch. Weight Consistency Specifies Regularities of Macaque Cortical Networks. *Cerebral Cortex*, 21(6):1254–1272, 2011. doi: 10.1093/cercor/bhq201.
- N. T. Markov, M. Ercsey-Ravasz, C. Lamy, A. R. R. Gomes, L. Magrou, P. Misery, P. Giroud, P. Barone, C. Dehay, Z. Toroczkai, K. Knoblauch, D. C. V. Essen, and H. Kennedy. The role of long-range connections on the specificity of the macaque interareal cortical network. *Proceedings of the National Academy of Sciences*, 110(13):5187–5192, 2013a. doi: 10.1073/pnas.1218972110.
- N. T. Markov, M. Ercsey-Ravasz, D. C. Van Essen, K. Knoblauch, Z. Toroczkai, and H. Kennedy. Cortical High-Density Counterstream Architectures. *Science*, 342(6158):1238406, 2013b. doi: 10.1126/science.1238406.
- N. T. Markov, M. M. Ercsey-Ravasz, A. R. Ribeiro Gomes, C. Lamy, L. Magrou, J. Vezoli, P. Misery, A. Falchier, R. Quilodran, M. A. Gariel, J. Sallet, R. Gamanut, C. Huissoud, S. Clavagnier, P. Giroud, D. Sappey-Marinier, P. Barone, C. Dehay, Z. Toroczkai, K. Knoblauch, D. C. Van Essen, and H. Kennedy. A Weighted and Directed Interareal Connectivity Matrix for Macaque Cerebral Cortex. *Cerebral Cortex*, 24(1):17–36, 2014a. doi: 10.1093/cercor/bhs270.
- N. T. Markov, J. Vezoli, P. Chameau, A. Falchier, R. Quilodran, C. Huissoud, C. Lamy, P. Misery, P. Giroud, S. Ullman, P. Barone, C. Dehay, K. Knoblauch, and H. Kennedy. The anatomy of hierarchy: Feedforward and feedback pathways in macaque visual cortex: Cortical counter-streams. *Journal of Comparative Neurology*, 522(1):225–259, 2014b. doi: 10.1002/cne.23458.
- H. Markram, M. Toledo-Rodriguez, Y. Wang, A. Gupta, G. Silberberg, and C. Wu. Interneurons of the neocortical inhibitory system. *Nature Reviews Neuroscience*, 5(10):793–807, 2004. doi: 10.1038/nrn1519.
- S. K. McConnell. Fates of visual cortical neurons in the ferret after isochronic and heterochronic transplantation. *The Journal of Neuroscience*, 8(3):945–974, 1988.

- D. McFadden. Chapter 13: Quantitative Methods for Analyzing Travel Behaviour of Individuals: Some Recent Developments. In D. A. Hensher and P. R. Stopher, editors, *Behavioural Travel Modelling*, pages 279–318. Croom Helm, London, UK, 1979. ISBN 978-0-85664-819-9.
- G. McSherry and I. Smart. Cell production gradients in the developing ferret isocortex. *Journal of Anatomy*, 144:1–14, 1986.
- G. M. McSherry. Mapping of cortical histogenesis in the ferret. *Development*, 81(1): 239–252, 1984.
- M. Medalla and H. Barbas. Diversity of laminar connections linking periarculate and lateral intraparietal areas depends on cortical structure. *European Journal of Neuroscience*, 23(1):161–179, 2006. doi: 10.1111/j.1460-9568.2005.04522.x.
- M. Medalla and H. Barbas. Anterior Cingulate Synapses in Prefrontal Areas 10 and 46 Suggest Differential Influence in Cognitive Control. *Journal of Neuroscience*, 30(48):16068–16081, 2010. doi: 10.1523/JNEUROSCI.1773-10.2010.
- M. Medalla, P. Lera, M. Feinberg, and H. Barbas. Specificity in Inhibitory Systems Associated with Prefrontal Pathways to Temporal Cortex in Primates. *Cerebral Cortex*, 17(suppl 1):i136–i150, 2007. doi: 10.1093/cercor/bhm068.
- C. Meissirel, C. Dehay, M. Berland, and H. Kennedy. Segregation of callosal and association pathways during development in the visual cortex of the primate. *Journal of Neuroscience*, 11(11):3297–3316, 1991.
- J. F. Mejias, J. D. Murray, H. Kennedy, and X.-J. Wang. Feedforward and feedback frequency-dependent interactions in a large-scale laminar network of the primate cortex. *Science Advances*, 2(11):e1601335, 2016. doi: 10.1126/sciadv.1601335.
- D. S. Melchitzky, G. González-Burgos, G. Barrionuevo, and D. A. Lewis. Synaptic targets of the intrinsic axon collaterals of supragranular pyramidal neurons in monkey prefrontal cortex. *The Journal of Comparative Neurology*, 430(2):209–221, 2001. doi: 10.1002/1096-9861(20010205)430:2<209::AID-CNE1026>3.0.CO;2-#.
- P. A. Merolla, J. V. Arthur, R. Alvarez-Icaza, A. S. Cassidy, J. Sawada, F. Akopyan, B. L. Jackson, N. Imam, C. Guo, Y. Nakamura, B. Brezzo, I. Vo, S. K. Esser, R. Appuswamy, B. Taba, A. Amir, M. D. Flickner, W. P. Risk, R. Manohar, and D. S. Modha. A million spiking-neuron integrated circuit with a scalable communication network and interface. *Science*, 345(6197):668–673, 2014. doi: 10.1126/science.1254642.

- H. S. Meyer, R. Egger, J. M. Guest, R. Foerster, S. Reissl, and M. Oberlaender. Cellular organization of cortical barrel columns is whisker-specific. *Proceedings of the National Academy of Sciences*, 110(47):19113–19118, 2013. doi: 10.1073/pnas.1312691110.
- G. Michalareas, J. Vezoli, S. van Pelt, J.-M. Schoffelen, H. Kennedy, and P. Fries. Alpha-Beta and Gamma Rhythms Subserve Feedback and Feedforward Influences among Human Visual Cortical Areas. *Neuron*, 89(2):384–397, 2016. doi: 10.1016/j.neuron.2015.12.018.
- L. E. Mickelsen, M. Bolisetty, B. R. Chimileski, A. Fujita, E. J. Beltrami, J. T. Costanzo, J. R. Naparstek, P. Robson, and A. C. Jackson. Single-cell transcriptomic analysis of the lateral hypothalamic area reveals molecularly distinct populations of inhibitory and excitatory neurons. *Nature Neuroscience*, 22(4):642–656, 2019. doi: 10.1038/s41593-019-0349-8.
- E. K. Miller, M. Lundqvist, and A. M. Bastos. Working Memory 2.0. *Neuron*, 100(2):463–475, 2018. doi: 10.1016/j.neuron.2018.09.023.
- S. Miyama, T. Takahashi, R. S. Nowakowski, and V. S. Caviness. A gradient in the duration of the G1 phase in the murine neocortical proliferative epithelium. *Cerebral Cortex*, 7(7):678–689, 1997. doi: 10.1093/cercor/7.7.678.
- M. Müller-Linow, C. C. Hilgetag, and M.-T. Hütt. Organization of Excitable Dynamics in Hierarchical Biological Networks. *PLoS Computational Biology*, 4(9), 2008. doi: 10.1371/journal.pcbi.1000190.
- D. S. Modha and R. Singh. Network architecture of the long-distance pathways in the macaque brain. *Proceedings of the National Academy of Sciences*, 107(30):13485–13490, 2010. doi: 10.1073/pnas.1008054107.
- B. J. Molyneaux, P. Arlotta, J. R. L. Menezes, and J. D. Macklis. Neuronal subtype specification in the cerebral cortex. *Nature Reviews Neuroscience*, 8(6):427–437, 2007. doi: 10.1038/nrn2151.
- B. J. Molyneaux, P. Arlotta, R. M. Fame, J. L. MacDonald, K. L. MacQuarrie, and J. D. Macklis. Novel Subtype-Specific Genes Identify Distinct Subpopulations of Callosal Projection Neurons. *Journal of Neuroscience*, 29(39):12343–12354, 2009. doi: 10.1523/JNEUROSCI.6108-08.2009.
- D. Morales and A. Kania. Cooperation and crosstalk in axon guidance cue integration: Additivity, synergy, and fine-tuning in combinatorial signaling. *Developmental Neurobiology*, 77(7):891–904, 2017. doi: 10.1002/dneu.22463.

- V. B. Mountcastle. Modality and Topographic Properties of Single Neurons of Cat's Somatic Sensory Cortex. *Journal of Neurophysiology*, 20(4):408–434, 1957.
- V. B. Mountcastle. The Evolution of Ideas Concerning the Function of the Neocortex. *Cerebral Cortex*, 5(4):289–295, 1995. doi: 10.1093/cercor/5.4.289.
- K. L. Narr, R. M. Bilder, A. W. Toga, R. P. Woods, D. E. Rex, P. R. Szeszko, D. Robinson, S. Sevy, H. Gunduz-Bruce, Y.-P. Wang, H. DeLuca, and P. M. Thompson. Mapping Cortical Thickness and Gray Matter Concentration in First Episode Schizophrenia. *Cerebral Cortex*, 15(6):708–719, 2005. doi: 10.1093/cercor/bhh172.
- R. Nieuwenhuys and C. A. J. Broere. A map of the human neocortex showing the estimated overall myelin content of the individual architectonic areas based on the studies of Adolf Hopf. *Brain Structure and Function*, 222(1):465–480, 2017. doi: 10.1007/s00429-016-1228-7.
- R. Nieuwenhuys, C. A. J. Broere, and L. Cerliani. A new myeloarchitectonic map of the human neocortex based on data from the Vogt–Vogt school. *Brain Structure and Function*, 220(5):2551–2573, 2015. doi: 10.1007/s00429-014-0806-9.
- L. G. Nowak and J. Bullier. The timing of information transfer in the visual system. In K. S. Rockland, J. H. Kaas, and A. Peters, editors, *Cerebral Cortex: Volume 12: Extrastriate Cortex in Primates*, pages 205–233. Plenum Press, New York, USA, 1997. ISBN 978-0-306-45530-8.
- L. G. Nowak, M. H. Munk, P. Girard, and J. Bullier. Visual latencies in areas V1 and V2 of the macaque monkey. *Visual Neuroscience*, 12(2):371–384, 1995.
- T. J. Nowakowski, A. Bhaduri, A. A. Pollen, B. Alvarado, M. A. Mostajo-Radji, E. D. Lullo, M. Haeussler, C. Sandoval-Espinosa, S. J. Liu, D. Velmeshev, J. R. Ounadjela, J. Shuga, X. Wang, D. A. Lim, J. A. West, A. A. Leyrat, W. J. Kent, and A. R. Kriegstein. Spatiotemporal gene expression trajectories reveal developmental hierarchies of the human cortex. *Science*, 358(6368):1318–1323, 2017. doi: 10.1126/science.aap8809.
- J. O'Kusky and M. Colonnier. A laminar analysis of the number of neurons, glia, and synapses in the visual cortex (area 17) of adult macaque monkeys. *The Journal of Comparative Neurology*, 210(3):278–290, 1982. doi: 10.1002/cne.902100307.
- D. D. O'Leary and B. B. Stanfield. A transient pyramidal tract projection from the visual cortex in the hamster and its removal by selective collateral elimination. *Brain Research*, 392(1-2):87–99, 1986.

- D. D. M. O’Leary and S. E. Koester. Development of projection neuron types, axon pathways, and patterned connections of the mammalian cortex. *Neuron*, 10(6): 991–1006, 1993. doi: 10.1016/0896-6273(93)90049-W.
- M. J. Oswald, M. L. Tantirigama, I. Sonntag, S. M. Hughes, and R. M. Empson. Diversity of layer 5 projection neurons in the mouse motor cortex. *Frontiers in Cellular Neuroscience*, 7:174, 2013. doi: 10.3389/fncel.2013.00174.
- T. Otsuka and Y. Kawaguchi. Firing-Pattern-Dependent Specificity of Cortical Excitatory Feed-Forward Subnetworks. *The Journal of Neuroscience*, 28(44):11186–11195, 2008. doi: 10.1523/JNEUROSCI.1921-08.2008.
- T. Otsuka and Y. Kawaguchi. Cortical Inhibitory Cell Types Differentially Form Intralaminar and Interlaminar Subnetworks with Excitatory Neurons. *The Journal of Neuroscience*, 29(34):10533–10540, 2009. doi: 10.1523/JNEUROSCI.2219-09.2009.
- T. Otsuka and Y. Kawaguchi. Cell Diversity and Connection Specificity between Callosal Projection Neurons in the Frontal Cortex. *The Journal of Neuroscience*, 31(10):3862–3870, 2011. doi: 10.1523/JNEUROSCI.5795-10.2011.
- H. V. Oviedo, I. Bureau, K. Svoboda, and A. M. Zador. The functional asymmetry of auditory cortex is reflected in the organization of local cortical circuits. *Nature Neuroscience*, 13(11):1413–1420, 2010. doi: 10.1038/nn.2659.
- N. Palomero-Gallagher and K. Zilles. Cortical layers: Cyto-, myelo-, receptor- and synaptic architecture in human cortical areas. *NeuroImage*, 2017. doi: 10.1016/j.neuroimage.2017.08.035.
- D. Pandya, M. Petrides, and P. B. Cipolloni. *Cerebral Cortex: Architecture, Connections, and the Dual Origin Concept*. Oxford University Press, New York, 2015. ISBN 978-0-19-933050-8.
- D. N. Pandya and F. Sanides. Architectonic parcellation of the temporal operculum in rhesus monkey and its projection pattern. *Zeitschrift für Anatomie und Entwicklungsgeschichte*, 139(2):127–161, 1973.
- D. N. Pandya and E. H. Yeterian. Architecture and Connections of Cortical Association Areas. In A. Peters and E. G. Jones, editors, *Association and auditory cortices*, volume 4 of *Cerebral cortex*, pages 3–61. Plenum Press, New York, 1985. ISBN 0-306-42040-6.

- D. N. Pandya, B. Seltzer, and H. Barbas. Input-output organization of the primate cerebral cortex. In H. Steklis and J. Erwin, editors, *Comparative Primate Biology, Vol.4: Neurosciences*, pages 39–80. Alan R. Liss, New York, 1988.
- H.-J. Park and K. J. Friston. Structural and Functional Brain Networks: From Connections to Cognition. *Science*, 342(6158):1238411, 2013. doi: 10.1126/science.1238411.
- C. C. H. Petersen. The Functional Organization of the Barrel Cortex. *Neuron*, 56(2):339–355, 2007. doi: 10.1016/j.neuron.2007.09.017.
- F. Petroni, S. Panzeri, C. C. Hilgetag, R. Kötter, and M. P. Young. Simultaneity of responses in a hierarchical visual network. *Neuroreport*, 12(12):2753–2759, 2001.
- F. Polleux. Genetic Mechanisms Specifying Cortical Connectivity: Let’s MakeSome Projections Together. *Neuron*, 46(3):395–400, 2005. doi: 10.1016/j.neuron.2005.04.017.
- F. Polleux, C. Dehay, A. Goffinet, and H. Kennedy. Pre- and Post-mitotic Events Contribute to the Progressive Acquisition of Area-specific Connectional Fate in the Neocortex. *Cerebral Cortex*, 11(11):1027–1039, 2001. doi: 10.1093/cercor/11.11.1027.
- T. Popovitchenko and M.-R. Rasin. Transcriptional and Post-Transcriptional Mechanisms of the Development of Neocortical Lamination. *Frontiers in Neuroanatomy*, 11, 2017. doi: 10.3389/fnana.2017.00102.
- T. C. Potjans and M. Diesmann. The Cell-Type Specific Cortical Microcircuit: Relating Structure and Activity in a Full-Scale Spiking Network Model. *Cerebral Cortex*, 24(3):785–806, 2014. doi: 10.1093/cercor/bhs358.
- J. D. Power, B. L. Schlaggar, C. N. Lessov-Schlaggar, and S. E. Petersen. Evidence for Hubs in Human Functional Brain Networks. *Neuron*, 79(4):798–813, 2013. doi: 10.1016/j.neuron.2013.07.035.
- D. J. Price and C. Blakemore. Regressive events in the postnatal development of association projections in the visual cortex. *Nature*, 316(6030):721–724, 1985. doi: 10.1038/316721a0.
- D. J. Price, J. M. Ferrer, C. Blakemore, and N. Kato. Postnatal development and plasticity of corticocortical projections from area 17 to area 18 in the cat’s visual cortex. *Journal of Neuroscience*, 14(5):2747–2762, 1994.

- D. J. Price, H. Kennedy, C. Dehay, L. Zhou, M. Mercier, Y. Jossin, A. M. Goffinet, F. Tis-sir, D. Blakey, and Z. Molnár. The development of cortical connections. *European Journal of Neuroscience*, 23(4):910–920, 2006. doi: 10.1111/j.1460-9568.2006.04620.x.
- M. E. Raichle. The Restless Brain. *Brain Connectivity*, 1(1):3–12, 2011. doi: 10.1089/brain.2011.0019.
- S. Raiguel, M. M. Van Hulle, D.-K. Xiao, V. L. Marcar, and G. A. Orban. Shape and Spatial Distribution of Receptive Fields and Antagonistic Motion Surrounds in the Middle Temporal Area (V5) of the Macaque. *European Journal of Neuroscience*, 7(10):2064–2082, 1995. doi: 10.1111/j.1460-9568.1995.tb00629.x.
- P. Rakic. Neurons in Rhesus Monkey Visual Cortex: Systematic Relation between Time of Origin and Eventual Disposition. *Science*, 183(4123):425–427, 1974. doi: 10.1126/science.183.4123.425.
- P. Rakic. Neurogenesis in adult primate neocortex: an evaluation of the evidence. *Nature Reviews Neuroscience*, 3(1):65–70, 2002.
- P. Rakic. Confusing cortical columns. *Proceedings of the National Academy of Sciences*, 105(34):12099–12100, 2008. doi: 10.1073/pnas.0807271105.
- P. Rakic, J. P. Bourgeois, M. F. Eckenhoff, N. Zecevic, and P. S. Goldman-Rakic. Concurrent overproduction of synapses in diverse regions of the primate cerebral cortex. *Science*, 232(4747):232–235, 1986. doi: 10.1126/science.3952506.
- A. T. Reid, A. Krumnack, E. Wanke, and R. Kötter. Optimization of cortical hierarchies with continuous scales and ranges. *NeuroImage*, 47(2):611–617, 2009. doi: 10.1016/j.neuroimage.2009.04.061.
- N. L. Rempel-Clower and H. Barbas. The laminar pattern of connections between prefrontal and anterior temporal cortices in the Rhesus monkey is related to cortical structure and function. *Cerebral Cortex*, 10(9):851–865, 2000. doi: 10.1093/cercor/10.9.851.
- V. Reyes-Puerta, J.-J. Sun, S. Kim, W. Kilb, and H. J. Luhmann. Laminar and Columnar Structure of Sensory-Evoked Multineuronal Spike Sequences in Adult Rat Barrel Cortex In Vivo. *Cerebral Cortex*, page bhu007, 2014. doi: 10.1093/cercor/bhu007.
- C. Ribault, K. Sekimoto, and A. Triller. From the stochasticity of molecular processes to the variability of synaptic transmission. *Nature Reviews Neuroscience*, 12(7): 375–387, 2011. doi: 10.1038/nrn3025.

- M. J. Roberts, E. Lowet, N. M. Brunet, M. Ter Wal, P. Tiesinga, P. Fries, and P. De Weerd. Robust Gamma Coherence between Macaque V1 and V2 by Dynamic Frequency Matching. *Neuron*, 78(3):523–536, 2013. doi: 10.1016/j.neuron.2013.03.003.
- K. S. Rockland. Five points on columns. *Frontiers in Neuroanatomy*, 4:22, 2010. doi: 10.3389/fnana.2010.00022.
- K. S. Rockland and D. N. Pandya. Laminar origins and terminations of cortical connections of the occipital lobe in the rhesus monkey. *Brain Research*, 179(1):3–20, 1979. doi: 10.1016/0006-8993(79)90485-2.
- M. Rubinov. Constraints and spandrels of interareal connectomes. *Nature Communications*, 7:13812, 2016. doi: 10.1038/ncomms13812.
- M. Rubinov, R. J. F. Ypma, C. Watson, and E. T. Bullmore. Wiring cost and topological participation of the mouse brain connectome. *Proceedings of the National Academy of Sciences*, 112(32):10032–10037, 2015. doi: 10.1073/pnas.1420315112.
- P. A. Salin and J. Bullier. Corticocortical connections in the visual system: structure and function. *Physiological Reviews*, 75(1):107–154, 1995.
- R. Salvador, J. Suckling, M. R. Coleman, J. D. Pickard, D. Menon, and E. Bullmore. Neurophysiological Architecture of Functional Magnetic Resonance Images of Human Brain. *Cerebral Cortex*, 15(9):1332–1342, 2005. doi: 10.1093/cercor/bhi016.
- J. R. Sanes and M. Yamagata. Formation of lamina-specific synaptic connections. *Current Opinion in Neurobiology*, 9(1):79–87, 1999. doi: 10.1016/S0959-4388(99)80010-5.
- F. Sanides. *Die Architektonik des Menschlichen Stirnhirns*, volume 98 of *Monographien aus dem Gesamtgebiete der Neurologie und Psychiatrie*. Springer Berlin Heidelberg, Berlin, Heidelberg, 1962. ISBN 978-3-540-02886-4 978-3-642-86210-6.
- F. Sanides. Functional architecture of motor and sensory cortices in primates in the light of a new concept of neocortex evolution. In C. R. Noback and W. Montagna, editors, *The Primate Brain*, pages 137–208. Appleton-Century-Crofts, New York, USA, 1970.
- F. Sanides. Representation in the cerebral cortex and its areal lamination patterns. In G. Bourne, editor, *The Structure and Function of Nervous Tissue*, volume 5, pages 329–453. Academic Press, New York, USA, 1972.

- F. Sanides and J. Hoffmann. Cyto- and myeloarchitecture of the visual cortex of the cat and of the surrounding integration cortices. *Journal für Hirnforschung*, 11(1): 79–104, 1969.
- H. Sato, Y. Shimanuki, M. Saito, H. Toyoda, T. Nokubi, Y. Maeda, T. Yamamoto, and Y. Kang. Differential Columnar Processing in Local Circuits of Barrel and Insular Cortices. *The Journal of Neuroscience*, 28(12):3076–3089, 2008. doi: 10.1523/JNEUROSCI.0172-08.2008.
- J. W. Scannell and M. P. Young. The connectional organization of neural systems in the cat cerebral cortex. *Current Biology*, 3(4):191–200, 1993. doi: 10.1016/0960-9822(93)90331-H.
- J. W. Scannell, C. Blakemore, and M. P. Young. Analysis of connectivity in the cat cerebral cortex. *The Journal of Neuroscience*, 15(2):1463–1483, 1995.
- J. W. Scannell, G. A. Burns, C. C. Hilgetag, M. A. O’Neill, and M. P. Young. The Connectional Organization of the Cortico-thalamic System of the Cat. *Cerebral Cortex*, 9(3):277–299, 1999. doi: 10.1093/cercor/9.3.277.
- J. W. Scannell, S. Grant, B. R. Payne, and R. Baddeley. On variability in the density of corticocortical and thalamocortical connections. *Philosophical Transactions of the Royal Society B: Biological Sciences*, 355(1393):21, 2000. doi: 10.1098/rstb.2000.0547.
- M. Schmidt, R. Bakker, C. C. Hilgetag, M. Diesmann, and S. J. van Albada. Multi-scale account of the network structure of macaque visual cortex. *Brain Structure and Function*, 223(3):1409–1435, 2018a. doi: 10.1007/s00429-017-1554-4.
- M. Schmidt, R. Bakker, K. Shen, G. Bezgin, M. Diesmann, and S. J. v. Albada. A multi-scale layer-resolved spiking network model of resting-state dynamics in macaque visual cortical areas. *PLOS Computational Biology*, 14(10):e1006359, 2018b. doi: 10.1371/journal.pcbi.1006359.
- M. T. Schmolesky, Y. Wang, D. P. Hanes, K. G. Thompson, S. Leutgeb, J. D. Schall, and A. G. Leventhal. Signal Timing Across the Macaque Visual System. *Journal of Neurophysiology*, 79(6):3272–3278, 1998.
- L. H. Scholtens, R. Schmidt, M. A. de Reus, and M. P. van den Heuvel. Linking Macroscale Graph Analytical Organization to Microscale Neuroarchitectonics in the Macaque Connectome. *The Journal of Neuroscience*, 34(36):12192–12205, 2014. doi: 10.1523/JNEUROSCI.0752-14.2014.

- L. H. Scholtens, M. A. de Reus, and M. P. van den Heuvel. Linking contemporary high resolution magnetic resonance imaging to the von Economo legacy: A study on the comparison of MRI cortical thickness and histological measurements of cortical structure. *Human Brain Mapping*, 36(8):3038–3046, 2015. doi: 10.1002/hbm.22826.
- M. L. Schwartz and P. S. Goldman-Rakic. Prenatal specification of callosal connections in rhesus monkey. *The Journal of Comparative Neurology*, 307(1):144–162, 1991. doi: 10.1002/cne.903070113.
- M. L. Schwartz, P. Rakic, and P. S. Goldman-Rakic. Early phenotype expression of cortical neurons: evidence that a subclass of migrating neurons have callosal axons. *Proceedings of the National Academy of Sciences*, 88(4):1354–1358, 1991. doi: 10.1073/pnas.88.4.1354.
- A. Schüz and G. Palm. Density of neurons and synapses in the cerebral cortex of the mouse. *The Journal of Comparative Neurology*, 286(4):442–455, 1989. doi: 10.1002/cne.902860404.
- J. Seidlitz, F. Váša, M. Shinn, R. Romero-Garcia, K. J. Whitaker, P. E. Vértes, K. Wagstyl, P. K. Reardon, L. Clasen, S. Liu, A. Messinger, D. A. Leopold, P. Fonagy, R. J. Dolan, P. B. Jones, I. M. Goodyer, A. Raznahan, and E. T. Bullmore. Morphometric Similarity Networks Detect Microscale Cortical Organization and Predict Inter-Individual Cognitive Variation. *Neuron*, 97(1):231–247.e7, 2018. doi: 10.1016/j.neuron.2017.11.039.
- E. Seiradake, E. Y. Jones, and R. Klein. Structural Perspectives on Axon Guidance. *Annual Review of Cell and Developmental Biology*, 32(1):577–608, 2016. doi: 10.1146/annurev-cellbio-111315-125008.
- M. Senden, G. Deco, M. A. de Reus, R. Goebel, and M. P. van den Heuvel. Rich club organization supports a diverse set of functional network configurations. *NeuroImage*, 96:174–182, 2014. doi: 10.1016/j.neuroimage.2014.03.066.
- P. Shaw, N. J. Kabani, J. P. Lerch, K. Eckstrand, R. Lenroot, N. Gogtay, D. Greenstein, L. Clasen, A. Evans, J. L. Rapoport, J. N. Giedd, and S. P. Wise. Neurodevelopmental Trajectories of the Human Cerebral Cortex. *The Journal of Neuroscience*, 28(14):3586–3594, 2008. doi: 10.1523/JNEUROSCI.5309-07.2008.
- S. Shipp. The importance of being agranular: a comparative account of visual and motor cortex. *Philosophical Transactions of the Royal Society B: Biological Sciences*, 360(1456):797–814, 2005. doi: 10.1098/rstb.2005.1630.

- S. Shipp. Neural Elements for Predictive Coding. *Frontiers in Psychology*, 7, 2016. doi: 10.3389/fpsyg.2016.01792.
- R. L. Sidman, I. L. Miale, and N. Feder. Cell proliferation and migration in the primitive ependymal zone; An autoradiographic study of histogenesis in the nervous system. *Experimental Neurology*, 1(4):322–333, 1959. doi: 10.1016/0014-4886(59)90024-X.
- G. Silberberg, A. Gupta, and H. Markram. Stereotypy in neocortical microcircuits. *Trends in Neurosciences*, 25(5):227–230, 2002. doi: 10.1016/S0166-2236(02)02151-3.
- R. A. Silver. Neuronal arithmetic. *Nature Reviews Neuroscience*, 11(7):474–489, 2010. doi: 10.1038/nrn2864.
- I. H. Smart. Histogenesis of the mesocortical area of the mouse telencephalon. *Journal of Anatomy*, 138(3):537–552, 1984.
- I. H. Smart and M. Smart. Growth patterns in the lateral wall of the mouse telencephalon: I. Autoradiographic studies of the histogenesis of the isocortex and adjacent areas. *Journal of Anatomy*, 134(Pt 2):273–298, 1982.
- C. U. M. Smith. Does history repeat itself? Cortical columns 1. Introduction. *Cortex; a journal devoted to the study of the nervous system and behavior*, 46(3):279–280, 2010a. doi: 10.1016/j.cortex.2008.12.001.
- C. U. M. Smith. Does history repeat itself? Cortical columns 2. From cytoarchitectonics to columns. *Cortex; a journal devoted to the study of the nervous system and behavior*, 46(5):591–592, 2010b. doi: 10.1016/j.cortex.2008.12.003.
- C. U. M. Smith. Does history repeat itself? Cortical columns 3. A cortex of columns. *Cortex; a journal devoted to the study of the nervous system and behavior*, 46(6):713–714, 2010c. doi: 10.1016/j.cortex.2008.12.002.
- C. U. M. Smith. Does history repeat itself? Cortical columns 4. Déjà vu? *Cortex; a journal devoted to the study of the nervous system and behavior*, 46(8):947–948, 2010d. doi: 10.1016/j.cortex.2009.02.002.
- P. Somogyi, G. Tamás, R. Lujan, and E. H. Buhl. Salient features of synaptic organisation in the cerebral cortex. *Brain Research Reviews*, 26(2–3):113–135, 1998. doi: 10.1016/S0165-0173(97)00061-1.
- C. Song and J. R. Moyer. Layer- and subregion-specific differences in the neurophysiological properties of rat medial prefrontal cortex pyramidal neurons. *Journal of Neurophysiology*, 119(1):177–191, 2018. doi: 10.1152/jn.00146.2017.

- O. Sporns, D. R. Chialvo, M. Kaiser, and C. C. Hilgetag. Organization, development and function of complex brain networks. *Trends in Cognitive Sciences*, 8(9):418–425, 2004. doi: 10.1016/j.tics.2004.07.008.
- N. Spruston. Pyramidal neurons: dendritic structure and synaptic integration. *Nature Reviews Neuroscience*, 9(3):206–221, 2008. doi: 10.1038/nrn2286.
- L. R. Squire, D. Berg, F. E. Bloom, S. du Lac, A. Ghosh, and N. Spitzer, editors. *Fundamental Neuroscience*. Elsevier Academic Press, London, UK, 3rd edition, 2008. ISBN 978-0-12-374019-9.
- B. B. Stanfield and D. D. M. O’Leary. The transient corticospinal projection from the occipital cortex during the postnatal development of the rat. *Journal of Comparative Neurology*, 238(2):236–248, 1985. doi: 10.1002/cne.902380210.
- E. Stoeckli. Where does axon guidance lead us? *F1000Research*, 6:78, 2017. doi: 10.12688/f1000research.10126.1.
- B. Suter, R. S. Nowakowski, P. G. Bhide, and V. S. Caviness. Navigating Neocortical Neurogenesis and Neuronal Specification: A Positional Information System Encoded by Neurogenetic Gradients. *The Journal of Neuroscience*, 27(40):10777–10784, 2007. doi: 10.1523/JNEUROSCI.3091-07.2007.
- L. L. Symonds and A. C. Rosenquist. Laminar origins of visual corticocortical connections in the cat. *The Journal of comparative neurology*, 229(1):39–47, 1984. doi: 10.1002/cne.902290104.
- J. Szentagothai. The Ferrier Lecture, 1977: The Neuron Network of the Cerebral Cortex: A Functional Interpretation. *Proceedings of the Royal Society of London. Series B. Biological Sciences*, 201(1144):219–248, 1978. doi: 10.1098/rspb.1978.0043.
- T. Takahashi, R. S. Nowakowski, and V. S. Caviness. The cell cycle of the pseudostratified ventricular epithelium of the embryonic murine cerebral wall. *The Journal of Neuroscience*, 15(9):6046–6057, 1995.
- Y. Tang, H. Gao, W. Zou, and J. Kurths. Identifying Controlling Nodes in Neuronal Networks in Different Scales. *PLoS ONE*, 7(7), 2012. doi: 10.1371/journal.pone.0041375.
- L. Telley, G. Agirman, J. Prados, N. Amberg, S. Fièvre, P. Oberst, G. Bartolini, I. Vitali, C. Cadilhac, S. Hippenmeyer, L. Nguyen, A. Dayer, and D. Jabaudon. Temporal patterning of apical progenitors and their daughter neurons in the developing neocortex. *Science*, 364(6440):eaav2522, 2019. doi: 10.1126/science.aav2522.

- M. Tessier-Lavigne and C. S. Goodman. The Molecular Biology of Axon Guidance. *Science*, 274(5290):1123–1133, 1996. doi: 10.1126/science.274.5290.1123.
- P. Tewarie, A. Hillebrand, E. van Dellen, M. M. Schoonheim, F. Barkhof, C. H. Polman, C. Beaulieu, G. Gong, B. W. van Dijk, and C. J. Stam. Structural degree predicts functional network connectivity: A multimodal resting-state fMRI and MEG study. *NeuroImage*, 97:296–307, 2014a. doi: 10.1016/j.neuroimage.2014.04.038.
- P. Tewarie, M. D. Steenwijk, B. M. Tijms, M. Daams, L. J. Balk, C. J. Stam, B. M. Uitdehaag, C. H. Polman, J. J. Geurts, F. Barkhof, P. J. Pouwels, H. Vrenken, and A. Hillebrand. Disruption of structural and functional networks in long-standing multiple sclerosis. *Human Brain Mapping*, 2014b. doi: 10.1002/hbm.22596.
- A. M. Thomson and A. P. Bannister. Interlaminar Connections in the Neocortex. *Cerebral Cortex*, 13(1):5–14, 2003. doi: 10.1093/cercor/13.1.5.
- A. M. Thomson, D. C. West, Y. Wang, and A. P. Bannister. Synaptic Connections and Small Circuits Involving Excitatory and Inhibitory Neurons in Layers 2–5 of Adult Rat and Cat Neocortex: Triple Intracellular Recordings and Biocytin Labelling In Vitro. *Cerebral Cortex*, 12(9):936–953, 2002. doi: 10.1093/cercor/12.9.936.
- D. Tomasi, R. Wang, G.-J. Wang, and N. D. Volkow. Functional Connectivity and Brain Activation: A Synergistic Approach. *Cerebral Cortex*, 24(10):2619–2629, 2014. doi: 10.1093/cercor/bht119.
- S. Tomasi, R. Caminiti, and G. M. Innocenti. Areal Differences in Diameter and Length of Corticofugal Projections. *Cerebral Cortex*, 22:1463–1472, 2012. doi: 10.1093/cercor/bhs011.
- E. K. Towilson, P. E. Vértes, S. E. Ahnert, W. R. Schafer, and E. T. Bullmore. The Rich Club of the *C. elegans* Neuronal Connectome. *The Journal of Neuroscience*, 33(15):6380–6387, 2013. doi: 10.1523/JNEUROSCI.3784-12.2013.
- M. P. van den Heuvel and O. Sporns. An Anatomical Substrate for Integration among Functional Networks in Human Cortex. *The Journal of Neuroscience*, 33(36):14489–14500, 2013a. doi: 10.1523/JNEUROSCI.2128-13.2013.
- M. P. van den Heuvel and O. Sporns. Network hubs in the human brain. *Trends in Cognitive Sciences*, 17(12):683–696, 2013b. doi: 10.1016/j.tics.2013.09.012.
- M. P. van den Heuvel, R. S. Kahn, J. Goñi, and O. Sporns. High-cost, high-capacity backbone for global brain communication. *Proceedings of the National Academy of Sciences*, 109(28):11372–11377, 2012. doi: 10.1073/pnas.1203593109.

- M. P. van den Heuvel, L. H. Scholtens, and M. A. de Reus. Topological organization of connectivity strength in the rat connectome. *Brain Structure and Function*, 221(3):1719–1736, 2016. doi: 10.1007/s00429-015-0999-6.
- M. P. v. d. van den Heuvel, L. H. Scholtens, L. Feldman Barrett, C. C. Hilgetag, and M. A. de Reus. Bridging Cytoarchitectonics and Connectomics in Human Cerebral Cortex. *Journal of Neuroscience*, 35(41):13943–13948, 2015. doi: 10.1523/JNEUROSCI.2630-15.2015.
- D. C. Van Essen, H. A. Drury, J. Dickson, J. Harwell, D. Hanlon, and C. H. Anderson. An Integrated Software Suite for Surface-based Analyses of Cerebral Cortex. *Journal of the American Medical Informatics Association*, 8(5):443–459, 2001. doi: 10.1136/jamia.2001.0080443.
- T. van Haeften, L. Baks-te Bulte, P. H. Goede, F. G. Wouterlood, and M. P. Witter. Morphological and numerical analysis of synaptic interactions between neurons in deep and superficial layers of the entorhinal cortex of the rat. *Hippocampus*, 13(8):943–952, 2003. doi: 10.1002/hipo.10144.
- T. van Kerkoerle, M. W. Self, B. Dagnino, M.-A. Gariel-Mathis, J. Poort, C. van der Togt, and P. R. Roelfsema. Alpha and gamma oscillations characterize feedback and feed-forward processing in monkey visual cortex. *Proceedings of the National Academy of Sciences*, 111(40):14332–14341, 2014. doi: 10.1073/pnas.1402773111.
- S. Varier and M. Kaiser. Neural Development Features: Spatio-Temporal Development of the *Caenorhabditis elegans* Neuronal Network. *PLoS Computational Biology*, 7(1):e1001044, 2011. doi: 10.1371/journal.pcbi.1001044.
- M. Verhage, A. S. Maia, J. J. Plomp, A. B. Brussaard, J. H. Heeroma, H. Vermeer, R. F. Toonen, R. E. Hammer, T. K. v. Den, Berg, M. Missler, H. J. Geuze, and T. C. Südhof. Synaptic Assembly of the Brain in the Absence of Neurotransmitter Secretion. *Science*, 287(5454):864–869, 2000. doi: 10.1126/science.287.5454.864.
- J. Vezoli, A. Falchier, B. Jouve, K. Knoblauch, M. Young, and H. Kennedy. Quantitative Analysis of Connectivity in the Visual Cortex: Extracting Function from Structure. *The Neuroscientist*, 10(5):476–482, 2004. doi: 10.1177/1073858404268478.
- N. Vitureira and Y. Goda. The interplay between Hebbian and homeostatic synaptic plasticity. *The Journal of Cell Biology*, 203(2):175–186, 2013. doi: 10.1083/jcb.201306030.
- O. Vogt. Die myeloarchitektonische Felderung des menschlichen Stirnhirns. *J Psychol Neurol*, 15(4/5):221–232, 1910.

- C. von Economo. *Zellaufbau der Grosshirnrinde des Menschen*. Springer, Berlin, 1927.
- C. von Economo. *Cellular Structure of the Human Cerebral Cortex*. Karger Medical and Scientific Publishers, Basel, Switzerland, 2009. ISBN 978-3-8055-9061-7.
- U. Voss, R. Holzmann, A. Hobson, W. Paulus, J. Koppehele-Gossel, A. Klimke, and M. A. Nitsche. Induction of self awareness in dreams through frontal low current stimulation of gamma activity. *Nature Neuroscience*, 17(6):810–812, 2014. doi: 10.1038/nn.3719.
- P. E. Vértes, A. F. Alexander-Bloch, N. Gogtay, J. N. Giedd, J. L. Rapoport, and E. T. Bullmore. Simple models of human brain functional networks. *Proceedings of the National Academy of Sciences*, 109(15):5868–5873, 2012. doi: 10.1073/pnas.1111738109.
- N. Wagatsuma, T. C. Potjans, M. Diesmann, and T. Fukai. Layer-dependent attentional processing by top-down signals in a visual cortical microcircuit model. *Frontiers in Computational Neuroscience*, 5:31, 2011. doi: 10.3389/fncom.2011.00031.
- K. Wagstyl, L. Ronan, I. M. Goodyer, and P. C. Fletcher. Cortical thickness gradients in structural hierarchies. *NeuroImage*, 111:241–250, 2015. doi: 10.1016/j.neuroimage.2015.02.036.
- Z. Wang, Z. Dai, G. Gong, C. Zhou, and Y. He. Understanding Structural-Functional Relationships in the Human Brain A Large-Scale Network Perspective. *The Neuroscientist*, page 1073858414537560, 2014. doi: 10.1177/1073858414537560.
- P. V. Watkins, J. P. Y. Kao, and P. O. Kanold. Spatial pattern of intra-laminar connectivity in supragranular mouse auditory cortex. *Frontiers in Neural Circuits*, 8:15, 2014. doi: 10.3389/fncir.2014.00015.
- S. P. Wise and E. G. Jones. The organization and postnatal development of the commissural projection of the rat somatic sensory cortex. *The Journal of Comparative Neurology*, 168(3):313–343, 1976. doi: 10.1002/cne.901680302.
- K. P. Wylie, E. Kronberg, K. Maharajh, J. Smucny, M. A. Cornier, and J. R. Tregellas. Between-network connectivity occurs in brain regions lacking layer IV input. *NeuroImage*, 116:50–58, 2015. doi: 10.1016/j.neuroimage.2015.05.010, 10.1016/j.neuroimage.2015.05.010.
- D. Xing, C.-I. Yeh, S. Burns, and R. M. Shapley. Laminar analysis of visually evoked activity in the primary visual cortex. *Proceedings of the National Academy of Sciences*, 109(34):13871–13876, 2012. doi: 10.1073/pnas.1201478109.

- X. Xu and E. M. Callaway. Laminar Specificity of Functional Input to Distinct Types of Inhibitory Cortical Neurons. *The Journal of Neuroscience*, 29(1):70–85, 2009. doi: 10.1523/JNEUROSCI.4104-08.2009.
- X.-K. Xu, J. Zhang, and M. Small. Rich-club connectivity dominates assortativity and transitivity of complex networks. *Physical Review E*, 82(4):046117, 2010. doi: 10.1103/PhysRevE.82.046117.
- N. Yamamoto, K. Yamada, T. Kurotani, and K. Toyama. Laminar specificity of extrinsic cortical connections studied in coculture preparations. *Neuron*, 9(2):217–228, 1992. doi: 10.1016/0896-6273(92)90161-6.
- I. B. Yáñez, A. Muñoz, J. Contreras, J. Gonzalez, E. Rodriguez-Veiga, and J. DeFelipe. Double bouquet cell in the human cerebral cortex and a comparison with other mammals. *The Journal of Comparative Neurology*, 486(4):344–360, 2005. doi: 10.1002/cne.20533.
- W. J. Youden. Index for rating diagnostic tests. *Cancer*, 3(1):32–35, 1950. doi: 10.1002/1097-0142(1950)3:1<32::AID-CNCR2820030106>3.0.CO;2-3.
- M. P. Young. Objective analysis of the topological organization of the primate cortical visual system. *Nature*, 358(6382):152–155, 1992. doi: 10.1038/358152a0.
- M. P. Young. The Organization of Neural Systems in the Primate Cerebral Cortex. *Proceedings of the Royal Society of London. Series B: Biological Sciences*, 252(1333):13–18, 1993. doi: 10.1098/rspb.1993.0040.
- M. P. Young, J. W. Scannell, G. A. Burns, and C. Blakemore. Analysis of connectivity: neural systems in the cerebral cortex. *Reviews in the neurosciences*, 5(3):227–250, 1994.
- R. Yuste. *Dendritic Spines*. MIT Press, 2010. ISBN 978-0-262-01350-5.
- G. Zamora-López, C. Zhou, and J. Kurths. Graph analysis of cortical networks reveals complex anatomical communication substrate. *Chaos: An Interdisciplinary Journal of Nonlinear Science*, 19(1):015117, 2009. doi: 10.1063/1.3089559.
- G. Zamora-López, C. Zhou, and J. Kurths. Cortical hubs form a module for multisensory integration on top of the hierarchy of cortical networks. *Frontiers in Neuroinformatics*, 4:1, 2010. doi: 10.3389/neuro.11.001.2010.
- G. Zamora-López, C. Zhou, and J. Kurths. Exploring Brain Function from Anatomical Connectivity. *Frontiers in Neuroscience*, 5:83, 2011. doi: 10.3389/fnins.2011.00083.

- B. Zikopoulos and H. Barbas. Changes in Prefrontal Axons May Disrupt the Network in Autism. *The Journal of Neuroscience*, 30(44):14595–14609, 2010. doi: 10.1523/JNEUROSCI.2257-10.2010.
- B. Zikopoulos and H. Barbas. Altered neural connectivity in excitatory and inhibitory cortical circuits in autism. *Frontiers in Human Neuroscience*, 7:609, 2013. doi: 10.3389/fnhum.2013.00609.
- K. Zilles. Architektonik und funktionelle Neuroanatomie der Hirnrinde des Menschen. In H. Förstl, M. Hautzinger, and G. Roth, editors, *Neurobiologie psychischer Störungen*, pages 75–140. Springer Berlin Heidelberg, 2006. ISBN 978-3-540-25694-6 978-3-540-30887-4.
- K. Zilles and K. Amunts. Receptor mapping: architecture of the human cerebral cortex. *Current opinion in neurology*, 22(4):331–339, 2009. doi: 10.1097/WCO.0b013e32832d95db.
- K. Zilles and K. Amunts. Architecture of the Cerebral Cortex. In J. K. Mai and G. Paxinos, editors, *The Human Nervous System*, pages 836–895. Academic Press, San Diego, 3rd edition, 2012a. ISBN 978-0-12-374236-0.
- K. Zilles and K. Amunts. Segregation and Wiring in the Brain. *Science*, 335(6076): 1582–1584, 2012b. doi: 10.1126/science.1221366.
- K. Zilles and N. Palomero-Gallagher. Multiple Transmitter Receptors in Regions and Layers of the Human Cerebral Cortex. *Frontiers in Neuroanatomy*, 11, 2017. doi: 10.3389/fnana.2017.00078.
- K. Zilles, N. Palomero-Gallagher, and K. Amunts. Development of cortical folding during evolution and ontogeny. *Trends in Neurosciences*, 36(5):275–284, 2013. doi: 10.1016/j.tins.2013.01.006.

Acknowledgements

First and foremost, I would like to thank Claus. Thank you for giving me this exciting project to work on - I enjoyed working on the conceptual side of things and not being held back much by the vagaries of conducting (*in vivo*) experiments. But mostly, thank you for giving me time to develop, both professionally and personally. During the time in your lab, I made the transition from student to researcher and adult, in an environment that was very supportive in both respects.

Many thanks also go to Simon Grant as well as Helen Barbas. Simon, working with you on our publication was very instructive, and I took away a lot that helped me with later manuscripts. Helen, thank you very much for welcoming me in your lab and giving me the opportunity to measure neuron densities myself - I gained not only additional data points, but a deeper familiarity with the subject matter, which is indispensable for conducting worthwhile research. Also, I hope you like where we took your structural model.

Thank you for bouncing ideas back and forth, advice, proofreading manuscripts and providing me with cake as well as, most importantly, distraction from the minutiae of research: Alexandros, Andrea, Caroline, Farid, Leigh-Anne, Melissa, René, I was fortunate you were around!

And, of course, thank you Georg, Alex and Cara for putting everything in perspective.

September 2019,

Sarah

This work has received funding from the German Research Foundation (SFB936/A1).

Prior publications

The following articles resulted directly from the work on this dissertation:

Beul, S. F., and Hilgetag, C. C. (2015). Towards a “canonical” agranular cortical microcircuit. *Frontiers in Neuroanatomy* 8, 165. doi:10.3389/fnana.2014.00165.

Beul, S. F., Grant, S., and Hilgetag, C. C. (2015). A predictive model of the cat cortical connectome based on cytoarchitecture and distance. *Brain Structure and Function* 220, 3167–3184. doi:10.1007/s00429-014-0849-y.

Beul, S. F., Barbas, H., and Hilgetag, C. C. (2017). A Predictive Structural Model of the Primate Connectome. *Scientific Reports* 7, 43176. doi:10.1038/srep43176.

Beul, S. F., Goulas, A., and Hilgetag, C. C. (2018). Comprehensive computational modelling of the development of mammalian cortical connectivity underlying an architectonic type principle. *PLOS Computational Biology* 14, e1006550. doi:10.1371/journal.pcbi.1006550.

Beul, S. F., and Hilgetag, C. C. (2019). Neuron density fundamentally relates to architecture and connectivity of the primate cerebral cortex. *NeuroImage* 189, 117051. doi:10.1016/j.neuroimage.2019.01.010.

Beul, S. F., and Hilgetag, C. C. (2019). Systematic modelling of the development of laminar projection origins in the cerebral cortex: Interactions of spatio-temporal patterns of neurogenesis and cellular heterogeneity. Under review.

Beul, S. F., Goulas, A., and Hilgetag, C. C. (2019). An architectonic type principle applies to the establishment of laminar patterns of cortico-cortical connections. In preparation.

Additionally, during this time I co-authored the following articles:

Hilgetag, C. C., Medalla, M., Beul, S. F., and Barbas, H. (2016). The primate connectome in context: Principles of connections of the cortical visual system. *NeuroImage* 134, 685–702. doi:10.1016/j.neuroimage.2016.04.017.

Hilgetag, C. C., Beul, S. F., van Albada, S. J., and Goulas, A. (2019). An architectonic type principle integrates macroscopic cortico-cortical connections with intrinsic cortical circuits of the primate brain. *Network Neuroscience* 3(4), 905–923. doi:10.1162/netn_a_00100.

Curriculum Vitae

Lebenslauf entfällt aus datenschutzrechtlichen Gründen

Lebenslauf entfällt aus datenschutzrechtlichen Gründen

Supplementary figures

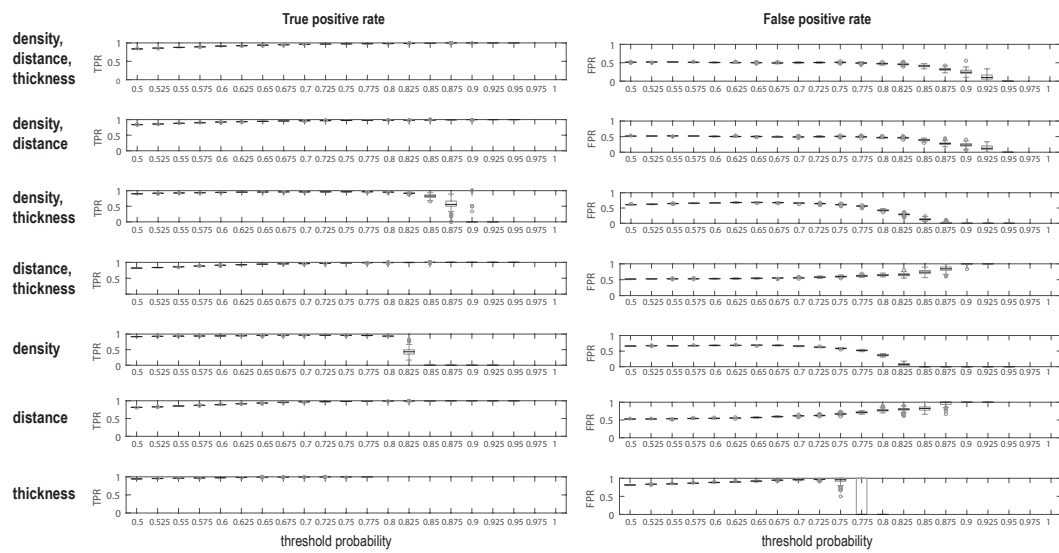


Figure C.1: True positive rate and false positive rate for classification of projection existence from all possible combinations of parameters in the macaque cortex. Distribution of rates across all 100 rounds of cross-validation is shown for all threshold probabilities. Overall performance was best for the combination of $|\log\text{-ratio}_{\text{density}}|$ and Euclidean distance. Note that the addition of $|\log\text{-ratio}_{\text{thickness}}|$ to these two parameters did not improve performance. Boxplots indicate median rates by a black bar and outliers by grey circles.

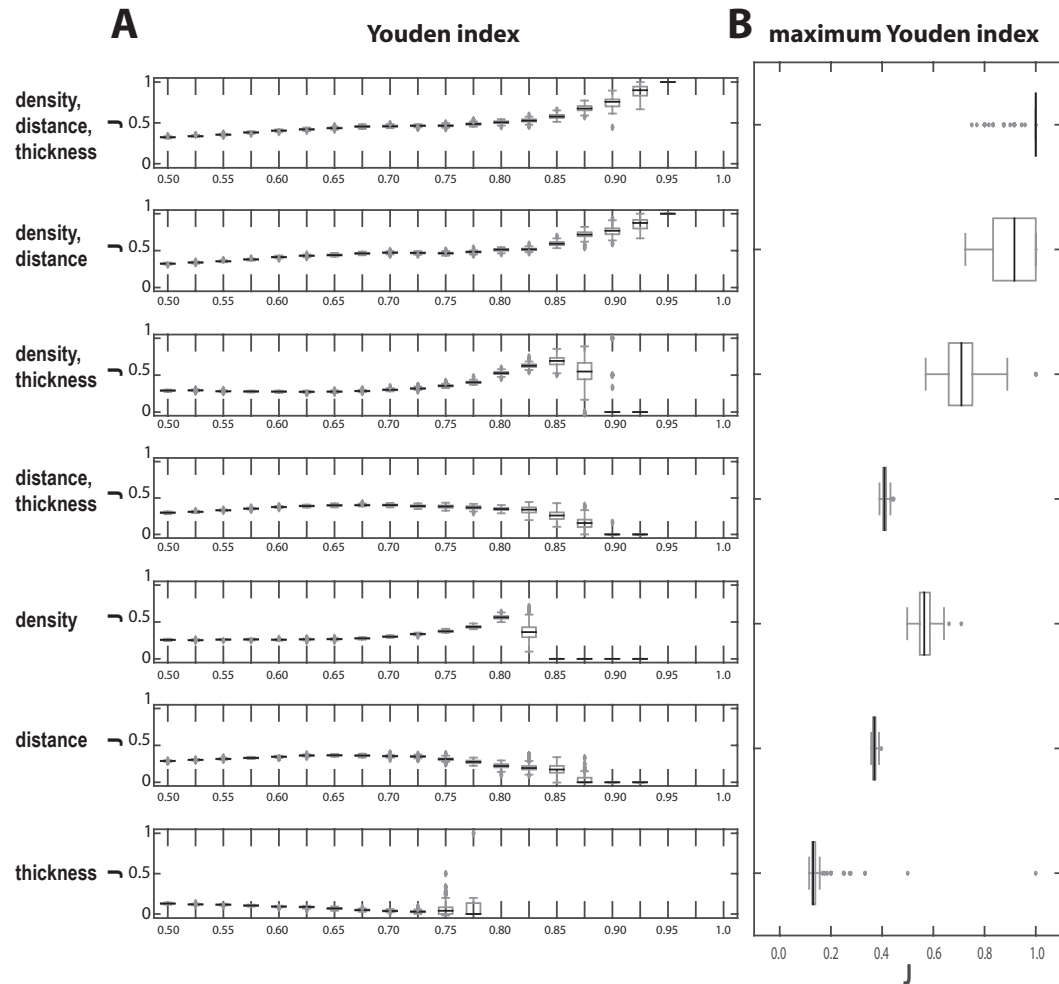


Figure C.2: Youden index J for classification of projection existence from all possible combinations of parameters in the macaque cortex. **(A)** Distribution of J across all 100 rounds of cross-validation is shown for all threshold probabilities. Overall performance was best for the combination of $|\log\text{-ratio}_{\text{density}}|$ and Euclidean distance. Note that the addition of $|\log\text{-ratio}_{\text{thickness}}|$ to these two parameters did not improve performance. **(B)** Distribution of maximum J (across all threshold probabilities) for all 100 rounds of cross-validation. Kruskal-Wallis-test showed that the distributions were significantly different ($H = 661.0$, $p < .001$). Post hoc tests (Bonferroni-corrected) revealed that the distributions of 'density, distance, thickness' and 'density, distance' were not significantly different from each other ($p > .05$), while all other pair-wise tests reached statistical significance (all $p < .05$). Boxplots indicate median J by a black bar and outliers by grey circles.

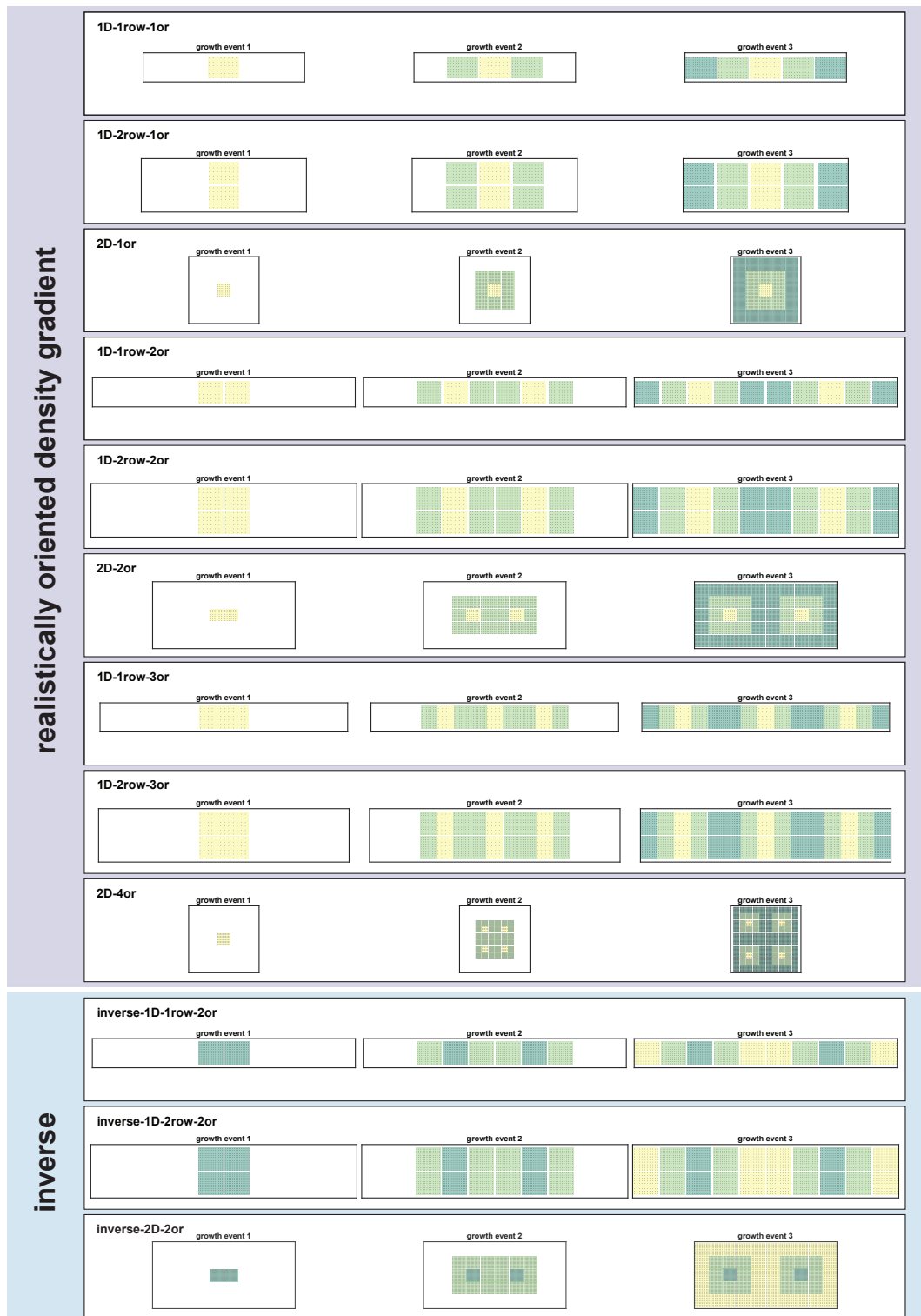


Figure C.3: Developmental trajectories of all 21 growth layouts.

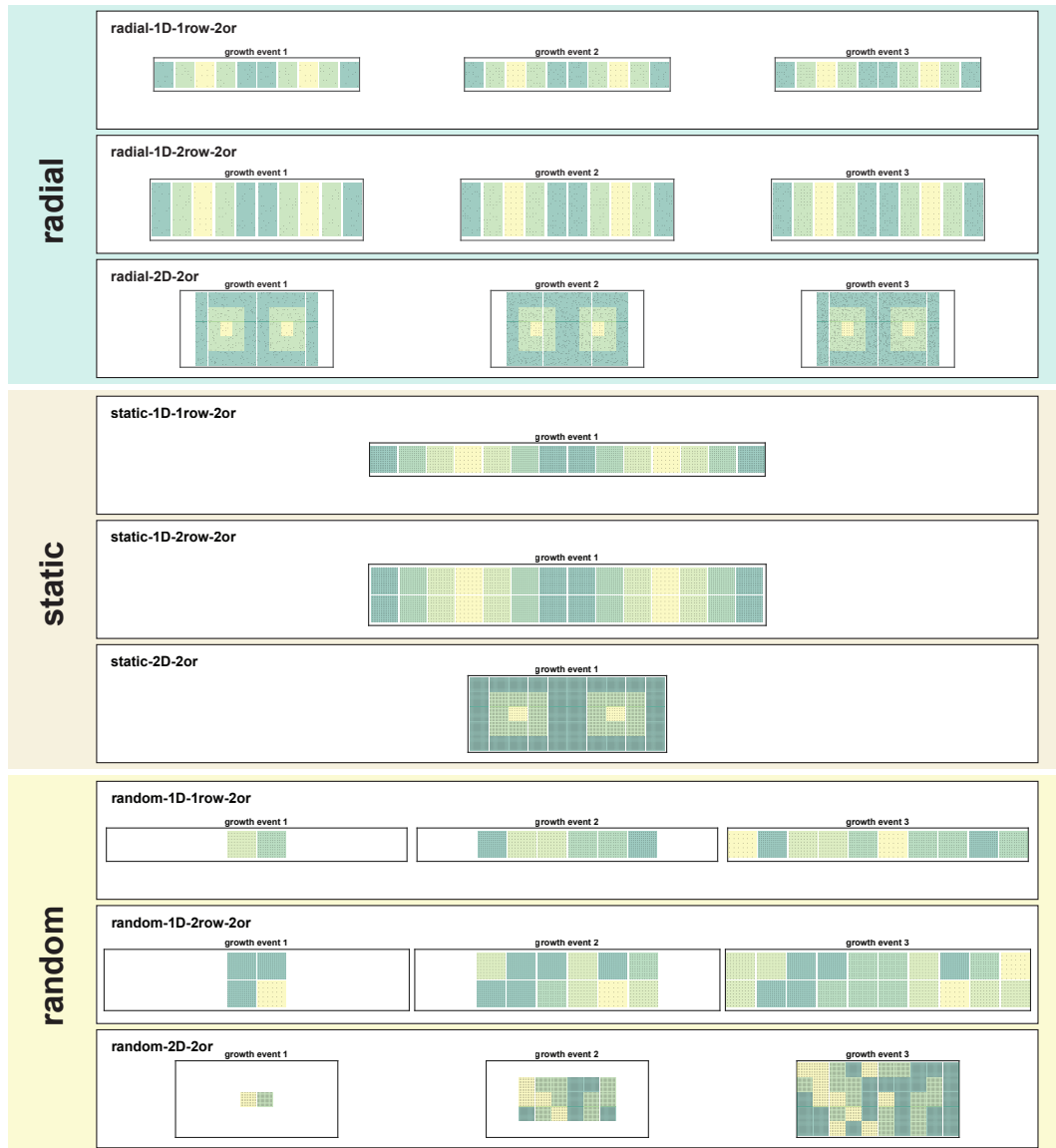


Figure C.3: Developmental trajectories of all 21 growth layouts (cont.). Illustration of the spatio-temporal growth trajectory for each growth layout. The successive population of the cortical sheet with neurons is shown for the first three growth events. For static growth, all neurons grow simultaneously, hence only one growth event is shown. Abbreviations and background colours as in Table 2.1.

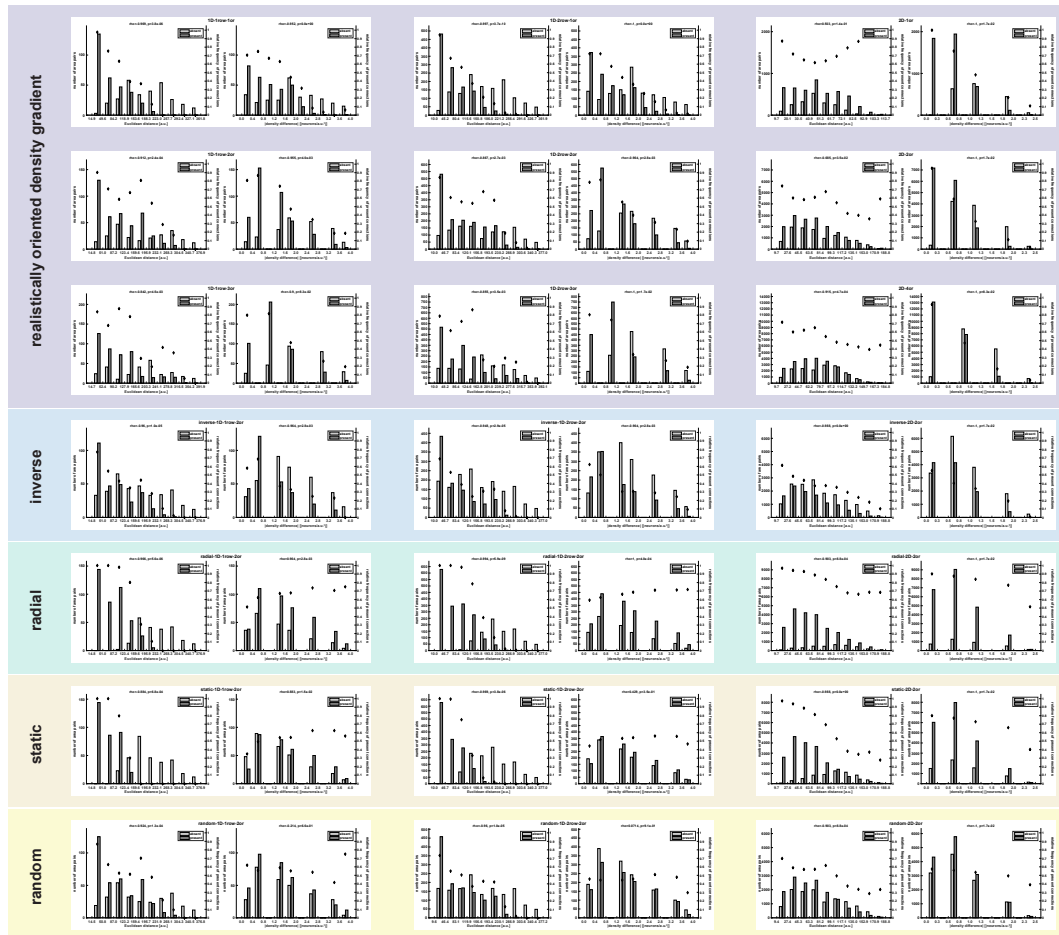


Figure C.4: Correlation of relative connection frequency with distance and absolute density difference for all growth layouts. Distribution of absent and present connections across distance (left panels) and absolute density difference (right panels) for all growth layouts. Absolute numbers of absent and present projections (bars) are depicted alongside the corresponding relative frequency of present connections (diamonds). Simulation instances were chosen to be representative of the median values shown in Figure 3.22. Spearman rank correlation results for each particular instance are shown on top of each plot. A.u.: arbitrary unit. Abbreviations and background colours as in Table 2.1.

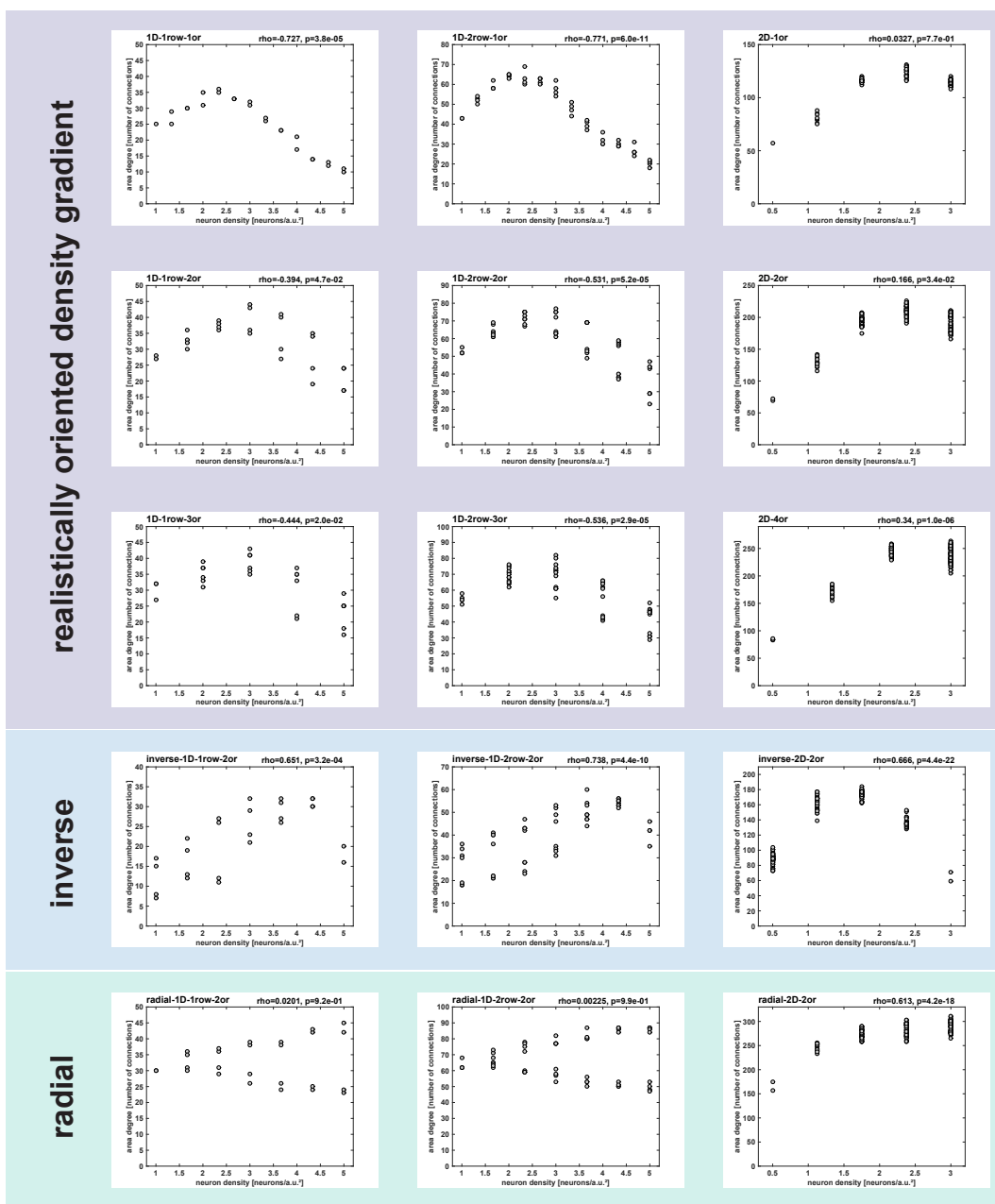


Figure C.5: Correlation of area degree with neuron density for all growth layouts.

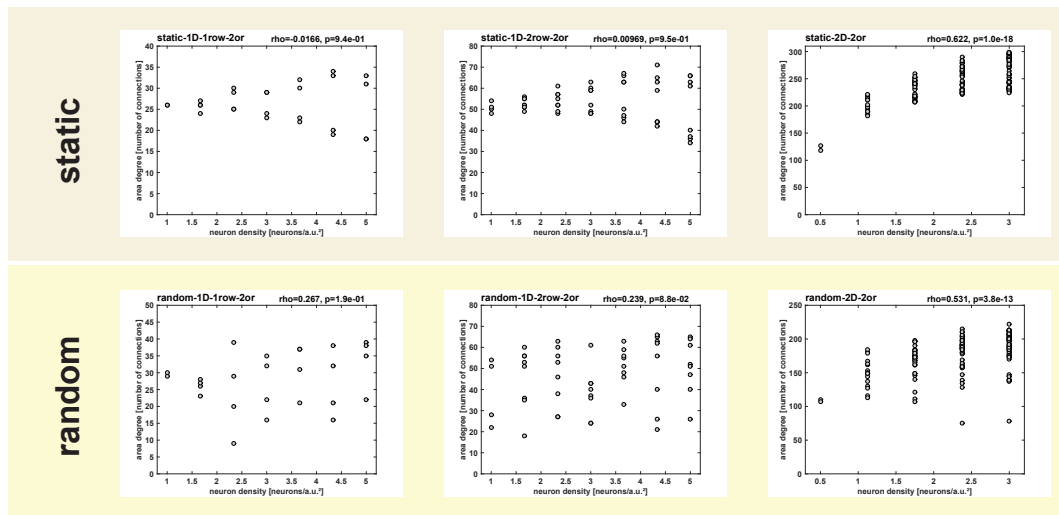


Figure C.5: Correlation of area degree with neuron density for all growth layouts (cont.). Variation of area degree (number of connections) across areas' neuron density is shown. Simulation instances were chosen to be representative of the median values shown in Figure 3.24. Spearman rank correlation results for each particular instance are shown on top of each plot. A.u.: arbitrary unit. Abbreviations and background colours as in Table 2.1.

A delay infragranular compartment growth

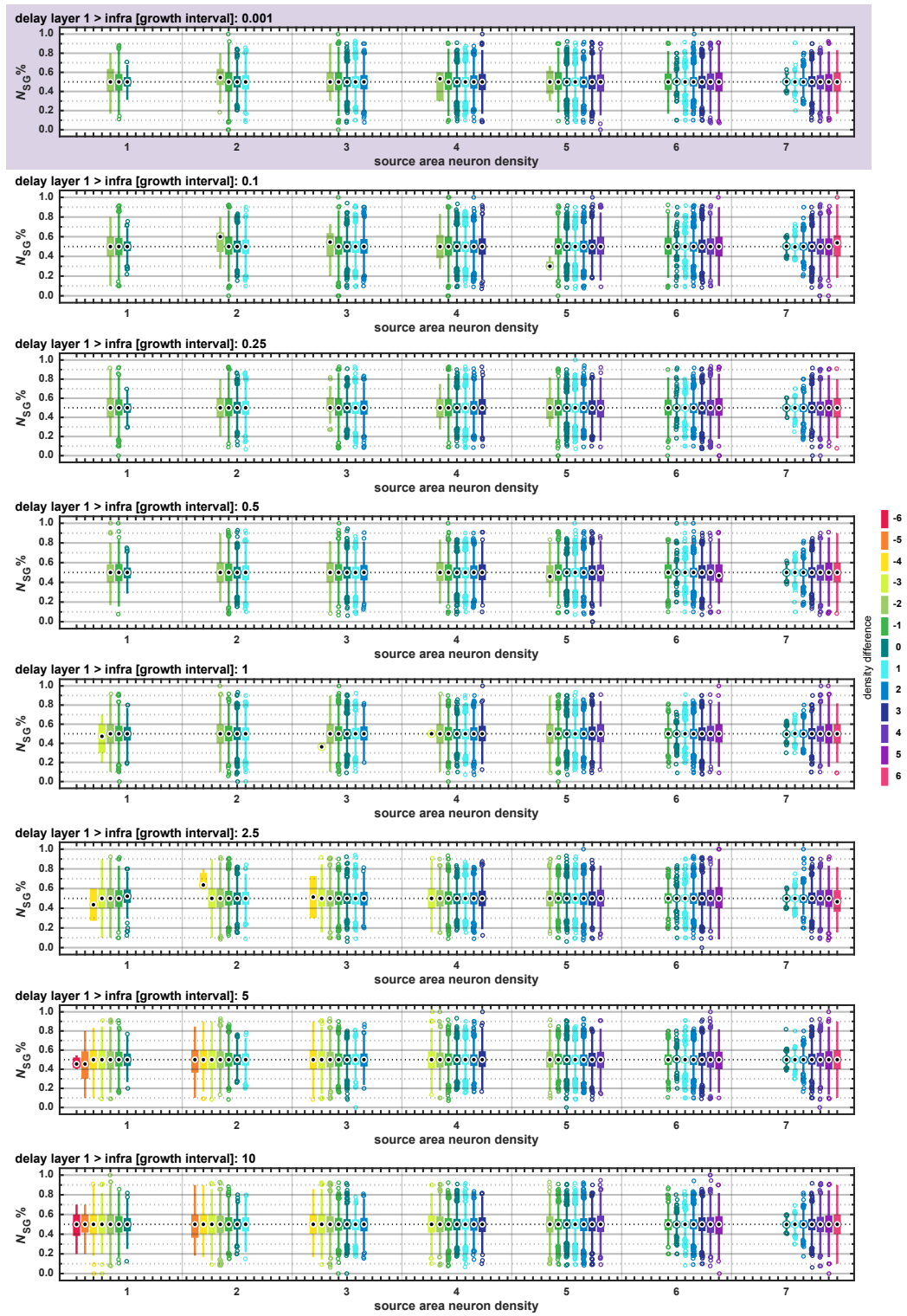


Figure C.6: Supragranular contribution across source area densities.

B delay supragranular compartment growth

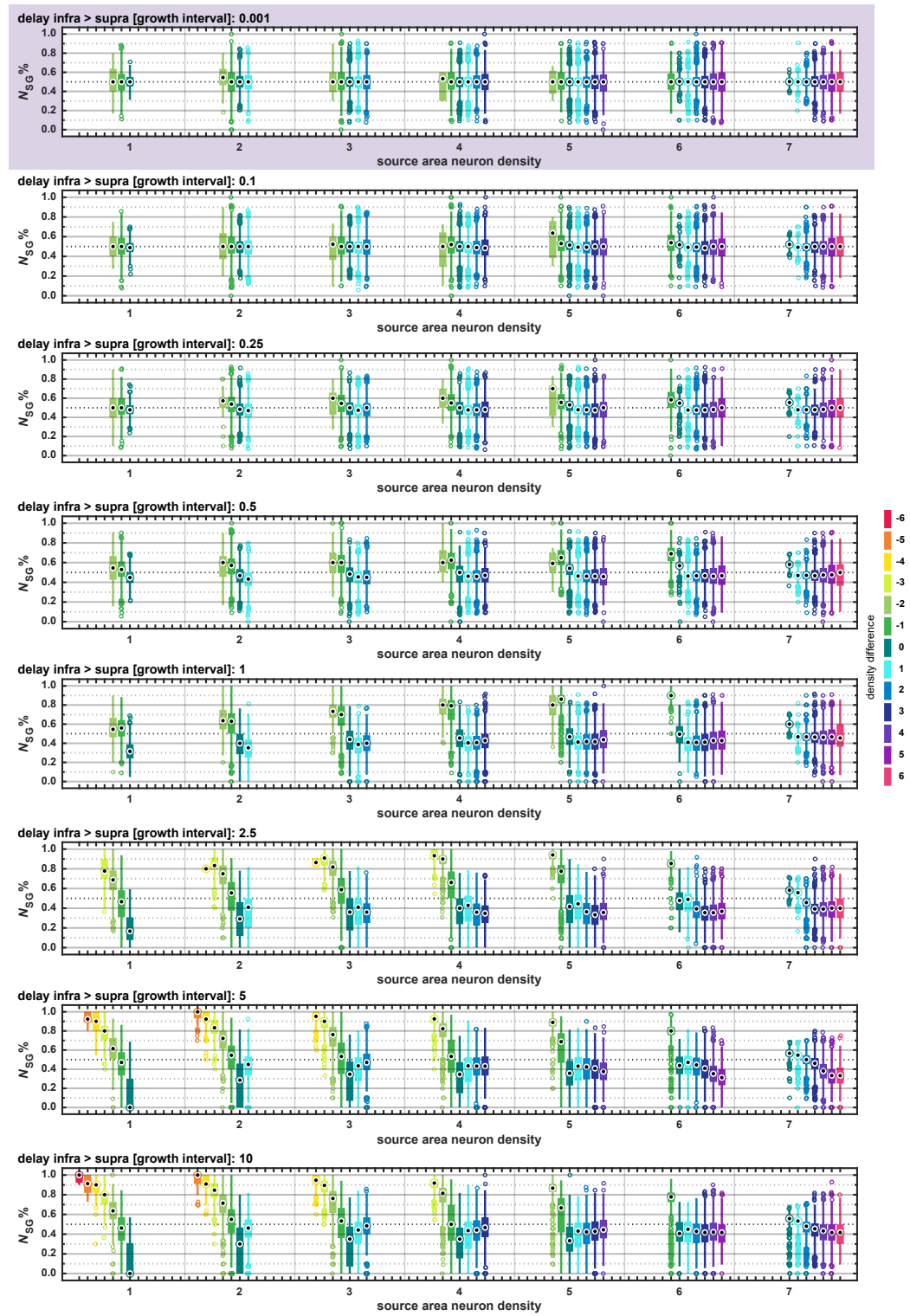


Figure C.6: Supragranular contribution across source area densities (cont.).

C supragranular compartment neuron density



Figure C.6: Supragranular contribution across source area densities (cont.).

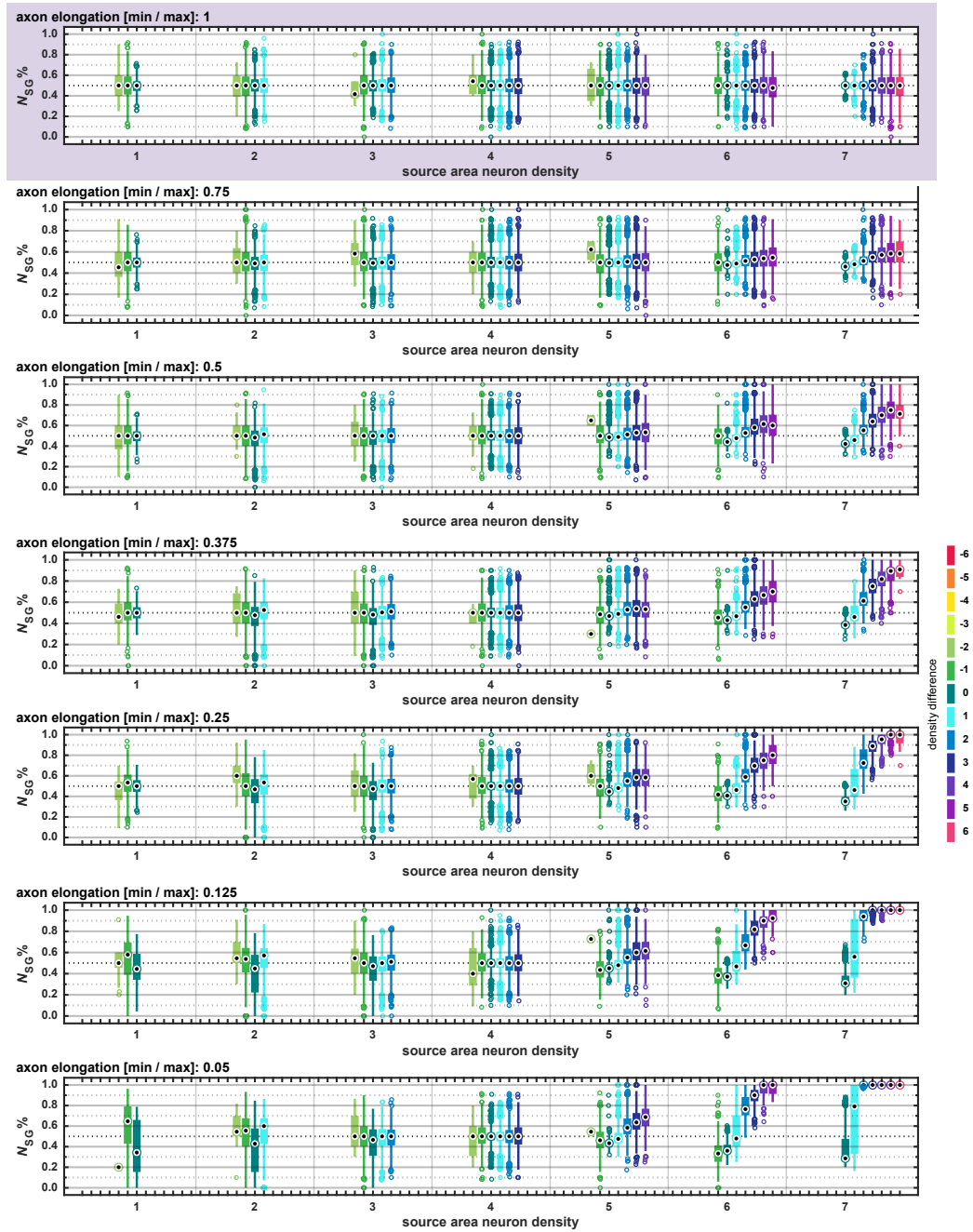
D axon elongation

Figure C.6: Supragranular contribution across source area densities (cont.). Box plots show the distribution of supragranular contribution ($N_{SG}\%$) across density differences (ranked, see color scale) categorised according to the neuron densities of the source areas (ranked). For each feature ((A) delay infragranular compartment, (B) delay supragranular compartment, (C) supragranular compartment neuron density scaling, (D) axon elongation), projections are shown for each implemented parameter value. Thus, one row of box plots corresponds to one box in Figure 3.28. Box plots show distribution across 50 simulation instances (projections for all 50 instances are collapsed), indicating median (target), interquartile range (box), data range (whiskers) and outliers (circles, outside of 2.7 standard deviations). Parameter values that correspond to baseline are highlighted in purple.

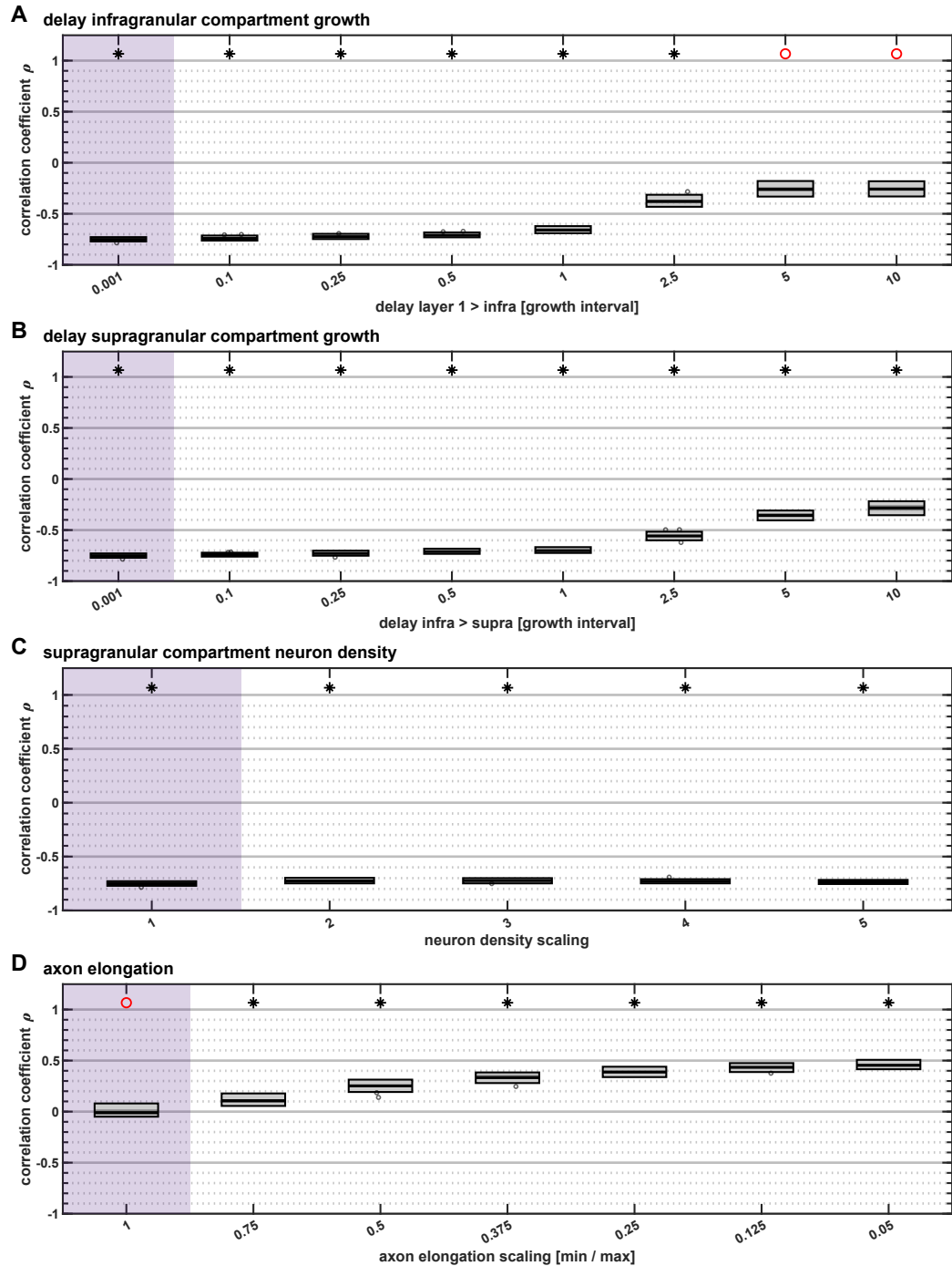


Figure C.7: Correlation of area degree with neuron density. Spearman rank correlation coefficients for the correlation between area degree (number of connections) and area neuron density. We used a sign test to determine whether the distribution of associated Spearman rank correlation p -values had a median value smaller than $\alpha = 0.05$. The result of the sign test is indicated on top; black star: median $p < 0.05$, red circle: median $p \geq 0.05$. Box plots show distribution across 50 simulation instances per implementation, indicating median (line), interquartile range (dark grey box), data range (light grey box) and outliers (circles, outside of 2.7 standard deviations). Parameter values that correspond to baseline (i.e., with no feature implemented), are highlighted in purple.

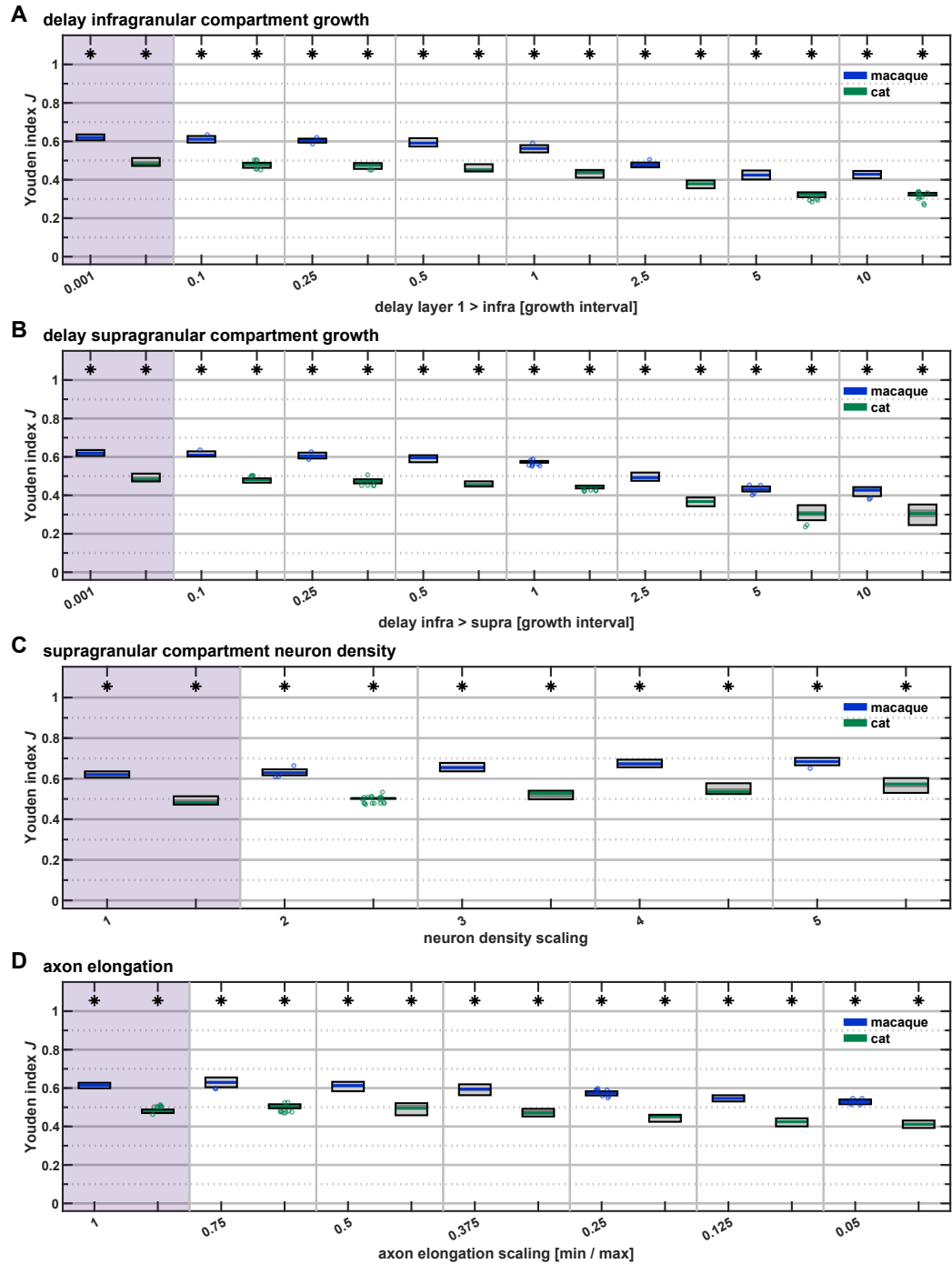


Figure C.8: Simulation-to-empirical classification performance.

Figure C.8: Simulation-to-empirical classification performance. We trained a classifier on simulated data and used it to classify connection existence from relative differentiation and spatial proximity in the macaque (blue) and cat (green) cortex. Classification performance is indicated by the Youden index J for the four implemented features. Whether the classifier performed better than chance was assessed by a permutation test, where J was calculated for prediction from randomly permuted labels and a z-test was performed. We used a sign test to determine whether the distribution of associated z-test p -values had a median value smaller than $\alpha = 0.05$. The result of the sign test is indicated on top; black star: performance better than chance with median $p < 0.05$, red circle: performance not better than chance with median $p \geq 0.05$. Box plots show distribution across 50 simulation instances per implementation, indicating median (line), interquartile range (dark grey box), data range (light grey box) and outliers (circles, outside of 2.7 standard deviations). Parameter values that correspond to baseline (i.e., with no feature implemented), are highlighted in purple.

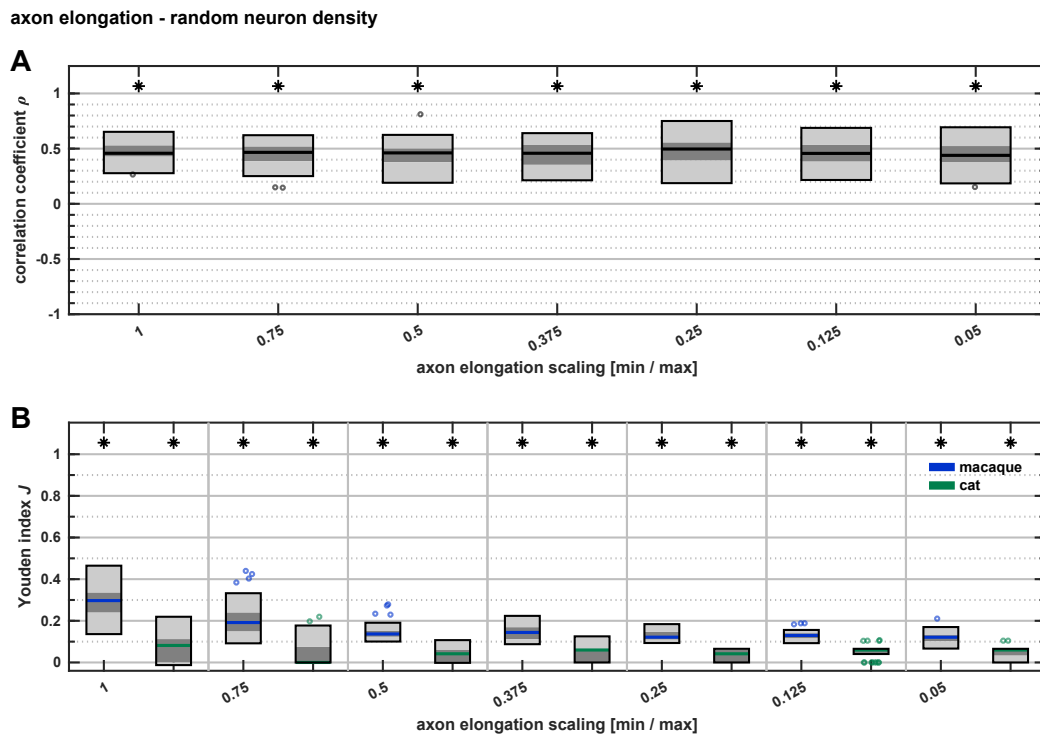


Figure C.9: Axon elongation without ordered succession of neuron density values. Results for implementation of scaling in axon elongation with randomly assigned area neuron densities. That is, this implementation lacked the ordered gradient of areas with higher neuron density forming at later points in time that was present in the other implementations. **(A)** Spearman rank correlation coefficients for the correlation between area degree (number of connections) and area neuron density, as in Figure C.7. **(B)** Classification performance for simulation-to-empirical classification performance from relative differentiation and spatial proximity, as in Figure C.8. The results of sign tests are indicated on top; black star: performance better than chance with median $p < 0.05$, red circle: performance not better than chance with median $p \geq 0.05$. Box plots show distribution across 50 simulation instances per implementation, indicating median (line), interquartile range (dark grey box), data range (light grey box) and outliers (circles, outside of 2.7 standard deviations).

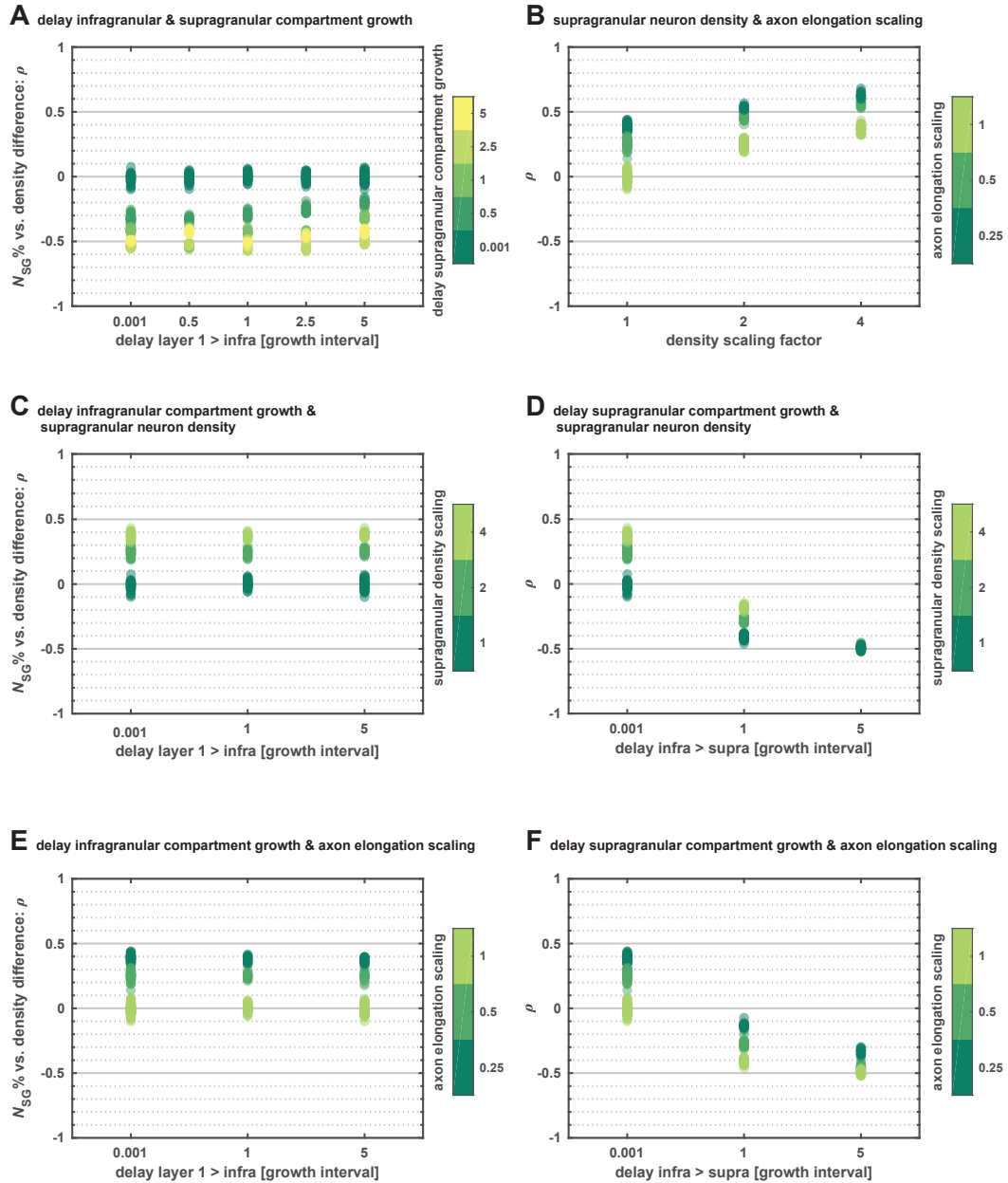


Figure C.10: Pairwise combination of features. Spearman rank correlation coefficients for the correlation between the supragranular contribution of a projection and the neuron density difference between the connected areas. We simulated implementations of all pairwise combinations of features at a reduced set of parameter values.

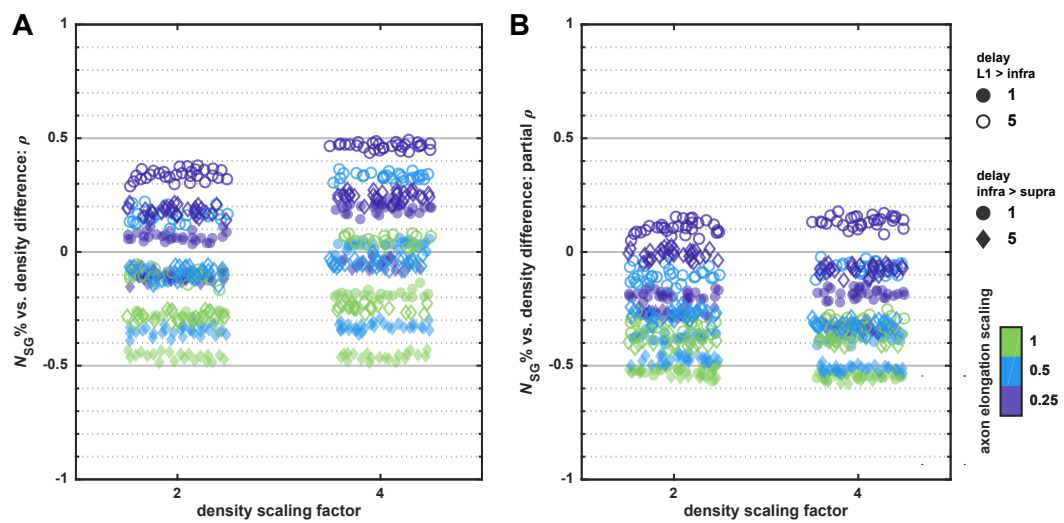


Figure C.11: Combination of all features. Spearman rank correlation coefficients for the correlation between the supragranular contribution of a projection and the neuron density difference between the connected areas. We simulated implementations of all four features simultaneously, at a reduced set of parameter values. **(A)** Correlation coefficients for the correlation of supragranular contribution values with neuron density difference between connected areas. **(B)** Partial correlation coefficients for the correlation of supragranular contribution value with neuron density difference, controlling for the supra-to-total neuron ratio (as in Figure 3.29B).

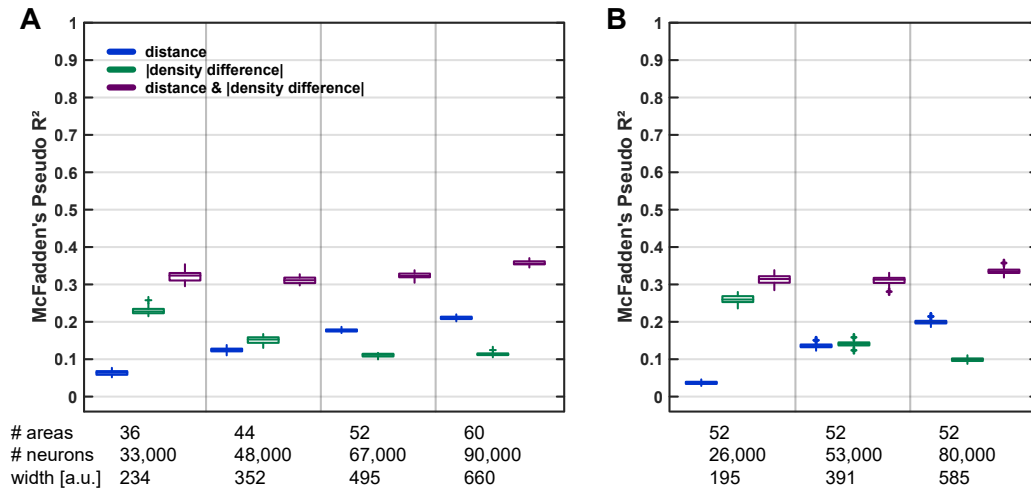


Figure C.12: Classification of connection existence using logistic regression in simulated cortical sheets of different sizes. We simulated at least 50 instances of seven implementations of the realistically oriented density gradient 1D 2rows 2origins growth layout. Across seven different implementations of the *in silico* model we varied the number of neurons populating the simulated cortical sheet, thereby changing its spatial extent. For four implementations (**A**), we scaled the number of cortical areas with the square root of the number of neurons (specifically, number of areas equalled the square root of the number of neurons divided by 5, to reach an appropriate range for the number of areas), as suggested by Braitenberg (2001) for a hypothetical scheme of cortical connectivity. For three further implementations (**B**), we kept the number of areas constant and effectively increased area sizes by adding more neurons. Number of areas, approximate number of neurons and approximate width of the cortical sheet for each implementation are given below the abscissa. The logistic regressions were performed analogous to those shown in Figure 3.23, as described in Section 2.4.4.2. While spatial distance (blue) did not contribute substantially to the classification of connection existence in small cortical sheets, its contribution to classification performance increased as the spatial extent (denoted here by arbitrary units, a.u.) of the simulated cortical sheet increased. The rise in spatial proximity's predictive power occurred irrespective of whether the expansion of the cortical sheet coincided with an increase in the number of cortical areas (**A**) or not (**B**).

Supplementary tables

1	area 1	DLS	dorsolateral suprasylvian area
2	area 2	DP	dorsoposterior auditory field
4	area 4	EPp	posterior part of the posterior ectosylvian gyrus
7	area 7	ER	entorhinal cortex
17	area 17	Hipp	hippocampus proper
18	area 18	Ia	agranular insula
19	area 19	Ig	granular insula
35	area 35	IL	infralimbic area
36	area 36	LA	anterior limbic cortex
20a	area 20a	P	posterior auditory field
20b	area 20b	PFCdl	dorsolateral prefrontal cortex
21a	area 21a	PFCdm	dorsomedial prefrontal cortex
21b	area 21b	PFCr	rostral prefrontal cortex
3a	area 3a	PFCv	ventral prefrontal cortex
3b	area 3b	PL	prelimbic area
4g	area 4 _γ	PLLS	posterolateral lateral suprasylvian area
5al	lateral area 5a	PMLS	posteromedial lateral suprasylvian area
5am	medial area 5a	POA	presylvian oculomotor area
5bl	lateral area 5b	PS	posterior suprasylvian area
5bm	medial area 5b	pSb	presubiculum, parasubiculum, and postsubicular cortex
5m	medial area 5	RS	retrosplenial cortex
6l	lateral area 6	Sb	subiculum
6m	medial area 6	SII	second somatosensory area
AAF	anterior auditory field	SIV	fourth somatosensory area
AES	anterior ectosylvian sulcus	SSAi	inner (deep) suprasylvian sulcal region of area 5
AI	primary auditory field	SSAo	outer suprasylvian sulcal region of area 5
AII	secondary auditory field	SSF	suprasylvian fringe
ALG	anterolateral gyrus	SVA	splenial visual area
ALLS	anterolateral lateral suprasylvian area	Tem	temporal auditory field
AMLS	anteromedial lateral suprasylvian area	V	ventral auditory field
Amyg	amygdala	VLS	ventrolateral suprasylvian area
CGa	anterior cingulate cortex	VP	ventroposterior auditory field
CGp	posterior cingulate cortex		

Table D.1: Anatomical abbreviations in the cat cortex.

Appendix D. Supplementary tables

Source area	Target area	Connection strength	Border distance	Type difference	Level difference	Source area	Target area	Connection strength	Border distance	Type difference	Level difference	Source area	Target area	Connection strength	Border distance	Type difference	Level difference
17	18	3	1	0	-1	PS	PFCr	0	4	-	-	PMLS	ALG	0	2	-	-
17	PS	0	3	4	-3	PS	PFCdl	1	3	-2	-	PMLS	6l	1	4	3	-
17	VLS	2	4	2	-2	PS	PFCv	1	3	0	-	PMLS	5Am	0	3	2	-
17	19	3	2	1	-3	PS	PFCdm	1	4	-1	-	PMLS	5AI	0	3	2	-
17	PMLS	3	3	1	-4	PS	IG	2	2	0	-	PMLS	5Bm	0	2	2	-
17	SVA	0	1	3	-4	PS	LA	1	4	-	-	PMLS	5BI	2	2	1	-
17	21a	2	3	1	-6	VLS	17	0	4	-2	2	PMLS	5m	0	2	-	-
17	PLLS	1	4	2	-5	VLS	18	1	3	-2	1	PMLS	SSAo	0	2	2	-
17	ALLS	0	4	2	-7	VLS	19	1	2	-1	-1	PMLS	SSAI	0	2	2	-
17	AMLS	2	3	2	-8	VLS	PMLS	3	1	-1	-2	PMLS	PFCr	0	5	-	-
17	20a	3	2	4	-7	VLS	21a	0	1	-1	-4	PMLS	PFCdl	0	5	1	-
17	DLS	0	4	2	-8	VLS	PLLS	0	2	0	-3	PMLS	IA	1	4	-	-
17	21b	2	3	2	-8	VLS	20a	2	2	2	-5	PMLS	IG	1	4	3	-
17	20b	0	2	4	-9	VLS	DLS	2	1	0	-6	SVA	17	0	1	-3	4
17	7	0	2	3	-10	VLS	7	0	2	1	-8	SVA	18	0	1	-3	3
17	AES	0	5	3	-9	VLS	CGA	1	3	2	-9	SVA	19	3	2	-2	1
17	ALG	0	3	-	-	VLS	AES	1	4	1	-7	SVA	PMLS	1	3	-2	0
17	4g	0	3	3	-	VLS	EPp	1	2	0	-	SVA	21a	0	3	-2	-2
17	6m	0	2	3	-	19	17	3	2	-1	3	SVA	PLLS	1	4	-1	-1
17	5Am	0	3	3	-	19	18	3	1	-1	2	SVA	AMLS	1	3	-1	-4
17	5AI	0	4	3	-	19	PS	0	2	3	0	SVA	20a	2	2	1	-3
17	5Bm	0	3	3	-	19	VLS	2	2	1	1	SVA	DLS	0	4	-1	-4
17	5BI	0	3	2	-	19	PMLS	3	2	0	-1	SVA	20b	2	1	1	-5
17	5m	0	2	-	-	19	SVA	3	2	2	-1	SVA	7	3	2	0	-6
17	SSAo	0	4	3	-	19	21a	3	1	0	-3	SVA	CGP	2	1	1	-6
17	SSAI	0	4	3	-	19	PLLS	2	3	1	-2	SVA	CGA	2	1	1	-7
18	17	3	1	0	1	19	ALLS	1	3	1	-4	SVA	SSF	1	4	-	-
18	PS	0	2	4	-2	19	AMLS	2	2	1	-5	SVA	5Am	0	3	0	-
18	VLS	1	3	2	-1	19	20a	3	1	3	-4	SVA	5AI	1	4	0	-
18	19	3	1	1	-2	19	DLS	2	2	1	-5	SVA	5Bm	0	3	0	-
18	PMLS	3	2	1	-3	19	21b	1	1	1	-5	SVA	5BI	2	3	-1	-
18	SVA	0	1	3	-3	19	20b	1	2	3	-6	SVA	5m	1	2	-	-
18	21a	2	2	1	-5	19	7	2	1	2	-7	SVA	SSAo	2	4	0	-
18	PLLS	1	3	2	-4	19	CGP	0	3	3	-7	SVA	LA	1	2	-	-
18	ALLS	1	3	2	-6	19	CGA	0	2	3	-8	21a	17	3	3	-1	6
18	AMLS	3	2	2	-7	19	AES	0	5	2	-6	21a	18	3	2	-1	5
18	20a	2	1	4	-6	19	ALG	3	1	-	-	21a	PS	0	2	3	3
18	DLS	0	3	2	-7	19	SSF	1	3	-	-	21a	VLS	0	1	1	4
18	21b	2	2	2	-7	19	EPp	1	2	1	-	21a	19	3	1	0	3
18	20b	0	1	4	-8	19	4g	0	4	2	-	21a	PMLS	1	1	0	2
18	7	1	1	3	-9	19	6l	1	4	3	-	21a	SVA	0	3	2	2
18	AES	0	5	3	-8	19	6m	0	3	2	-	21a	PLLS	1	2	1	1
18	ALG	0	2	-	-	19	5Am	0	3	2	-	21a	ALLS	0	3	1	-1
18	4g	0	3	3	-	19	5AI	1	3	2	-	21a	AMLS	2	2	1	-2
18	5Am	0	3	3	-	19	5Bm	1	2	2	-	21a	20a	2	2	3	-1
18	5AI	0	3	3	-	19	5BI	2	2	1	-	21a	DLS	0	2	1	-2
18	5Bm	0	2	3	-	19	5m	0	2	-	-	21a	21b	2	1	1	-2
18	5BI	1	2	2	-	19	SSAo	0	3	2	-	21a	20b	0	3	3	-3
18	5m	0	2	-	-	19	SSAI	0	3	2	-	21a	7	2	1	2	-4
18	SSAo	0	3	3	-	19	IA	0	4	-	-	21a	AES	0	5	2	-3
18	SSAI	0	3	3	-	19	IG	0	4	3	-	21a	35	2	4	3	-6
PS	17	0	3	-4	3	PMLS	17	3	3	-1	4	21a	36	1	3	3	-6
PS	18	0	2	-4	2	PMLS	18	2	2	-1	3	21a	ALG	0	1	-	-
PS	19	1	2	-3	0	PMLS	PS	0	3	3	1	21a	EPp	1	2	1	-
PS	PMLS	1	3	-3	-1	PMLS	VLS	3	1	1	2	21a	5Am	0	3	2	-
PS	SVA	1	2	-1	-1	PMLS	19	3	2	0	1	21a	5AI	1	3	2	-
PS	21a	1	2	-3	-3	PMLS	SVA	0	3	2	0	21a	5Bm	0	2	2	-
PS	PLLS	3	3	-2	-2	PMLS	21a	1	1	0	-2	21a	5BI	2	2	1	-
PS	ALLS	0	3	-2	-4	PMLS	PLLS	2	1	1	-1	21a	5m	0	2	-	-
PS	AMLS	1	4	-2	-5	PMLS	ALLS	0	2	1	-3	21a	SSAo	0	3	2	-
PS	20a	2	1	0	-4	PMLS	AMLS	2	1	1	-4	21a	SSAI	0	3	2	-
PS	21b	1	1	-2	-5	PMLS	20a	3	3	3	-3	PLLS	17	1	4	-2	5
PS	20b	2	1	0	-6	PMLS	DLS	0	2	1	-4	PLLS	18	2	3	-2	4
PS	7	1	3	-1	-7	PMLS	21b	1	2	1	-4	PLLS	PS	3	3	2	2
PS	CGA	1	3	0	-8	PMLS	20b	0	3	3	-5	PLLS	VLS	1	2	0	3
PS	AES	2	3	-1	-6	PMLS	7	0	1	2	-6	PLLS	19	1	3	-1	2
PS	35	1	2	0	-9	PMLS	CGA	1	2	3	-7	PLLS	PMLS	1	1	-1	1
PS	36	2	1	0	-9	PMLS	AES	1	4	2	-5	PLLS	SVA	0	4	1	1
PS	SSF	2	2	-	-	PMLS	35	1	4	3	-8	PLLS	21a	0	2	-1	-1

Table D.2: Projection data and structural measures in the cat cortex.

Appendix D. Supplementary tables

Source area	Target area	Connection strength	Border distance	Type difference	Level difference	Source area	Target area	Connection strength	Border distance	Type difference	Level difference	Source area	Target area	Connection strength	Border distance	Type difference	Level difference
PLLS	ALLS	2	1	0	-2	AMLS	7	2	1	1	-2	DLS	Epp	2	1	0	-
PLLS	AMLS	1	2	0	-3	AMLS	CGA	1	2	2	-3	DLS	IA	2	3	-	-
PLLS	20a	2	3	2	-2	AMLS	AES	1	3	1	-1	DLS	IG	2	3	2	-
PLLS	DLS	3	1	0	-3	AMLS	ALG	1	2	-	-	21b	17	2	3	-2	8
PLLS	21b	0	2	0	-3	AMLS	4g	1	4	1	-	21b	18	2	2	-2	7
PLLS	20b	0	4	2	-4	AMLS	4	1	3	2	-	21b	VLS	1	1	0	6
PLLS	7	1	2	1	-5	AMLS	6m	1	3	1	-	21b	19	1	1	-1	5
PLLS	CGA	1	3	2	-6	AMLS	5Am	1	3	1	-	21b	PMLS	1	2	-1	4
PLLS	AES	3	3	1	-4	AMLS	5AI	2	2	1	-	21b	21a	2	1	-1	2
PLLS	35	1	5	2	-7	AMLS	5Bm	1	2	1	-	21b	PLLS	0	2	0	3
PLLS	ALG	0	3	-	-	AMLS	5BI	2	2	0	-	21b	AMLS	0	3	0	0
PLLS	EPp	2	2	0	-	AMLS	5m	1	2	-	-	21b	20a	2	1	2	1
PLLS	6l	1	5	2	-	AMLS	SSAo	0	1	1	-	21b	DLS	1	1	0	0
PLLS	6m	1	4	1	-	AMLS	SSAi	1	1	1	-	21b	20b	0	2	2	-1
PLLS	5Am	0	4	1	-	AMLS	PFCr	0	5	-	-	21b	7	2	2	1	-2
PLLS	5AI	0	3	1	-	AMLS	PFCdl	0	5	0	-	21b	35	2	3	2	-4
PLLS	5Bm	0	3	1	-	AMLS	LA	1	3	-	-	21b	36	1	2	2	-4
PLLS	5BI	1	3	0	-	20a	17	3	2	-4	7	21b	EPp	1	1	0	-
PLLS	5m	0	3	-	-	20a	18	2	1	-4	6	21b	5Am	0	4	1	-
PLLS	SSAo	0	2	1	-	20a	PS	0	1	0	4	21b	5AI	1	4	1	-
PLLS	SSAi	0	2	1	-	20a	VLS	2	2	-2	5	21b	5Bm	0	3	1	-
PLLS	PFCr	0	6	-	-	20a	19	3	1	-3	4	21b	5BI	2	3	0	-
PLLS	PFCdl	1	5	0	-	20a	PMLS	3	3	-3	3	21b	5m	0	3	-	-
PLLS	PFCv	0	5	2	-	20a	SVA	0	2	-1	3	21b	SSAo	0	4	1	-
PLLS	PFCdm	1	5	1	-	20a	21a	2	2	-3	1	21b	SSAi	0	3	1	-
PLLS	IA	1	4	-	-	20a	PLLS	1	3	-2	2	20b	17	0	2	-4	9
PLLS	IG	2	3	2	-	20a	ALLS	0	4	-2	0	20b	18	0	1	-4	8
ALLS	17	0	4	-2	7	20a	AMLS	0	3	-2	-1	20b	PS	2	1	0	6
ALLS	18	0	3	-2	6	20a	DLS	0	2	-2	-1	20b	VLS	0	3	-2	7
ALLS	PS	0	3	2	4	20a	21b	2	1	-2	-1	20b	19	1	2	-3	6
ALLS	VLS	1	3	0	5	20a	20b	3	1	0	-2	20b	PMLS	0	3	-3	5
ALLS	19	1	3	-1	4	20a	7	2	2	-1	-3	20b	SVA	2	1	-1	5
ALLS	PMLS	0	2	-1	3	20a	CGP	2	3	0	-3	20b	21a	0	3	-3	3
ALLS	21a	0	3	-1	1	20a	AES	0	4	-1	-2	20b	PLLS	0	4	-2	4
ALLS	PLLS	2	1	0	2	20a	35	2	2	0	-5	20b	ALLS	0	4	-2	2
ALLS	AMLS	1	1	0	-1	20a	36	1	2	0	-5	20b	AMLS	1	3	-2	1
ALLS	20a	0	4	2	0	20a	ALG	0	2	-	-	20b	20a	3	1	0	2
ALLS	DLS	2	2	0	-1	20a	SSF	1	3	-	-	20b	DLS	0	3	-2	1
ALLS	20b	0	4	2	-2	20a	EPp	2	2	-2	-	20b	7	2	2	-1	-1
ALLS	7	1	2	1	-3	20a	6m	1	3	-1	-	20b	CGP	2	2	0	-1
ALLS	CGA	1	3	2	-4	20a	5Am	0	4	-1	-	20b	CGA	1	2	0	-2
ALLS	AES	2	3	1	-2	20a	5AI	1	4	-1	-	20b	AES	1	4	-1	0
ALLS	SSF	1	1	-	-	20a	5Bm	0	3	-1	-	20b	35	2	1	0	-3
ALLS	EPp	1	2	0	-	20a	5BI	0	3	-2	-	20b	36	1	1	0	-3
ALLS	6m	1	4	1	-	20a	5m	0	3	-	-	20b	SSF	1	3	-	-
ALLS	5Am	0	3	1	-	20a	SSAo	0	4	-1	-	20b	EPp	2	2	-2	-
ALLS	5AI	0	2	1	-	20a	SSAi	0	4	-1	-	20b	6m	1	3	-1	-
ALLS	5Bm	0	3	1	-	20a	PFCr	0	5	-	-	20b	5Am	0	4	-1	-
ALLS	5BI	2	2	0	-	20a	PFCdl	1	4	-2	-	20b	5AI	1	4	-1	-
ALLS	5m	2	3	-	-	20a	PFCv	1	4	0	-	20b	5Bm	0	3	-1	-
ALLS	SSAo	0	1	1	-	20a	PFCdm	0	4	-1	-	20b	5BI	0	3	-2	-
ALLS	SSAi	0	2	1	-	20a	IA	1	3	-	-	20b	5m	0	3	-	-
ALLS	PFCr	0	6	-	-	20a	IG	1	3	0	-	20b	SSAo	0	4	-1	-
ALLS	PFCdl	1	5	0	-	20a	RS	2	2	-1	-	20b	SSAi	0	4	-1	-
ALLS	PFCv	0	5	2	-	DLS	17	0	4	-2	8	20b	PFCr	0	4	-	-
ALLS	PFCdm	1	5	1	-	DLS	18	0	3	-2	7	20b	PFCdl	1	3	-2	-
ALLS	IG	2	3	2	-	DLS	VLS	2	1	0	6	20b	PFCv	1	3	0	-
AMLS	17	3	3	-2	8	DLS	19	0	2	-1	5	20b	PFCdm	0	4	-1	-
AMLS	18	3	2	-2	7	DLS	PMLS	0	2	-1	4	20b	IA	1	2	-	-
AMLS	PS	0	4	2	5	DLS	SVA	0	4	1	4	20b	IG	1	3	0	-
AMLS	19	2	2	-1	5	DLS	21a	0	2	-1	2	20b	LA	1	3	-	-
AMLS	PMLS	3	1	-1	4	DLS	PLLS	3	1	0	3	20b	RS	2	1	-1	-
AMLS	SVA	1	3	1	4	DLS	AMLS	0	3	0	0	7	17	0	2	-3	10
AMLS	21a	2	2	-1	2	DLS	20a	0	2	2	1	7	18	1	1	-3	9
AMLS	PLLS	0	2	0	3	DLS	21b	1	1	0	0	7	PS	0	3	1	7
AMLS	ALLS	1	1	0	1	DLS	20b	0	3	2	-1	7	VLS	0	2	-1	8
AMLS	20a	0	3	2	1	DLS	7	0	3	1	-2	7	19	2	1	-2	7
AMLS	DLS	0	3	0	0	DLS	CGA	1	4	2	-3	7	PMLS	0	1	-2	6
AMLS	20b	1	3	2	-1	DLS	AES	2	3	1	-1	7	SVA	3	2	0	6

Table D.2: Projection data and structural measures in the cat cortex (cont.). 260

Appendix D. Supplementary tables

Source area	Target area	Connection strength	Border distance	Type difference	Level difference	Source area	Target area	Connection strength	Border distance	Type difference	Level difference	Source area	Target area	Connection strength	Border distance	Type difference	Level difference
7	21a	2	1	-2	4	CGA	SSAI	1	3	-1	-	35	20b	1	1	0	3
7	PLLS	1	2	-1	5	CGA	PFCr	3	3	-	-	35	7	1	3	-1	2
7	20a	1	2	1	3	CGA	PFCdl	3	3	-2	-	35	CGP	1	3	0	2
7	DLS	0	3	-1	2	CGA	PFCv	2	3	0	-	35	CGA	2	3	0	1
7	21b	1	2	-1	2	CGA	PFCdm	3	2	-1	-	35	ER	3	1	-	-
7	20b	0	2	1	1	CGA	IA	2	2	-	-	35	36	3	1	0	0
7	CGP	3	2	1	0	CGA	IG	2	3	0	-	35	AI	1	4	-4	-
7	CGA	1	1	1	-1	CGA	LA	2	1	-	-	35	All	2	3	-3	-
7	AES	0	4	0	1	CGA	RS	2	2	-1	-	35	DP	2	4	-	-
7	35	1	3	1	-2	CGA	PL	1	2	-	-	35	P	2	4	-2	-
7	ALG	3	1	-	-	CGA	pSb	1	3	-	-	35	SSF	1	4	-	-
7	SSF	2	3	-	-	AES	17	0	5	-3	9	35	EPp	1	3	-2	-
7	EPp	2	3	-1	-	AES	18	0	5	-3	8	35	Tem	1	2	0	-
7	4g	1	3	0	-	AES	PS	2	3	1	6	35	3a	1	3	-2	-
7	6l	2	3	1	-	AES	19	0	5	-2	6	35	3b	1	2	-3	-
7	6m	3	2	0	-	AES	PMLS	1	4	-2	5	35	1	1	3	-2	-
7	5Am	1	2	0	-	AES	21a	1	5	-2	3	35	2	1	3	-2	-
7	5AI	2	2	0	-	AES	PLLS	3	3	-1	4	35	SII	1	3	-1	-
7	5Bm	2	1	0	-	AES	ALLS	2	3	-1	2	35	SIV	2	3	-1	-
7	5BI	3	1	-1	-	AES	AMLS	1	3	-1	1	35	6m	2	4	-1	-
7	5m	3	1	-	-	AES	20a	2	4	1	2	35	5Am	0	4	-1	-
7	SSAo	2	2	0	-	AES	DLS	2	3	-1	1	35	5AI	0	4	-1	-
7	SSAI	2	2	0	-	AES	20b	2	4	1	0	35	5Bm	1	4	-1	-
7	PFCr	1	4	-	-	AES	7	0	4	0	-1	35	5BI	0	4	-2	-
7	PFCdl	1	4	-1	-	AES	CGP	2	5	1	-1	35	5m	1	3	-	-
7	PFCv	0	4	1	-	AES	CGA	2	4	1	-2	35	SSAo	0	4	-1	-
7	PFCdm	1	3	0	-	AES	35	1	3	1	-3	35	SSAI	0	4	-1	-
7	IA	1	3	-	-	AES	36	1	3	1	-3	35	PFCr	1	3	-	-
7	IG	1	4	1	-	AES	SSF	1	2	-	-	35	PFCdl	1	2	-2	-
7	LA	1	2	-	-	AES	EPp	1	3	-1	-	35	PFCv	2	2	0	-
7	RS	2	3	0	-	AES	SIV	2	1	0	-	35	PFCdm	1	3	-1	-
CGP	20a	1	3	0	3	AES	4g	2	5	0	-	35	IA	3	1	-	-
CGP	20b	1	2	0	1	AES	4	1	5	1	-	35	IG	1	2	0	-
CGP	7	3	2	-1	0	AES	6l	1	4	1	-	35	LA	2	4	-	-
CGP	CGA	3	1	0	-1	AES	6m	2	5	0	-	35	RS	1	2	-1	-
CGP	AES	1	5	-1	1	AES	POA	2	3	-	-	35	PL	2	3	-	-
CGP	DP	2	5	-	-	AES	5Am	2	4	0	-	35	IL	2	2	-	-
CGP	P	2	5	-2	-	AES	5AI	2	3	0	-	35	pSb	2	2	-	-
CGP	SSF	1	5	-	-	AES	5Bm	2	5	0	-	35	Sb	2	3	-	-
CGP	EPp	3	4	-2	-	AES	5BI	0	4	-1	-	36	PS	2	1	0	9
CGP	6m	3	2	-1	-	AES	5m	2	4	-	-	36	PMLS	1	4	-3	8
CGP	POA	2	4	-	-	AES	SSAo	2	3	0	-	36	SVA	1	2	-1	8
CGP	PFCr	3	4	-	-	AES	SSAI	1	2	0	-	36	PLLS	1	4	-2	7
CGP	PFCdl	3	4	-2	-	AES	PFCr	1	4	-	-	36	ALLS	1	4	-2	5
CGP	PFCv	3	4	0	-	AES	PFCdl	2	3	-1	-	36	AMLS	1	4	-2	4
CGP	PFCdm	3	3	-1	-	AES	PFCv	0	3	1	-	36	20a	1	2	0	5
CGP	IA	2	3	-	-	AES	IA	1	2	-	-	36	20b	1	1	0	3
CGP	IG	2	4	0	-	AES	IG	2	1	1	-	36	CGP	1	3	0	2
CGP	LA	2	2	-	-	ER	20a	2	2	-	-	36	CGA	1	3	0	1
CGP	RS	1	1	-1	-	ER	20b	2	1	-	-	36	AES	2	3	-1	3
CGP	PL	1	3	-	-	ER	CGP	1	3	-	-	36	ER	2	2	-	-
CGP	pSb	1	2	-	-	ER	CGA	1	3	-	-	36	35	3	1	0	0
CGA	20a	2	2	0	4	ER	35	3	1	-	-	36	AI	1	3	-4	-
CGA	20b	2	2	0	2	ER	36	2	2	-	-	36	All	2	2	-3	-
CGA	AES	1	4	-1	2	ER	6m	1	3	-	-	36	DP	1	3	-	-
CGA	ER	2	3	-	-	ER	PFCr	1	4	-	-	36	P	0	3	-2	-
CGA	35	2	3	0	-1	ER	PFCv	2	3	-	-	36	SSF	1	3	-	-
CGA	36	1	3	0	-1	ER	PFCdm	1	3	-	-	36	EPp	2	2	-2	-
CGA	DP	2	5	-	-	ER	LA	2	3	-	-	36	Tem	3	1	0	-
CGA	P	2	5	-2	-	ER	RS	1	2	-	-	36	3a	1	3	-2	-
CGA	SSF	1	4	-	-	ER	PL	3	2	-	-	36	3b	1	2	-3	-
CGA	EPp	1	4	-2	-	ER	IL	2	1	-	-	36	1	1	3	-2	-
CGA	6m	2	1	-1	-	ER	pSb	2	1	-	-	36	2	1	3	-2	-
CGA	5Am	1	2	-1	-	ER	Sb	2	2	-	-	36	SII	1	3	-1	-
CGA	5AI	1	3	-1	-	35	PMLS	1	4	-3	8	36	SIV	1	3	-1	-
CGA	5Bm	2	2	-1	-	35	PLLS	1	5	-2	7	36	6m	1	4	-1	-
CGA	5BI	1	2	-2	-	35	ALLS	1	5	-2	5	36	5Am	0	4	-1	-
CGA	5m	1	1	-	-	35	AMLS	1	4	-2	4	36	5AI	0	4	-1	-
CGA	SSAo	2	3	-1	-	35	20a	1	2	0	5	36	5Bm	1	4	-1	-

Table D.2: Projection data and structural measures in the cat cortex (cont.). 261

Appendix D. Supplementary tables

Source area	Target area	Connection strength	Border distance	Type difference	Level difference	Source area	Target area	Connection strength	Border distance	Type difference	Level difference	Source area	Target area	Connection strength	Border distance	Type difference	Level difference
36	5BI	0	4	-2	-	DP	P	2	1	-	-	EPp	6m	2	5	1	-
36	5m	1	3	-	-	DP	VP	1	2	-	-	EPp	PFCr	0	4	-	-
36	SSAo	0	4	-1	-	DP	RS	2	4	-	-	EPp	PFCdl	1	3	0	-
36	SSAi	0	4	-1	-	P	20a	1	3	2	-	EPp	PFCv	0	3	2	-
36	PFCr	1	3	-	-	P	20b	1	3	2	-	EPp	PFCdm	1	4	1	-
36	PFCdl	1	2	-2	-	P	CGP	2	5	2	-	EPp	IA	2	2	-	-
36	PFCv	2	2	0	-	P	CGA	2	5	2	-	EPp	IG	2	2	2	-
36	PFCdm	1	3	-1	-	P	35	2	4	2	-	EPp	LA	1	5	-	-
36	IA	1	1	-	-	P	36	0	3	2	-	Tem	All	2	1	-3	-
36	IG	3	2	0	-	P	AI	3	1	-2	-	Tem	EPp	2	1	-2	-
36	LA	2	4	-	-	P	All	3	1	-1	-	Tem	PFCr	1	3	-	-
36	RS	1	2	-1	-	P	AAF	1	2	1	-	Tem	PFCdl	1	2	-2	-
36	PL	2	3	-	-	P	DP	2	1	-	-	Tem	PFCv	1	2	0	-
36	IL	2	3	-	-	P	VP	2	1	1	-	Tem	IA	2	1	-	-
36	pSb	2	2	-	-	P	V	2	1	-	-	Tem	IG	2	1	0	-
ALG	17	0	3	-	-	P	EPp	2	1	0	-	Tem	PL	2	3	-	-
ALG	18	0	2	-	-	P	Tem	1	2	2	-	3a	AES	1	4	1	-
ALG	19	3	1	-	-	P	RS	2	4	1	-	3a	3b	2	1	-1	-
ALG	PMLS	0	2	-	-	VP	CGP	1	5	1	-	3a	1	2	2	0	-
ALG	21a	0	1	-	-	VP	36	1	2	1	-	3a	2	2	2	0	-
ALG	PLLS	0	3	-	-	VP	AI	2	2	-3	-	3a	SII	3	3	1	-
ALG	AMLS	1	2	-	-	VP	All	2	2	-2	-	3a	4g	3	1	1	-
ALG	7	3	1	-	-	VP	AAF	1	3	0	-	3a	4	2	1	2	-
AI	CGP	0	6	4	-	VP	DP	2	2	-	-	3a	6l	2	1	2	-
AI	35	1	4	4	-	VP	P	2	1	-1	-	3a	5Am	3	3	1	-
AI	AII	2	1	1	-	VP	V	2	1	-	-	3a	5AI	3	3	1	-
AI	AAF	3	1	3	-	VP	EPp	2	1	-1	-	3a	5Bm	0	3	1	-
AI	DP	2	1	-	-	VP	Tem	2	1	1	-	3a	5BI	0	3	0	-
AI	P	2	1	2	-	V	EPp	1	2	-	-	3a	5m	0	2	-	-
AI	VP	2	2	3	-	SSF	PS	2	2	-	-	3a	SSAo	1	3	1	-
AI	V	3	2	-	-	SSF	7	1	3	-	-	3a	SSAi	2	3	1	-
AI	SSF	1	1	-	-	SSF	CGP	2	5	-	-	3b	AES	1	3	2	-
AI	EPp	1	2	2	-	SSF	CGA	2	4	-	-	3b	3a	2	1	1	-
AI	Tem	1	2	4	-	SSF	AES	2	2	-	-	3b	1	2	1	1	-
AII	CGP	0	5	3	-	SSF	All	1	2	-	-	3b	2	2	1	1	-
AII	AES	1	1	2	-	SSF	EPp	2	1	-	-	3b	SII	3	2	2	-
AII	35	2	3	3	-	SSF	SIV	2	2	-	-	3b	4g	2	2	2	-
AII	36	1	2	3	-	SSF	4g	1	5	-	-	3b	4	2	2	3	-
AII	AI	3	1	-1	-	SSF	4	1	5	-	-	3b	6l	2	2	3	-
AII	AAF	2	2	2	-	SSF	6l	1	5	-	-	3b	5Am	2	2	2	-
AII	P	2	1	1	-	SSF	5Am	0	4	-	-	3b	5AI	3	2	2	-
AII	SSF	2	2	-	-	SSF	5AI	2	3	-	-	3b	5Bm	1	2	2	-
AII	EPp	2	2	1	-	SSF	5Bm	0	4	-	-	3b	5BI	1	3	1	-
AII	PFCr	1	4	-	-	SSF	5BI	1	3	-	-	3b	5m	1	1	-	-
AII	PFCdl	1	3	1	-	SSF	5m	1	4	-	-	3b	SSAo	1	2	2	-
AII	PFCv	1	3	3	-	SSF	SSAo	1	2	-	-	3b	SSAi	1	2	2	-
AII	PFCdm	1	4	2	-	SSF	SSAi	2	1	-	-	1	3a	2	2	0	-
AII	IA	2	2	-	-	SSF	PFCr	1	5	-	-	1	3b	2	1	-1	-
AII	IG	2	1	3	-	SSF	PFCdl	1	4	-	-	1	2	2	1	0	-
AAF	CGP	0	5	1	-	SSF	PFCv	1	4	-	-	1	SII	3	2	1	-
AAF	CGA	0	4	1	-	SSF	PFCdm	1	5	-	-	1	4g	2	3	1	-
AAF	AES	1	1	0	-	SSF	LA	1	5	-	-	1	4	1	3	2	-
AAF	36	2	4	1	-	EPp	PS	2	1	2	-	1	6l	2	3	2	-
AAF	AI	3	1	-3	-	EPp	21a	1	2	-1	-	1	6m	1	3	1	-
AAF	AII	2	2	-2	-	EPp	20a	2	2	2	-	1	5Am	3	1	1	-
AAF	DP	2	2	-	-	EPp	21b	1	1	0	-	1	5AI	1	2	1	-
AAF	P	2	2	-1	-	EPp	20b	2	2	2	-	1	5Bm	2	2	1	-
AAF	VP	1	3	0	-	EPp	7	1	3	1	-	1	5BI	0	3	0	-
AAF	V	2	3	-	-	EPp	CGP	1	4	2	-	1	5m	2	1	-	-
AAF	SSF	2	1	-	-	EPp	CGA	1	4	2	-	1	SSAo	1	2	1	-
AAF	EPp	1	2	-1	-	EPp	AES	1	3	1	-	1	SSAi	2	2	1	-
AAF	Tem	1	3	1	-	EPp	35	2	3	2	-	2	3a	2	2	0	-
DP	20a	1	3	-	-	EPp	36	1	2	2	-	2	3b	2	1	-1	-
DP	20b	1	3	-	-	EPp	AI	1	2	-2	-	2	1	2	1	0	-
DP	CGP	2	5	-	-	EPp	All	1	2	-1	-	2	SII	3	1	1	-
DP	CGA	2	5	-	-	EPp	P	2	1	0	-	2	4g	2	3	1	-
DP	35	2	4	-	-	EPp	VP	2	1	1	-	2	4	1	3	2	-
DP	36	1	3	-	-	EPp	V	1	2	-	-	2	6l	2	3	2	-
DP	All	2	2	-	-	EPp	SSF	2	1	-	-	2	6m	1	3	1	-

Table D.2: Projection data and structural measures in the cat cortex (cont.). 262

Source area	Target area	Connection strength	Border distance	Type difference	Level difference	Source area	Target area	Connection strength	Border distance	Type difference	Level difference	Source area	Target area	Connection strength	Border distance	Type difference	Level difference
2	5Am	2	2	1	-	4g	5BI	2	4	-1	-	6m	LA	2	1	-	-
2	5AI	2	1	1	-	4g	5m	2	3	-	-	6m	PL	2	1	-	-
2	5Bm	0	3	1	-	4g	SSAo	2	4	0	-	6m	IL	2	2	-	-
2	5BI	2	2	0	-	4g	SSAi	2	4	0	-	POA	20a	1	4	-	-
2	5m	2	2	-	-	4g	LA	2	2	-	-	POA	20b	1	3	-	-
2	SSAo	2	1	1	-	4	CGA	2	1	0	-	POA	7	2	4	-	-
2	SSAi	1	1	1	-	4	AES	1	5	-1	-	POA	CGP	2	4	-	-
2	IA	1	2	-	-	4	ER	1	4	-	-	POA	AES	2	3	-	-
2	IG	1	1	2	-	4	35	1	4	0	-	POA	SII	1	3	-	-
SII	AES	2	1	0	-	4	36	1	4	0	-	POA	SIV	2	3	-	-
SII	35	1	3	1	-	4	3a	2	1	-2	-	POA	6m	2	2	-	-
SII	36	1	3	1	-	4	3b	2	2	-3	-	POA	IA	1	1	-	-
SII	3a	3	3	-1	-	4	1	2	3	-2	-	POA	IG	2	2	-	-
SII	3b	3	2	-2	-	4	2	2	3	-2	-	5Am	7	1	2	0	-
SII	1	3	2	-1	-	4	SII	2	4	-1	-	5Am	CGA	1	2	1	-
SII	2	3	1	-1	-	4	4g	2	1	-1	-	5Am	AES	1	4	0	-
SII	SIV	1	1	0	-	4	6I	2	2	0	-	5Am	SIV	2	4	0	-
SII	4g	3	4	0	-	4	5Am	2	3	-1	-	5Am	4g	2	4	0	-
SII	4	3	4	1	-	4	5AI	1	4	-1	-	5Am	4	2	3	1	-
SII	6I	2	4	1	-	4	5Bm	2	3	-1	-	5Am	6I	0	4	1	-
SII	6m	1	4	0	-	4	5BI	1	3	-2	-	5Am	6m	1	3	0	-
SII	POA	2	3	-	-	4	5m	2	2	-	-	5Am	5AI	1	1	0	-
SII	5Am	2	3	0	-	4	SSAo	1	4	-1	-	5Am	5Bm	3	1	0	-
SII	5AI	1	2	0	-	4	SSAi	1	4	-1	-	5Am	5BI	0	2	-1	-
SII	5Bm	2	4	0	-	4	LA	2	2	-	-	5Am	5m	2	1	-	-
SII	5BI	0	3	-1	-	6I	20a	1	4	0	-	5Am	SSAo	2	2	0	-
SII	5m	2	3	-	-	6I	20b	1	4	0	-	5Am	SSAi	2	3	0	-
SII	SSAo	0	2	0	-	6I	7	2	3	-1	-	5Am	PFCr	0	5	-	-
SII	SSAi	3	1	0	-	6I	CGA	3	2	0	-	5Am	PFCv	0	4	1	-
SII	IA	1	2	-	-	6I	EPp	1	4	-2	-	5Am	PFCdm	0	4	0	-
SII	IG	1	1	1	-	6I	SIV	2	4	-1	-	5Am	IA	1	3	-	-
SIV	CGA	1	4	1	-	6I	6m	3	1	-1	-	5Am	LA	1	3	-	-
SIV	AES	2	1	0	-	6I	5Am	0	4	-1	-	5AI	19	1	3	-2	-
SIV	35	1	3	1	-	6I	5AI	2	4	-1	-	5AI	20a	1	4	1	-
SIV	36	2	3	1	-	6I	5Bm	1	4	-1	-	5AI	20b	1	4	1	-
SIV	SSF	2	2	-	-	6I	5BI	2	4	-2	-	5AI	7	2	2	0	-
SIV	3b	1	3	-2	-	6I	5m	1	3	-	-	5AI	CGA	1	3	1	-
SIV	4g	1	5	0	-	6I	SSAo	1	4	-1	-	5AI	AES	1	3	0	-
SIV	4	1	5	1	-	6I	SSAi	1	4	-1	-	5AI	SII	1	2	0	-
SIV	6I	2	4	1	-	6I	PFCr	1	1	-	-	5AI	SIV	2	3	0	-
SIV	6m	2	5	0	-	6I	PFCdl	2	1	-2	-	5AI	4g	2	4	0	-
SIV	POA	2	3	-	-	6I	PFCv	1	2	0	-	5AI	4	1	4	1	-
SIV	5Am	2	4	0	-	6I	PFCdm	1	2	-1	-	5AI	6I	2	4	1	-
SIV	5AI	2	3	0	-	6I	LA	2	2	-	-	5AI	6m	1	4	0	-
SIV	5Bm	2	5	0	-	6I	PL	2	2	-	-	5AI	5Am	2	1	0	-
SIV	5BI	0	4	-1	-	6m	7	3	2	0	-	5AI	5Bm	1	2	0	-
SIV	5m	2	4	-	-	6m	CGP	3	2	1	-	5AI	5BI	2	1	-1	-
SIV	SSAo	1	3	0	-	6m	CGA	3	1	1	-	5AI	5m	2	2	-	-
SIV	SSAi	2	2	0	-	6m	AES	1	5	0	-	5AI	SSAo	2	1	0	-
SIV	PFCr	0	4	-	-	6m	ER	1	3	-	-	5AI	SSAi	0	2	0	-
SIV	PFCdl	1	3	-1	-	6m	35	1	4	1	-	5AI	PFCr	0	5	-	-
SIV	PFCv	1	3	1	-	6m	36	1	4	1	-	5AI	PFCdl	1	4	-1	-
SIV	PFCdm	1	4	0	-	6m	EPp	1	5	-1	-	5AI	PFCv	0	4	1	-
SIV	IA	2	2	-	-	6m	SIV	2	5	0	-	5AI	PFCdm	0	5	0	-
SIV	IG	2	1	1	-	6m	4g	1	1	0	-	5AI	IA	1	3	-	-
SIV	LA	1	5	-	-	6m	6I	3	1	1	-	5AI	LA	1	4	-	-
4g	CGA	2	2	1	-	6m	5Am	1	3	0	-	5Bm	19	1	2	-2	-
4g	AES	1	5	0	-	6m	5AI	1	4	0	-	5Bm	7	2	1	0	-
4g	3a	2	1	-1	-	6m	5Bm	1	3	0	-	5Bm	CGA	1	2	1	-
4g	3b	2	2	-2	-	6m	5BI	2	3	-1	-	5Bm	AES	1	5	0	-
4g	1	2	3	-1	-	6m	5m	1	2	-	-	5Bm	SII	2	4	0	-
4g	2	2	3	-1	-	6m	SSAo	2	4	0	-	5Bm	SIV	2	5	0	-
4g	SII	2	4	0	-	6m	SSAi	0	4	0	-	5Bm	4g	2	4	0	-
4g	4	2	1	1	-	6m	PFCr	1	2	-	-	5Bm	4	2	3	1	-
4g	6I	2	1	1	-	6m	PFCdl	2	2	-1	-	5Bm	6I	1	4	1	-
4g	6m	2	1	0	-	6m	PFCv	0	2	1	-	5Bm	6m	1	3	0	-
4g	5Am	3	4	0	-	6m	PFCdm	2	1	0	-	5Bm	5Am	3	1	0	-
4g	5AI	3	4	0	-	6m	IA	2	3	-	-	5Bm	5AI	2	2	0	-
4g	5Bm	3	4	0	-	6m	IG	2	4	1	-	5Bm	5BI	2	1	-1	-

Table D.2: Projection data and structural measures in the cat cortex (cont.). 263

Appendix D. Supplementary tables

Source area	Target area	Connection strength	Border distance	Type difference	Level difference	Source area	Target area	Connection strength	Border distance	Type difference	Level difference	Source area	Target area	Connection strength	Border distance	Type difference	Level difference
5Bm	5m	2	1	-	-	SSAo	PFCdm	0	5	0	-	PFCv	CGP	3	4	0	-
5Bm	SSAo	2	2	0	-	SSAo	IA	1	3	-	-	PFCv	CGA	2	3	0	-
5Bm	SSAi	2	3	0	-	SSAo	LA	1	4	-	-	PFCv	ER	1	3	-	-
5Bm	PFCr	0	5	-	-	SSAi	7	1	2	0	-	PFCv	SSF	1	4	-	-
5Bm	PFCdl	0	4	-1	-	SSAi	CGA	1	3	1	-	PFCv	EPp	1	3	-2	-
5Bm	PFCv	0	4	1	-	SSAi	AES	1	2	0	-	PFCv	5Am	0	4	-1	-
5Bm	PFCdm	0	4	0	-	SSAi	SSF	2	1	-	-	PFCv	5Bm	0	4	-1	-
5Bm	IA	1	3	-	-	SSAi	3b	1	2	-2	-	PFCv	5m	0	3	-	-
5Bm	LA	1	3	-	-	SSAi	SII	2	1	0	-	PFCv	SSAo	0	4	-1	-
5BI	19	1	2	-1	-	SSAi	SIV	2	2	0	-	PFCv	SSAi	0	4	-1	-
5BI	7	2	1	1	-	SSAi	4g	2	4	0	-	PFCv	PFCr	2	1	-	-
5BI	CGA	1	2	2	-	SSAi	4	1	4	1	-	PFCv	PFCdl	2	1	-2	-
5BI	SSF	1	3	-	-	SSAi	6l	1	4	1	-	PFCv	PFCdm	2	1	-1	-
5BI	4g	2	4	1	-	SSAi	5Am	2	3	0	-	PFCv	IA	2	1	-	-
5BI	4	1	3	2	-	SSAi	5AI	2	2	0	-	PFCv	IG	1	2	0	-
5BI	6l	2	4	2	-	SSAi	5Bm	2	3	0	-	PFCv	LA	1	2	-	-
5BI	6m	2	3	1	-	SSAi	5BI	1	2	-1	-	PFCv	RS	1	4	-1	-
5BI	5Am	0	2	1	-	SSAi	5m	2	3	-	-	PFCv	IL	1	2	-	-
5BI	5AI	3	1	1	-	SSAi	SSAo	1	1	0	-	PFCdm	PS	1	4	1	-
5BI	5Bm	2	1	1	-	SSAi	PFCr	0	5	-	-	PFCdm	7	1	3	0	-
5BI	5m	2	2	-	-	SSAi	PFCdl	0	4	-1	-	PFCdm	CGP	3	3	1	-
5BI	SSAo	2	1	1	-	SSAi	PFCv	0	4	1	-	PFCdm	CGA	3	2	1	-
5BI	SSAi	1	2	1	-	SSAi	PFCdm	0	5	0	-	PFCdm	ER	1	3	-	-
5BI	PFCr	0	5	-	-	SSAi	IA	1	3	-	-	PFCdm	SSF	1	5	-	-
5BI	PFCdl	1	5	0	-	SSAi	LA	1	4	-	-	PFCdm	EPp	1	4	-1	-
5BI	PFCv	0	5	2	-	PFCr	7	1	4	-	-	PFCdm	5Am	0	4	0	-
5BI	PFCdm	0	4	1	-	PFCr	CGP	3	4	-	-	PFCdm	5Bm	0	4	0	-
5BI	IA	1	4	-	-	PFCr	CGA	3	3	-	-	PFCdm	5m	0	3	-	-
5BI	LA	1	3	-	-	PFCr	AES	1	4	-	-	PFCdm	SSAo	0	5	0	-
5m	7	2	1	-	-	PFCr	SSF	1	5	-	-	PFCdm	SSAi	0	5	0	-
5m	CGA	1	1	-	-	PFCr	5Am	0	5	-	-	PFCdm	PFCr	2	1	-	-
5m	AES	1	4	-	-	PFCr	5Bm	0	5	-	-	PFCdm	PFCdl	2	2	-1	-
5m	SSF	1	4	-	-	PFCr	5m	0	4	-	-	PFCdm	PFCv	1	1	1	-
5m	SIV	1	4	-	-	PFCr	SSAo	0	5	-	-	PFCdm	IA	2	2	-	-
5m	4g	2	3	-	-	PFCr	SSAi	0	5	-	-	PFCdm	IG	2	3	1	-
5m	4	2	2	-	-	PFCr	PFCdl	2	1	-	-	PFCdm	LA	2	2	-	-
5m	6l	1	3	-	-	PFCr	PFCv	1	1	-	-	PFCdm	RS	1	4	0	-
5m	6m	1	2	-	-	PFCr	PFCdm	2	1	-	-	PFCdm	PL	2	1	-	-
5m	5Am	2	1	-	-	PFCr	IA	2	2	-	-	PFCdm	IL	1	2	-	-
5m	5AI	2	2	-	-	PFCr	IG	2	3	-	-	IA	17	0	3	-	-
5m	5Bm	2	1	-	-	PFCr	LA	1	3	-	-	IA	18	0	3	-	-
5m	5BI	0	2	-	-	PFCr	RS	2	5	-	-	IA	PS	1	2	-	-
5m	SSAo	1	3	-	-	PFCdl	PS	1	3	2	-	IA	PLLS	1	4	-	-
5m	SSAi	1	3	-	-	PFCdl	20a	1	4	2	-	IA	ALLS	1	4	-	-
5m	PFCr	0	4	-	-	PFCdl	20b	1	3	2	-	IA	CGP	2	3	-	-
5m	PFCdl	0	3	-	-	PFCdl	7	1	4	1	-	IA	CGA	2	2	-	-
5m	PFCv	0	3	-	-	PFCdl	CGP	3	4	2	-	IA	AES	1	2	-	-
5m	PFCdm	0	3	-	-	PFCdl	CGA	3	3	2	-	IA	ER	1	2	-	-
5m	IA	1	2	-	-	PFCdl	AES	1	3	1	-	IA	35	3	1	-	-
5m	LA	1	2	-	-	PFCdl	SSF	1	4	-	-	IA	36	1	1	-	-
SSAo	7	2	2	0	-	PFCdl	EPp	1	3	0	-	IA	AI	1	3	-	-
SSAo	CGA	1	3	1	-	PFCdl	5Am	0	4	1	-	IA	AI1	1	2	-	-
SSAo	AES	1	3	0	-	PFCdl	5AI	1	4	1	-	IA	EPp	2	2	-	-
SSAo	SSF	1	2	-	-	PFCdl	5Bm	0	4	1	-	IA	SII	1	2	-	-
SSAo	3b	1	2	-2	-	PFCdl	5BI	1	5	0	-	IA	SIV	1	2	-	-
SSAo	SIV	1	3	0	-	PFCdl	5m	0	3	-	-	IA	6m	2	3	-	-
SSAo	4g	2	4	0	-	PFCdl	SSAo	0	4	1	-	IA	5Am	1	3	-	-
SSAo	4	1	4	1	-	PFCdl	SSAi	0	4	1	-	IA	5AI	2	3	-	-
SSAo	6l	1	4	1	-	PFCdl	PFCr	3	1	-	-	IA	5Bm	1	3	-	-
SSAo	6m	2	4	0	-	PFCdl	PFCv	1	1	2	-	IA	5BI	1	4	-	-
SSAo	5Am	3	2	0	-	PFCdl	PFCdm	2	2	1	-	IA	5m	1	2	-	-
SSAo	5AI	3	1	0	-	PFCdl	IA	2	1	-	-	IA	SSAo	1	3	-	-
SSAo	5Bm	1	2	0	-	PFCdl	IG	2	2	2	-	IA	SSAi	1	3	-	-
SSAo	5BI	2	1	-1	-	PFCdl	LA	2	3	-	-	IA	PFCr	2	2	-	-
SSAo	5m	2	3	-	-	PFCdl	RS	1	4	1	-	IA	PFCdl	2	1	-	-
SSAo	SSAi	2	1	0	-	PFCdl	PL	2	2	-	-	IA	PFCv	2	1	-	-
SSAo	PFCr	0	5	-	-	PFCv	PS	1	3	0	-	IA	PFCdm	2	2	-	-
SSAo	PFCdl	0	4	-1	-	PFCv	20a	1	4	0	-	IA	LA	2	3	-	-
SSAo	PFCv	0	4	1	-	PFCv	20b	1	3	0	-	IA	PL	3	2	-	-

Table D.2: Projection data and structural measures in the cat cortex (cont.). 264

Source area	Target area	Connection strength	Border distance	Type difference	Level difference
IA	IL	1	3	-	-
IG	17	0	4	-4	-
IG	18	0	4	-4	-
IG	PS	3	2	0	-
IG	PLLS	1	3	-2	-
IG	ALLS	1	3	-2	-
IG	7	1	4	-1	-
IG	CGP	2	4	0	-
IG	CGA	2	3	0	-
IG	AES	2	1	-1	-
IG	ER	1	3	-	-
IG	35	2	2	0	-
IG	36	3	2	0	-
IG	AI	1	2	-4	-
IG	AII	1	1	-3	-
IG	EPp	2	2	-2	-
IG	SII	1	1	-1	-
IG	SIV	2	1	-1	-
IG	4g	1	4	-1	-
IG	4	1	4	0	-
IG	6l	1	3	0	-
IG	6m	2	4	-1	-
IG	5Am	1	3	-1	-
IG	5AI	2	2	-1	-
IG	5Bm	1	4	-1	-
IG	5BI	1	3	-2	-
IG	5m	1	3	-	-
IG	SSAo	1	2	-1	-
IG	SSAI	1	2	-1	-
IG	PFCr	2	3	-	-
IG	PFCdl	3	2	-2	-
IG	PFCv	1	2	0	-
IG	PFCdm	2	3	-1	-
IG	LA	2	4	-	-
IG	PL	2	3	-	-
IG	IL	2	4	-	-
LA	CGP	2	2	-	-
LA	CGA	2	1	-	-
LA	P	0	6	-	-
LA	5Am	1	3	-	-
LA	5AI	1	4	-	-
LA	5Bm	2	3	-	-
LA	5BI	1	3	-	-
LA	5m	1	2	-	-
LA	SSAo	2	4	-	-
LA	SSAI	1	4	-	-
LA	PFCr	2	3	-	-
LA	PFCdl	2	3	-	-
LA	PFCv	1	2	-	-
LA	PFCdm	2	2	-	-
LA	IA	2	3	-	-
LA	IG	2	4	-	-
LA	RS	2	3	-	-

Source area	Target area	Connection strength	Border distance	Type difference	Level difference
LA	PL	2	1	-	-
LA	IL	2	2	-	-
RS	20a	2	2	1	-
RS	20b	2	1	1	-
RS	CGP	1	1	1	-
RS	CGA	2	2	1	-
RS	ER	2	2	-	-
RS	35	2	2	1	-
RS	36	1	2	1	-
RS	DP	2	4	-	-
RS	P	2	4	-1	-
RS	PFCr	2	5	-	-
RS	PFCdl	1	4	-1	-
RS	PFCv	1	4	1	-
RS	PFCdm	1	4	0	-
RS	LA	2	3	-	-
RS	PL	1	4	-	-
PL	CGP	2	3	-	-
PL	CGA	1	2	-	-
PL	ER	1	2	-	-
PL	35	2	3	-	-
PL	36	1	3	-	-
PL	6m	2	1	-	-
PL	5Am	0	4	-	-
PL	5Bm	0	4	-	-
PL	5m	0	3	-	-
PL	SSAo	0	5	-	-
PL	SSAI	0	5	-	-
PL	PFCr	2	2	-	-
PL	PFCdl	1	2	-	-
PL	PFCv	1	1	-	-
PL	PFCdm	1	1	-	-
PL	IA	2	2	-	-
PL	LA	2	1	-	-
PL	IL	2	1	-	-
PL	Sb	1	4	-	-
IL	CGP	2	4	-	-
IL	CGA	2	3	-	-
IL	ER	2	1	-	-
IL	35	2	2	-	-
IL	36	1	3	-	-
IL	PFCr	1	3	-	-
IL	PFCdl	1	3	-	-
IL	PFCv	1	2	-	-
IL	PFCdm	1	2	-	-
IL	IA	1	3	-	-
IL	LA	2	2	-	-
IL	PL	2	1	-	-
IL	Sb	2	3	-	-
pSb	20a	1	2	-	-
pSb	20b	1	1	-	-
pSb	CGP	1	2	-	-
pSb	CGA	2	3	-	-

Source area	Target area	Connection strength	Border distance	Type difference	Level difference
pSb	ER	3	1	-	-
pSb	35	2	2	-	-
pSb	36	2	2	-	-
pSb	PFCr	1	5	-	-
pSb	PFCv	1	4	-	-
pSb	PFCdm	1	4	-	-
pSb	LA	2	4	-	-
pSb	PL	2	3	-	-
pSb	IL	1	2	-	-
pSb	Sb	2	1	-	-
Sb	20a	1	3	-	-
Sb	20b	1	2	-	-
Sb	CGA	1	4	-	-
Sb	ER	2	2	-	-
Sb	PFCr	1	6	-	-
Sb	PFCdl	1	5	-	-
Sb	PFCv	1	5	-	-
Sb	PFCdm	0	5	-	-
Sb	IA	2	4	-	-
Sb	IG	1	5	-	-
Sb	LA	2	5	-	-
Sb	RS	2	2	-	-
Sb	PL	3	4	-	-
Sb	IL	3	3	-	-
Hipp	ER	3	3	-	-
Hipp	35	1	4	-	-
Hipp	pSb	2	2	-	-
Hipp	Sb	2	1	-	-
Amyg	20a	1	3	-	-
Amyg	20b	1	2	-	-
Amyg	CGA	1	4	-	-
Amyg	ER	2	1	-	-
Amyg	35	2	1	-	-
Amyg	36	2	2	-	-
Amyg	Tem	1	3	-	-
Amyg	SII	1	4	-	-
Amyg	SIV	1	4	-	-
Amyg	4g	1	4	-	-
Amyg	4	1	4	-	-
Amyg	6l	2	4	-	-
Amyg	6m	2	3	-	-
Amyg	PFCr	2	4	-	-
Amyg	PFCdl	2	3	-	-
Amyg	PFCv	2	3	-	-
Amyg	PFCdm	2	3	-	-
Amyg	IA	2	2	-	-
Amyg	IG	2	3	-	-
Amyg	LA	1	3	-	-
Amyg	PL	3	2	-	-
Amyg	IL	2	1	-	-
Amyg	pSb	2	2	-	-
Amyg	Sb	2	3	-	-

Table D.2: Projection data and structural measures in the cat cortex (cont.). Projection data collation for the cat cortex published in Scannell and colleagues (1995) and structural measures associated with each projection. See Supplementary Table D.1 for a list of abbreviations.

Projections predicted to be absent		Source area	Target area						
		10	11	24c	13	24c	25	F6	24a
		12	11	24d	13	24d	25	F7	24a
		13	11	46d	13	46d	25	OPAI	24a
		14	11	46v	13	46v	25	OPRO	24a
		25	11	8b	13	8b	25	9	24d
		32	11	8l	13	8m	25	11	24d
		24a	11	8m	13	9/46d	25	12	24d
		24c	11	8r	13	9/46v	25	13	24d
		24d	11	9/46d	13	F3	25	14	24d
		46d	11	9/46v	13	F6	25	23	24d
		46v	11	F3	13	OPAI	25	25	24d
		8b	11	F4	13	OPRO	25	32	24d
		8l	11	F5	13	9	32	24a	24d
		8m	11	F6	13	10	32	24c	24d
		8r	11	F7	13	11	32	46d	24d
		9/46d	11	OPAI	13	12	32	46v	24d
		9/46v	11	OPRO	13	13	32	8b	24d
		F6	11	9	14	14	32	8l	24d
		F7	11	10	14	25	32	8m	24d
		9	12	11	14	24a	32	8r	24d
		10	12	12	14	24c	32	9/46d	24d
		11	12	13	14	24d	32	9/46v	24d
		13	12	25	14	46d	32	F2	24d
		14	12	32	14	46v	32	F3	24d
		25	12	24a	14	8b	32	F4	24d
		32	12	24c	14	8m	32	F6	24d
		24a	12	24d	14	9/46d	32	F7	24d
		24c	12	46d	14	F3	32	9	46v
		24d	12	46v	14	F4	32	10	46v
		46d	12	8r	14	F6	32	11	46v
		46v	12	9/46d	14	F7	32	12	46v
		8b	12	9/46v	14	OPAI	32	13	46v
		8l	12	F6	14	OPRO	32	14	46v
		8m	12	OPAI	14	9	24a	25	46v
		8r	12	24d	23	11	24a	32	46v
		9/46d	12	8b	23	12	24a	24a	46v
		9/46v	12	8l	23	13	24a	24c	46v
		F5	12	8m	23	14	24a	24d	46v
		F6	12	F1	23	25	24a	46d	46v
		F7	12	F2	23	32	24a	8b	46v
		OPAI	12	F3	23	24c	24a	8l	46v
		OPRO	12	F4	23	24d	24a	8m	46v
		9	13	9	25	46d	24a	8r	46v
		10	13	10	25	46v	24a	9/46d	46v
		11	13	11	25	8b	24a	9/46v	46v
		12	13	12	25	8m	24a	F3	46v
		14	13	13	25	9/46d	24a	F6	46v
		25	13	14	25	F2	24a	F7	46v
		32	13	32	25	F3	24a	2	8r
		24a	13	24a	25	F4	24a	9	8r

Projections predicted to be present		Source area	Target area						
		10	9	10	9	10	9	10	9
		11	9	11	9	11	9	11	9
		12	9	12	9	12	9	12	9
		13	9	13	9	13	9	13	9
		14	9	14	9	14	9	14	9
		25	9	25	9	25	9	25	9
		32	9	32	9	32	9	32	9
		24a	9	24a	9	24a	9	24a	9
		24c	9	24c	9	24c	9	24c	9
		24d	9	24d	9	24d	9	24d	9
		46d	9	46d	9	46d	9	46d	9
		46v	9	46v	9	46v	9	46v	9
		8b	9	8b	9	8b	9	8b	9
		8m	9	8m	9	8m	9	8m	9
		8r	9	8r	9	8r	9	8r	9
		9/46d	9	9/46d	9	9/46d	9	9/46d	9
		9/46v	9	9/46v	9	9/46v	9	9/46v	9
		F2	9	F2	9	F2	9	F2	9
		F3	9	F3	9	F3	9	F3	9
		F6	9	F6	9	F6	9	F6	9
		F7	9	F7	9	F7	9	F7	9
		9	11	9	11	9	11	9	11

Table D.3: Classification of unsampled projections in the macaque cortex. 266

Source area	Target area								
11	8r	32	F3	F3	F4	F7	F6	F5	peri
12	8r	24a	F3	F5	F4	5	LIP	OPRO	peri
13	8r	24c	F3	F6	F4	7a	LIP	TEad	peri
14	8r	24d	F3	F7	F4	7m	LIP	TEav	peri
24c	8r	46d	F3	OPAI	F4	DP	LIP	TH/TF	peri
24d	8r	46v	F3	OPRO	F4	STPi	LIP	ento	TEad
46d	8r	8b	F3	9	F6	V3a	LIP	peri	TEad
46v	8r	8l	F3	10	F6	12	OPAI	TEav	TEad
8b	8r	8m	F3	11	F6	13	OPAI	TEO	TEad
8l	8r	8r	F3	12	F6	14	OPAI	TH/TF	TEad
8m	8r	9/46d	F3	13	F6	25	OPAI	2	TEav
9/46d	8r	F1	F3	14	F6	32	OPAI	ento	TEav
9/46v	8r	F2	F3	25	F6	24a	OPAI	peri	TEav
F2	8r	F4	F3	32	F6	8b	OPAI	TEad	TEav
F3	8r	F6	F3	24a	F6	F4	OPAI	teo	TEav
F4	8r	F7	F3	24c	F6	OPRO	OPAI	TH/TF	TEav
F5	8r	13	F4	24d	F6	12	OPRO	ento	TH/TF
F6	8r	23	F4	46d	F6	13	OPRO	peri	TH/TF
F7	8r	32	F4	46v	F6	25	OPRO	TEad	TH/TF
OPRO	ento	24a	F4	8b	F6	32	OPRO	TEav	TH/TF
peri	ento	24d	F4	8l	F6	24a	OPRO	7m	V3a
TEad	ento	8b	F4	8m	F6	ento	OPRO	DP	V3a
TEav	ento	8l	F4	8r	F6	F4	OPRO	LIP	V3a
TH/TF	ento	8m	F4	9/46d	F6	F5	OPRO	MT	V3a
9	F3	8r	F4	9/46v	F6	OPAI	OPRO	V2	V3a
13	F3	9/46d	F4	F2	F6	peri	OPRO	V4	V3a
23	F3	F1	F4	F3	F6	2	peri		
25	F3	F2	F4	F4	F6	ento	peri		

Table D.3: Classification of unsampled projections in the macaque cortex (cont.). The status of projections not sampled in the adult macaque data set was predicted from the posterior probabilities resulting from the trained classifier (Figure 3.11). Projections were predicted to be absent if their associated $|\log\text{-ratio}_{density}|$ and Euclidean distance yielded a posterior probability for a projection to be present of $p_{\text{present}} \leq 0.15$, and predicted to be present if $p_{\text{present}} \geq 0.85$.

Appendix D. Supplementary tables

Label in M132	Label in reference	Description of sampling site in morphological measures reference	Reference
3	3b	„caudal bank of the central sulcus (Vogt and Vogt's area 3b)”	ER02
5	5	„rostral bank of the intraparietal sulcus (Brodmann's area 5, corresponding to I-II of Preuss and Goldman-Rakic)”	ER02
7a	7a	„the [...] anterior banks of the dorsal superior temporal sulcus (including areas [...] 7a)”	ER97
7b	7b	„exposed rostral portion of the inferior parietal lobule (Vogt and Vogt's area 7b)”	ER02
7m	7m	„precuneate gyrus, caudal and ventral to the tip of the cingulate sulcus [...] area 7m of Cavada and Goldman-Rakic; PGM of Pandya and Seltzer; PE of von Bonin and Bailey)”	E99a
8l, 8m	FEF	„medial portion of the anterior bank of the arcuate sulcus, which corresponds to the portion of the FEF related to the parietal visual stream. (Bullier et al., 1996)”	ER98b
9	9	„anterior lateral portion of the superior frontal gyrus (corresponding to Walker's and Petrides and Pandya's area 9 or Preuss and Goldman-Rakic's area 9d) [...], the anterior medial portion of the superior frontal gyrus (area 9m of Preuss and Goldman-Rakic, corresponding to Walker's area 9)”	E11a
9/46d	46	„medial frontal gyrus (corresponding to Walker's and Petrides and Pandya's area 46 or Preuss and Goldman-Rakic's area 46vr)”	E11a
10	10	„medial wall of the frontal pole, inferior and adjacent to the rostral extent of the cingulate sulcus (area 10)” (E00), “the medial portion of the frontal pole anterior to the rostral sulcus (corresponding to area 10 of Walker, Preuss and Goldman-Rakic and Petrides and Pandya)” (E11a)	E00, E11a
11	11	„lateral orbital gyrus adjacent to the fronto-orbital sulcus (area 11)”	E00
12	12	„inferofrontal gyrus, adjacent to the fronto-orbital sulcus (area 12 orbital [...]) Preuss and Goldman-Rakic)”	E00
13	13	„end of the orbital cortex between the medial orbital sulcus and the lateral orbital sulcus, inferior to the intermediate orbital sulcus (area 12orb of Preuss and Goldman-Rakic, corresponding to Walker's area 13 and Petrides and Pandya's area 14)”	E11a
23	Posterior cingulate	„caudal region of the cingulate gyrus (corresponding to Brodmann's area 23)”	E05
24a, 24b, 24c, 24d	Anterior cingulate	„rostral portion of the cingulate gyrus (corresponding to Brodmann's area 24)”	E05
45A	12	„inferior frontal gyrus (corresponding to Walker's area 46, Petrides and Pandya's area 45A or Preuss and Goldman-Rakic's area 12vl)”	E11a
46d, 46v	46	„the LPFC (area 46)” (C15); „caudal LPFC (Brodmann's Area 46)” (GML17)	C15, GML17
core	A1	„tissue including A1 was excised from the inferior bank of the lateral sulcus”	E10b
F1	4	„rostral bank of central sulcus (Brodmann's area 4; corresponding to 4c of Preuss et al.)”	ER02
F4	6	„exposed lateral portion of the precentral gyrus [Brodmann's area 6; corresponding to premotor area PMv of Strick (Strick, 1985) or F4 of Matelli and colleagues (Matelli et al., 1985, 1991)]”	ER02
LIP	LIPv	„lateral bank of the intraparietal sulcus (including area LIPv)”	ER97
MT	MT	„posterior [...] banks of the dorsal superior temporal sulcus (including areas MT [...])”	ER97
STPI	STP	„middle third of the dorsal bank of the superior temporal sulcus (area STP of Bruce et al. (1981), rSTP of Hikosaka et al. (1988), STPp of Felleman & Van Essen (1991) and TPOr of Cusick et al. (1995))”	E99b
TEad	TE	„rostral third of the ventral bank of the superior temporal sulcus (cytoarchitectural area TEa of Seltzer & Pandya (1978) and TEad(s) of Yukie (1997))”	E99b
TEav	TEav	„area TEav of Saleem et al. (2000), including area 36c of Suzuki and Amaral (1994; Figure 1)”	E11b
TEO	TEO	„dorsolateral portion of the occipitotemporal transition (TEO)” (E10a)	ER98a, E10a

Table D.4: Correspondence of areas in the macaque cortex across parcellations.

Label in M132	Label in reference	Description of sampling site in morphological measures reference	Reference
TEpd	TEpd	„rostral third of the ventral bank of the superior temporal sulcus (IT; cytoarchitectural area TEa of Seltzer and Pandya, 1978; TEad(s) of Yukie, 1997; PIT of Felleman and Van Essen, 1991)” (E05), “the inferior temporal gyrus anterior to the posterior middle temporal sulcus, corresponding to area TEpd of Yukie et al. (1990) (see also Seltzer and Pandya, 1978)” (E09), “the middle third of the inferior temporal gyrus immediately anterior to the posterior middle temporal sulcus (TE, TEp of Seltzer and Pandya 1978, TEpd of Yukie 1997)” (E10a)	E05, E09, E10a
V1	V1	„superior pole of the exposed occipital operculum, corresponding to the central 5–8° in the visual field representation in the primary visual cortex (V1) (Daniel and Whitteridge, 1961)” (E09)	ER97, ER98a, E05, E09, E10a
V2	V2	„posterior bank of the inferior occipital sulcus (V2; corresponding approximately to the central 1–2 degrees) (Gattass et al. 1981; Levitt, Kiper, and Movshon 1994; Roe and T'so 1995)” (E10a)	ER97, ER98a, E01, E10a
V4	V4	„middle third of the prelunate gyrus (V4; corresponding approximately to 10–20 degrees in the visual representation) (Gattass et al. 1988)” (E10a)	ER98a, E10a

Table D.4: Correspondence of areas in the macaque cortex across parcellations (cont.). Connectivity data were published in the M132 parcellation (Markov et al., 2014a), while the morphological measures were published in reports using alternative parcellations of the macaque cortex. This table shows how areas were matched across parcellations and indicates which references the morphological measures were collated from. See main text for references. C15, Coskren et al. (2015); ER97, Elston and Rosa (1997); ER98a, Elston and Rosa (1998b); ER98b, Elston and Rosa (1998a); E99a, Elston et al. (1999a); E99b, Elston et al. (1999b); E00, Elston (2000); E01, Elston et al. (2001); ERO2, Elston and Rockland (2002); E05, Elston et al. (2005); E09, Elston et al. (2009); E10a, Elston et al. (2010a); E10b, Elston et al. (2010b); E11a, Elston et al. (2011a); E11b, Elston et al. (2011b); GML17, Gilman et al. (2017).

	Absent projections		Present projections		t-statistic	p-value	Effect size r
	Mean	Group size	Mean	Group size			
Area-based measures							
log-ratio _{density}	0.67	402	0.33	641	$t_{(1041)} = 14.5$	<.001	0.41
geodesic distance [mm]	30.9	995	22.6	1410	$t_{(2403)} = 22.0$	<.001	0.41
Cellular morphological measures							
$\Delta_{\text{soma size}}$ [μm^2]	71.7	190	58.8	288	$t_{(476)} = 2.7$	0.007	0.12
$\Delta_{\text{spine count}}$ [#]	3525	205	2687	290	$t_{(493)} = 4.3$	<.001	0.19
$\Delta_{\text{spine density}}$ [#/ $10\mu\text{m}$]	8.9	205	7.3	290	$t_{(493)} = 3.1$	0.002	0.14
$\Delta_{\text{tree size}}$ [μm^2]	48420	220	37191	323	$t_{(541)} = 4.0$	<.001	0.17

Table D.5: Structural measures in connected and unconnected pairs of macaque cortex areas in reduced data set. A cutoff was applied to the macaque connectivity data, removing connections with less than five constituent axons. Absolute values of relative structural measures are averaged across area pairs without (absent) and with (present) a linking projection. T-statistics, p-values and effect size r are results of two-tailed independent samples t-tests comparing the two respective distributions for equal means.

	Regression covariate	t-statistic	p-value	R ² _{adj}	J	accuracy	# observations	
Covariates included individually								
(1)	 log-ratio_{density} 	-0.89	-11.7	0.0000	0.220	0.338	0.721	1043
(2)	geodesic distance	-0.97	-18.5	0.0000	0.223	0.266	0.657	2405
(3)	 Δ_{soma size} 	-0.25	-2.7	0.0073	0.020	0.045	0.603	478
(4)	 Δ_{spine count} 	-0.41	-4.2	0.0000	0.048	0.169	0.634	495
(5)	 Δ_{spine density} 	-0.30	-3.1	0.0021	0.026	0.061	0.590	495
(6)	 Δ_{tree size} 	-0.36	-3.9	0.0001	0.038	0.118	0.624	543
(7)	intercept	0.35	8.4	0.0000	0.000	0.000	0.586	2405
(8) Covariates included simultaneously								
	 log-ratio_{density} 	-0.76	-4.5	0.0000	0.466	0.518	0.777	350
	geodesic distance	-1.07	-6.3	0.0000				
	 Δ_{soma size} 	0.61	3.4	0.0007				
	Δ _{spine count}	-0.31	-1.2	0.2451				
	Δ _{spine density}	-0.07	-0.3	0.7547				
	Δ _{tree size}	-0.02	-0.1	0.9083				
(9) log-ratio_{density} excluded								
	geodesic distance	-1.22	-8.7	0.0000	0.376	0.414	0.728	434
	Δ _{soma size}	0.24	1.8	0.0667				
	Δ _{spine count}	0.08	0.4	0.7263				
	Δ _{spine density}	-0.44	-2.2	0.0272				
	 Δ_{tree size} 	-0.30	-2.2	0.0296				
(10) geodesic distance excluded								
	 log-ratio_{density} 	-1.05	-7.0	0.0000	0.329	0.445	0.749	350
	 Δ_{soma size} 	0.38	2.5	0.0108				
	 Δ_{spine count} 	-0.60	-2.4	0.0150				
	Δ _{spine density}	0.13	0.6	0.5371				
	Δ _{tree size}	0.08	0.5	0.6016				
(11) Δ_{soma size} excluded								
	 log-ratio_{density} 	-0.46	-3.3	0.0010	0.428	0.478	0.761	394
	geodesic distance	-1.00	-6.8	0.0000				
	Δ _{spine count}	-0.15	-0.7	0.5082				
	Δ _{spine density}	-0.03	-0.1	0.8808				
	Δ _{tree size}	-0.12	-0.7	0.4636				
(12) Δ_{spine count} excluded								
	 log-ratio_{density} 	-0.75	-4.4	0.0000	0.463	0.485	0.766	350
	geodesic distance	-1.09	-6.5	0.0000				
	 Δ_{soma size} 	0.58	3.3	0.0010				
	Δ _{spine density}	-0.27	-1.7	0.0902				
	Δ _{tree size}	-0.10	-0.6	0.5328				
(13) Δ_{spine density} excluded								
	 log-ratio_{density} 	-0.77	-4.6	0.0000	0.466	0.518	0.777	350

Table D.6: Classification of connection existence by logistic regression in reduced data set.

		Regression			R^2_{adj}	J	accuracy	# observations
	covariate	t-statistic	p-value					
(13)	geodesic distance	-1.06	-6.3	0.0000				
cont.	 Δsoma size 	0.62	3.4	0.0006				
	 Δspine count 	-0.37	-2.0	0.0423				
	Δ tree size	0.00	0.0	0.9869				
(14)	 Δtree size excluded							
	 log-ratio_{density} 	-0.77	-4.7	0.0000	0.466	0.518	0.777	350
	geodesic distance	-1.07	-6.3	0.0000				
	 Δsoma size 	0.61	3.4	0.0007				
	Δ spine count	-0.32	-1.3	0.1895				
	Δ spine density	-0.06	-0.3	0.7712				

Table D.6: Classification of connection existence by logistic regression in reduced data set (cont.). A cutoff was applied to the macaque connectivity data, removing connections with less than five constituent axons. We performed binary logistic regression analyses (enumerated in brackets), each including a different set of the structural measures as covariates and connectivity (grouped into 'absent' and 'present' connections) as the dependent variable. Bold-faced covariates significantly contributed to classification performance as indicated by the p-value. Across all regression analyses, absolute neuron density ratio, geodesic distance and soma size difference consistently emerged as meaningful predictors.

FLNe	Individual correlation		Partial correlation	
	r	p-value	r	p-value
log-ratio _{density}	-0.19	<0.0001	-0.05	0.4487
geodesic distance	-0.47	<0.0001	-0.51	<0.0001
Δ soma size	-0.11	0.0516	0.09	0.1965
Δ spine count	-0.17	0.0028	0.00	0.9467
Δ spine density	-0.12	0.0468	-0.13	0.0610
Δ tree size	-0.13	0.0197	-0.19	0.0056
ranked strength	ρ	p-value	ρ	p-value
ranked log-ratio _{density}	0.20	<0.0001	0.13	0.0690
ranked geodesic distance	0.44	<0.0001	0.46	<0.0001
ranked Δ soma size	0.15	0.0116	-0.14	0.0528
ranked Δ spine count	0.12	0.0372	-0.02	0.7246
ranked Δ spine density	0.09	0.1112	0.12	0.0836
ranked Δ tree size	0.15	0.0053	0.20	0.0052

Table D.7: Correlation between projection strength and structural measures in reduced data set. A cutoff was applied to the macaque connectivity data, removing connections with less than five constituent axons. Pearson correlation coefficients and associated p-values for correlations between projection strength, expressed either as $\ln(\text{FLNe})$ or as ranked strengths, and absolute values of relative structural measures or ranked absolute values of relative structural measures. Correlations were assessed both for each measure independently (individual correlation) and while accounting for all other five measures (partial correlation).

	Individual correlation		Partial correlation	
	r	p-value	r	p-value
Overall degree (29x29)				
Neuron density	-0.61	0.0017	-0.62	0.0328
Soma size	0.45	0.0631	-0.02	0.9467
Spine count	0.14	0.5915	-0.02	0.9388
Spine density	0.01	0.9574	-0.26	0.4107
Dendritic tree size	0.43	0.0729	0.17	0.5994
Out-degree (29x29)				
Neuron density	-0.65	0.0006	-0.61	0.0354
Soma size	0.34	0.1666	-0.22	0.4893
Spine count	0.24	0.3455	0.05	0.8787
Spine density	0.19	0.4627	-0.14	0.6691
Dendritic tree size	0.35	0.1535	0.01	0.9710
In-degree (29x29)				
Neuron density	-0.45	0.0258	-0.44	0.1501
Soma size	0.43	0.0777	0.16	0.6215
Spine count	0.03	0.9226	-0.08	0.8089
Spine density	-0.13	0.6196	-0.27	0.3981
Dendritic tree size	0.40	0.1033	0.23	0.4635
In-degree (cortex-wide)				
Neuron density	-0.41	0.0488	-0.22	0.4839
Soma size	0.48	0.0457	0.35	0.2704
Spine count	0.14	0.5915	0.11	0.7302
Spine density	-0.10	0.6998	-0.38	0.2277
Dendritic tree size	0.46	0.0552	0.14	0.6741

Table D.8: Correlation between area degree and structural measures in reduced data set. A cutoff was applied to the macaque connectivity data, removing connections with less than five constituent axons. Pearson correlation coefficients and associated p-values for correlations between the structural measures for each area and overall area degree (total number of maintained connections), out-degree, in-degree or cortex-wide in-degree. Correlations were assessed both for each measure independently (individual correlation) and while accounting for the other five measures (partial correlation). Geodesic distance could not be included because it is a relational property not defined for individual areas. Bonferroni correction for multiple tests results in an adjusted significance threshold of $\alpha_{adj} = 0.05/5 = 0.01$ for the individual correlations.

Appendix D. Supplementary tables

Immature $N_{sc}\%$ vs. adult $N_{sc}\%$	Source Area	Target area	Immature $N_{sc}\%$	Adult $N_{sc}\%$
Neonatal $N_{sc}\%$ [K89]				
	STS	V1	0.36	0.05
	V2	V1	0.68	0.53
	V4	V1	0.63	0.24
Fetal $N_{sc}\%$ [B02]				
	V1	V4	0.85	1.00
	V2	V4	0.96	0.95
	V3A	V4	0.73	0.63
	MT	V4	0.65	0.56
	FST	V4	0.47	0.11
	LIP	V4	0.55	0.17
	TEO	V4	0.69	0.30
	TE	V4	0.43	0.29
	TH-TF	V4	0.06	0.002
	FEF	V4	0.73	0.75
Enucleated $N_{sc}\%$ vs. intact $N_{sc}\%$	Source area	Target area	Enucleated infant $N_{sc}\%$ [M18]	Intact adult $N_{sc}\%$ [C15]
	entorhinal	V2	0.00	-/-
	FEF	V2	0.33	-/-
	FST	V2	0.14	0.07
	LIP	V2	0.37	0.05
	MST	V2	0.08	0.02
	MT	V2	0.60	0.27
	peri	V2	0.02	0.04
	PGa	V2	0.22	0.02
	PIP	V2	0.33	0.01
	STP	V2	0.15	0.16
	subiculum	V2	0.00	-/-
	TE	V2	0.06	0.02
	TEO	V2	0.39	0.09
	TH/TF	V2	0.00	0.01
	V1	V2	1.00	0.74
	V3	V2	0.59	0.32
	V3A	V2	0.49	0.03
	V4	V2	0.41	0.25
	7A	V4	0.05	0.04
	FEF	V4	0.44	-/-
	FST	V4	0.20	0.17
	LIP	V4	0.24	0.22
	MST	V4	0.16	0.04
	MT	V4	0.35	0.46
	peri	V4	0.00	0.0004
	PIP	V4	0.44	0.15
	STP	V4	0.04	0.02
	TE	V4	0.05	0.09
	TEO	V4	0.45	0.43
	TH/TF	V4	0.05	0.01
	V1	V4	0.00	0.98
	V2	V4	0.83	0.93
	V3	V4	0.65	0.66
	V3A	V4	0.63	0.00

Table D.9: Projection data in the immature macaque cortex. Values for Batardière and colleagues (2002) extracted from their Figure 7A. K89, Kennedy et al. (1989); B02, Batardière et al. (2002); M18, Magrou et al. (2018); C15, Chaudhuri et al. (2015).

	ρ	p-value	R ²
adult $N_{SG}\%$ vs. immature $N_{SG}\%$			
Neonate (K89)	1.00	0.3333	0.77
Fetal (B02)	0.94	0.0000	0.75
immature $N_{SG}\%$ vs. architectonic type difference			
Neonate (K89)	1.00	0.3333	0.95
Fetal (B02)	0.87	0.0011	0.74
adult $N_{SG}\%$ vs. architectonic type difference			
Neonate (K89)	1.00	0.3333	0.92
Fetal (B02)	0.87	0.0009	0.74
immature $N_{SG}\%$ vs. neuron density difference			
Neonate (K89)	1.00	0.3333	0.82
Fetal (B02)	0.73	0.0311	0.37
adult $N_{SG}\%$ vs. neuron density difference			
Neonate (K89)	1.00	0.3333	1.00
Fetal (B02)	0.72	0.0369	0.54
adult $N_{SG}\%$ / immature $N_{SG}\%$ vs. architectonic type difference			
Neonate (K89)	1.00	0.3333	0.91
Fetal (B02)	0.77	0.0093	0.62
adult $N_{SG}\%$ / immature $N_{SG}\%$ vs. neuron density difference			
Neonate (K89)	1.00	0.3333	0.99
Fetal (B02)	0.58	0.1080	0.38

Table D.10: Correlations of laminar projection patterns and architectonic differentiation in the immature macaque cortex. See Figure 3.19 for scatter plots of the underlying data. ρ and p-value: Spearman rank-correlation; R²: coefficient of determination for a linear regression model. Please note that the p-value for K89 correlations cannot be lower than 0.33 because only three data points are available. K89, Kennedy et al. (1989); B02, Batardière et al. (2002).

	Individual correlation			Partial correlation		
	ρ	p-value	R ²	ρ	p-value	R ²
$N_{SG}\%$ enucleated vs. $N_{SG}\%$ intact	0.47	0.0083	0.27	0.58	0.0013	0.48
$N_{SG}\%$ enucleated vs. architectonic type difference	0.73	1.2e-6	0.44	0.86	4.2e-10	0.62
$N_{SG}\%$ enucleated vs. neuron density difference	0.48	0.0185	0.21	0.60	0.0033	0.47

Table D.11: Correlations with laminar projection patterns after enucleation. See Figure 3.20 for scatter plots of the underlying data. ρ and p-value: Spearman rank-correlation; R²: coefficient of determination for a linear regression model. Projections originating in V1 were excluded because V1 was affected very strongly by the enucleation and the resulting $N_{SG}\%$ -values are outliers.

set	growth mode	# origins	Connectivity statistics				Relative connection frequency				Logistic regression performance				Area degree				
			median fraction connected areas	median number of connections	distance		absolute density difference		median McFadden's Pseudo R ²	distance McFadden's Pseudo R ²	validation p-values of correlation: sign test	relative connection frequency vs distance	correlation relative connection frequency vs distance	validation p-values of correlation: sign test	distance & absolute density difference	median McFadden's Pseudo R ²	median ρ	correlation vs neuron density	validation p-values of correlation: sign test
					correlation relative connection frequency vs distance	validation p-values of correlation: sign test	correlation relative connection frequency vs distance	validation p-values of correlation: sign test											
realistically oriented gradient	1D 1 row	1	0.517	280	-0.99	9.54E-08	-9.9	2.08E-23	-0.98	0.0E+00	-9.9	2.08E-23	0.407	0.154	0.513	-0.74	2.19E-05	-9.9	2.08E-23
	1D 2 rows	1	0.466	1019	-0.99	9.54E-08	-9.9	2.08E-23	-1.00	0.0E+00	-9.9	2.08E-23	0.373	0.161	0.458	-0.79	1.32E-11	-9.9	2.08E-23
	2D	1	0.708	4154	0.50	1.43E-01	10.1	1.0E+00	-1.00	1.67E-02	-9.9	2.08E-23	0.000	0.266	0.269	0.03	7.43E-01	10.1	1.0E+00
	1D 1 row	2	0.629	372	-0.89	6.10E-04	-9.9	2.08E-23	-0.96	2.78E-03	-9.9	2.08E-23	0.166	0.150	0.381	-0.42	3.26E-02	-5.5	1.90E-08
	1D 2 rows	2	0.563	1339	-0.85	2.68E-03	-9.9	2.08E-23	-0.96	2.78E-03	-9.9	2.08E-23	0.137	0.143	0.314	-0.52	7.57E-05	-9.9	2.08E-23
	2D	2	0.590	13103	-0.77	1.37E-02	-8.1	2.75E-16	-1.00	1.67E-02	-9.9	2.08E-23	0.016	0.256	0.288	0.17	3.41E-02	-5.1	1.70E-07
inverse gradient	1D 1 row	3	0.611	395	-0.88	1.10E-03	-9.9	2.08E-23	-0.90	8.33E-02	3.9	1.0E+00	0.188	0.152	0.424	-0.44	2.15E-02	-7.7	6.80E-15
	1D 2 rows	3	0.549	1412	-0.85	3.50E-03	-9.9	2.08E-23	-1.00	1.67E-02	-9.9	2.08E-23	0.155	0.151	0.359	-0.56	8.83E-06	-9.9	2.08E-23
	2D	3	0.578	18626	-0.92	4.67E-04	-9.9	2.08E-23	-1.00	8.33E-02	10.1	1.0E+00	0.017	0.285	0.320	0.34	1.52E-06	-9.9	2.08E-23
	1D 1 row	2	0.438	259	-0.95	2.38E-05	-9.9	2.08E-23	-0.96	2.78E-03	-9.9	2.08E-23	0.175	0.077	0.284	0.67	1.95E-04	-9.9	2.08E-23
	1D 2 rows	2	0.393	933	-0.95	2.93E-05	-9.9	2.08E-23	-1.00	3.97E-04	-9.9	2.08E-23	0.164	0.051	0.224	0.72	1.53E-09	-9.9	2.08E-23
	2D	2	0.408	7988	-0.99	0.0E+00	-9.9	2.08E-23	-1.00	1.67E-02	-9.9	2.08E-23	0.029	0.040	0.074	0.67	2.97E-22	-9.9	2.08E-23
radial	1D 1 row	2	0.654	365	-0.98	1.54E-06	-9.9	2.08E-23	0.96	2.78E-03	-8.9	2.79E-19	0.743	0.013	0.745	0.00	9.49E-01	10.1	1.0E+00
	1D 2 rows	2	0.659	1459	-0.99	5.93E-09	-9.9	2.08E-23	0.96	2.78E-03	-9.3	7.02E-21	0.703	0.006	0.705	0.00	9.54E-01	10.1	1.0E+00
	2D	2	0.864	17693	-0.93	6.51E-05	-9.9	2.08E-23	-1.00	1.67E-02	-9.9	2.08E-23	0.099	0.020	0.126	0.59	7.49E-17	-9.9	2.08E-23
static	1D 1 row	2	0.528	319	-0.93	7.57E-05	-9.9	2.08E-23	0.85	2.38E-02	-2.3	1.07E-02	0.746	0.009	0.750	0.00	9.12E-01	10.1	1.0E+00
	1D 2 rows	2	0.522	1266	-0.97	3.78E-06	-9.9	2.08E-23	0.46	3.02E-01	6.7	1.0E+00	0.724	0.003	0.730	0.00	9.27E-01	10.1	1.0E+00
	2D	2	0.758	16283	-0.95	0.0E+00	-9.9	2.08E-23	-1.00	1.67E-02	-9.9	2.08E-23	0.215	0.010	0.236	0.62	6.41E-19	-9.9	2.08E-23
random	1D 1 row	2	0.515	307	-0.95	2.38E-05	-9.9	2.08E-23	-0.18	3.57E-01	7.1	1.0E+00	0.171	0.001	0.174	0.29	1.30E-01	3.9	1.0E+00
	1D 2 rows	2	0.462	1096	-0.95	1.02E-05	-9.9	2.08E-23	-0.36	2.54E-01	6.7	1.0E+00	0.148	0.000	0.148	0.25	7.98E-02	1.3	9.03E-01
	2D	2	0.549	12165	-0.84	4.46E-03	-9.9	2.08E-23	-1.00	1.67E-02	-8.5	9.48E-18	0.022	0.003	0.025	0.54	9.56E-14	-9.9	2.08E-23

Table D.12

Table D.12: Summary of connectivity statistics, correlation with relative projection frequency, classification performance logistic regression, and correlation with area degree in silico. This table lists the median values indicated by the box plots in Figures 3.21 through 3.24. Where applicable, the table additionally lists the associated median p-value of Spearman rank correlations as well as the z-value and p-value of a left-tailed sign test testing the distribution of rank correlation p-values for a median of $\alpha = 0.05$. Background colours as in Table 2.1.

Accuracy										
macaque										
cat										
validation of 'median p-value against chance performance': sign test										
prediction performance										
validation of 'median p-value against chance performance': sign test										
median p-value against chance perf.										
set	growth mode	# origins	median accuracy	median p-value against chance perf.	z-val	p-value	median accuracy	median p-value against chance perf.	z-val	p-value
realistically oriented gradient	1D 1 row	1	0.805	0.0E+00	-9.90	2.08E-23	0.699	6.37E-18	-9.90	2.08E-23
	1D 2 rows	1	0.781	4.54E-43	-9.90	2.08E-23	0.640	6.45E-19	-9.90	2.08E-23
	2D	1	0.811	3.14E-24	-9.90	2.08E-23	0.830	2.57E-10	-9.90	2.08E-23
	1D 1 row	2	0.854	0.0E+00	-9.90	2.08E-23	0.820	6.03E-17	-9.90	2.08E-23
	1D 2 rows	2	0.860	0.0E+00	-9.90	2.08E-23	0.797	1.89E-16	-9.90	2.08E-23
	2D	2	0.841	4.61E-35	-9.90	2.08E-23	0.767	7.93E-15	-9.90	2.08E-23
	1D 1 row	3	0.837	0.0E+00	-9.90	2.08E-23	0.796	2.92E-17	-9.90	2.08E-23
	1D 2 rows	3	0.843	0.0E+00	-9.90	2.08E-23	0.757	4.00E-17	-9.90	2.08E-23
inverse gradient	2D	3	0.847	5.33E-41	-9.90	2.08E-23	0.767	6.32E-16	-9.90	2.08E-23
	1D 1 row	2	0.782	7.70E-40	-9.90	2.08E-23	0.586	3.59E-15	-9.90	2.08E-23
	1D 2 rows	2	0.744	3.48E-35	-9.90	2.08E-23	0.500	1.84E-13	-9.90	2.08E-23
radial	2D	2	0.852	1.65E-22	-9.90	2.08E-23	0.667	3.10E-06	-9.90	2.08E-23
	1D 1 row	2	0.739	7.89E-33	-9.90	2.08E-23	0.671	4.24E-10	-9.90	2.08E-23
	1D 2 rows	2	0.751	1.38E-34	-9.90	2.08E-23	0.682	2.60E-11	-9.90	2.08E-23
static	2D	2	0.644	3.20E-01	5.50	1.0E+00	0.771	3.20E-01	5.90	1.0E+00
	1D 1 row	2	0.701	1.89E-39	-9.90	2.08E-23	0.602	1.28E-11	-9.90	2.08E-23
	1D 2 rows	2	0.703	1.12E-39	-9.90	2.08E-23	0.602	6.91E-12	-9.90	2.08E-23
random	2D	2	0.869	1.40E-39	-9.90	2.08E-23	0.897	6.17E-13	-9.90	2.08E-23
	1D 1 row	2	0.880	1.70E-23	-9.90	2.08E-23	0.722	4.65E-04	-9.70	1.51E-22
	1D 2 rows	2	0.801	1.05E-19	-9.90	2.08E-23	0.556	8.81E-03	-9.90	2.08E-23
	2D	2	1.000	4.05E-02	0.71	7.60E-01	1.000	6.10E-02	3.88	1.0E+00

Table D.13: Summary classification of empirical connectivity from simulated connectivity.

Youden index <i>J</i>										
macaque										
cat										
validation of 'median p-value against chance performance': sign test										
validation of 'median p-value against chance performance': sign test										
prediction performance										
prediction performance										
set	growth mode	# origins	median accuracy	median p-value against chance perf.	z-val	p-value	median accuracy	median p-value against chance perf.	z-val	p-value
realistically oriented gradient	1D 1 row	1	0.805	0.0E+00	-9.90	2.08E-23	0.699	6.37E-18	-9.90	2.08E-23
	1D 2 rows	1	0.781	4.54E-43	-9.90	2.08E-23	0.640	6.45E-19	-9.90	2.08E-23
	2D	1	0.811	3.14E-24	-9.90	2.08E-23	0.830	2.57E-10	-9.90	2.08E-23
	1D 1 row	2	0.854	0.0E+00	-9.90	2.08E-23	0.820	6.03E-17	-9.90	2.08E-23
	1D 2 rows	2	0.860	0.0E+00	-9.90	2.08E-23	0.797	1.89E-16	-9.90	2.08E-23
	2D	2	0.841	4.61E-35	-9.90	2.08E-23	0.767	7.93E-15	-9.90	2.08E-23
	1D 1 row	3	0.837	0.0E+00	-9.90	2.08E-23	0.796	2.92E-17	-9.90	2.08E-23
	1D 2 rows	3	0.843	0.0E+00	-9.90	2.08E-23	0.757	4.00E-17	-9.90	2.08E-23
	2D	3	0.847	5.33E-41	-9.90	2.08E-23	0.767	6.32E-16	-9.90	2.08E-23
inverse gradient	1D 1 row	2	0.782	7.70E-40	-9.90	2.08E-23	0.586	3.59E-15	-9.90	2.08E-23
	1D 2 rows	2	0.744	3.48E-35	-9.90	2.08E-23	0.500	1.84E-13	-9.90	2.08E-23
	2D	2	0.852	1.65E-22	-9.90	2.08E-23	0.667	3.10E-06	-9.90	2.08E-23
radial	1D 1 row	2	0.739	7.89E-33	-9.90	2.08E-23	0.671	4.24E-10	-9.90	2.08E-23
	1D 2 rows	2	0.751	1.38E-34	-9.90	2.08E-23	0.682	2.60E-11	-9.90	2.08E-23
	2D	2	0.644	3.20E-01	5.50	1.0E+00	0.771	3.20E-01	5.90	1.0E+00
static	1D 1 row	2	0.701	1.89E-39	-9.90	2.08E-23	0.602	1.28E-11	-9.90	2.08E-23
	1D 2 rows	2	0.703	1.12E-39	-9.90	2.08E-23	0.602	6.91E-12	-9.90	2.08E-23
	2D	2	0.869	1.40E-39	-9.90	2.08E-23	0.897	6.17E-13	-9.90	2.08E-23
random	1D 1 row	2	0.880	1.70E-23	-9.90	2.08E-23	0.722	4.65E-04	-9.70	1.51E-22
	1D 2 rows	2	0.801	1.05E-19	-9.90	2.08E-23	0.556	8.81E-03	-9.90	2.08E-23
	2D	2	1.000	4.05E-02	0.71	7.60E-01	1.000	6.10E-02	3.88	1.0E+00

% classified										
macaque										
cat										
median fraction classified										
median fraction classified										
set	growth mode	# origins	median fraction classified	median fraction classified						
realistically oriented gradient	1D 1 row	1	0.548	0.471						
	1D 2 rows	1	0.493	0.438						
	2D	1	0.423	0.414						
	1D 1 row	2	0.510	0.409						
	1D 2 rows	2	0.409	0.328						
	2D	2	0.346	0.309						
	1D 1 row	3	0.551	0.451						
	1D 2 rows	3	0.461	0.384						
	2D	3	0.392	0.343						
inverse gradient	1D 1 row	2	0.376	0.341						
	1D 2 rows	2	0.300	0.274						
	2D	2	0.077	0.049						
radial	1D 1 row	2	0.743	0.723						
	1D 2 rows	2	0.730	0.701						
	2D	2	0.500	0.500						
static	1D 1 row	2	0.827	0.861						
	1D 2 rows	2	0.817	0.834						
	2D	2	0.426	0.393						
random	1D 1 row	2	0.137	0.139						
	1D 2 rows	2	0.116	0.133						
	2D	2	0.000	0.000						

Table D.13: Summary classification of empirical connectivity from simulated connectivity (cont.). This table lists the median values for classification accuracy, Youden index *J* and fraction of empirical connections classified as indicated by the box plots in Figures 3.25 through 3.27. For accuracy and Youden index, it additionally lists the associated median p-value of a z-test against chance performance as assessed by permutation analysis, as well as the z-value and p-value of a left-tailed sign test testing the distribution of z-test p-values for a median of $\alpha = 0.05$. Background colours as in Table 2.1.

Eidesstattliche Erklärung

Ich versichere ausdrücklich, dass ich die Arbeit selbständig und ohne fremde Hilfe verfasst, andere als die von mir angegebenen Quellen und Hilfsmittel nicht benutzt und die aus den benutzten Werken wörtlich oder inhaltlich entnommenen Stellen einzeln nach Ausgabe (Auflage und Jahr des Erscheinens), Band und Seite des benutzten Werkes kenntlich gemacht habe. Ferner versichere ich, dass ich die Dissertation bisher nicht einem Fachvertreter an einer anderen Hochschule zur Überprüfung vorgelegt oder mich anderweitig um Zulassung zur Promotion beworben habe. Ich erkläre mich einverstanden, dass meine Dissertation vom Dekanat der Medizinischen Fakultät mit einer gängigen Software zur Erkennung von Plagiaten überprüft werden kann.

Unterschrift: